Advancing Step-Growth Polymers: Novel Macromolecular Design and Electrostatic Interactions in Polyesters and Polyurethanes

Musan Zhang

Dissertation submitted to the faculty of the Virginia Polytechnic Institute and State University in partial fulfillment of the requirements for the degree of

Doctor of Philosophy
In
Chemistry

Timothy E. Long, Chair
Robert B. Moore
S. Richard Turner
Abby Whittington

May 2, 2013
Blacksburg, VA

Keywords: Step-Growth Polymers, Polyesters, Ionomers, Polyurethanes, Morphology

Advancing Step-Growth Polymers: Novel Macromolecular Design and Electrostatic Interactions in Polyesters and Polyurethanes

Musan Zhang

ABSTRACT

Conventional melt transesterification successfully synthesized high molecular weight segmented copolyesters. The cycloaliphatic monomers 2,2,4,4-tetramethyl-1,3-cyclobutanediol (CBDO) and dimethyl-1,4-cyclohexane dicarboxylate (DMCD) afforded sterically hindered, ester carbonyls in high-T_g polyester precursors. Reaction between the polyester polyol precursor and a primary or secondary alcohol at melt polymerization temperatures revealed reduced transesterification of the polyester hard segment as a result of enhanced steric hindrance adjacent to the ester linkages. Subsequent polymerization of a 4,000 g/mol polyol with monomers comprising the low-T_g block yielded high molecular weight polymers that exhibited enhanced mechanical properties compared to a non-segmented copolyester control. Atomic force microscopy uncovered unique needle-like, interconnected, microphase separated surface morphologies, and small-angle X-ray scattering confirmed the presence of bulk microphase separation.

This new synthetic strategy enabled selective control of ionic charge placement into the hard segment or soft segment block of segmented copolyesters using melt transesterification. The ionic placement impacted the microphase-separated morphology, which influenced its thermomechanical properties and resulting mechanical performance. Melt transesterification of low-T_g, sodium sulfonated copolyesters achieved up to 15 mol% ionic content. The 10 and 15 mol% sodium sulfonated copolyesters exhibited water-dispersibility, which enabled cation

dialysis exchanges to divalent metal cations. The sulfonated copolyesters containing divalent metal cations exhibited enhanced rubbery plateau moduli to higher temperatures.

Novel trialkylphosphonium ionic liquids chain extenders enabled the successful synthesis of poly(ethylene glycol)-based, cationic polyurethanes with pendant phosphoniums in the hard segments (HS). Aqueous size exclusion chromatography (SEC) confirmed the charged polyurethanes, which varied the phosphonium alkyl substituent length (ethyl and butyl) and cationic HS content (25, 50, 75 mol%), achieved high absolute molecular weights. Dynamic mechanical analysis (DMA) demonstrated the triethylphosphonium (TEP) and tributylphosphonium (TBP) polyurethanes displayed similar thermomechanical properties, including increased rubbery plateau moduli and flow temperatures. Fourier transform infrared spectroscopy (FTIR) emphasized the significance of ion-dipole interaction on hydrogen bonding. Atomic force microscopy (AFM), small-angle X-ray scattering (SAXS), and wide-angle X-ray diffraction (WAXD) supported microphase separated morphologies in the trialkylphosphonium polyurethanes, despite the presence of ionic interactions. Sorption isotherm experiments revealed TBP polyurethanes displayed similar water sorption profiles to the noncharged analogue and lower water absorptivity compared to TEP. The phosphonium polyurethanes displayed significantly improved tensile strain; however, lower tensile stress of the TEP polyurethane was presumably due to absorbed water. In addition, we also explored applications of the trialkylphosphonium polyurethanes as nucleic acid delivery vectors and demonstrated their abilities to form colloidally stable polyplexes in salt-containing media.

ACKNOWLEDGEMENTS

I would first like to thank Dr. Long for accepting an over-optimistic "biologist" with no previous chemistry research experience into his group. Thank you for your support throughout my graduate career and for providing me so many rich opportunities in research, academic, and industrial experiences. If fate holds an academic path for me, I will never forget what I have learned from you mentorship, especially your enthusiastic passion for polymer science, students, and education. I would also like to thank my committee members Dr. Richard Turner, Dr. Robert Moore, and Dr. Abby Whittington for their guidance and thought-provoking questions, especially during exams. Dr. Moore's visco and morphology classes (in addition to being extremely entertaining) hinted at the similarities between intricate and unique morphological structures and art, my passion and hobby. I am thankful for Dr. Turner's inexplicable knowledge of polyesters, which helped me so much when I was on a synthetic roadblock. I owe the success during my last year of my work on the trialkylphosphonium and imidazolium diol to Dr. Turner, who provided me with a reference to synthesize a halogenated diol with TWO primary hydroxyls. Finally, I would like to thank Dr. Abby Whittington for encouraging me during exams to view problems from a bioengineer's perspective.

I am gracious for the staff at Virginia Tech Chemistry and MII, especially Laurie Good, Tammy Jo Hiner, and Teresa Dickerson for being so helpful with all the technical details related to funding, Hokiemart, impromptu academic emergencies, and getting paid. I am especially grateful for Valerie Owens, Naya Sou, and Brent Bowden, for their moral support, attention to detail, and organizational skills when dealing with the chaotic vortex that is the Long group.

I am so appreciative for members of our group, past and current. I am thankful for my mentor Gozde Ozturk, who never once spoke an ill word about her experience but instead

offered advice on how to survive graduate school. Also, I'm so grateful to have met friends like Jenny England and Alice Savage – for lunches and non-science related escapes. I would like to thank my undergraduate students in research – Adam, Joe, Eliot, Jen, Nick, Courtney, and Niki. I'm also very grateful for amusing and wise postdocs and senior students, especially Matt Hunley, Erin Murphy, and Christian Schreiner. I am thankful beyond words to have been able to move to ICTAS II and work with the three most talented guys in Polymer Chemistry: Adam, Sean, and Mike. Dr. Adam Smith - for being a friend, mentor, and role model with a familiar accent. Sean Hemp – for being such a skilled chemist and fearless leader with remarkable enthusiasm, faith, and drive. Mike Allen – for being a friend and partner from Day 1 of this grad school journey - suffice it to say, we experienced many ups and downs, but we both enjoyed poking fun of the irony and absurdity…and laughing never got old. Ashley – I know you will bring your creativity and brilliance to our beloved polyester research. To the younger students – stay optimistic and idealistic throughout your time in grad school. Do not be self-defeating; share your successes and challenges with each other, ask for help from older students, and learn to create your own ideas. For the two people who shared this crazy Spring 2013 semester: Asem- thank you so much for being a strong role model and mentor; John – I'm so glad the Big Bang said yes, "the world began with a yes."

Finally, to my parents – my role models who embody determination, compassion, and wit. I have the opportunities to make choices in my life today because of the sacrifices they have made and I am beyond humbled. To my younger sisters – Lucy and Stacy – the two of you are my best friends in this entire world…thanks for living in cooler places than Blacksburg, Virginia for momentary escapes. My younger brother Justin, who is starting undergrad next year – when you find your passion in life, jump in – you won't regret it.

Table of Contents

Chapter 1: Introduction 1
1.1 Dissertation Overview 1
1.2 References 4
Chapter 2: Traditional and Novel Synthetic Approaches in Polyester Step-Growth Polymerization 5
2.1 Abstract 5
2.2 Introduction and Historical Perspective 6
2.3 Synthesis of Step-Growth Polymers 8
2.3.1 Polycondensation Polymers 9
2.3.2 Polyaddition Polymers 35
2.4 Novel Synthetic Approaches in Step-Growth Polymerization 50
2.4.1 Non-aqueous emulsion polymerization 50
2.4.2 Lipase-catalyzed polymerization 52
2.4.3 Chain-growth polycondensation 55
2.5 Polyesters for Current and Emerging Technologies 55
2.6 Conclusions 60
2.7 References 62
Chapter 3: Stimuli-Responsive Hydrogels for Controlled Insulin Delivery 71
3.1 Abstract 71
3.2 Introduction 72
3.3 Challenges in Insulin Delivery 73
3.4 Hydrogels in Insulin Delivery 75
3.4.1 Temperature-Responsive Hydrogels 76
3.4.2 pH-Responsive Hydrogels 84
3.4.3 Glucose-Responsive Hydrogels 88
3.5 Conclusions 91
3.6 References 92
Chapter 4: Melt Transesterification and Characterization of Segmented Block Copolyesters Containing 2,2,4,4-Tetramethyl-1,3-cyclobutanediol 96
4.1 Abstract 96
4.2 Introduction 97

4.3 Experimental Section 99
4.4 Results and Discussion 102
4.5 Conclusions 117
4.6 References 118
Chapter 5: Influence of Charge Placement on the Thermal and Morphological Properties of Sulfonated Segmented Copolyesters 121
5.1 Abstract 121
5.2 Introduction 122
5.3 Experimental Section 124
5.4 Results and Discussion 127
5.5 Conclusions 142
5.6 References 144
5.7 Supporting Information 146
Chapter 6: Impact of Divalent Metal Cations on Thermal and Rheological Properties of Randomly Sulfonated Polyesters 149
6.1 Abstract 149
6.2 Introduction 150
6.3 Experimental Section 152
6.4 Results and Discussion 155
6.5 Conclusions 161
6.6 References 168
6.7 Supporting Information 169
Chapter 7: Water-Dispersible Cationic Polyurethanes Containing Pendant Trialkylphosphoniums 171
7.1 Abstract 171
7.2 Introduction 172
7.3 Experimental Section 174
7.4 Results and Discussion 177
7.5 Conclusions 193
7.6 References 195
7.7 Supporting Information 197
Chapter 8: Trialkylphosphonium Polyesters for Nonviral Nucleic Acid Delivery 203

8.1 Abstract 203
8.2 Introduction 204
8.3 Experimental Section 206
8.4 Results and Discussion 209
8.5 Conclusions 216
8.6 References 217
8.7 Supporting Information 218
Chapter 9: Overall Conclusions 220
Chapter 10: Suggested Future Work 221
10.1 Polymerized Imidazolium and Phosphonium Ionic Liquids for Step-Growth Biopolymers 221

List of Figures

Figure 2.1. Peptide dendritic monomers derived from amino acids produced a fast curing hydrogel for sealant-repaired corneal incisions.[74] 22

Figure 2.2. General structure for polyimides. 25

Figure 2.3. Chemical structures of commonly used dianhydrides for polyimide synthesis. 26

Figure 2.4. Chemical structures of common diamines used in polyimide synthesis. 27

Figure 2.5. Sub-nanometer ultrathin polyimide films on Au(111) substrates. a) Monomers used in polyimide formation. b) Hydrogen-bonded planar sheets of monomers prior to annealing. White boxed area indicates the hydrogen bonded structure between the PTCDA and DATP. c) Polyimide ultrathin film through the annealing of the hydrogen bonded monomers. Blue circled area highlights unreacted DATP and PTCDA monomers. White boxed area shows parallel polyimide strands after thermal imidization.[30] 30

Figure 2.6. List of commonly used aliphatic and aromatic diisocyanates for polyurethane synthesis. 41

Figure 2.7. Schematic of the microstructure transition of shape-memory poly(ester-urethanes) under strain deformation and shape recovery.[60] 46

Figure 2.8, Micrographs of epoxy-cured polymer composites. a) Optical micrograph of amine-filled microcapsules in solution for self-healing epoxy composites. b) Fluorescence micrograph reflecting the response of microcapsules under applied pressure.[67] 49

Figure 2.9. Nonaqueous emulsion polycondensation.[74] 51

Figure 2.10. Size and shape of polyester nanoparticles synthesized using oil-in-oil emulsion polymerization a) SEM image and b) particle distribution from SEM image. Polyester nanoparticles displayed an average particle size of 38 ± 7 nm.[74] 52

Figure 2.11. Growth of bio-based polymers derived from renewable resources from 2003 to 2007.[98] 56

Figure 3.1 *In vitro* release of FITC labeled dextran. Filled squares and circles represent 23 and 35 weight% of polymer, respectively.[73] 77

Figure 3.2. Shear storage modulus (G'), shear loss modulus (G''), and complex viscosity (ŋ*) show clear changes indicating the gelation temperature and sol-gel transition.[75] Reprinted with permission from Brahim, S.; Narinesingh, D.; Guiseppi-Elie, A., *Biomacromolecules* 2003, *4* (3), 497-503. Copyright 2003 American Chemical Society. 79

Figure 3.3. Comparison of insulin release rate for ReGel-1 and ReGel-2. ReGel-1 have a PEG unit of 1,000 g/mol and ReGel2: have a PEG unit of 1,450.[75] Reprinted with permission from Brahim, S.; Narinesingh, D.; Guiseppi-Elie, A., *Biomacromolecules* 2003, *4* (3), 497-503. Copyright 2003 American Chemical Society. 80

Figure 3.4. Effect of PLGA molecular weight on phase transition of PEG-PLGA-PEG.[62] Reprinted with permission from Jeong, B.; Bae, Y. H.; Kim, S. W., *Macromolecules* 1999, *32* (21), 7064-7069. Copyright 1999 American Chemical Society. 81

Figure 3.5. Phase diagram for PEG-PLGA-PEG triblocks.[62] Reprinted with permission from Jeong, B.; Bae, Y. H.; Kim, S. W., *Macromolecules* 1999, *32* (21), 7064-7069. Copyright 1999 American Chemical Society. 81

Figure 3.6. Electrostatic interactions provide strong complexes between the protonated PAE and partially negative carbonyl from the insulin amino acid. The dotted line depicts potential hydrogen bonding between the carbonyl and protonated amine. 82

Figure 3.7. Mechanism controlling the complexation and release of insulin.[37] (Image reproduced from Ref. 37) 83

Figure 3.8. Insulin release profile showed clear response to the changes in glucose based on time and concentration.[98] (Image reproduced from Ref. 98) 89

Figure 3.9. Changing glucose and pH concentrations control solute diffusion through swollen and collapsed hydrogels.[99] (Image reproduced from Ref. 99) 90

Figure 3.10. Examples of methacrylic tertiary amines used in pH-responsive polymeric systems. 90

Figure 4.1. Plot of T_g as a function of poly(CBDO-DMCD) M_n. 105

Figure 4.2. Plot of T_g as a function of inverse M_n provides a theoretical T_g for high molecular weight poly(CBDO-DMCD). 106

Figure 4.3. Transesterification study demonstrated a decrease in M_n as a function of reaction temperature and alcohol steric hindrance. 108

Figure 4.4. Dynamic mechanical analysis of 20, 30, and 40 wt% hard segment copolyesters. Dynamic mechanical properties analyzed in tension mode: 1 Hz, 3 °C/min. 112

Figure 4.5. Tensile properties of 30 and 40 wt% hard segment (HS) copolyesters. Tensile data are reported as an average of 5 replications under tensile mode and crosshead speed of 10 mm/min. 113

Figure 4.6. Atomic force images in tapping mode of segmented copolyesters. (a) 30 wt% hard segment content. (b) 40 wt% hard segment content. 114

Figure 4.7. SAXS profiles of scattering intensity versus scattering vector for poly[(CBDO-DMCD)-*co*-(DEG-DMAp)] copolyester. 116

Figure 5.1. HS T_g as a function of sulfonated dimethylisophthalate (poly(sCBDO-DMCD)) or dimethyl isophthalate (poly(dCBDO-DMCD)) molar content. 130

Figure 5.2. Dynamic mechanical analysis of sulfonated HS copolyesters. 133

Figure 5.3. Dynamic mechanical analysis of sulfonated SS copolyesters. 133

Figure 5.4. *In situ* VT-SAXS profile demonstrating the disappearance of the scattering peak maximum ($q \approx 0.35$ nm^{-1}) from 130 to 145 °C. VT-SAXS profiles were collected approximately every 10 sec from 30 – 200 °C under a heating ramp rate of 10 °C/min. Each scattering profile represents a 5 °C interval. 135

Figure 5.5. Log-log plots of *G'* vs. *G''* obtained from dynamic melt rheology. The transition to temperature-independent *G'* vs. *G''* curves (slope = 2) was used to identify the ODT. 136

Figure 5.6. Atomic force microscopy phase images of non-sulfonated and sulfonated segmented block copolyesters containing 30 wt% HS. a) Non-sulfonated, b) 3 mol% sulfonated HS, c) 5 mol% sulfonated HS, d) 3 mol% sulfonated SS, and e) 5 mol% sulfonated SS. 138

Figure 5.7. Tensile testing plots displaying a) stress at break, b) strain at break, and c) Young's modulus as a function of sulfonation content in HS (circle) or SS (triangle). Tensile data are represented as an average of five samples. 139

Figure 5.8. Hysteresis studies depicting three loading and unloading cycles for 7 mol% soft segment sulfonated copolyesters pulled to a) 80% and b) 120% strain at 80 mm/min with 30 sec delays between cycles. 141

Figure 6.1. Dynamic light scattering traces of 5 wt% sodium sulfonated polyesters in water and water with 0.25 M NaBr. 164

Figure 6.2. Influence of monovalent and divalent salt concentrations on the hydrodynamic diameter of 15 mol% sulfonated copolyesters in 10 wt% polymer solutions. Divalent salts increased the polymer hydrodynamic diameter at approximately 16 mM salt concentrations. 164

Figure 6.3. Dynamic mechanical analysis of Na-10s and Na-15s copolyesters. 165

Figure 6.4. Dynamic mechanical analysis of 15 mol% sulfonated copolyesters as a function of countercation composition. 165

Figure 6.5. Temperature sweep experiments obtained from dynamic melt rheology demonstrates the influence of divalent metal cations on 15 mol% sulfonated copolyesters. Molecular weight influences were eliminated using dialysis cation exchange. 166

Figure 6.6. Representative thermogravimetric sorption/desorption/sorption curve obtained from Mg-15s copolyester. 166

Figure 6.7. TTS master curves of $\leq$ 5 mol% sodium sulfonated copolyester (T_{ref} = 40 °C) demonstrating an extended rubbery plateau as a function of sulfonation level. Filled and unfilled symbols represent the storage and loss moduli, respectively. 167

Figure 6.8. TTS master curve of Zn-15s copolyester (T_{ref} = 30 °C). Filled and unfilled symbols represent the storage (G') and loss (G'') moduli, respectively. 167

Figure 7.1. Representative aqueous SEC light scattering chromatograms of phosphonium PU (54/23/23 water/methanol/acetic acid (v/v/v %), 0.1 M sodium acetate). 179

Figure 7.2. Dynamic mechanical analysis of noncharged and phosphonium PU (75 mol% HS). 182

Figure 7.3. FTIR spectra of noncharged and phosphonium polyurethanes: a) N-H stretch between 3000 – 3500 cm^{-1} and b) carbonyl stretch between 1600 – 1750 cm^{-1}. 184

Figure 7.4. Atomic force microscopy phase images: a) BD(75), b) TEP(75), and c) TBP(75) polyurethanes. The scale bars represent 200 nm. 186

Figure 7.5. Representative tensile stress-strain curves of noncharged and phosphonium polyurethanes. Arrow designates the stress and strain at break for BD(75). 189

Figure 7.6. Sorption isotherm of noncharged and phosphonium polyurethanes (75 mol% HS) at 25 °C. 190

Figure 7.7. DNA binding gel shift assay of cationic polyurethanes with various TBP mol% content. Arrows designate +/- ratio at complete DNA binding. 192

Figure 7.8. Polyplex stability (+/- ratio = 4) over 24 h in salt solution, Dulbecco's modified Eagle's media (DMEM). 192

Figure 8.1. Picture of phosphonium polyesters demonstrating colorless appearance. 211

Figure 8.2 MTT cytotoxicity as a function of polymer concentration after 4 h incubation on HeLa cell viability. 214

Figure 8.3 GFP expression in HeLa cells using TEPAA and poly(TEPAA-co-PEG) segmented copolyester. 215

Figure 10.1 Representative micelle structure formed from ionic associations of surfactant polar headgroups. 223

Figure 10.2. Versatile imidazolium diols with various functionality. 224

List of Tables

Table 2.1. Growth of polymer fibers from 1996 to 2000.[6] 11

Table 2.2. Stereoisomers of starch-modified monomers for polyesters derived from renewable resources. Specific stereoisomers of the monomers determine monomer melting temperatures and final polyester properties.[97] 58

Table 3.1 Two PLGA-PEG-PLGA polymers were synthesized from varying PEG molecular weights and molar ratios of DL-lactide: glycolide. Zentner et al. reported similar molecular weight and PDI from ReGel2 79

Table 3.2 Calcium binding affinity (mean ± standard deviation, *n*=3) of poly(MAA-*g*-EG) compared to C934p and PCP in buffered solution at pH 6.7. 86

Table 4.1. Molecular weight control of poly(CBDO-DMCD) polyols using stoichiometric imbalance. 104

Table 4.2. Molecular weight characterization of poly[(CBDO-DMCD)-*co*-(DEG-DMAp)] copolyesters. 111

Table 5.1. T_g of soft segment sulfonated copolyesters. T_g values are determined from the second heat of a heat/cool/heat experiment 131

Table 6.1. Summary of sodium sulfonated random copolyester compositions and thermal properties. 163

Table 6.2. Summary of thermal properties and flow activation energies for 15 mol% sulfonated copolyesters containing various countercations. The molecular weights of the sulfonated copolyesters are identical. 163

Table 7.1. Absolute molecular weights of butanediol (BD), triethylphosphonium diol (TEP), tributylphosphonium diol (TBP) chain extended polyurethanes (PU) containing various mol% hard segment (HS) content. 180

Table 7.2. Thermal properties of BD, TEP, and TBP chain extended PU containing various mol% HS content. 180

Table 7.3. Summary of SAXS scattering peak position, q, and interdomain spacing, *d*, of noncharged and phosphonium polyurethanes. 188

Table 7.4. Tensile properties of noncharged and phosphonium polyurethanes. 188

Table 8.1 Summary of trialkylphosphonium-containing polyester compositions and thermal properties. 213

List of Schemes

Scheme 2.1. Equilibrium addition-elimination mechanism for polyesterification reactions.[3] 13

Scheme 2.2. Thermal degradation of PET through chain scission and anhydride formation..... 17

Scheme 2.3. Synthesis of polyamides through direct amidation or self-amidation of an amino acid.[11] 20

Scheme 2.4. General reaction between dianhydrides and diamines to form the polyimide through an amic acid intermediate followed by dehydration and cyclization of the amic acid. Note that there are several isomeric possibilities during the amic acid stage leading to increased solubility. However, these isomers are essentially eliminated during the cyclization..... 26

Scheme 2.5. Nucleophilic aromatic substitution mechanism commonly used to synthesize poly(arylene ether sulfones) or poly(arylene ether ketones). 34

Scheme 2.6 Possible side reactions from excess isocyanates during polyurethane polymerization leading to branching or crosslinking. 37

Scheme 2.7. Synthetic scheme for the preparation of segmented polyurethanes using a prepolymer method. 39

Scheme 2.8. Synthesis of epichlorohydrin from glycerol, a byproduct of transesterification from vegetable oil, from Solvay Epicerol™ process. 47

Scheme 2.9. General epoxy resin curing between a diepoxide (functionality (f) = 2) and diamine (f=4). 48

Scheme 2.10. General synthetic strategy for the synthesis of isosorbide from starch.[97, 99] 57

Scheme 3.1 Synthesis of thermo-responsive biodegradable hydrogels from PEG and PLLA..... 76

Scheme 3.2. Synthesis of UV crosslinked CECS/poly(HEMA) with TEGDMA crosslinker..... 85

Scheme 4.1. Synthesis of high-T_g CBDO-containing polyester polyols. 103

Scheme 4.2 Synthesis of poly(CBDO-DMCD)-based segmented copolyesters. 109

Scheme 4.3. Synthesis of low-T_g poly(DEG-DMAp) homopolymer. 110

Scheme 4.4. Synthesis of CBDO-containing non-segmented copolyesters. 110

Scheme 5.1. Synthesis of high-T_g sulfonated poly(sCBDO-DMCD) polyols using melt-transesterification. 128

Scheme 5.2. Synthesis of segmented copolyesters containing sulfonated poly(CBDO-DMCD) hard segments using metal-catalyzed melt transesterification. 129

Scheme 5.3. Synthesis of soft segment sulfonated segmented copolyesters containing poly(CBDO-DMCD) hard segments..... 129

Scheme 6.1. Synthesis of sodium sulfonated random copolyesters..... 162

Scheme 7.1 Synthesis of trialkyl(1,3-dihydroxypropyl)phosphonium bromide..... 177

Scheme 7.2. Synthesis of trialkylphosphonium polyurethanes. 178

Scheme 8.1. Synthesis of trialkylphosphonium diols. 209
Scheme 8.2. Synthesis of poly(trialkylphosphonium succinate) (poly(TAPS)). 210
Scheme 8.3. Melt polycondensation of poly(neopentylglycol succinate) (poly(NPGS)). 212
Scheme 10.1. Synthesis of imidazole diol and alkylation with haloalkanes to afford imidazolium diols 222

Chapter 1: Introduction

1.1 *Dissertation Overview*

Step-growth polymers serve an extremely important role in emerging technologies and biomedical applications. As the scientific community becomes increasingly aware of their role in the outcome of our environment, polymer researchers have acknowledged the importance of polyesters as a green approach for solving many of these ecological concerns.[1-3] Many of the monomers are sustainable, renewable, and derived from non-petrochemical resources such as agricultural feedstock, and the polymer can be composted.[2] Because of the hydrolytic ester linkage within the polymeric backbone, polyesters have found utility in biodegradable products from packaging to biomedical applications and drug delivery devices.[4] Conveniently, the chemical environment surrounding the ester bond, polymer topology, and polymer architecture control the hydrolytic properties of the ester bond.[4-6]

Segmented block copolymers are an important class of polymers that are common in many industrially significant thermoplastic elastomers. One advantage of immiscible block copolymers is that they incorporate the properties of each block to tailor the specific polymer physical properties. Although the advantages of polyester block copolymers are apparent, it is often difficult to control the structural integrity of entirely polyester-based blocks due to the inherent nature of the labile ester bond. In this dissertation, we show that the block sequence control of the segmented copolyesters depends largely on the steric hindrance surrounding the electrophilic carbonyl ester.[7]

Recently, there has been an increasing interest in the rigid cycloaliphatic diol 2,2,4,4-tetramethyl-1,3-cyclobutanediol (CBDO) as a suitable monomer replacement in many bisphenol-A based polycarbonates.[8] The synthesis of entirely polyester-based segmented copolyesters

relies heavily on the sterically hindered CBDO to deter transesterification. In addition, we investigated the role of electrostatic interactions through sulfonation of the hard segment on the thermal, mechanical, and morphological properties of these copolymers. Successful bulk synthesis of polyester-based segmented copolymers introduces a new class of biodegradable and sustainable copolyesters for high performance thermoplastic elastomers to biomedical applications.

Melt transesterification of sulfonated dimethyl isophthalate (sDMI), diethylene glycol (DEG), and dimethyl adipate (DMAp) produced low-T_g ionomers with varying sulfonation levels (1 – 15 mol%). At higher sulfonation molar content near 10 – 15 mol%, the low T_g polymers produced free-standing films. Dynamic mechanical analysis demonstrated an increase in both the polymer terminal flow temperature and rubbery plateau modulus with increasing sulfonation content. Dynamic light scattering (DLS) indicated these polymers formed monodispersed nanoparticles with a hydrodynamic diameter of 10 nm in water. The addition of 0.05 M sodium bromide (NaBr) decreased the nanoparticle's polydispersity presumably due to the salt screening of the polymer electrostatic interactions in solution. The non-aggregated polymer in aqueous solution allowed us to utilize dialysis to exchange the countercation from Na^+ to Li^+, Mg^{2+}, Ca^{2+}, and Zn^{2+}. We investigated the influence of the cationic structure on the polymer thermomechanical properties and water sorption behavior. Dynamic mechanical analysis concluded that the divalent countercations significantly lengthened the breadth of the rubbery plateau modulus up to 180 °C. The results reveal unique property differences that distinguished the monovalent from the divalent cations.

The use of a phosphonium ion instead of an ammonium ion in polymeric vehicles is a relatively new topic in gene delivery. The design inspiration for our phosphonium polyurethanes

and polyesters was based on combining the colloidal stability and noncovalent complexing interactions, such as electrostatics and hydrogen bonding, to generate potentially biodegradable, nontoxic, and efficient delivery vectors.[3, 4] Novel trialkylphosphonium diols containing ethyl, propyl, and butyl substituents were synthesized in quantitative yields. The difunctional primary alcohols afforded equal reactivity and eliminated β-hydrogens for improved thermal stability. Segmented trialkylphosphonium polyurethanes with PEG soft segments effectively bound DNA and remain colloidally stable over 1 d. Cationic polyurethanes possess several desirable advantages including improved microphase separation and mechanical performance for a variety of applications from high performance engineering thermoplastics to novel biomaterials. Polyurethane compositions varied the HS content and alkyl substituent to elucidate their influence on thermomechanical properties and morphology.

The trialkylphosphonium polyesters maintained good coloration and exhibited an increase in their melt viscosity during melt polymerization. Thermal analysis reflected an increase in the T_g with the incorporation of cationic phosphoniums. Nonionic polyesters using the structural analogue, neopentylglycol, demonstrated monomer stoichiometric imbalance and polymerization conditions generated polyesters with controlled molecular weight. Variations in monomer structure and composition tuned the macromolecular architecture to enable structure-property characterization. Depending on the phosphonium diol alkyl substituent length and diacid structure, these polyesters were readily soluble in water. DNA delivery studies of the water-soluble polyesters were investigated.

1.2 *References*

1. Ozturk, G. I.; Pasquale, A. J.; Long, T. E., *The Journal of Adhesion 86* (4), 395-408.
2. Wanamaker, C. L.; O'Leary, L. E.; Lynd, N. A.; Hillmyer, M. A.; Tolman, W. B., *Biomacromolecules* **2007,** *8* (11), 3634-3640.
3. Wanamaker, C. L.; Tolman, W. B.; Hillmyer, M. A., *Biomacromolecules* **2009,** *10* (2), 443-448.
4. Ozturk, G.; Long, T. E., *J. Polym. Sci., Part A: Polym. Chem.* **2009,** *47* (20), 5437-5447.
5. Lin, Q.; Unal, S.; Fornof, A. R.; Armentrout, R. S.; Long, T. E., *Polymer* **2006,** *47* (11), 4085-4093.
6. Unal, S.; Ozturk, G.; Sisson, K.; Long, T. E., *Journal of Polymer Science Part A: Polymer Chemistry* **2008,** *46* (18), 6285-6295.
7. Zhang, M.; Ozturk, G. I.; Long, T. E., *Polym. Prepr. (Am. Chem. Soc., Div. Polym. Chem.)* **2009,** *50* (2), 549-550.
8. Kelsey, D. R.; Scardino, B. M.; Grebowicz, J. S.; Chuah, H. H., *Macromolecules* **2000,** *33* (16), 5810-5818.

Chapter 2: Traditional and Novel Synthetic Approaches in Polyester Step-Growth Polymerization

(From: Zhang, M.; June, S. M.; Long, T. E., 5.02 - Principles of Step-Growth Polymerization (Polycondensation and Polyaddition). In *Polymer Science: A Comprehensive Reference*, Matyjaszewski, K., Ed. Elsevier: Amsterdam, 2012; pp 7-47.)

2.1 *Abstract*

Step-growth polymerization enables future technologies and molecular design of diverse macromolecular architectures ranging from tailored long-chain branching to segmented block copolymers. Scientists and engineers continue to advance the traditional families of step-growth polymers with novel synthetic strategies, unique processing scenarios, and tailored interfaces. Many step-growth polymers impart sustainability into emerging technologies, including bio-derived monomers and biodegradable compositions. New reaction pathways including Michael addition reactions, ionene polyelectrolytes, and click modification strategies have re-energized this field. This chapter focuses on the structure-property-performance relationships that continue to advance macromolecular science and engineering.

2.2 *Introduction and Historical Perspective*

Since Wallace Carothers's early discoveries of polyesters and polyamides, with the many implications of the resulting Carothers's equation, the impact of engineering thermoplastics has continued to expand as new technologies demand high performance macromolecular architectures. In his pioneering work from 1929, Carothers described a vision for polycondensation that expressed the requirement for reactive monomeric functional groups to form a new bond through the elimination of a small molecule or condensate.[1, 2] The early work explored the reversible nature of polycondensation reactions and strategies to circumvent the strict requirements for successful step-growth polymerizations. Unlike conventional free-radical polymerization, early polycondensation polymers were reversible and susceptible to hydrolysis, which was an obstacle for obtaining high molecular weight polymers. In addition, Carothers acknowledged various types of polymer topologies through the alteration of monomer functionality.[2]

Eighty years after Carothers's early work, step-growth polymerization has emerged as a commercially viable approach for designing tailored polymers for a variety of applications. Although early interests in step-growth polymers were directed towards alternatives to vinyl-based polymers for commercial purposes, the unique advantages of step-growth polymers became increasingly apparent. For example, properties such as toughness, stiffness, and thermal stability were markedly improved compared to early free-radically derived polymers.[3] The versatility of these polymers advanced step-growth polymers into new industries, and this theme of expanding relevance to a variety of applications is still readily apparent today. This chapter outlines many synthetic methods for step-growth polymers and transitions to rapidly evolving applications in other disciplines. For example, step-growth polymers play an important role in biomedical applications due to their tunability and ability to modify mechanical, thermal, and

drug delivery properties compared to conventional small molecule drugs. It is remarkable that in a little over 50 years, step-growth polymerization has truly emerged as an interdisciplinary field of study.

The application of step-growth polymers could not have achieved such significance without an understanding of the synthetic principles that enables controlled and predictable morphological and mechanical properties of polymers. One unique advantage of step-growth polymerization is the ability to tailor the monomer choice, which directly affects the polymer backbone unlike many conventional free-radical polymers that have a non-functional hydrocarbon backbone. The development of novel monomers reenergized research interests and provided a new molecular handle to combine centered on the fundamental understanding of structure-property-morphology relationships to improve and tailor polymer performance. The ability to design the polymer backbone allows for control of mechanical, thermal, and flexibility of the polymer chain. In addition, multifunctional monomers can be designed to create diverse polymer topology. The understanding of polymer chemical composition and topology promotes morphology control, which relates to various desirable polymer properties such as enhanced mechanical and thermal properties. Polymer research has engaged in an increasing interest towards creating sophisticated, versatile, and multifunctional polymers, which offer "smart" capabilities such as dynamic assembly, stimuli-responsive, self-healing, and remendable properties.

In addition to creating polymers with tailored physical properties, polymer scientists are becoming increasingly aware of their contribution and responsibility to ameliorate environmental issues. Because step-growth polymers have expanded into various disciplines, global issues, such as diminishing natural resources, human disease, energy crisis, water purification, and

climate change, have all been unavoidable concerns which polymer chemists and engineers have been trying to solve. Thus, many of the research efforts have been redirected to some of the first polycondensation polymers that Wallace Carothers studied in 1929, i.e., polyesters.[4, 5] The revival of polyester synthesis interest stems mainly from the need to transition away from petroleum derived monomers and towards renewable resources. In addition, green chemistry promotes research in novel synthetic approaches such as enzyme-catalysis, solvent-free, and no byproduct polymerizations. The hydrolytically labile ester linkage allows polyesters to find applications not only in recyclable packaging, but also in biodegradable drug delivery devices and biomaterials.

This chapter focuses on the recent advances in the field of step-growth polymers and describes the basic principles first outlined by Wallace Carothers. Various polymer architectures are achieved through step-growth polymerization, and several examples of traditional classes of polycondensation and polyaddition polymers with novel applications will be reviewed. Applications of new chemistries, such as ionene synthesis, click chemistry, and Michael addition, expand the class of step-growth polymerizations. Finally, this chapter will explore synthetic strategies, such as enzyme-catalyzed and living polycondensation polymerization, that have been developed to circumvent challenges present in step-growth polymerization. Future directions for step-growth polymers feature new synthetic approaches that demonstrate the remarkable progress and discovery in step-growth polymerization since the time of Wallace Carothers.

2.3 *Synthesis of Step-Growth Polymers*

Step-growth polymerization occurs in "steps" to form new chemical bonds as described earlier in this chapter. There are two types of step-growth polymerization processes: polycondensation and polyaddition. Both classes of polymerizations proceed in the same fashion

of monomer to dimer to tetramer and high molecular weight polymer. The differences in the two classes of step-growth polymers as well as examples of these polymers are described in the following sections.

2.3.1 Polycondensation Polymers

Polycondensation polymers are a class of step-growth polymers in which the formation of a new functional group results in the elimination of a small molecule byproduct. Classical examples of polycondensation polymers include polyesters, polyamides, polyimides, and poly(arylene ethers). These polymers utilize organic reactions such as addition-elimination chemistry to afford polymers with specific functional linkages. The resulting polymer linkages provide properties such hydrolyzability, hydrogen-bonding interactions, and dipolar interactions. Careful monomer selection and polymer topology further tailor the mechanical properties of these polymers. The immense amount of established research demonstrates the expanding impact of polycondensation polymers in commercial industry.

2.3.1.1 Polyesters

Within the last 20 years, the number of polyester plant industries in Europe, USA, and Japan have grown and promoted the growth of polyester production to an estimated 3 billion pounds a year.[6] Because of the substantial growth of polyester plants now developing in China, it was estimated that in 2010, polyester production will surpass 100 billion pounds a year. China, itself, contributed 80% of the new polyester plants recently developed.[6] In the field of synthetic fibers, polyesters dominated the total amount of polymer-based fibers within the last decade.

Table 2.1 summarizes the contribution of common polymers in the fiber industry.[6] Interestingly, polyester fibers contributed to nearly 60% of all fiber production in 2000. This trend emphasized the importance of this polymer within economically important fiber production. PET fibers afforded approximately 45% of all PET produced.[7] Because of chain stiffness and crystallinity, PET fibers demonstrated excellent tensile properties, solvent resistance, toughness and fatigue resistance.[7] Solid-state resins accounts for the second largest application of PET. The demand for cheap packaging and bottles has become the main contributors for the demand for PET development.

Polyesters, most notably poly(ethylene terephthalate) (PET), also assume an important role in the food packaging industry. The large scale production of PET provided the packaging industry with cheaper production costs. PET films are often bi-axially stretched in order to induce crystallization. Interestingly, these films are optically clear although the film is nearly 50% crystalline.[3] In addition, these polymers possess mechanical properties capable of withstanding the large pressures of carbonated drinks. It is estimated that the polyester food packaging industry constitutes a significant amount of the overall polymeric applications. As these industries continue to expand, the demand for affordable and more environmentally-friendly polyesters with tailored properties will stimulate and influence the future research within this growing field.

Table 2.1. Growth of polymer fibers from 1996 to 2000.[6]

Fibers	Production (/10^{-8} kg)			Percent increase from 1999
	1996	1998	2000	
Polyester				
thread	60.1	93.4	98.0	6.2
staple fiber	50.8	68.9	73.4	
Polyamide				
thread	29	30.8	32.6	6.4
staple fiber	5.4	4.5	4.5	
Polypropylene				
thread	18.1	24.5	25.4*	5
staple fiber				
Polyacrylic	21.8	21.8	22.7	5.6
Cellulose	27.2	23.6	24.5	0.4
Other	0.9	1.8	1.8**	—
Total	215.0	269.4	283.9	3.5

* Including 10.0-13.6×10^{8} kg of polypropylene fibers.[6]
** Including 5.4×10^{7} kg of aramid and carbon fibers.[6]

One method that enables simple modification of polyester properties relates to the monomer selection. The discovery of new monomers promotes the continuing growth of applications for this field. Polyesters have emerged as an economically important commercial commodity and have found utility in a variety of applications including fibers, thermoplastic elastomers, coatings, and high performance polymers due to their outstanding mechanical and thermal properties.[3] Polyesters are polymers with ester linkages within the backbone. These ester linkages are hydrolytically unstable, and this attribute has launched a growing field of biodegradable polyester research from recyclable polymers for packaging to drug delivery vehicles with degradable and controllable drug delivery.[8-10] In addition to their degradation properties, polyesters also employ monomers derived from renewable resources. Over the years, polyesters continue to possess desirable advantages such as tunable properties for the packaging and fiber industries.

There is current interest within the industry to limit its dependency on nonrenewable petroleum derived monomers, and research is directed towards monomers derived from renewable resources. The research often involves new catalysts or simple methods to transform plant-based starches to useful diols. Typically, the cost of monomer becomes the limiting factor in polyester synthesis, and often a consideration between properties and cost of production becomes crucial for commercial polyesters. For example, exchanging ethylene glycol (EG) for longer glycols such as 1,4-butanediol (BD) increases crystallization rate and allows for faster production; however, the cost of production for PET is much less compared to poly(butylene terephthalate) PBT.[3]

Another recent interest centers around cardo-monomers for their application in novel aromatic polyesters.[11] Cardo monomers are monomers that contain looped or cyclic structures. Research literature suggested introducing these bulky groups into polyesters will increase free volume, chain stiffness, and enhance solubility. Successful high molecular weight cardo monomer-containing polyester employed phase-transfer-catalyzed interfacial polycondensation. Addition of the bulky group from the cardo diol substantially increased both the T_g's ranging from 207 – 287 °C.[11] Although the properties of the polyesters showed promise for thermoplastics, the challenging synthesis of the cardo diol limits its application in the field.

Scheme 2.1 illustrates the main mechanistic pathway in which polyester synthesis proceeds. Typically, a strong nucleophile such as an alcohol attacks an activated carbonyl such as a carboxylic acid or acyl halide to form the tetrahedral intermediate. Upon elimination of the condensate X-Y, the new ester linkage is formed. The entire reaction proceeds through an equilibrium mechanism. Various leaving groups and nucleophiles are summarized within Error!

Reference source not found. as well. The reaction conditions as well as the cost of monomer dictate the choice of monomer.

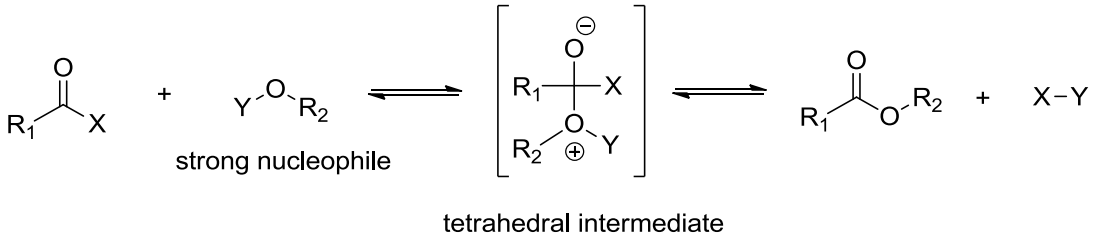

Direct Esterification: X = OH, Y = H
Alcoholysis: X = OR_3, Y = H
Acidolysis: X = OH, Y = R_4CO
Transesterification: X = OR_3, Y = R_4CO
Acyl chloride - Hydroxy: X = Cl, Y = H
Anhydride - Hydroxy: X = R_3COO, Y = H

Scheme 2.1. Equilibrium addition-elimination mechanism for polyesterification reactions.[3]

Understanding the principles of the equilibrium addition-elimination reaction for polyesterification becomes crucial to attain high molecular weight polymers. According to Error! Reference source not found., the forward reaction produces an ester functional group and a condensate byproduct. Conversely, the reverse reaction hydrolyzes the ester bond when the condensate or simply water is present and translates to depolymerization. Because the species within step-growth reactions are dynamic throughout the extent of the reaction, the equilibrium favors the reverse reaction or depolymerization as the polymerization proceeds forward due to higher concentration of the condensate.[2, 12] In order to address this concern, many polyester syntheses are conducted in the melt phase at elevated temperatures well above the boiling point of the byproduct or condensate and removal of the condensate drives the reaction towards polymerization.

Melt polymerization represents a common synthetic approach for many step-growth polymers such as polyesters. Temperature ranges for bulk polymerization must be at least 10-

20 °C above the melting point of the polymer. However, because many bulk polymerization occurs at high temperatures 150 – 350 °C, careful consideration must be paid in order to limit the effects of side reaction such thermooxidation.[13] Bulk reactions are therefore conducted under an inert atmosphere. As the reaction proceeds from monomer to oligomer to polymer, the role of chain entanglement begins to dominate the melt reaction through the form of higher melt viscosity. The following equation describes the relationship between melt viscosity (η_o) and molecular weight (M) using a power relationship that was first described by Fox and Flory in 1951:[14]

$$\eta_0 \propto M^{3.4}$$

This equation suggests that a gradual increase in molecular weight results in a large increase in melt viscosity.

The melt viscosity plays a direct role in the molecular weight control of any step-growth bulk polymerization. A common misconception in melt step-growth polymerization is that the kinetics of step-growth polymerization within the melt decreases with time due to the change in reactivity of end groups.[1, 2, 15] In reality, the reactivity of the end groups does not change with polymerization extent, because reactivity of functional groups is directly related to the collision position, energy, and frequency of the reactive groups. The more accurate reason for the differences in step-growth polymerization kinetics is attributed to the dynamics of the reactive species. As the reaction proceeds from monomers to oligomers to polymers, the rate of diffusion for each of these species changes dramatically. Monomers will diffuse through the melt much faster than oligomers or polymers due to chain entanglements. For this reason, the accessibility of the oligomers and polymer end groups will be less than that of the monomer, and thus, reaction kinetics during step-growth polymerization will not remain constant.

In addition to melt viscosity effects, the removal of the condensate and of low molecular weight byproducts also becomes essential for accelerating the reaction and increasing molecular weight. Various techniques ameliorate these issues such as purging the system with nitrogen gas to facilitate removal of the condensate. In addition, vigorous stirring will also promote diffusion of the reactive end groups and removal of the condensate. High vacuum is applied to the final stages of bulk polymerizations to attain high molecular weight. Because of the reaction mechanism of step-growth polymerization, high molecular weight of polycondensation polymers will not occur until high conversion of polymerization occurs.

Due to these reasons, step-growth reactions require long reaction times and catalysts to increase reaction rates. For example, synthesis of polyesters with aromatic carboxylic acids and glycols utilizes metal glycolates through high ligand exchanges.[16] The rate constant of the reaction depends much on the pK_a of the carboxylic acid as well as the sterics and the electronic contributions of the aromatic ring. Typical polyester polycondensation catalyst employed are metal alkylates such as tin, antimony, and titanium. These catalysts are sensitive to hydroxyl or carboxylic acid groups.[3] Metal alkylates form metal alcoholate complexes to facilitate ligand exchange. In contrast, Lewis acid catalysts, such as zinc or manganese, coordinate with the carbonyl oxygen of the ester to increase nucleophilicity of the carbonyl compound.

Consideration for side reactions within bulk polymerizations must be taken. Short chain oligomers contribute to nearly 2-3% of the polymer produced. Cyclic oligomers are often dependent on the monomers chosen. Cyclization occurs at any time of the polymerization process because step-growth polymerization allows for reaction of any accessible end group.[17] The reaction temperature strongly influences cyclization reactions, and, as a result, the decrease in end group concentrations severely affects the polymer molecular weight.[16] Other side

reactions which may occur at elevated temperature include the etherification of EG to form diethylene glycol or dioxane byproducts through dehydration. In many cases, simple modifications in catalyst choice from metal acids such as zinc, lead, and manganese acetates can prevent side reactions such as etherification.[16] Other side reactions occur via chain scission due to thermal degradation of the ester bond. **Scheme 2.2** below represents an example of polyester chain scission to produce the alkene-terminated oligomer which is subject to nucleophilic attack by the carboxylic acid. This side reaction causes defects within the polymer. Elimination of acetaldehyde also occurs and influences packaging applications. Substantial yellowing of the polymer also results as a consequence of thermal or oxidative degradation. Selecting an appropriate catalyst, removing oxygen from the reaction, providing an inert atmosphere, and reducing reaction temperatures are practical approaches to avoid side reactions.

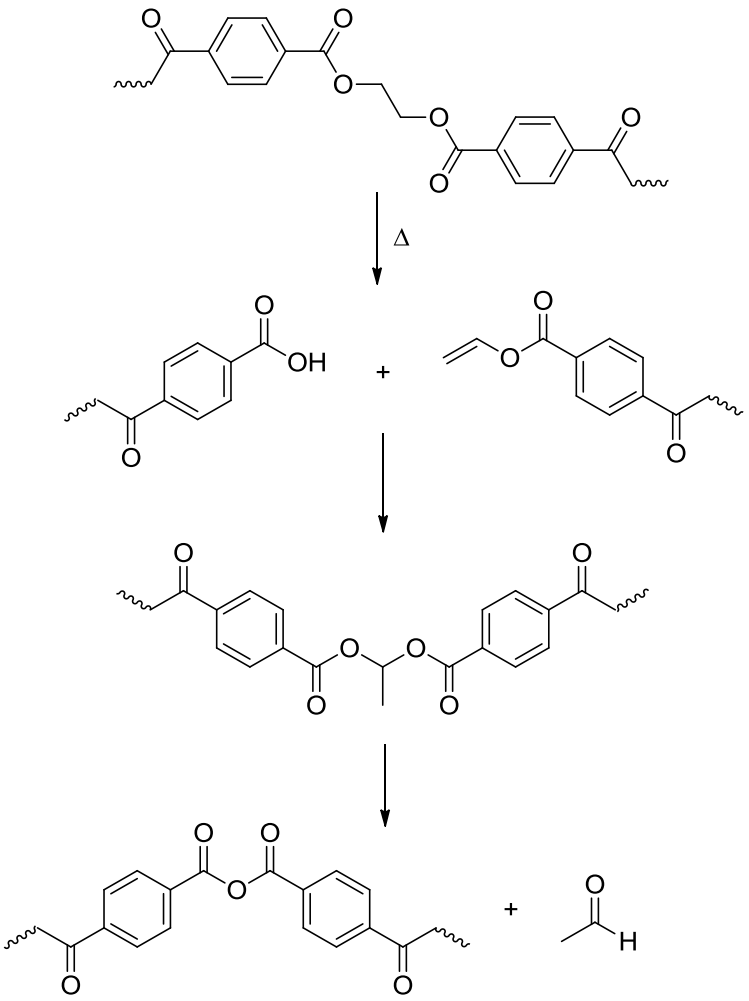

Scheme 2.2. Thermal degradation of PET through chain scission and anhydride formation.

Economically significant polyesters have principally focused on aliphatic-aromatic polyesters derived from diols with alkylene oxide units and diesters with terephthalate or isothalate units. PET dominates the commercial plastics application in fibers, molding resins, and film formation for packaging applications. Early development and commercialization of PET encountered difficulties, because the terephthalic acid (TA) used could not be obtained in high purity. However, this obstacle was solved through the use of the diester monomer, dimethyl terephthalate (DMT). PET possessed several advantages. Melt polymerization eliminated the use of volatile solvents, greatly reduced production costs, and simplified purification steps. In

addition, the ability to drive the reaction to high conversions through distillation of the diol monomer to facilitate polymerization and transesterification circumvented the strict requirement of 1:1 monomer stoichiometry in conventional step-growth polymerization. Thus, the 1:1 stoichiometry so vital for attaining high molecular weight polymers was not a necessity and an excess of diol monomer is commonly used to increase the formation of EG endcapped DMT. However, the removal of excess EG at the second stage using reduced pressure essentially approaches 1:1 stoichiometry.

Synthesis of PET occurs through two stages with the aid of metal acetate catalysts such as calcium, manganese, cobalt, and zinc. The first stage occurs at 190-195 °C, below the boiling point of EG, 197 °C, and above the melting point of DMT, 140-142 °C. At this point, the high reaction temperature facilitates methanol distillation and drives the reaction forward. Bis(2-hydroxyethyl) terephthalate and oligomers are formed during this initial stage. In the second stage, a step-wise increase in reaction temperature from 190 – 280 °C and reduced pressure during the last hour of the reaction increase the reaction rate and continue polymerization through transesterification and removal of EG. The final temperature of 280 °C maintains melt homogeneity. As the reaction proceeds, the molecular weight of PET increases, and crystallization occurs within the melt if the reaction temperature is not above the melting temperature of PET, 265 °C. Melt heterogeneity results in large polydispersities, because polymeric chains within crystals are inaccessible for ester-interchange. Catalysts are employed to facilitate the reaction. Metal-acetates catalyzes the first stage of the reaction, and antimony(III) oxide is often added during the second stage of the reaction to continue condensation.

In addition to melt polymerization, polyesters can be synthesized through interfacial condensation. One advantage of this method is that 1:1 stoichiometry is not required to acquire

high molecular weight, because polymerization occurs at the solvent interface. In addition, polymerization occurs rapidly and is only limited to the diffusion of monomers at the solvent interface. Synthesis of polyesters using this approach occurs through a reaction between an acyl halide and glycol in two immiscible solvents. Each solvent contains one of the reactive monomers and polymers can be isolated as a film or a filament through drawing the polymer from the interface. Interfacial polymerization can be quite advantageous for polymers which are unstable at high temperatures and have been used for the synthesis of polyesters, polyamides, polyurethanes, and polysulfonamides.[18] However, the use of solvent, monomer expense, and acidic byproduct are often undesirable in large scale production of polymers.

2.3.1.2 Polyamides

Polyamides contain amide functional groups within the polymer backbone. The unique properties of polyamides arise from the hydrogen-bonding capabilities of the amide functional group. These strong intermolecular interactions afford high melting and thermally stable polymers with excellent mechanical properties. **Scheme 2.3** below illustrates the synthesis of polyamides through two methods: direct amidation and self-amidation. Direct amidation utilizes two difunctional monomers, A-A and B-B, to form the new amide bond. Self-amidation are A-B type monomers from amino acid derivatives. Again, stoichiometric balance of the functional group in a 1:1 stoichiometry is a requirement for the synthesis of high molecular weight polymerization. In direct amidation, careful control of monomer stoichiometry is a necessity. For self-amidation, the bifunctional monomer achieves 1:1 stoichiometry. In both cases, however, monomer purity is required. Careful consideration must be taken to prevent side reactions which may limit the molecular weights of polyamides. Side reactions such as oligomeric cyclization occur with diamines containing less than four methylene units.

Decarboxylation is also a concern for lower diacid monomers. In addition, pressurized systems prevent the escape of volatile cyclic oligomers.

Direct Amidation (A-A + B-B):

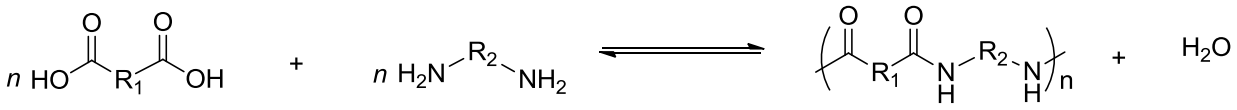

Self-amidation (A-B):

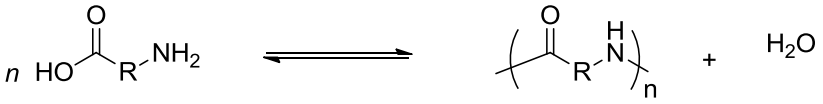

Scheme 2.3. Synthesis of polyamides through direct amidation or self-amidation of an amino acid.[11]

Many polyamides employ the salt solution method. Nylon-6,6 can be polymerized using this approach without addition of a catalyst. The salt solution method proceeds in three stages. In the first stage, the reaction between hexamethylene diamine and adipic acid forms the salt in solution. Conveniently, this method is quite exothermic, and the reaction proceeds through the precipitation of the salt from solution. On the industrial scale, a watery salt slurry were used directly for the second stage of the polymerization process. This method also provides the added advantage of a 1:1 stoichiometry inherent in AA-BB type monomers arising from the carboxylate and protonated amine during salt formation.

In the second stage, the salt further reacts under pressure and heat to form the prepolymer. Polymerization occurs under pressure, because the volatilization of hexamethylene diamine, which boils at 205 °C, will result in a loss of this monomer in the reaction and cause a stoichiometric imbalance of the functional groups. This stage can be achieved through an

autoclaving procedure and step-wise increase in temperature from 210 – 290 °C. The prepolymer formed during this event will typically be semicrystalline; however, further reaction is needed to remove the condensate, water, and drive the reaction forward. As the reaction continues and the polyamide chains grow, the melt viscosity increases, and melt-polymerization becomes difficult.

Because of the high melting temperatures of polyamides, prepolymers are typically reacted within melt extruders where solid-state polymerization occurs at atmospheric pressure and 290 °C. Further orientation of polymer chains through processing techniques induces higher degrees of crystallinity. Although one could imagine applying melt reaction conditions used in polyester synthesis to polyamide polymerization, such as elevating temperatures and reducing pressure to drive the reaction forward, however, several concerns prevent this polymerization technique and solid-state polymerization at atmospheric pressures are employed instead. At high reaction temperatures and reduced pressures, aliphatic polyamides undergo side-reactions that cause branching and substantial coloring of the polymer.

Control of polymer architecture allows for design of applications including drug delivery, molecular imaging, electroactive devices, and membrane technology. The growing field of polymer drug delivery takes advantage of the ability to design and regulate the delivery of drugs through controlled and predictable manners. Another advantage of polyamides arises from their similarity to naturally occurring polymers, namely polypeptides. Incorporation of amino acids as biobased monomers has become increasingly popular in the field of biomedicine due to their inherent biocompatibility and extensive monomer selection.

Wathier et al. described the synthesis of dendritic macromolecules from peptide monomers.[19] The advantages of the high surface functionalization and branching density from

dendrimers were needed for sufficient crosslinking reactions for forming wound-healing hydrogels. Dendrimers derived from lysine and cysteine with varying branch density were synthesized and crosslinked with poly(ethylene glycol dialdehyde) to form thiazolidine linkages. This reaction occurred quickly and spontaneously at relatively neutral pH (7.4) upon mixing the two solutions. Dynamic mechanical analysis revealed an increase in modulus with increasing dendron density. Due to the mild conditions and fast in-situ crosslinking of the hydrogel, this technique of crosslinking peptide-derived dendrons through the formation of thiazolidine linkages affords a facile and safe method for wound-healing sutures (**Figure 2.1**).

Figure 2.1. Peptide dendritic monomers derived from amino acids produced a fast curing hydrogel for sealant-repaired corneal incisions.[74]

In contrast to the linear aliphatic polyamides described above, there have been interests in the synthesis of aromatic polyamides (aramid). Garcia et al. recently reviewed the advances in aramids research.[20] The significant properties which arise from the stiffness of the polymer chains and high directionality from the anisotropic liquid crystalline solution pioneered the technologies for engineering commercial aramids. These properties provided excellent high thermal and mechanical properties that give rise to their outstanding tensile, mechanical, and

flame resistant properties.[20] Many aromatic polyamides can be directly spun into fibers from the polymer solution due to the alignment of the stiff polymer chains from the extended chain conformations in solution. Recent advances in aramid technologies have allowed aromatic polyamides to find application in membrane technologies and electroactive and optically active devices. Further developments in the area of aromatic polyamides aim to advance these high performance polymers and improve their outstanding mechanical properties.

There are currently two main methods for synthesizing aramids: low-temperature solution methods and high-temperature solution methods. Later developments in the synthesis of poly(*p*-phenylene terephthalate) (PPPT) replaced hexamethylphosphoramide (HMPA) with polar solvents such as *N*-methyl-2-pyrrolidone (NMP), *N*,*N*-dimethylformamide (DMF), and *N*,*N*-dimethylacetamide (DMAC) with calcium chloride to aid in disrupting the strong hydrogen bonds. Under the principles of step-growth polymerization, the requirement for extremely high monomer purity remains an obstacle in polyaramide synthesis. Molecular weight considerations are confronted during the synthesis of polyaramides. Polydispersity of approximately 2.0 results from low molecular weight aramide oligomers. The polydispersity reaches close to 3.0 when high molecular weight polymer is attained.

Research interests in aromatic polyamides currently focus on creating synthetic methods to attain soluble polyaramides. Due to the high degree of crystallinity, polyaramides are difficult to melt-extrude or redissolve for solution casting which limits their versatility in applications. Therefore, incorporating new monomers, which increase chain flexibility, disrupt chain regularity, decrease the hydrogen-bonding intermolecular interactions, and increase polymer solubility in solvents such as DMF, NMP, and dimethyl sulfoxide (DMSO). Typical

polymerization of polyaramides utilizes the acyl chloride method due to the reduced basicity of aromatic diamines.

2.3.1.3 Polyimides

Incorporation of heterocyclic and aromatic units within the polymer backbone provided excellent thermal stability and mechanical properties. Aramids and PET were two types of aromatic polymers that displayed desirable properties with high melting temperatures. These polymers were synthesized using aromatic monomers, and high molecular weight polymers were difficult to reprocess due to thermal degradation and high processing temperatures. The main demand for aromatic or heterocyclic polymers with low processing temperatures stemmed from the aerospace industry which required adhesive or polymer-composite formulations with high thermal stability and optimal mechanical properties under harsh environments.[3, 21, 22] Polyimides currently find application in a variety of technologies. In addition to high performance resins, structural foams, and molecular composites, polyimides are utilized in electronics and microelectronics devices. Polyimides elicited interest in membrane technologies specifically for gas separation and fuel cell applications. Because of their ease of processing, ability to acquire high thermal stability, and naturally high free-volume properties, the field of polyimide research continues to expand even today.

Polyimides were the first known polycondensation polymers in which the aromatic or heterocyclic units were formed during polymerization. Cyclization of the monomers was the method of incorporating cyclic groups into the polymer backbone rather than the addition of aromatic or cyclic monomers. **Figure 2.2** below illustrates a general formula for the structure of polyimides where "R" groups are aromatic or aliphatic units. A demand for low processing

temperatures and high thermal stability launched the first investigation involving endcapped low molecular weight oligomers with maleimide.[22, 23] Because of the low molecular weight, these oligomers had low melting and flow temperatures which allowed them to be easily processed.

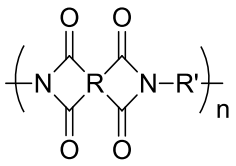

Figure 2.2. General structure for polyimides.

Scheme 2.4. illustrates the synthesis of polyimides between a dianhydride and a diamine. The anhydride ring-opening reaction results in the intermediate amic acid structure. Due to the various isomers achieved in the amic acid form, the polymer remains soluble and processible. Upon reaction between the carboxylic acid and amide to eliminate water and create the cyclic imide functional group, the polymer loses these structural isomers, and the polymer becomes insoluble. A list of common aliphatic and aromatic dianhydride and diamines are shown in **Figure 2.3.** and **Figure 2.4**. The high melting temperature of the resulting polymer further complicates the synthesis of aromatic polyimides. Thus, aromatic polyimides are commonly synthesized in polar aprotic solvents such as DMF, DMAC, and NMP at low reaction temperatures to acquire the amic acid. The amic acid form of the polymer is still processible and soluble in solvent; however, the aromatic polyimide is insoluble. Further heating of the polymer cyclodehydrates the amic acid to form the imide bond.

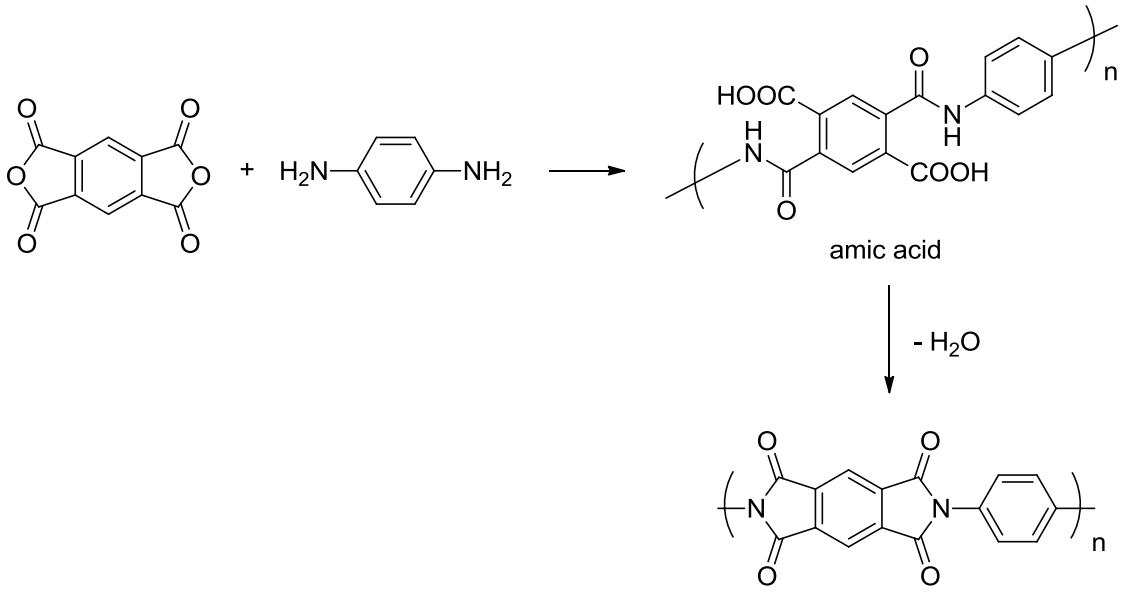

Scheme 2.4. General reaction between dianhydrides and diamines to form the polyimide through an amic acid intermediate followed by dehydration and cyclization of the amic acid. Note that there are several isomeric possibilities during the amic acid stage leading to increased solubility. However, these isomers are essentially eliminated during the cyclization.

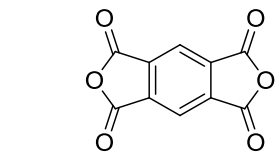

pyromellitic dianhydride (PMDA)

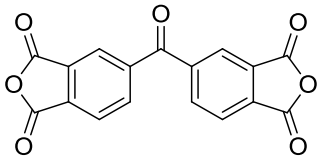

3,3',4,4'-Benzophenonetetracarboxylic dianhydride (BTDA)

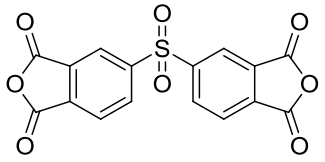

3,3',4,4'-Diphenylsulfonetetracarboxylic dianhydride (DSDA)

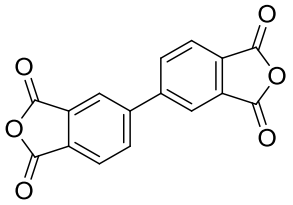

3,3',4,4'-Biphenyltetracarboxylic dianhydride (BPDA)

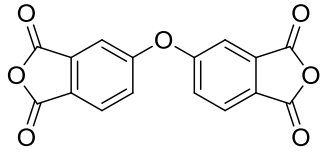

4,4'-Oxydiphthalic anhydride (ODPA)

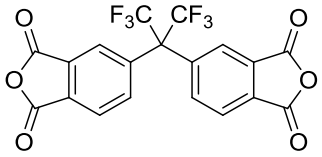

2,2'-Bis(3,4-dicarboxyphenyl) hexafluoropropane dianhydride (6FDA)

Figure 2.3. Chemical structures of commonly used dianhydrides for polyimide synthesis.

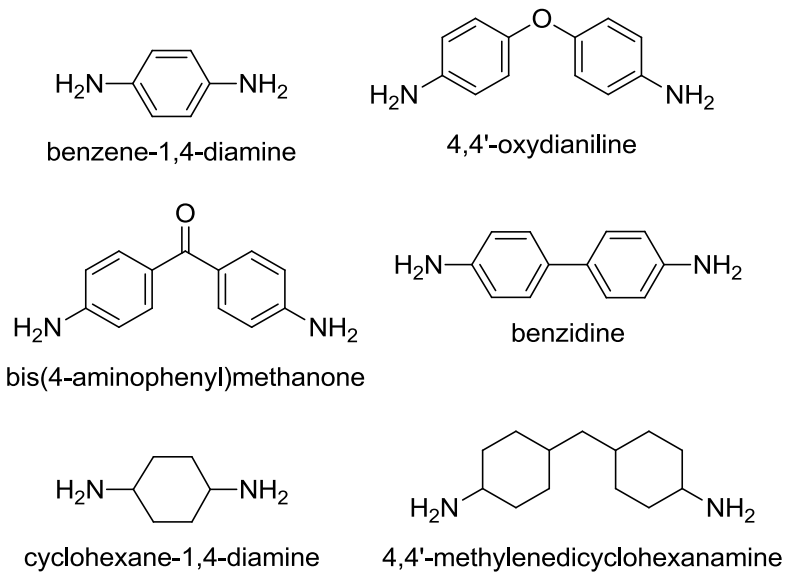

Figure 2.4. Chemical structures of common diamines used in polyimide synthesis.

Similar to many step-growth polymerizations, polyimide synthesis also follows a nucleophilic addition-elimination mechanism in which each reaction step is in equilibrium. Thus, the forward reaction encourages the formation of the polymer, and the reverse reaction favors depolymerization. Polyimide syntheses are condensation reactions, and the condensate, water, must be removed from the reaction during the cyclization step to prevent undesirable low molecular weight polymer. In addition, the reaction in solution is further complicated, and imide bond formation actually requires two mechanistic steps. The first step involves the ring opening of the dianhydride through a nucleophilic substitution reaction and elimination of the carboxylic acid. In this case, the carboxylic acid equates to the condensate which is covalently attached to the polymer to form the amic acid. Therefore, this equilibrium process cannot be driven through the elimination of the condensate. However, this first step is conveniently exothermic due to ring-opening, and the reaction temperature controls the kinetics. Increasing the temperature will favor lower molecular weight polyimides while cooling the reaction favors higher molecular weight polymers.

Because the reaction is in equilibrium, reaction conditions such as monomer reactivity, solvent polarity, and temperature strongly influence polyimide synthesis.[24] Reaction rates increase as the basicity of the diamines increases. However, if the basicity of the diamines is adequate, lowering the temperature of the reaction will not greatly affect the reaction kinetics.[25, 26] In addition to reaction temperature and monomer reactivity, solvent polarity also played a large role in the reaction kinetics.[27, 28] Polar aprotic solvents increase reaction rates due to hydrogen-bonding polymer-solvent complexation and stabilization of the amic acid. In the second step, tertiary alkyl amines or aromatic pyridines catalyze the thermal imidization.

During the synthesis of polyimides, dry conditions must be obtained to eliminate possible side reactions, such as hydrolysis of the dianhydride to form the dicarboxylic acid. In addition, water enhances the reverse reaction through hydrolysis of the amic acid to produce the dicarboxylic acid and the amine. Interestingly, the polydispersity of the polyamic acid increases, reaches a maximum, and slowly decreases with time due to the reverse reaction.[22] This effect can be seen directly with the increase and subsequent decrease in solution viscosity. Another complication that arises during the polyimide synthesis is the phase separation reaction during thermal imidization condensation second step. Phase separation of the polyimide from the poly(amic acid) prevents a homogenous polymerization.

Melt polymerization and solution polymerization of polyimides have been described.[3, 22, 29] Melt polymerization of tetracarboxylic acid and diamines occur much in the same way as polyamides through an initial low molecular weight salt formation from low heating at 110 – 138 °C.[24] Upon an increase in temperature to 250 – 300 °C for several hours, the reaction condenses water and the imide functional group is formed. The main drawback for this approach centers on the requirement for the reaction temperature to be above the highest thermal transition

temperature of the polyimide. The nucleophilicity of the diamine also plays a large role in the melt polymerization of polyimides. Aromatic diamines are not basic enough to form the salt with carboxylic acid. Thus, only aliphatic diamines containing at least 7 methylene units are used to form high molecular weight polyimides. The addition of flexible ether linkages incorporated through the dianhydride monomer reduced polyimide melting temperatures.

Polyimides find application in electronic devices and membrane technologies. Fasel et al. recently described the condensation reaction of sub-nanometer thick linear and crosslinked polyimide films through thermal annealing of 4,4'-diamino-*p*-terphenyl (DAPT) or 2,4,6-tris(4-aminophenyl)-1,3,5-triazine (TAPT), with 3,4,9,10-perylenetetracarboxylic-dianhydride (PTCDA) on Au(111) crystals (**Figure 2.5.a**)[30] Interestingly, the researchers found that monomer deposition formed planar, organized supramolecular monolayers upon the substrate. **Figure 2.5.b** reflects the organization of the hydrogen bonded DATP-PTCDA suprastructure using scanning tunneling microscopy (STM). Upon thermal annealing at 267 °C, the reaction formed imprinted parallel polyimides strands, which pre-organized through the hydrogen bonding of the monomers as seen in **Figure 2.5.c.**

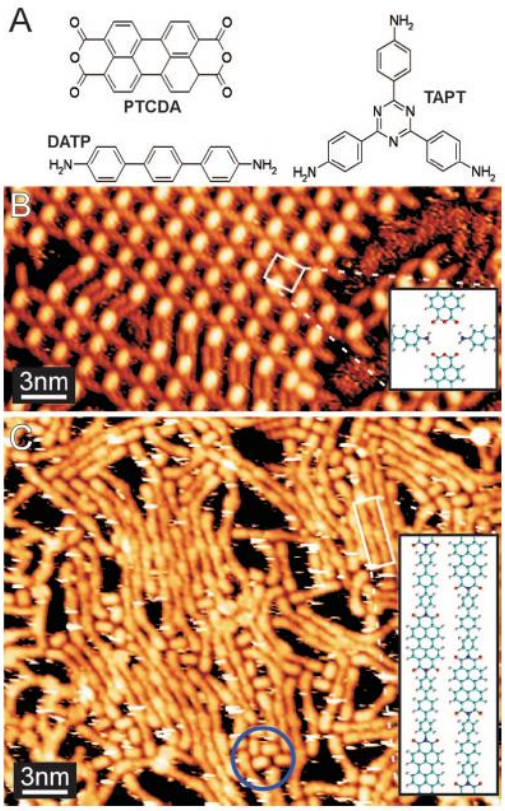

Figure 2.5. Sub-nanometer ultrathin polyimide films on Au(111) substrates. a) Monomers used in polyimide formation. b) Hydrogen-bonded planar sheets of monomers prior to annealing. White boxed area indicates the hydrogen bonded structure between the PTCDA and DATP. c) Polyimide ultrathin film through the annealing of the hydrogen bonded monomers. Blue circled area highlights unreacted DATP and PTCDA monomers. White boxed area shows parallel polyimide strands after thermal imidization.[30]

Further investigation using STM with triamine monomers indicated a porous network structure rather than parallel polymer strands. The authors concluded ultrathin polyimides films were deposited onto Au(111) substrates to form pre-organized suprastructures through the hydrogen-bonding interaction between the dianhydride and diamines. Upon thermal annealing, STM images revealed ordered polyimide strands when diamines (DATP) and dianhydrides (PTCDA) were reacted due to the preorganization of the monomers. Reaction of the triamine (TAPT) with the dianhydride (PTCDA) displayed a different porous network structure after

thermal imidization. This method proved promising as a facile and controllable approach to synthesize thin polyimide films containing specific morphological structures.

In addition to relevance in the electronics field, polyimides are gaining attention in the area of fuel cell applications. Watanabe et al. recently demonstrated durable aliphatic and aromatic polyimide ionomers were suitable for electrolyte membranes.[31] Synthesis of sulfonated polyimides produced highly conductive clear ductile polymer films (0.18 S cm^{-1}) which surpassed Nafion®, the standard benchmark for fuel cell membranes, at 140 °C and 100% relative humidity. These sulfonated polyimide ionomers possessed excellent thermal and oxidative stability. Furthermore, scanning transmission electron microscopy (STEM) images revealed spherical ionic clusters whose size, distribution, and microphase separation could be controlled through the degree of polyimide branching. Small, homogenous, and well-distributed ionic domains are thought to increase proton transport and conductivity for fuel cell applications.

2.3.1.4 Poly(arylene ethers)

Poly(arylene ethers) (PAEs) are high performance polymers that have arylene-ether linkages in the polymer backbone. These polymers have found extensive application due to their thermal stability, enhanced mechanical properties, and excellent resistance to hydrolysis and oxidation.[3, 21, 32] In addition, multiple organic synthetic methods allowed this class of aromatic polymers to be expanded and explored to fine tune not only the composition of the polymer but also cost-effective methods that eliminate or reduce side reactions. Properties of PAEs are in part attributed to the aromatic ether linkage which gives rise to chain flexibility. This flexible linkage affords desirable secondary transitions such as benzene ring flips to occur which impart desirable impact properties.

The versatility of PAEs originates from the multiple synthetic methods available for creating these polymers. The three major divisions of organic synthetic reactions are highlighted below, and their advantages and disadvantages will be discussed:

1) Electrophilic aromatic substitution
2) Nucleophilic aromatic substitution
3) Metal-catalyzed coupling reactions

Electrophilic aromatic substitution reactions for the synthesis of PAEs are typically Friedal Craft reactions. This reaction can occur in bulk or in solution with the aid of a metal catalyst such as $FeCl_3$, $AlCl_3$, and $AlBr_3$.[21, 33] Reaction of an activated arenesulfonyl halide with benzene yields the poly(sulfone). Replacing benzene with diphenyl ether easily incorporates ether linkages into the polymer backbone to synthesize poly(ether sulfones). This method will generate an acid byproduct. Alternatively, the reaction between diphenyl ether and terephthaloyl chloride also generates poly(arylene ether ketones).

Both bulk and solution polymerizations are possible with the Friedal Craft reaction. The bulk reaction entails creating low molecular polymer in the melt. Subsequent heating of the ground polymer at 230-250 °C facilitates the removal of the acid while reducing possible radical side reactions on the sulfonyl chloride.[34] Unfortunately this synthetic approach causes some side reactions and crosslinking which leads to an irregular polymer backbone. Lowering the temperature of the second heating stage and using limited amounts of catalyst (0.1 – 4 wt%) reduces the possibility of side reactions.[35] Polymerization can also occur in solution using $AlCl_3$ and methylene chloride as the solvent. However, the main drawbacks of this approach include purification of the catalyst and low molecular weight due to insolubility of the polymer.

The main approach for synthesizing PAEs is through the nucleophilic aromatic substitution of an activated aryl halide. This synthetic route occurs in solution and requires higher temperatures than the electrophilic aromatic substitution reaction. However, side reactions are less likely to occur, and the reaction is more tolerable of other functional groups. **Scheme 2.5** illustrates the nucleophilic aromatic substitution mechanism, and there are several features which distinguish this reaction. The first step reaction in which the nucleophile adds to the electropositive carbon is the rate-limiting step. The electronegative halide creates a partially electropositive charge on the carbon through induction and causes the nucleophile to preferentially add at that site.

Because this step is rate-determining, the strength of the nucleophile and the electronegativity of the halide substituent dictate the rate of reaction. Thus, the rate of reaction follows this trend for the halide leaving group: F>>Cl>Br>I. Addition of the nucleophile to the activated arene generates the Meisenheimer complex, a resonance stabilized intermediate, was supported through the isolation of the salt and examination of the influence of the electron withdrawing group on the reaction rate. Therefore, electron-withdrawing groups such as NO_2, SO_2, and CO encourage and stabilize this first step. The fast and second step involves the re-aromatization of the benzene ring and the removal of the leaving group.

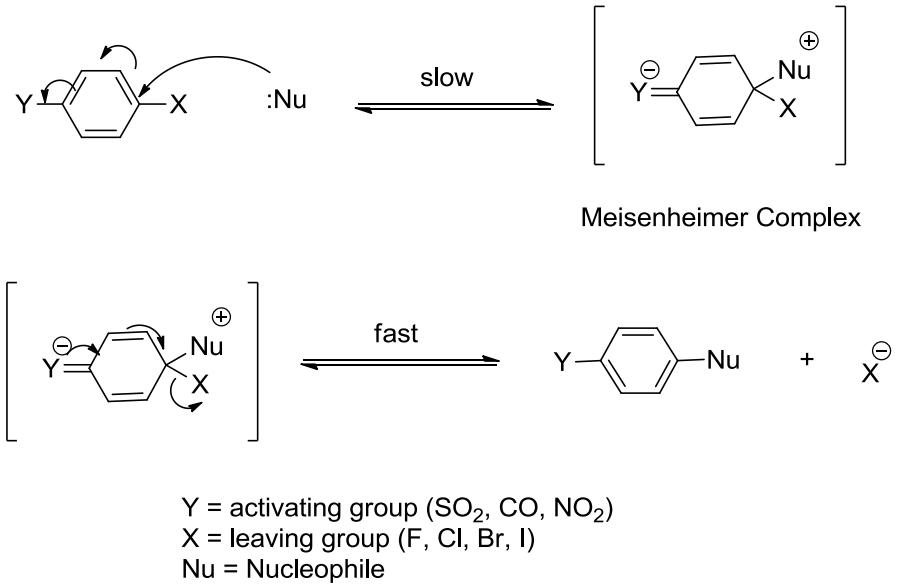

Y = activating group (SO_2, CO, NO_2)
X = leaving group (F, Cl, Br, I)
Nu = Nucleophile

Scheme 2.5. Nucleophilic aromatic substitution mechanism commonly used to synthesize poly(arylene ether sulfones) or poly(arylene ether ketones).

Other approaches utilizing metal-coupling reactions have also been explored. The Ullman reaction is a common method for synthesizing PAEs between diphenol and aromatic halide using a copper catalyst. This synthetic route affords greater variability of polymer composition, because activating groups are not needed. The main drawbacks include purification and removal of the copper catalyst as well as the need for expensive brominated catalysts. Other metal-coupling reactions have also been investigated including the reaction with nickel catalyst and halogenated aromatic compounds.[21, 32, 33, 36] Less expensive aromatic chlorides and milder reaction conditions are advantages of this approach.

PAEs have recently been explored for their fuel cell application, because the aromatic groups can be subjected to ionization to generate the charged species.[33] McGrath et al. recently investigated the effect of polymer block length on the bulk morphology of poly(arylene ether sulfones) for proton exchange membranes.[36] TEM micrographs illustrated the effects of charge placement on the morphology of the sulfonated poly(arylene ether sulfones). [36] Randomly

sulfonated copolymers showed lack of long-range microphase separation. TEM investigated the morphological features in PAE multiblock systems for block lengths as small as 5k-5k of the sulfonated to unsulfonated blocks. As the block length increased, the extent of microphase separation became more regular, and the interlamellar spacing also increased with block length.

2.3.2 Polyaddition Polymers

The second class of step-growth polymers is polyaddition polymers. Polyaddition polymers do not form small molecule byproducts, and polymer examples of this class includes polyurethanes and epoxy resins. New classes of step-growth reactions are expanding this class of step-growth polymers and will be described in later sections of this chapter.

2.3.2.1 Polyurethanes

Polyurethanes (PU) are polymers with carbamate linkages within the backbone. Polyurethanes were developed in the 1930s by Otto Bayer et al at I. G. Farbenindustrie at Leverkusen, Germany and quickly became a main competitor for nylon and polyamides.[37, 38] Since then, the applications of polyurethanes have expanded to encompass coatings, shoe soles, foams, and thermoplastic elastomers. Within the past decade, polyurethanes have also reached the biomedical industry and now have found application in implants, soft tissue replacement, angioplasty balloons, drug delivery, and biocompatible tissue scaffolds.[39] The unique ability to control the chemical structure as well as in fine-tuning polymer chain stiffness, flexibility, and morphology enables this class of step-growth polymers to acquire desirable properties for a variety of applications.

There are many approaches for forming the carbamate linkage; the standard method includes the nucleophilic addition reaction between a diol and diisocyanate. Conveniently, this reaction does not produce a condensate byproduct and thus, falls into the category of polyaddition step-growth polymers. Polymerization occurs readily without removal of the reaction condensate. The isocyanate functional group has the ability to form different types of linkages including urethane, urea, and amide bonds which further increases this monomer's versatility in polymer synthesis. The reaction between an isocyanate and carboxylic acid gives rise to the amide linkage and carbon dioxide. Formation of polymer foams often takes advantage of this byproduct to create voids within the polymer.

One concern with the synthesis of polyurethanes is the possibility of crosslinking or hyperbranching side reactions. Careful control of monomer stoichiometry and reaction temperature can eliminate side reactions. These reactions occur through the additional reaction of the urethane or urea nitrogen to unreacted isocyanates. **Scheme 2.6** below illustrates possible side reactions that occur from the nucleophilic nitrogen of the urethane linkage.

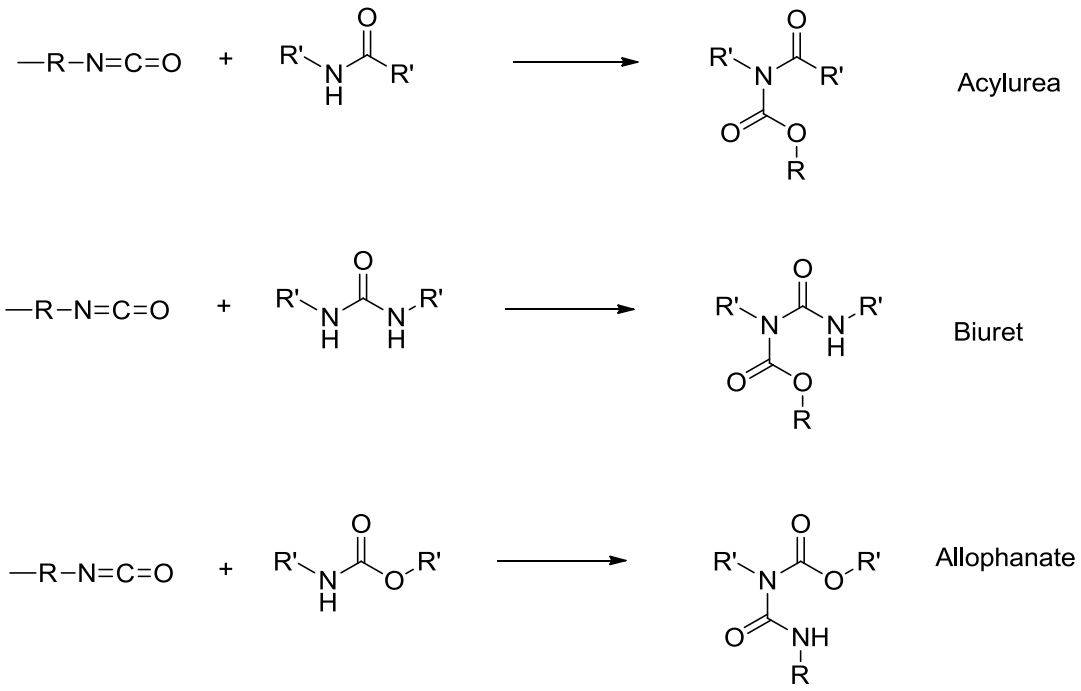

Scheme 2.6 Possible side reactions from excess isocyanates during polyurethane polymerization leading to branching or crosslinking.

The outstanding properties of polyurethanes can be attributed to the hydrogen bonding between the urethane and urea groups. This intermolecular interaction also contributes to the crystallinity; however, the hydrogen-bonding interaction in urethane linkages is weaker than urea and amide groups.[40-42] The hydrogen-bonding unit within the hard segment block gives rise to the high T_g and the microphase separation behavior typically seen in segmented polyurethanes. The degree of hydrogen bonding and morphology of the segmented polyurethanes depend largely on the choice of chain extender. Many thermoplastic elastomers take advantage of strong hydrogen-bonding intermolecular interaction to impart exceptional elastomeric properties such as high strain and low mechanical hysteresis.

Segmented block copolymers of polyurethanes have also remained one of the main types of polyurethanes. Segmented polyurethanes are synthesized with chain-extenders or without chain extenders. **Scheme 2.7** illustrates a conventional 2-step approach utilizing the prepolymer

method for synthesizing segmented block polyurethanes. Soft segment blocks including polyether polyols are often reacted with excess diisocyanate. The isocyanate-functionalized the soft segment block is called the prepolymer. Soft segment blocks should have low T_g below -50 °C.[42] Other soft segment block polyols include polyesters, polybutadiene, polycaprolactone, and polycarbonate.[3] Subsequent addition of a diol chain-extender will react with the prepolymer and excess diisocyanate to produce a hard segment block with a higher density of urethane linkages. Hard segment block properties are tailored through the diisocyanate and can form highly crystalline domains.

The block structure allows for microphase separation to create physical crosslinks due to the incompatibility of the polymer blocks, which can be further facilitated through hard segment crystallization in the case of polyurethane. Monomer stoichiometry and the soft-segment molecular weight define the hard segment content. The careful choice of hard block and soft block composition, and hence thermal transitions for the corresponding block, determines the application and processing window. The flexible soft segment block attributes to the high elongations typically seen in polyurethane elastomers, and the hard segment block provides mechanical stability and acts as physical crosslinks.

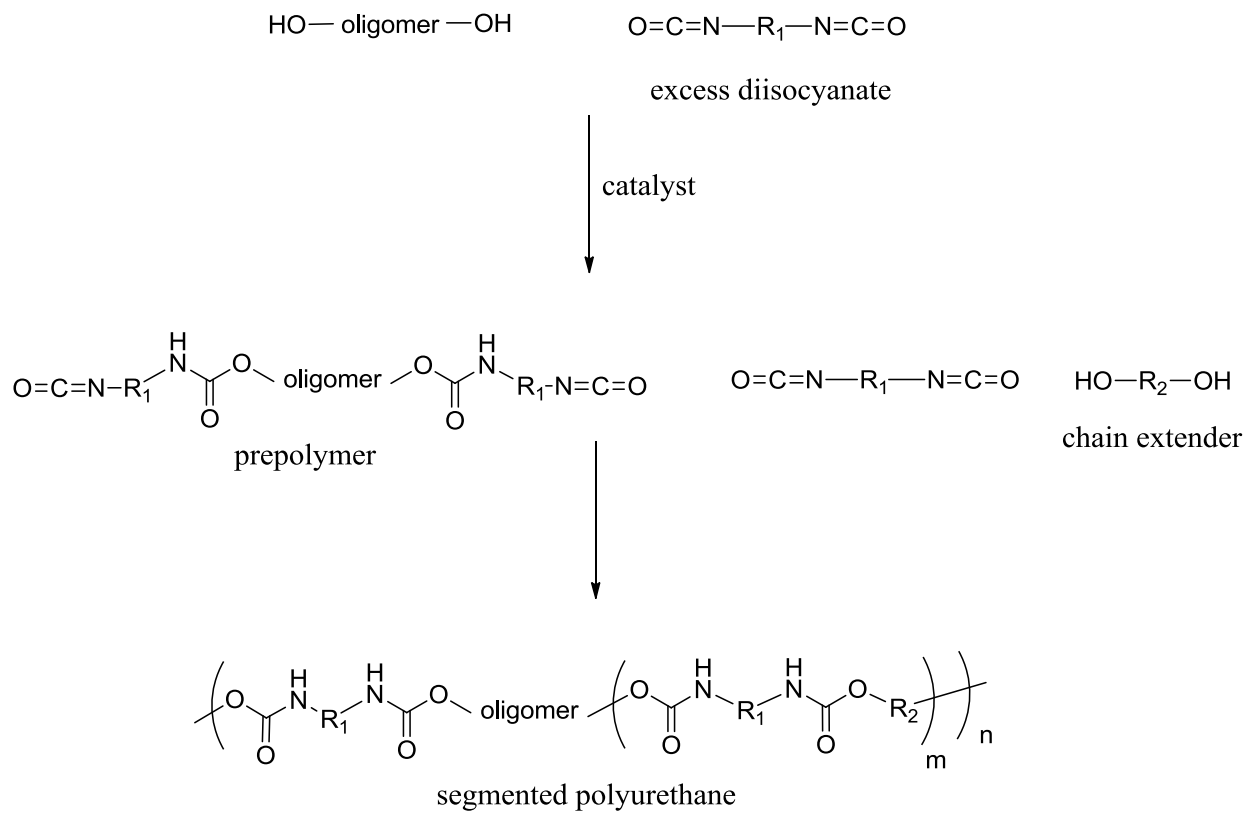

Scheme 2.7. Synthetic scheme for the preparation of segmented polyurethanes using a prepolymer method.

Figure 2.6 represents a list of commonly used diisocyanates and their chemical structure. There are many synthetic routes that are taken to synthesize diisocyanates including Curtis, Hoffman, and Lossen rearrangement. The use of Hoffman and Lossen rearrangements are commonly used to synthesize aliphatic diisocyanates.[38] Aromatic diisocyanate monomers produce mechanically tougher polymers. Aromatic diisocyanates are more reactive, thermally and hydrolytically stable and less volatile than their aliphatic counterparts; however, they are generally less UV stable and can cause yellowing of the polymer. Selection of aliphatic diisocyanates, such as HMDI, also has the added complexity of mixed stereoisomers which can play a large role in the thermal and mechanical properties of the polymer. Reactivity of diisocyanates with other functional groups

also differ. Reactions of amines with diisocyanates are faster and more reactive than hydroxyl groups, water, and carboxyl groups. In addition, steric hindrance of these functional groups also directly affects the reaction kinetics.

Polyurethane synthesis typically employs tertiary amines or organotin compounds to increase the reaction rates and facilitate the linear polymerization rather than branching and crosslinking side reactions or reactions with water. The reaction kinetics of polyurethane synthesis directly relate to the basicity and steric hindrance of the tertiary amines. For example, triethylene diamine with a pKa of 8.2 is more basic than triethylene amine whose pKa is 10.8, and the relative reaction rate of butanol to phenyl isocyanate is 3.3:0.9 with triethylene diamines and triethylene amine, respectively.[38] Although the reaction rates for the nucleophilic addition reaction increases with amine basicity, the side reactions which produce crosslinked or hyperbranched structures as illustrated in **Scheme 2.6** can also increase as well. Careful control of the catalyst choice and reaction temperatures can lower the probability of branching or crosslinking side reactions.

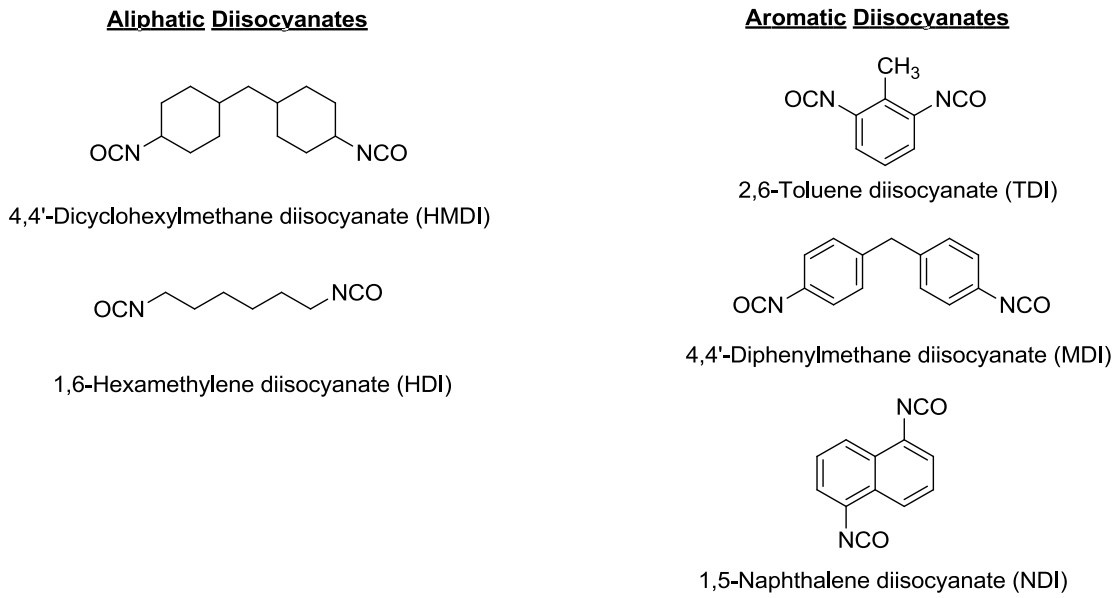

Figure 2.6. List of commonly used aliphatic and aromatic diisocyanates for polyurethane synthesis.

Unlike conventional ABA triblocks which generally have block molecular weights ranging from 30,000 to 100,000 g mol^{-1} depending on the polymerization method, segmented block copolymers have alternating block lengths with molecular weights between 1,000 – 5,000 g mol^{-1}.[42] Moreover, the molecular weight, composition, and weight content of ABA immiscible triblocks often form unique long range morphological features such as spherical, cylindrical, biocontinuous gyroids, and biocontinuous lamellar.[43] Specifically, it is the microphase separation of the immiscible blocks which attributes to useful elastomeric and mechanical properties.[32] The correlation between molecular weight of these blocks and the influence on morphology has been heavily studied within the past decade.[43-48] In contrast to the well-defined block copolymers often synthesized using living polymerization techniques, segmented block copolymers, such as polyurethanes, do not have well defined block structures but a distribution of block length. This characteristic leads to the loss of long-range microphase separation; however, phase separation can still be seen.

Synthesis of segmented thermoplastic copolymers using step-growth polymerization finds wider applications due to the ability to tailor the polymer backbone through monomer choice. Thus, hard segment and soft segment block compositions can be easily modified which translates to better control of the elastomeric properties. Studies on non-chain extended polyurethane systems showed differences in microphase separation behavior compared to polyureas due to differences in the degree of hydrogen bonding. Wilkes, Yilgor, and others investigated the effects of diisocyanate symmetry on the morphological behavior of poly(ether-urethanes).[49-51] The synthetic method used in the experiment involved stoichiometrically reacting 1,000 g mol^{-1} poly(tetramethylene oxide) (1K PTMO) polyols with various symmetrical (MDI, TDI, HMDI) and unsymmetrical (HMDI, TDI, and MDI) diisocyanates to afford high molecular weight polymer.

AFM images of poly(ether-urethanes) and poly(ether-ureas) synthesized with symmetrical or unsymmetrical diisocyanates revealed only symmetrical diisocyanates PPDI, HDI, and CHDI resulted in any mechanical integrity and microphase separation through AFM investigations.[42] Unsymmetrical diisocyanates produced low-T_g, structurally inadequate polymer films and lacked microphase separation when investigated with AFM. The results demonstrated the importance and influence of diisocyanate symmetry on the polymer morphology and the mechanical properties of the poly(ether-urethanes). In contrast, poly(ether-ureas), which have bidentate hydrogen-bonding capabilities, indicated no influence of diisocyanate symmetry on the microphase separation. However, the symmetry of the diisocyanate, which most likely affected the hard segment crystallinity, affected morphology and structure of the phases.[42]

In addition to symmetry of the diisocyanate, segmented polyurethanes are also complicated through a variety of factors which influence the morphology and phase separation

such as chemical composition of the blocks, molecular weight, crystallizability of the hard segment, and thermal history.[42] High molecular weight prepolymers increase the microphase separation of the segmented block copolymer, while prepolymers with high polydispersities will encourage phase-mixing.[42] One of the most important factors, which determine the morphologies and the properties of segmented polyurethanes, depends on the choice of isocyanate. The symmetry of the isocyanate and the extent of electrostatic strength can regulate the crystallinity of the hard segment.

Although the study from Yilgor et al.[42] examined the influence of diisocyanate symmetry and hydrogen-bonding capabilities on the morphology of the segmented polyurethane, the effects of molecular weight on morphological structure was not investigated. The specific relationship between molecular weights of segmented block and polymer morphology poses more complications mainly due to the difficulties of controlling block molecular weights in prepolymer methods. Although the molecular weight of the prepolymer used in many segmented polyurethane synthesis is often known, the effective molecular weight of the hard segment block is difficult to elucidate. One method to bypass this obstacle is to react two prepolymers with known molecular weights such as polyols and an α,ω-difunctionally terminated oligomer, preferably with isocyanate groups. This approach avoids the use of chain-extenders and allows for a systematic study of the influence of block molecular weight on polymer morphology.

Recently, Meijer et al. investigated the crystal structures of linear-aliphatic polyurethanes containing 5-10 methylene units using transmission electron microscopy (TEM) and X-ray and electron diffraction analysis.[52] Hydrogen bonding of the polyurethanes produced crystals with lamellar crystal thicknesses between 5 and 10 nm. Further investigations showed that these hydrogen bonded crystal lattices were formed through fully extended chain conformations in an

ordered triclinic lattice. Furthermore, the hydrogen bonds were set between antiparallel chains very similar in fashion to aliphatic linear polyamides.

One of the more interesting polymer properties that have elicited much attention is the special shape-memory characteristics that have been found in many thermoplastic segmented polyurethanes.[53-57] Shape memory polymers (SMPs) are generally polymer networks that have the ability to hold a certain physical shape after deformation and return to the original physical state after being exposed to an external stimulus such as temperature, light, and pH. Many shape memory polyurethanes (SMPUs) have already been reported,[54, 56-59] and research is increasing the understanding in this area to better tailor the switching properties. In many cases, the composition of the various segments in the segmented polyurethanes contributes to a thermal transition which allows for the shape memory and shape recovery process to exist. Typically, a *switching* segment and *permanent* segment is established with the desired thermal transition temperature. The *switching* segment allows the polymer to morph and change its overall physical shape at the transition temperature, T_{trans}, and the *permanent* segments act as physical anchors whose thermal transition is generally above T_{trans} and retains the original primary shape. Upon heating the sample above T_{trans}, the flexible switching segment acquires more chain mobility to establish a new physical shape. Reheating the deformed polymer above T_{trans} entropically drives the polymer chain to convert back to the random-coil conformation.

Segmented polyurethanes been recently explored for shape memory applications since the block copolymers are able to form physical networks through microphase separation and crystallization of hard segment. In addition, the syntheses of segmented polyurethanes have been well-defined and various types of soft-segment precursors, diisocyanate monomer choice, and chain extenders allow for tailored polymers designs specifically for shape-memory

properties. In order for shape-memory properties to be useful in smart material applications, the reversibility and memory of the polymer shape must occur quickly and preferably with little hysteresis such that the properties of the polymer following repetitive physical deformation remains unchanged throughout deformation.

Shape memory poly(ester-urethanes) have found much interest from biomedical applications due to their shape-recovery properties and biodegradability from polyester blocks such as poly(lactic acid) and poly(ε-caprolactone). Wang et al. investigated the morphological consequences from deformation of poly(ester-urethanes) that have shape memory properties using FTIR.[60] Various other spectroscopic techniques have been employed to better understand the polymer microstructure transition that provides these shape memory and shape recovery properties including small-angle X-ray scattering (SAXS), wide-angle X-ray diffraction (WAXD), dynamic mechanical analysis (DMA), and atomic force microscopy (AFM). **Figure 2.7** depicts a representative schematic of poly(ester-urethanes) undergoing small and large strain and the shape recovery process under a thermal stimulus. Using FTIR, the investigators concluded the amorphous phase consisting of the soft segment PCL became more oriented under small induced strain. However, crystalline domains from the PCL as well as the hard segment urethane block remained largely unhindered. When larger strain is applied, the amorphous PCL becomes even more oriented and begins to undergo strain induced crystallization while the original crystallites from the PCL and hard segment phase also begin to align. Most importantly, the hydrogen bonding from the hard segments are slightly weakened and rearranged to adopt a newly fixed microstructure. Shape recovery largely relies on the entropy of the system to recover a more random-coil conformation of the amorphous chains and relies on restoring the intermolecular hydrogen-bonding interactions that were weakened during strain deformation.

The result confirmed others' work, which conclude that a recovery of the segmented polyurethane to its original shape which was largely dependent on the polymer microstructure.[59, 61, 62]

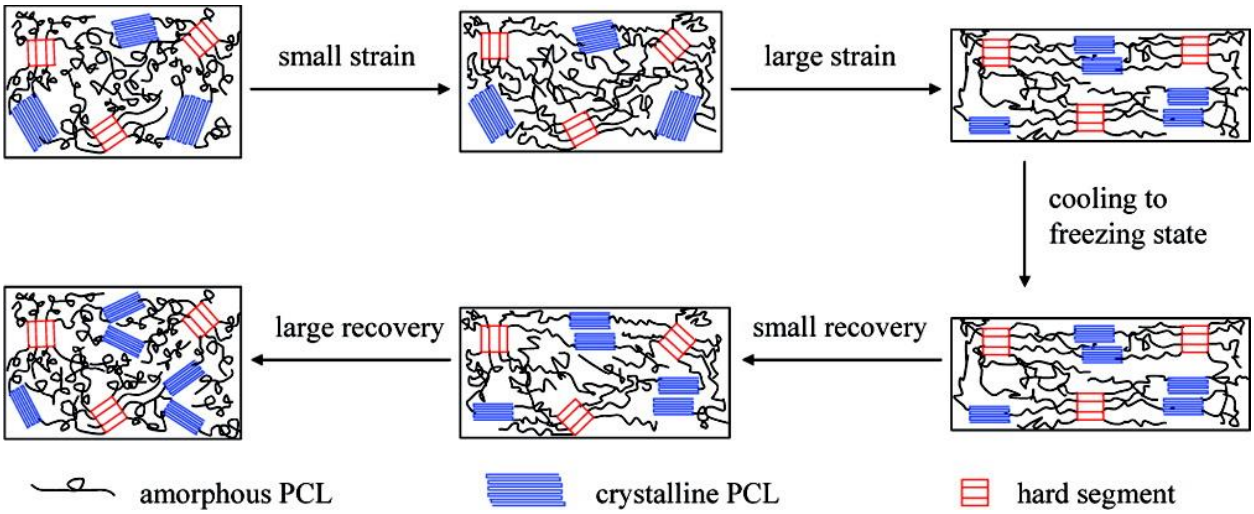

Figure 2.7. Schematic of the microstructure transition of shape-memory poly(ester-urethanes) under strain deformation and shape recovery.[60]

2.3.2.2 Epoxy resins

Epoxy resins are an important class of step-growth polymer which has allowed for a quick step-technique to synthesize thermoset networks. Epoxy thermosets are reactions between an epoxy resin, a small molecule or prepolymer that is functionalized with epoxide end groups, and a hardener or crosslinking agent. The crosslinking agent has a functionality $f>2$ to allow for oligomers formation, branching, and finally crosslinking.

One of the interesting factors about epoxy curing arises from the unique geometric structure of the epoxy ring. The development of epichlorohydrin facilitated the wide utility and application of this curing process to extend beyond small molecule diepoxies and include epoxy functionalized prepolymers. With the need to be more ecologically mindful, **Scheme 2.8**

highlights a green chemistry approach to synthesize epichlorohydrin from glycerol, a transesterification byproduct from vegetable oil.

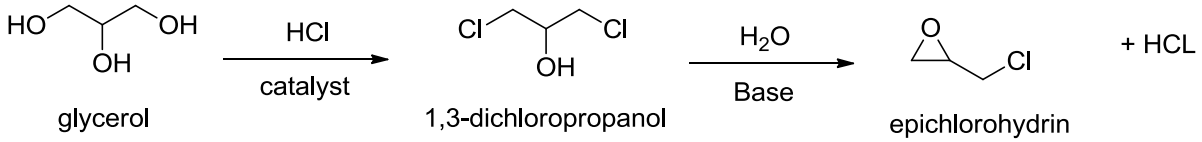

Scheme 2.8. Synthesis of epichlorohydrin from glycerol, a byproduct of transesterification from vegetable oil, from Solvay Epicerol™ process.

The epoxy ring itself is a heterocyclic three-membered planar ring.[63] Although the chemical compositions of the carbon and oxygen within the ring are sp^3-hybridized and should have characteristic 109.5° tetrahedral structures, the formation of the three-membered ring compresses the internal angles of the epoxy ring to nearly 60°. Thus, the hybridized orbitals of the carbon atoms are more similar to the trigonal planar sp^2 orbitals. Many previous literatures reviewed the effect of chemistry and hyperconjugation of the strained three-membered ring.[64, 65] The compressed internal angle of the epoxide ring translates to a very large ring-strain energy of approximately 113 kJ mol^{-1}. The release of ring-strain contributes to the major driving force for the fast and efficient mode of curing used in thermosets.

The epoxy curing occurs through a complex process in which the dynamics and the polymer structure changes during the curing chemistry. Reaction occurring between an epoxy resin and a hardener such as a diamines first occurs through the production of the small oligomers. Because the hardener has a functionality greater than 2, branching and eventual crosslinking will occur. During the branching stage, the polymer is still soluble in the reaction medium; however, as the reaction continues to cure, the reaction product will lose solubility or begin to swell in the reaction solvent and gelation takes place. Because the curing process is such a dynamic and complicated progression, properties of the polymers also change throughout

the reaction.[66] In fact, the curing process directly influences the viscoelastic properties as the monomers and reactants transition from oligomers to branched and finally crosslinked networks. The choice of epoxy resin, hardener, and crosslink density directly influences the polymer storage modulus increase as the epoxy resin cures. Because the chain mobility of the polymer thermoset decreases with crosslinking, the T_g also begins to rise as the curing process occurs.

Scheme 2.9 represents a general epoxy resin curing reaction between a diepoxide and diamines. The reaction of the epoxide ring can occur between an electrophile or a nucleophile to generate the ring-opening reaction and the subsequent alcohol. In general, the primary and secondary alcohol can be produced, since in theory, both carbons of the epoxide ring are likely to be reacted with the nucleophile or electrophile. However, the sterics of the reaction generally leads to the attack of the less sterically hindered carbon and subsequently, the secondary alcohol as seen in **Scheme 2.9**. Common nucleophiles used in epoxy reactions are alcohols, amines, and carboxylic acids. Alkyl halides and isocyanates are possible electrophilic reactants with epoxides as well.

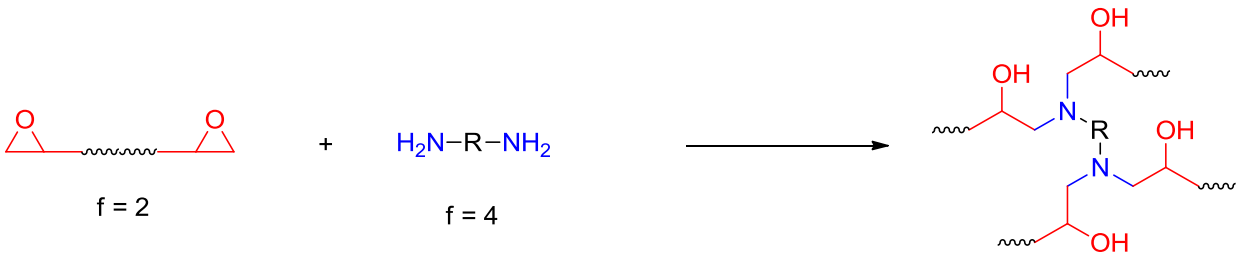

Scheme 2.9. General epoxy resin curing between a diepoxide (functionality (f) = 2) and diamine (f=4).

Epoxy curing has found vast utility in self-healing applications since the reaction occurs quickly and without any aid of catalysts. In many self-healing systems, microcapsules containing a reactant or catalyst are generated and blended into a binary polymer matrix. Upon stress or mechanical damage, the microcapsule will rupture and react with the surrounding matrix to

repair the polymer damage. The curing agent or compound held within the microcapsule contains the same chemistry as the polymer matrix to repair the damage with the same polymer composition to maintain matrix homogeneity. Epoxide reactions offer advantages such as a fast cure which is often necessary for quick polymer repair.

Recently, Sottos and coworkers developed a method to prepare microcapsules containing reactive amines using interfacial polymerization rather than conventional emulsion techniques to create the walls of the microparticles.[67] These particles were intended for epoxy adhesive applications with potential self-healing properties. The capsules contained the very reactive diethylene triamine which was created using a water-in-oil emulsion method and stabilized in a nanoclay suspension with polyisobutylene (PIB). Upon removal of PIB, the particles were quickly reacted with toluene diisocyanate (TDI) to create a polyurea wall. Careful addition of the TDI allowed for unaggregated microparticles with diameters averaging about 26 ± 10 μm (Error! Reference source not found.). The amine-containing capsules were blended with epoxy resin and curing was performed upon added pressure to rupture the capsules.

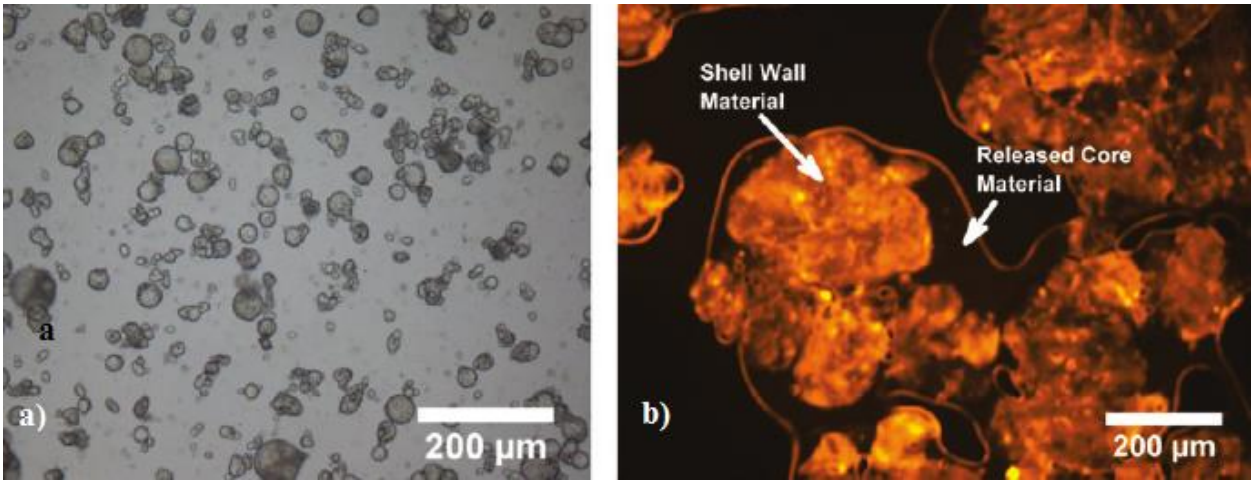

Figure 2.8, Micrographs of epoxy-cured polymer composites. a) Optical micrograph of amine-filled microcapsules in solution for self-healing epoxy composites. b) Fluorescence micrograph reflecting the response of microcapsules under applied pressure.[67]

2.4 *Novel Synthetic Approaches in Step-Growth Polymerization*

2.4.1 Non-aqueous emulsion polymerization

Polymer nanoparticles find many applications in engineering and life sciences. Nanoparticles are of particular interest for the development of polymeric drug delivery vehicle, magnetic imaging devices, and biosensors.[68-71] Formation of nanoparticles typically employs emulsion polymerization which involves two immiscible solvent, organic and aqueous. However, due to the nature of the reaction conditions, most nanoparticles were synthetically restricted to free-radical polymerizations. The first reported step-growth nanoparticles utilized the "Grubbs second generation" ruthenium catalysts to perform acyclic diene metathesis (ADMET) in an aqueous emulsion.[72] The ADMET polycondensation of *para*-divinylbenzenes produced conjugated nanoparticles. Fluorescent conjugated nanoparticles were also recently reported using the oxidative coupling Glaser reaction.[73] The Glaser coupling reaction conveniently avoided strict stoichiometric conditions to afford diethynyls from terminal monosubstituted alkynes. The application of emulsion polymerization has been limited for step-growth polymers since an aqueous condition would essentially compete with the equilibrium reaction and encourage hydrolytic depolymerization.

Encouragingly, Klapper et al. have developed a unique approach for the synthesis of polymer nanoparticles using oil-in-oil emulsions.[74] This particular method is desirable for many step-growth polymerizations in which traditional oil-in-water emulsion techniques would cause hydrolysis of the polymer. In addition, the group has investigated the nonaqueous emulsion techniques for a variety of step-growth polymers including polyamides, polyurethanes, and polyesters, although this technique was not limited to step-growth polymerization. Synthesis of polar step-growth polymers such as polyesters and polyurethanes using the oil-in-oil technique

required a polar aprotic solvent such as DMF dispersed in cyclohexane or acetonitrile. For the first time, polyester nanoparticles where synthesized under mild conditions with regular and well-defined shape and size using oil-in-oil emulsion polymerization (**Figure 2.9**). First, acetonitrile in cyclohexane was combined with an amphiphilic block copolymer poly(isoprene-*b*-methyl methacrylate) (PI-PMMA) which served as the surfactant stabilizer in a traditional emulsion polymerization. The diol was dissolved in the DMF phase and emulsified into the cyclohexane phase as micelles. Dropwise addition of the dichloride and base, pyridine or triethyleneamine, allowed diffusion of the dichloride from the continuous cyclohexane phase into the dispersed micelles.

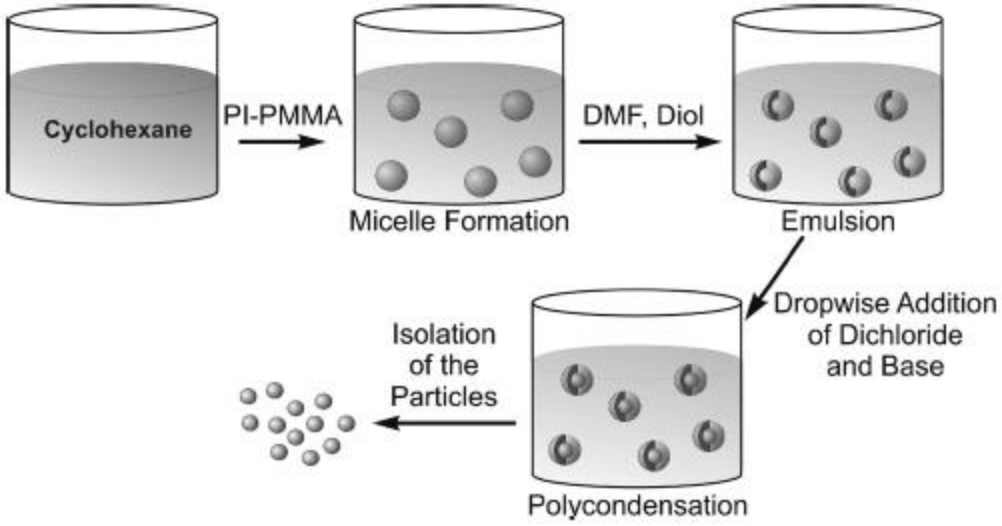

Figure 2.9. Nonaqueous emulsion polycondensation.[74]

Figure 2.10 below shows scanning electron micrograph (SEM) of polyester nanoparticles formed using this emulsion technique. Particle sizes were narrowly distributed and produced nano-scaled spherical beads of approximately 38 nm based on SEM. Weight-average molecular weights of the polyester beads were approximately 22,000 g mol^{-1} which was significantly higher

than previously investigated emulsion techniques.[74] The summarized techniques reveal the complexities, challenges, and triumphs of emulsion polymerization for step-growth nanoparticles.

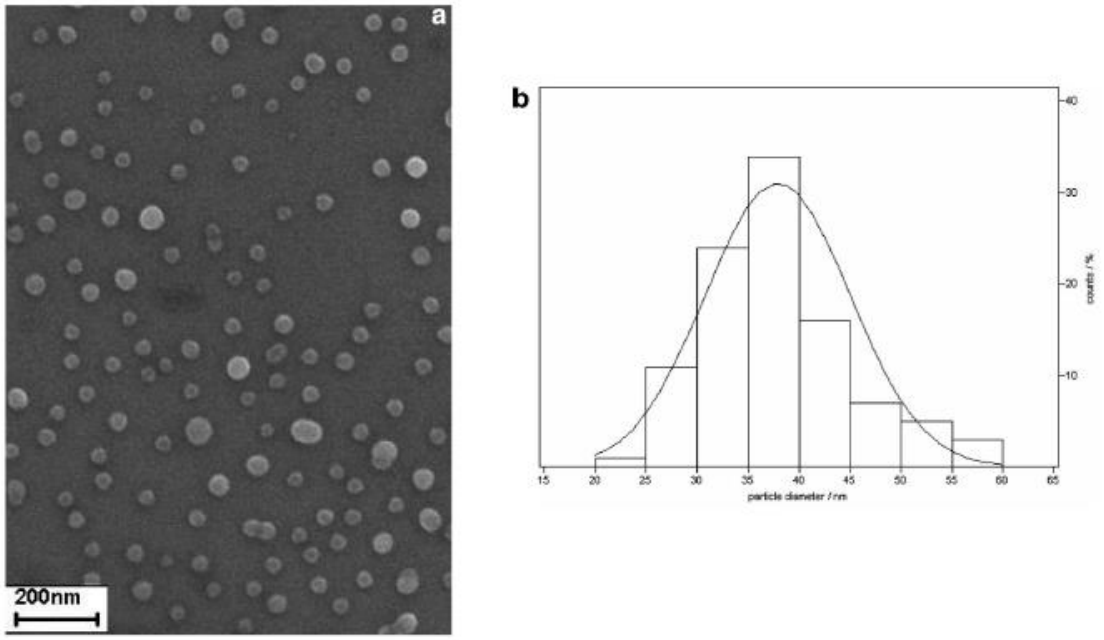

Figure 2.10. Size and shape of polyester nanoparticles synthesized using oil-in-oil emulsion polymerization a) SEM image and b) particle distribution from SEM image. Polyester nanoparticles displayed an average particle size of 38 ± 7 nm.[74]

2.4.2 Lipase-catalyzed polymerization

The use of lipase-catalyzed coupling reactions in step-growth chemistry has also elicited much attention for their eco-friendly approach for polymer synthesis. Lipases facilitate many of hydrolysis reactions of triglycerides into glycerol and fatty acids. In the category of polyesters, lipases have been utilized for ring-opening polymerization of cyclic monomers as well as condensation of hydroxyl and acid end groups.[75, 76] Early work described the use of porcine pancreatic lipases (PPL) to synthesize polyesters through linear polycondensation of ω-hydroxyesters and ring-opening polymerization of ε-caprolactone.[77] Unfortunately, these enzyme-catalyzed polymerizations suggested low rates of propagation and required long reaction

times. Further investigations revealed the rate of initiation was highly dependent on the choice of the nucleophilic initiator; however, kinetic studies of PPL-catalyzed PCL demonstrated controlled linear first-order kinetics independent of initiator concentration.[78] In addition, low molecular weights were attributed to the PPL-catalyzed hydrolysis reaction. Nevertheless, bio-derived renewable enzyme-catalyzed polymerizations offer distinct advantages for step-growth polymerization such as tolerance of aqueous mediums and high regio- and enantioselectivity.[79, 80] Furthermore, the avoidance of transition metal catalysts enables this method to be potentially useful for synthesis of bioresorbable polyesters for biomedical applications.

Much of the work from Gross's research has focused on the use of a highly selective immobilized enzyme Novozyme-435, a *lipase B* enzyme from *Candida antartica* (CALB), to synthesize polyesters and polyester block copolymers.[81, 82] The crystal structure of CALB was discovered in 2006, and it was hypothesized that the catalytic active center consists of three critical amino acids: serine (Ser105), histidine (His224), and aspartic acid (Asp187).[80] The three-dimensional structure of the active site assembled through a series of hydrogen-bonding interactions. Imidazole serves as a general base upon insertion of an ester substrate to promote acyl-enzyme intermediate formation and subsequent release of the alcohol byproduct.[83] The acyl-enzyme intermediate allows for a nucleophilic attack of the carbonyl, and the imidazolium ring from histadine facilitates protonation and release of the newly formed ester.

Early work has demonstrated the effectiveness of CALB-catalyzed sorbitol- or octanediol-containing aliphatic polyester polymerization in the absence of solvent.[81, 84] Further advances revealed the versatility of this enzyme to tailor macromolecular structure. Solvent-free cobalt crosslinking of a CALB-catalyzed copolymer containing unsaturated fatty acids illustrated a green approach to synthesize polymer coatings. Branched topologies were also achieved

through lipase catalysis of ε-caprolactone and an AB_2 monomer, 2,2-bis(hydroxymethyl)butyric acid.[85] Another example of lipase-catalyzed hyperbranched polyesters utilized trimethylolpropane as the branch core and linear aliphatic diacids and diols.[86] Graft polymer brushes has also been described.[87] 2-Hydroxyethyl methacrylate or ω-hydroxyl-ω'-methacrylate-poly(ethylene glycol) served as initiators of the lipase-catalyzed ring-opening polymerization of ω-pentadecalactone. Subsequent free-radical polymerization of the resulting vinyl macromonomer afforded highly dense polymer properties with intriguing crystallization behavior.

The efforts of many enzyme-catalyzed polyesters research have centered on the formation of block copolyesters for potential bio-derived thermoplastic elastomers. Living or controlled polymerizations have been traditional synthetic approaches to afford well-controlled block copolymers. However, the use volatile solvents and transesterification of the polyester blocks have limited the versatility of this synthetic method. Ring-opening polymerization with an ω-hydroxy-terminated polybutadiene macroinitiator and subsequent free-radical polymerization of the macromonomer represents one method used to achieve a diblock structure.[88] Other examples of block copolymer synthesis have also been described in the literature.[89-91]

Lipase-catalyzed polymerization has proven to be an efficient method to synthesize polyesters based the principles of green chemistry. Extensive research elucidated the kinetics and mechanisms of the polymerization and served as a platform that launched further investigations on the applicability of this approach to synthesize tailored macromolecular architectures. Although the body of research in lipase-catalyzed polymerizations is only in its infancy, the initial understanding and examples of polyester encourage its continuing exploration.

This synthetic method reflects the interdisciplinary efforts of step-growth research to bridge together the fields of biochemistry, polymer chemistry, and life sciences, take advantage of nature's design, and respond to the growing challenges of sustainability.

2.4.3 Chain-growth polycondensation

2.5 *Polyesters for Current and Emerging Technologies*

Polyesters offer a rich and diverse structure-property window with a vast array of difunctional and multifunctional monomers of sufficient purity for quantitative conversions. Polyesters also suggest more recently a rapidly growing importance due to their inherent biodegradability and opportunities for bio-based carboxylic acid and hydroxyl monomers. Thus, one can envision continued research and commercial interests because of the decreased reliance on fossil fuels, opportunities for quantitative conversion to starting monomers, and biodegradation for lessened impact on our environment. In addition, tailored polyesters in the biomedical arena have enabled numerous therapeutic delivery systems that permit time-release drug delivery, gene delivery vectors, and biodegradable tissue scaffolds for regenerative medicine.[92-95] New discoveries within the polyester family have catalyzed many new technologies. Many macromolecular parameters are easily tuned using step-growth polymerization methodologies, including composition, molecular weight, molecular weight distribution, topology, sequence, and stereochemistry. Thus, polyester design enables a systematic investigation of structure-property relationships and carefully tailored properties for diverse performance, ranging from food packaging to biomedical devices.

There is rapidly growing interest in the identification of monomers derived from renewable resources with special attention on synthetic pathways based on the principles of

green chemistry.[96] The transition from petrochemical-derived monomers to renewable resources reflects the awareness of consumers and industry on the importance of incorporating more sustainable chemistry commercial products. In fact, plastics production currently accounts for nearly 7% of worldwide oil and gas consumption.[94, 96, 97] Due to the rising concern pertaining to the limited amount of fossil fuels and the variability of fossil fuel costs, there is a renewed interest in utilizing renewable resources to produce high performance polymers. Researchers are focused on the utility of biomass, plant derived resources, to produce novel monomers. **Figure 2.11** illustrates a 38% growth of bio-based polymers derived from renewable resources from 2003 to 2007. Industrial polymers derived from starch have nearly doubled in the contribution of all bio-based polymers in 2007.

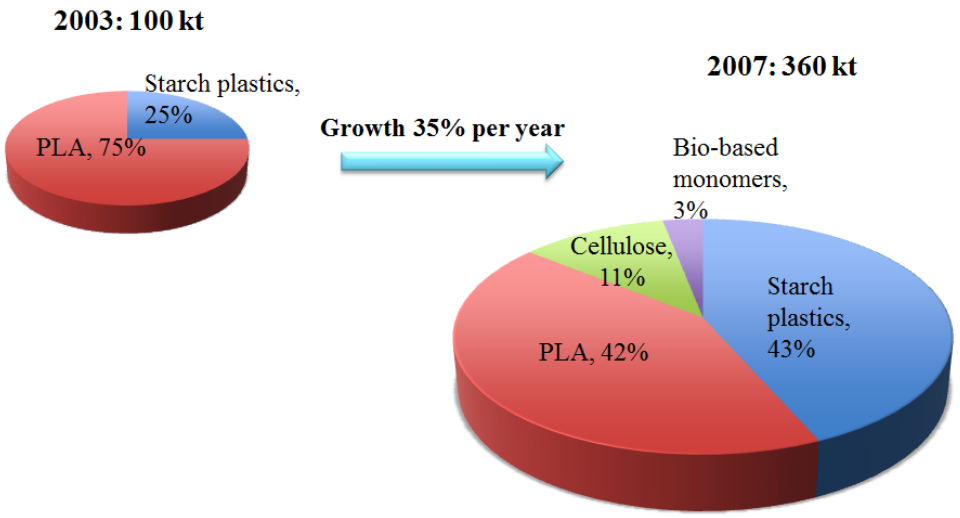

Figure 2.11. Growth of bio-based polymers derived from renewable resources from 2003 to 2007.[98]

The development of cyclic diols from cereal-based polysaccharides, 1,4:3,6-dianhydrohexitols, have also received attention due to their increased rigidity within the polymer backbone. Recently, a review from Pascault et al.[97] discussed the advantages of utilizing these monomers for polymer synthesis.

Table 2.2 summarizes the three isomers of 1,4:3,6-dianhydrohexitol monomers: isosorbide, isomannide, and isoidide. Stereochemical variation of the hydroxyl group afforded differences in the monomer melting temperature, reaction kinetics, and polymer thermal properties. **Scheme 2.10** describes the synthesis of 1,4:3,6-dianhydrohexitols. Initial enzymatic degradation of starch resulted in glucose or mannose, which was further catalytically reduced to sorbitol and mannitol. Subsequent dehydration and cyclization of sorbitol and mannitol produced the bicyclic diols, isosorbide and isomannide, respectively. Of the three isomers, isosorbide is the only one produced on a large industrial scale. A recurring requirement to afford high molecular weight step-growth polymers is the necessity for sufficient monomer purity. Limitations arising from monomer purity have been the central obstacle preventing transition of sugar-based diols into large scale commercial production. In particular, monomer degradation and deleterious side reaction during the monomer synthesis leads to discoloration of the resulting polymers as well as reduced molecular weight.

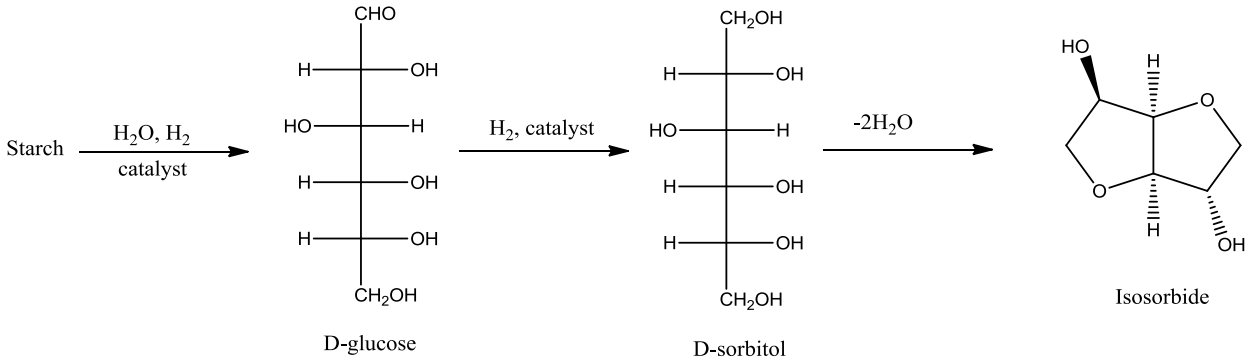

Scheme 2.10. General synthetic strategy for the synthesis of isosorbide from starch.[97, 99]

Table 2.2. Stereoisomers of starch-modified monomers for polyesters derived from renewable resources. Specific stereoisomers of the monomers determine monomer melting temperatures and final polyester properties.[97]

Chemical Name	Isosorbide 1,4:3,6-dianhydro-D-glucidol	Isomannide 1,4:3,6-dianhydro-D-mannitol	Isoidide 1,4:3,6-dianhydro-L-iditol
Molecular Structure	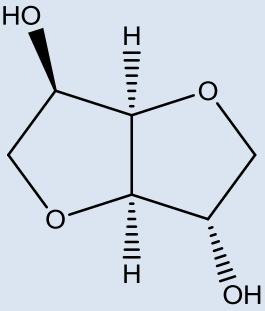	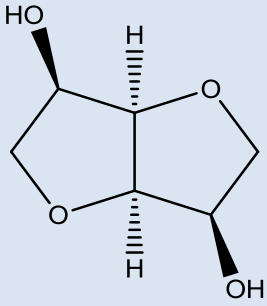	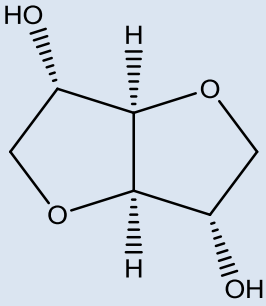
Melting Temperature	61 – 62 °C	81 – 85 °C	64 °C

The ability to effectively increase polyester T_g and avoid petroleum derived aromatic monomers reflects some of the main advantages for utilizing these cyclic diols. The kinked structure of isosorbide prevented crystallization; however isosorbide, a rigid bicyclic diol, effectively stiffened the polymer main chain and increased T_g. The highest all-aliphatic isosorbide-containing polyester displayed the highest T_g of approximately 60 °C,[100] while terephthalate-containing isosorbide polyesters revealed at T_g near 190 °C.[101] Recently, more attention is directed towards entirely aliphatic polyesters due to their potential biodegradability.[102-104]

Kricheldorf et al. investigated all-aliphatic copolyesters derived from isosorbide, 1,4-cyclohexane dicarboxylic acid (CHDA), and succinic acid to develop biodegradable polyesters from renewable monomers.[105] These copolyesters indicated tunable high T_g's depending on the stereochemistry of the bicyclic diol. Homopolymers of CHDA and isosorbide revealed the highest T_g (146 °C) followed by isomannide (133 °C) and isoidide (115 °C).[105] Replacing the

cyclic diacid with an aliphatic linear diacid, succinic acid, essentially lowered the T_g to 77 °C. Thus, the results concluded that isosorbide and its derivatives are suitable diols for the synthesis of polyesters with tunable glass transition temperatures.

Biodegradable poly(lactide)s (PLAs) have emerged in packaging applications as a solution to reduce waste production. Renewable lactide monomers are derived from corn or sugar feedstocks, processed to D-glucose, and finally fermented to result in the cyclic dimer, lactide.[98, 104] Using various metal catalysts, lactide monomers undergo ring-opening polymerization to produce the linear aliphatic polyester. Degradation of PLA produces lactic acid, which further metabolizes into carbon dioxide and water. Recent work from the Hillmyer research group demonstrated successful ring-opening polymerization of lactide and menthide monomers from renewable feedstock yielding thermoplastic elastomers.[106-108]

In addition to polymers derived from starch, vegetable oil-derived polymers including triglycerides and fatty acids such as stearic, oleic, and linoleic acid have also been described.[97, 109] Triglycerides are typically hydrolyzed to produce glycerol and a mixture of fatty acids. Furthermore, these potential monomers are naturally occurring, exhibited biocompatibility, and suggested potential impact in many biomedical applications. Due to the presence of unsaturated functionality in the mixture of fatty acid monomer, these monomers are suitable for many post-reactions such as dimerization or epoxidation reactions. Similar to separation and purification difficulties for isomannides, byproduct removal presents a challenge for the large-scale production and utilization of these triglyceride-based monomers for industrial applications. Typically, fractional distillations are often employed to separate the various components of the fatty acid products. Another challenge limiting the utilization of triglycerides in step-growth polymerization is the lack of perfect difunctionality in the monomer structure.[97] Many common

fatty acid monomers only contain a single carboxylic acid site; however, ricinoleic acid, being an exception, is a naturally occurring difunctional fatty acid that is suitable for various polyester syntheses.

Current efforts have been strongly undertaken in the industry to provide a company built upon transformation of large scale chemical production based on green chemistry principles. In 2004, the United States Department of Energy compiled a list of the top 12 sugar-derived monomers that are able to compete against petrochemically derived monomers.[110] One industrial example that addressed this concern is the chemical company Segetis, whose efforts are highly dependent on expanding technology based entirely on renewable resources. Their technology centers on levulinic ester ketals, a primary bio-based precursor for many various monomers. These initiatives further comments on the importance of sustainability both in the academic and industrial scale.

2.6 *Conclusions*

Although much of this chapter focused on traditional step-growth polymers, there is a renewed interest in discovering novel monomers, functionalities, and methods for future step-growth processes. As polymer scientists, the techniques and synthetic methods used to generate traditional step-growth polymers have developed significantly since Carothers's early pioneering work. However, the principles of step-growth polymerization continue to serve as the inspiration for many new step-growth polymers. Step-growth polymers have proven to be especially useful in achieving a variety of macromolecular structures with tailored performance. In order to address future challenges in polymer science, we must tackle questions in an interdisciplinary manner. We must strive to reduce our dependency on petroleum feedstocks, and we need to

design high performance polymers with a keen attention to sustainability. Step-growth polymerization processes are excellent platforms to achieve these critical goals.

2.7 *References*

1. Carothers, W. H.; Arvin, J. A., *J. Am. Chem. Soc.* **1929,** *51* (8), 2560-2570.
2. Carothers, W. H., *J. Am. Chem. Soc.* **1929,** *51* (8), 2548-2559.
3. Rogers, M. E.; Long, T. E., *Synthetic Methods in Step-Growth Polymers*. John Wiley & Sons, Inc.: Hoboken, 2003.
4. Persson, P. V.; Casas, J.; Iversen, T.; Córdova, A., *Macromolecules* **2006,** *39* (8), 2819-2822.
5. Nadeau, V.; Leclair, G.; Sant, S.; Rabanel, J.-M.; Quesnel, R.; Hildgen, P., *Polymer* **2005,** *46* (25), 11263-11272.
6. Perepelkin, K. E., *Fibre Chemistry* **2001,** *33* (4), 249-251.
7. Odian, G., *Principles of Polymerization*. 2004.
8. Zentner, G. M.; Rathi, R.; Shih, C.; McRea, J. C.; Seo, M.-H.; Oh, H.; Rhee, B. G.; Mestecky, J.; Moldoveanu, Z.; Morgan, M.; Weitman, S., *J. Controlled Release* **2001,** *72* (1-3), 203-215.
9. Wu, D. C.; Liu, Y.; He, C. B., *Macromolecules* **2008,** *41* (1), 18-20.
10. Simon, M.; Behrens, I.; Dailey, L. A.; Wittmar, M.; Kissel, T., *European Journal of Pharmaceutics and Biopharmaceutics* **2007,** *66* (2), 165-172.
11. Honkhambe, P. N.; Bhairamadgi, N. S.; Biyani, M. V.; Wadgaonkar, P. P.; Salunkhe, M. M., *Eur. Polym. J.* **2010,** *46* (4), 709-718.
12. Pang, K.; Kotek, R.; Tonelli, A., *Prog. Polym. Sci.* **2006,** *31* (11), 1009-1037.
13. Antheunis, H.; van der Meer, J.-C.; de Geus, M.; Heise, A.; Koning, C. E., *Biomacromolecules* **2010,** *11* (4), 1118-1124.
14. Fox, T. G.; Flory, P. J., *The Journal of Physical Chemistry* **1951,** *55* (2), 221-234.
15. Carothers, W. H., *Trans. Faraday Soc.* **1936,** *32*, 39-53.
16. Scheirs, J.; Long, T. E., *Modern polyesters: Chemistry and Technology of Polyesters and Copolyesters*. John Wiley & Sons: Hoboken, NJ, 2003.
17. Kricheldorf, H. R., *Acc. Chem. Res.* **2009,** *42* (8), 981-992.
18. Billmeyer, F. W., *Textbook of Polymer Science*. Wiley: New York, 1984.
19. Wathier, M.; Jung, P. J.; Camahan, M. A.; Kim, T.; Grinstaff, M. W., *J. Am. Chem. Soc.* **2004,** *126* (40), 12744-12745.
20. García, J. M.; García, F. C.; Serna, F.; de la Peña, J. L., *Prog. Polym. Sci.* **2010,** *35* (5), 623-686.
21. Feger, C.; Khojasteh, M. M.; McGrath, J. E., *Polyimides: Materials, chemistry and characterization*. Elsevier: Amsterdam, 1989.
22. Ghosh, M. K.; Mittal, K. L., *Polyimides: Fundamentals and Applications*. Marcel Dekker: 1996.
23. Sroog, C. E., *Prog. Polym. Sci.* **1991,** *16* (4), 561-694.
24. Adrova, N. A., *Polyimides, a new class of thermally stable polymers.* Technomic Pub. co: Stamford, Conn, 1970; Vol. 7.
25. Kaas, R. L., *J. Polym. Sci., Polym. Chem. Ed.* **1981,** *19* (Copyright (C) 2010 American Chemical Society (ACS). All Rights Reserved.), 2255-67.
26. Snyder, R. W.; Sheen, C. W., *Appl. Spectrosc.* **1988,** *42* (Copyright (C) 2010 American Chemical Society (ACS). All Rights Reserved.), 655-8.
27. Jeon, J.-Y.; Tak, T.-M., *J. Appl. Polym. Sci.* **1996,** *61* (Copyright (C) 2010 American Chemical Society (ACS). All Rights Reserved.), 529-544.

28. Vinogradova, S. V.; Vygodskii, Y. S., *Faserforsch. Textiltech.* **1977,** *28* (Copyright (C) 2010 American Chemical Society (ACS). All Rights Reserved.), 581-7.
29. Odian, G., *Principles of Polymerization, 4th Edition*. 2004; p 768 pp.
30. Treier, M.; Richardson, N. V.; Fasel, R., *J. Am. Chem. Soc.* **2008,** *130* (43), 14054-14055.
31. Asano, N.; Aoki, M.; Suzuki, S.; Miyatake, K.; Uchida, H.; Watanabe, M., *J. Am. Chem. Soc.* **2006,** *128* (5), 1762-1769.
32. Noshay, A.; McGrath, J. E., *Block Copolymers: Overview and Critical Survey*. Academic Press: 1977.
33. Harrison, W. L.; Hickner, M. A.; Kim, Y. S.; McGrath, J. E., *Fuel Cells* **2005,** *5* (2), 201-212.
34. Rogers, M. E.; Long, T. E., *Synthetic Methods in Step-Growth Polymers*. 2003; p 605 pp.
35. Cohen, S. M.; Young, R. H., *J. Polym. Sci., Polym. Chem. Ed.* **1966,** *4*, 722.
36. Lee, M.; Park, J. K.; Lee, H.-S.; Lane, O.; Moore, R. B.; McGrath, J. E.; Baird, D. G., *Polymer* **2009,** *50* (25), 6129-6138.
37. Bayer, O.; Rinke, H.; Siefken, W.; Ortner, L.; Schild, H. 1942.
38. Hepburn, C., *Polyurethane Elastomers*. Elsevier Applied Science: London, 1992.
39. Puskas, J. E.; Chen, Y., *Biomacromolecules* **2004,** *5* (4), 1141-1154.
40. Yilgor, E.; Yilgor, I.; Yurtsever, E., *Polymer* **2002,** *43* (24), 6551-6559.
41. Yilgor, E.; Yurtsever, E.; Yilgor, I., *Polymer* **2002,** *43* (24), 6561-6568.
42. Yilgor, I.; Yilgor, E., *Polymer Reviews* **2007,** *47* (4), 487-510.
43. Meuler, A. J.; Hillmyer, M. A.; Bates, F. S., *Macromolecules (Washington, DC, U. S.)* **2009,** *42* (Copyright (C) 2010 American Chemical Society (ACS). All Rights Reserved.), 7221-7250.
44. Hayward, R. C.; Pochan, D. J., *Macromolecules (Washington, DC, U. S.)* **2010,** *43* (Copyright (C) 2010 American Chemical Society (ACS). All Rights Reserved.), 3577-3584.
45. Jinnai, H.; Spontak, R. J., *Polymer* **2009,** *50* (Copyright (C) 2010 American Chemical Society (ACS). All Rights Reserved.), 1067-1087.
46. Jinnai, H.; Spontak, R. J.; Nishi, T., *Macromolecules (Washington, DC, U. S.)* **2010,** *43* (Copyright (C) 2010 American Chemical Society (ACS). All Rights Reserved.), 1675-1688.
47. Tsarkova, L.; Sevink, G. J. A.; Krausch, G., *Adv. Polym. Sci.* **2010,** *227* (Copyright (C) 2010 American Chemical Society (ACS). All Rights Reserved.), 33-73.
48. Zhang, J.; Yu, X.; Yang, P.; Peng, J.; Luo, C.; Huang, W.; Han, Y., *Macromol. Rapid Commun.* **2010,** *31* (Copyright (C) 2010 American Chemical Society (ACS). All Rights Reserved.), 591-608.
49. Chang, Y.-J. P.; Wilkes, G. L., *Journal of Polymer Science: Polymer Physics Edition* **1975,** *13*, 455-476.
50. Wilkes, G. L.; Abouzahr, S., *Macromolecules* **1981,** *14* (2), 456-458.
51. Yilgor, I.; Yilgor, E.; Das, S.; Wilkes, G. L., *J. Polym. Sci., Part B: Polym. Phys.* **2009,** *47* (5), 471-483.
52. Fernandez, C. E.; Bermudez, M.; Munoz-Guerra, S.; Leon, S.; Versteegen, R. M.; Meijer, E. W., *Macromolecules* **2010,** *43* (9), 4161-4171.
53. Fenix, Y. K.; Zhang, L.; Wu, Z. Z., *Research Journal of Chemistry and Environment* **2007,** *11* (2), 78-83.
54. Liu, C.; Qin, H.; Mather, P. T., *J. Mater. Chem.* **2007,** *17* (16), 1543-1558.

55. Ratna, D.; Karger-Kocsis, J., *Journal of Materials Science* **2008,** *43* (1), 254-269.
56. Wagermaier, W.; Kratz, K.; Heuchel, M.; Lendlein, A., Characterization Methods for Shape-Memory Polymers. In *Shape-Memory Polymers*, 2010; Vol. 226, pp 97-145.
57. Yakacki, C. M.; Gall, K., Shape-Memory Polymers for Biomedical Applications. In *Shape-Memory Polymers*, 2010; Vol. 226, pp 147-175.
58. D'Hollander, S.; Van Assche, G.; Van Mele, B.; Du Prez, F., *Polymer* **2009,** *50* (19), 4447-4454.
59. D'Hollander, S.; Gommes, C. J.; Mens, R.; Adriaensens, P.; Du, P. F., *J. Mater. Chem.* **2010,** *20* (Copyright (C) 2010 American Chemical Society (ACS). All Rights Reserved.), 3475-3486.
60. Wang, W.; Jin, Y.; Ping, P.; Chen, X.; Jing, X.; Su, Z., *Macromolecules* **2010,** *43* (6), 2942-2947.
61. Jorcin, J.-B.; Scheltjens, G.; Van, I. Y.; Tourwe, E.; Van, A. G.; De, G. I.; Van, M. B.; Terryn, H.; Hubin, A., *Electrochim. Acta* **2010,** *55* (Copyright (C) 2010 American Chemical Society (ACS). All Rights Reserved.), 6195-6203.
62. Hong, S. J.; Youk, J. H.; Yu, W.-R., *Fibers Polym.* **2010,** *11* (Copyright (C) 2010 American Chemical Society (ACS). All Rights Reserved.), 749-756.
63. Halton, B., *Adv. in Ring Strain in Organic Chemistry* **1991,** *1*, 1-17.
64. de, M. A.; Kozhushkov, S. I.; Schill, H., *Chem. Rev. (Washington, DC, U. S.)* **2006,** *106* (Copyright (C) 2010 American Chemical Society (ACS). All Rights Reserved.), 4926-4996.
65. Padwa, A.; Murphree, S., *Prog. Heterocycl. Chem.* **2003,** *15* (Copyright (C) 2010 American Chemical Society (ACS). All Rights Reserved.), 75-99.
66. Ellis, B., *Chemistry and Technology of Epoxy Resins*. Chapman & Hall: London, UK, 1993.
67. McIlroy, D. A.; Blaiszik, B. J.; Caruso, M. M.; White, S. R.; Moore, J. S.; Sottos, N. R., *Macromolecules* **2010,** *43* (4), 1855-1859.
68. Du, S.; Kendall, K.; Morris, S.; Sweet, C., *J. Chem. Technol. Biotechnol.* **2010,** *85* (Copyright (C) 2010 American Chemical Society (ACS). All Rights Reserved.), 1223-1228.
69. Oyewumi, M. O.; Kumar, A.; Cui, Z., *Expert Rev. Vaccines* **2010,** *9* (Copyright (C) 2010 American Chemical Society (ACS). All Rights Reserved.), 1095-1107.
70. Taylor, A. C. In *Advances in nanoparticle reinforcement in structural adhesives*, Woodhead Publishing Ltd.: 2010; pp 151-182.
71. Zheng, J.; Cheng, G.-f.; Feng, W.-j.; He, P.-g.; Fang, Y.-z., *Huaxue Shijie* **2010,** *51* (Copyright (C) 2010 American Chemical Society (ACS). All Rights Reserved.), 310-313.
72. Pecher, J.; Mecking, S., *Macromolecules* **2007,** *40* (22), 7733-7735.
73. Baier, M. C.; Huber, J.; Mecking, S., *J. Am. Chem. Soc.* **2009,** *131* (40), 14267-14273.
74. Klapper, M.; Nenov, S.; Haschick, R.; Müller, K.; Müllen, K., *Acc. Chem. Res.* **2008,** *41* (9), 1190-1201.
75. Kobayashi, S., *Proceedings of the Japan Academy, Series B* **2010,** *86* (4), 338-365.
76. MacDonald, R. T.; Pulapura, S. K.; Svirkin, Y. Y.; Gross, R. A.; Kaplan, D. L.; Akkara, J.; Swift, G.; Wolk, S., *Macromolecules* **1995,** *28* (1), 73-78.
77. Knani, D.; Gutman, A. L.; Kohn, D. H., *J. Polym. Sci., Part A: Polym. Chem.* **1993,** *31* (5), 1221-1232.

78. Henderson, L. A.; Svirkin, Y. Y.; Gross, R. A.; Kaplan, D. L.; Swift, G., *Macromolecules* **1996,** *29* (24), 7759-7766.
79. Varma, I. K.; Albertsson, A.-C.; Rajkhowa, R.; Srivastava, R. K., *Prog. Polym. Sci.* **2005,** *30* (10), 949-981.
80. Gotor-Fernández, V.; Busto, E.; Gotor, V., *Adv. Synth. Catal.* **2006,** *348* (7-8), 797-812.
81. Fu, H.; Kulshrestha, A. S.; Gao, W.; Gross, R. A.; Baiardo, M.; Scandola, M., *Macromolecules* **2003,** *36* (26), 9804-9808.
82. Chen, B.; Hu, J.; Miller, E. M.; Xie, W.; Cai, M.; Gross, R. A., *Biomacromolecules* **2008,** *9* (2), 463-471.
83. Kobayashi, S., *Macromol. Rapid Commun.* **2009,** *30* (4-5), 237-266.
84. Mahapatro, A.; Kumar, A.; Kalra, B.; Gross, R. A., *Macromolecules* **2003,** *37* (1), 35-40.
85. Skaria, S.; Smet, M.; Frey, H., *Macromol. Rapid Commun.* **2002,** *23* (4), 292-296.
86. Kulshrestha, A. S.; Gao, W.; Fu, H.; Gross, R. A., *Biomacromolecules* **2007,** *8* (6), 1794-1801.
87. Kalra, B.; Kumar, A.; Gross, R. A.; Baiardo, M.; Scandola, M., *Macromolecules* **2004,** *37* (4), 1243-1250.
88. Kumar, A.; Gross, R. A.; Wang, Y.; Hillmyer, M. A., *Macromolecules* **2002,** *35* (20), 7606-7611.
89. Srivastava, R. K.; Albertsson, A.-C., *Macromolecules* **2005,** *39* (1), 46-54.
90. Dai, S.; Li, Z., *Biomacromolecules* **2008,** *9* (7), 1883-1893.
91. Frampton, M. B.; Subczynska, I.; Zelisko, P. M., *Biomacromolecules* **2010,** *11* (7), 1818-1825.
92. Zhao, Q.; Wang, S.; Cheng, X.; Yam, R. C. M.; Kong, D.; Li, R. K. Y., *Biomacromolecules* **2010,** *11* (5), 1364-1369.
93. Wolf, F. K.; Hofmann, A. M.; Frey, H., *Macromolecules* **2010,** *43* (7), 3314-3324.
94. Raquez, J. M.; Deléglise, M.; Lacrampe, M. F.; Krawczak, P., *Prog. Polym. Sci.* **2010,** *35* (4), 487-509.
95. Ma, X.; Tang, J.; Shen, Y.; Fan, M.; Tang, H.; Radosz, M., *J. Am. Chem. Soc.* **2009,** *131* (41), 14795-14803.
96. Williams, C. K.; Hillmyer, M. A., *Polymer Reviews* **2008,** *48* (1), 1-10.
97. Fenouillot, F.; Rousseau, A.; Colomines, G.; Saint-Loup, R.; Pascault, J. P., *Prog. Polym. Sci.* **2010,** *35* (5), 578-622.
98. Shen, L.; Worrell, E.; Patel, M., *Biofuels, Bioproducts and Biorefining* **2010,** *4* (1), 25-40.
99. Lin, Q.; Pasatta, J.; Long, T. E., *Journal of Polymer Science Part A: Polymer Chemistry* **2003,** *41* (16), 2512-2520.
100. Braun, D.; Bergmann, M., *J. Prakt. Chem.* **1992,** *334*, 298.
101. Storbeck, R.; Rehahn, M.; Ballauff, M., *Makrolmol. Chem.* **1993,** *194*, 53.
102. Ozturk, G.; Long, T. E., *J. Polym. Sci., Part A: Polym. Chem.* **2009,** *47* (20), 5437-5447.
103. Pan, P.; Inoue, Y., *Prog. Polym. Sci.* **2009,** *34* (7), 605-640.
104. Rasal, R. M.; Janorkar, A. V.; Hirt, D. E., *Prog. Polym. Sci.* **2010,** *35* (3), 338-356.
105. Garaleh, M.; Yashiro, T.; Kricheldorf, H. R.; Simon, P.; Chatti, S., *Macromol. Chem. Phys.* **2010,** *211* (11), 1206-1214.
106. Wanamaker, C. L.; O'Leary, L. E.; Lynd, N. A.; Hillmyer, M. A.; Tolman, W. B., *Biomacromolecules* **2007,** *8* (11), 3634-3640.

107. Wanamaker, C. L.; Tolman, W. B.; Hillmyer, M. A., *Biomacromolecules* **2009,** *10* (2), 443-448.
108. Wanamaker, C. L.; Tolman, W. B.; Hillmyer, M. A., *Macromolecular Symposia* **2009,** *283-284* (1), 130-138.
109. Fornof, A. R., *PMSE Preprints* **2004,** *90*.
110. Desai, S., *Chemistry and industry (London)* **2010,** (2), 21.

(1) Carothers, W. H.; Arvin, J. A., *J. Am. Chem. Soc.* **1929,** *51* (8), 2560-2570.
(2) Carothers, W. H., *J. Am. Chem. Soc.* **1929,** *51* (8), 2548-2559.
(3) Rogers, M. E.; Long, T. E., *Synthetic Methods in Step-Growth Polymers*. John Wiley & Sons, Inc.: Hoboken, 2003.
(4) Persson, P. V.; Casas, J.; Iversen, T.; Córdova, A., *Macromolecules* **2006,** *39* (8), 2819-2822.
(5) Nadeau, V.; Leclair, G.; Sant, S.; Rabanel, J.-M.; Quesnel, R.; Hildgen, P., *Polymer* **2005,** *46* (25), 11263-11272.
(6) Perepelkin, K. E., *Fibre Chemistry* **2001,** *33* (4), 249-251.
(7) Odian, G., *Principles of Polymerization*. 2004.
(8) Zentner, G. M.; Rathi, R.; Shih, C.; McRea, J. C.; Seo, M.-H.; Oh, H.; Rhee, B. G.; Mestecky, J.; Moldoveanu, Z.; Morgan, M.; Weitman, S., *J. Controlled Release* **2001,** *72* (1-3), 203-215.
(9) Wu, D. C.; Liu, Y.; He, C. B., *Macromolecules* **2008,** *41* (1), 18-20.
(10) Simon, M.; Behrens, I.; Dailey, L. A.; Wittmar, M.; Kissel, T., *European Journal of Pharmaceutics and Biopharmaceutics* **2007,** *66* (2), 165-172.
(11) Honkhambe, P. N.; Bhairamadgi, N. S.; Biyani, M. V.; Wadgaonkar, P. P.; Salunkhe, M. M., *Eur. Polym. J.* **2010,** *46* (4), 709-718.
(12) Pang, K.; Kotek, R.; Tonelli, A., *Prog. Polym. Sci.* **2006,** *31* (11), 1009-1037.
(13) Antheunis, H.; van der Meer, J.-C.; de Geus, M.; Heise, A.; Koning, C. E., *Biomacromolecules* **2010,** *11* (4), 1118-1124.
(14) Fox, T. G.; Flory, P. J., *The Journal of Physical Chemistry* **1951,** *55* (2), 221-234.
(15) Carothers, W. H., *Trans. Faraday Soc.* **1936,** *32*, 39-53.
(16) Scheirs, J.; Long, T. E., *Modern polyesters: Chemistry and Technology of Polyesters and Copolyesters*. John Wiley & Sons: Hoboken, NJ, 2003.
(17) Kricheldorf, H. R., *Acc. Chem. Res.* **2009,** *42* (8), 981-992.
(18) Billmeyer, F. W., *Textbook of Polymer Science*. Wiley: New York, 1984.
(19) Wathier, M.; Jung, P. J.; Camahan, M. A.; Kim, T.; Grinstaff, M. W., *J. Am. Chem. Soc.* **2004,** *126* (40), 12744-12745.
(20) García, J. M.; García, F. C.; Serna, F.; de la Peña, J. L., *Prog. Polym. Sci.* **2010,** *35* (5), 623-686.
(21) Feger, C.; Khojasteh, M. M.; McGrath, J. E., *Polyimides: Materials, chemistry and characterization*. Elsevier: Amsterdam, 1989.
(22) Ghosh, M. K.; Mittal, K. L., *Polyimides: Fundamentals and Applications*. Marcel Dekker: 1996.
(23) Sroog, C. E., *Prog. Polym. Sci.* **1991,** *16* (4), 561-694.

(24) Adrova, N. A., *Polyimides, a new class of thermally stable polymers.* Technomic Pub. co: Stamford, Conn, 1970; Vol. 7.
(25) Kaas, R. L., *J. Polym. Sci., Polym. Chem. Ed.* **1981,** *19* (Copyright (C) 2010 American Chemical Society (ACS). All Rights Reserved.), 2255-67.
(26) Snyder, R. W.; Sheen, C. W., *Appl. Spectrosc.* **1988,** *42* (Copyright (C) 2010 American Chemical Society (ACS). All Rights Reserved.), 655-8.
(27) Jeon, J.-Y.; Tak, T.-M., *J. Appl. Polym. Sci.* **1996,** *61* (Copyright (C) 2010 American Chemical Society (ACS). All Rights Reserved.), 529-544.
(28) Vinogradova, S. V.; Vygodskii, Y. S., *Faserforsch. Textiltech.* **1977,** *28* (Copyright (C) 2010 American Chemical Society (ACS). All Rights Reserved.), 581-7.
(29) Odian, G., *Principles of Polymerization, 4th Edition*. 2004; p 768 pp.
(30) Treier, M.; Richardson, N. V.; Fasel, R., *J. Am. Chem. Soc.* **2008,** *130* (43), 14054-14055.
(31) Asano, N.; Aoki, M.; Suzuki, S.; Miyatake, K.; Uchida, H.; Watanabe, M., *J. Am. Chem. Soc.* **2006,** *128* (5), 1762-1769.
(32) Noshay, A.; McGrath, J. E., *Block Copolymers: Overview and Critical Survey*. Academic Press: 1977.
(33) Harrison, W. L.; Hickner, M. A.; Kim, Y. S.; McGrath, J. E., *Fuel Cells* **2005,** *5* (2), 201-212.
(34) Rogers, M. E.; Long, T. E., *Synthetic Methods in Step-Growth Polymers*. 2003; p 605 pp.
(35) Cohen, S. M.; Young, R. H., *J. Polym. Sci., Polym. Chem. Ed.* **1966,** *4*, 722.
(36) Lee, M.; Park, J. K.; Lee, H.-S.; Lane, O.; Moore, R. B.; McGrath, J. E.; Baird, D. G., *Polymer* **2009,** *50* (25), 6129-6138.
(37) Bayer, O.; Rinke, H.; Siefken, W.; Ortner, L.; Schild, H. 1942.
(38) Hepburn, C., *Polyurethane Elastomers*. Elsevier Applied Science: London, 1992.
(39) Puskas, J. E.; Chen, Y., *Biomacromolecules* **2004,** *5* (4), 1141-1154.
(40) Yilgor, E.; Yilgor, I.; Yurtsever, E., *Polymer* **2002,** *43* (24), 6551-6559.
(41) Yilgor, E.; Yurtsever, E.; Yilgor, I., *Polymer* **2002,** *43* (24), 6561-6568.
(42) Yilgor, I.; Yilgor, E., *Polymer Reviews* **2007,** *47* (4), 487-510.
(43) Meuler, A. J.; Hillmyer, M. A.; Bates, F. S., *Macromolecules (Washington, DC, U. S.)* **2009,** *42* (Copyright (C) 2010 American Chemical Society (ACS). All Rights Reserved.), 7221-7250.
(44) Hayward, R. C.; Pochan, D. J., *Macromolecules (Washington, DC, U. S.)* **2010,** *43* (Copyright (C) 2010 American Chemical Society (ACS). All Rights Reserved.), 3577-3584.
(45) Jinnai, H.; Spontak, R. J., *Polymer* **2009,** *50* (Copyright (C) 2010 American Chemical Society (ACS). All Rights Reserved.), 1067-1087.
(46) Jinnai, H.; Spontak, R. J.; Nishi, T., *Macromolecules (Washington, DC, U. S.)* **2010,** *43* (Copyright (C) 2010 American Chemical Society (ACS). All Rights Reserved.), 1675-1688.
(47) Tsarkova, L.; Sevink, G. J. A.; Krausch, G., *Adv. Polym. Sci.* **2010,** *227* (Copyright (C) 2010 American Chemical Society (ACS). All Rights Reserved.), 33-73.
(48) Zhang, J.; Yu, X.; Yang, P.; Peng, J.; Luo, C.; Huang, W.; Han, Y., *Macromol. Rapid Commun.* **2010,** *31* (Copyright (C) 2010 American Chemical Society (ACS). All Rights Reserved.), 591-608.
(49) Chang, Y.-J. P.; Wilkes, G. L., *Journal of Polymer Science: Polymer Physics Edition* **1975,** *13*, 455-476.

(50) Wilkes, G. L.; Abouzahr, S., *Macromolecules* **1981,** *14* (2), 456-458.
(51) Yilgor, I.; Yilgor, E.; Das, S.; Wilkes, G. L., *J. Polym. Sci., Part B: Polym. Phys.* **2009,** *47* (5), 471-483.
(52) Fernandez, C. E.; Bermudez, M.; Munoz-Guerra, S.; Leon, S.; Versteegen, R. M.; Meijer, E. W., *Macromolecules* **2010,** *43* (9), 4161-4171.
(53) Fenix, Y. K.; Zhang, L.; Wu, Z. Z., *Research Journal of Chemistry and Environment* **2007,** *11* (2), 78-83.
(54) Liu, C.; Qin, H.; Mather, P. T., *J. Mater. Chem.* **2007,** *17* (16), 1543-1558.
(55) Ratna, D.; Karger-Kocsis, J., *Journal of Materials Science* **2008,** *43* (1), 254-269.
(56) Wagermaier, W.; Kratz, K.; Heuchel, M.; Lendlein, A., Characterization Methods for Shape-Memory Polymers. In *Shape-Memory Polymers*, 2010; Vol. 226, pp 97-145.
(57) Yakacki, C. M.; Gall, K., Shape-Memory Polymers for Biomedical Applications. In *Shape-Memory Polymers*, 2010; Vol. 226, pp 147-175.
(58) D'Hollander, S.; Van Assche, G.; Van Mele, B.; Du Prez, F., *Polymer* **2009,** *50* (19), 4447-4454.
(59) D'Hollander, S.; Gommes, C. J.; Mens, R.; Adriaensens, P.; Du, P. F., *J. Mater. Chem.* **2010,** *20* (Copyright (C) 2010 American Chemical Society (ACS). All Rights Reserved.), 3475-3486.
(60) Wang, W.; Jin, Y.; Ping, P.; Chen, X.; Jing, X.; Su, Z., *Macromolecules* **2010,** *43* (6), 2942-2947.
(61) Jorcin, J.-B.; Scheltjens, G.; Van, I. Y.; Tourwe, E.; Van, A. G.; De, G. I.; Van, M. B.; Terryn, H.; Hubin, A., *Electrochim. Acta* **2010,** *55* (Copyright (C) 2010 American Chemical Society (ACS). All Rights Reserved.), 6195-6203.
(62) Hong, S. J.; Youk, J. H.; Yu, W.-R., *Fibers Polym.* **2010,** *11* (Copyright (C) 2010 American Chemical Society (ACS). All Rights Reserved.), 749-756.
(63) Halton, B., *Adv. in Ring Strain in Organic Chemistry* **1991,** *1*, 1-17.
(64) de, M. A.; Kozhushkov, S. I.; Schill, H., *Chem. Rev. (Washington, DC, U. S.)* **2006,** *106* (Copyright (C) 2010 American Chemical Society (ACS). All Rights Reserved.), 4926-4996.
(65) Padwa, A.; Murphree, S., *Prog. Heterocycl. Chem.* **2003,** *15* (Copyright (C) 2010 American Chemical Society (ACS). All Rights Reserved.), 75-99.
(66) Ellis, B., *Chemistry and Technology of Epoxy Resins*. Chapman & Hall: London, UK, 1993.
(67) McIlroy, D. A.; Blaiszik, B. J.; Caruso, M. M.; White, S. R.; Moore, J. S.; Sottos, N. R., *Macromolecules* **2010,** *43* (4), 1855-1859.
(68) Du, S.; Kendall, K.; Morris, S.; Sweet, C., *J. Chem. Technol. Biotechnol.* **2010,** *85* (Copyright (C) 2010 American Chemical Society (ACS). All Rights Reserved.), 1223-1228.
(69) Oyewumi, M. O.; Kumar, A.; Cui, Z., *Expert Rev. Vaccines* **2010,** *9* (Copyright (C) 2010 American Chemical Society (ACS). All Rights Reserved.), 1095-1107.
(70) Taylor, A. C. In *Advances in nanoparticle reinforcement in structural adhesives*, Woodhead Publishing Ltd.: 2010; pp 151-182.
(71) Zheng, J.; Cheng, G.-f.; Feng, W.-j.; He, P.-g.; Fang, Y.-z., *Huaxue Shijie* **2010,** *51* (Copyright (C) 2010 American Chemical Society (ACS). All Rights Reserved.), 310-313.
(72) Pecher, J.; Mecking, S., *Macromolecules* **2007,** *40* (22), 7733-7735.
(73) Baier, M. C.; Huber, J.; Mecking, S., *J. Am. Chem. Soc.* **2009,** *131* (40), 14267-14273.

(74) Klapper, M.; Nenov, S.; Haschick, R.; Müller, K.; Müllen, K., *Acc. Chem. Res.* **2008,** *41* (9), 1190-1201.
(75) Number, I.-I. P.; A1, W.; Crawford, E.
(76) Kobayashi, S., *Proceedings of the Japan Academy, Series B* **2010,** *86* (4), 338-365.
(77) MacDonald, R. T.; Pulapura, S. K.; Svirkin, Y. Y.; Gross, R. A.; Kaplan, D. L.; Akkara, J.; Swift, G.; Wolk, S., *Macromolecules* **1995,** *28* (1), 73-78.
(78) Knani, D.; Gutman, A. L.; Kohn, D. H., *J. Polym. Sci., Part A: Polym. Chem.* **1993,** *31* (5), 1221-1232.
(79) Henderson, L. A.; Svirkin, Y. Y.; Gross, R. A.; Kaplan, D. L.; Swift, G., *Macromolecules* **1996,** *29* (24), 7759-7766.
(80) Varma, I. K.; Albertsson, A.-C.; Rajkhowa, R.; Srivastava, R. K., *Prog. Polym. Sci.* **2005,** *30* (10), 949-981.
(81) Gotor-Fernández, V.; Busto, E.; Gotor, V., *Adv. Synth. Catal.* **2006,** *348* (7-8), 797-812.
(82) Fu, H.; Kulshrestha, A. S.; Gao, W.; Gross, R. A.; Baiardo, M.; Scandola, M., *Macromolecules* **2003,** *36* (26), 9804-9808.
(83) Chen, B.; Hu, J.; Miller, E. M.; Xie, W.; Cai, M.; Gross, R. A., *Biomacromolecules* **2008,** *9* (2), 463-471.
(84) Kobayashi, S., *Macromol. Rapid Commun.* **2009,** *30* (4-5), 237-266.
(85) Mahapatro, A.; Kumar, A.; Kalra, B.; Gross, R. A., *Macromolecules* **2003,** *37* (1), 35-40.
(86) Skaria, S.; Smet, M.; Frey, H., *Macromol. Rapid Commun.* **2002,** *23* (4), 292-296.
(87) Kulshrestha, A. S.; Gao, W.; Fu, H.; Gross, R. A., *Biomacromolecules* **2007,** *8* (6), 1794-1801.
(88) Kalra, B.; Kumar, A.; Gross, R. A.; Baiardo, M.; Scandola, M., *Macromolecules* **2004,** *37* (4), 1243-1250.
(89) Kumar, A.; Gross, R. A.; Wang, Y.; Hillmyer, M. A., *Macromolecules* **2002,** *35* (20), 7606-7611.
(90) Srivastava, R. K.; Albertsson, A.-C., *Macromolecules* **2005,** *39* (1), 46-54.
(91) Dai, S.; Li, Z., *Biomacromolecules* **2008,** *9* (7), 1883-1893.
(92) Frampton, M. B.; Subczynska, I.; Zelisko, P. M., *Biomacromolecules* **2010,** *11* (7), 1818-1825.
(93) Zhao, Q.; Wang, S.; Cheng, X.; Yam, R. C. M.; Kong, D.; Li, R. K. Y., *Biomacromolecules* **2010,** *11* (5), 1364-1369.
(94) Wolf, F. K.; Hofmann, A. M.; Frey, H., *Macromolecules* **2010,** *43* (7), 3314-3324.
(95) Raquez, J. M.; Deléglise, M.; Lacrampe, M. F.; Krawczak, P., *Prog. Polym. Sci.* **2010,** *35* (4), 487-509.
(96) Ma, X.; Tang, J.; Shen, Y.; Fan, M.; Tang, H.; Radosz, M., *J. Am. Chem. Soc.* **2009,** *131* (41), 14795-14803.
(97) Williams, C. K.; Hillmyer, M. A., *Polymer Reviews* **2008,** *48* (1), 1-10.
(98) Fenouillot, F.; Rousseau, A.; Colomines, G.; Saint-Loup, R.; Pascault, J. P., *Prog. Polym. Sci.* **2010,** *35* (5), 578-622.
(99) Shen, L.; Worrell, E.; Patel, M., *Biofuels, Bioproducts and Biorefining* **2010,** *4* (1), 25-40.
(100) Lin, Q.; Pasatta, J.; Long, T. E., *Journal of Polymer Science Part A: Polymer Chemistry* **2003,** *41* (16), 2512-2520.
(101) Braun, D.; Bergmann, M., *J. Prakt. Chem.* **1992,** *334*, 298.
(102) Storbeck, R.; Rehahn, M.; Ballauff, M., *Makrolmol. Chem.* **1993,** *194*, 53.
(103) Ozturk, G.; Long, T. E., *J. Polym. Sci., Part A: Polym. Chem.* **2009,** *47* (20), 5437-5447.

(104) Pan, P.; Inoue, Y., *Prog. Polym. Sci.* **2009,** *34* (7), 605-640.
(105) Rasal, R. M.; Janorkar, A. V.; Hirt, D. E., *Prog. Polym. Sci.* **2010,** *35* (3), 338-356.
(106) Garaleh, M.; Yashiro, T.; Kricheldorf, H. R.; Simon, P.; Chatti, S., *Macromol. Chem. Phys.* **2010,** *211* (11), 1206-1214.
(107) Wanamaker, C. L.; O'Leary, L. E.; Lynd, N. A.; Hillmyer, M. A.; Tolman, W. B., *Biomacromolecules* **2007,** *8* (11), 3634-3640.
(108) Wanamaker, C. L.; Tolman, W. B.; Hillmyer, M. A., *Biomacromolecules* **2009,** *10* (2), 443-448.
(109) Wanamaker, C. L.; Tolman, W. B.; Hillmyer, M. A., *Macromolecular Symposia* **2009,** *283-284* (1), 130-138.
(110) Fornof, A. R., *PMSE Preprints* **2004,** *90*.
(111) Desai, S., *Chemistry and industry (London)* **2010,** (2), 21.

Chapter 3: Stimuli-Responsive Hydrogels for Controlled Insulin Delivery

3.1 *Abstract*

Insulin therapy plays a critical role in controlling blood glucose levels at healthy levels for diabetic patients. Unfortunately, conventional insulin delivery lacks the delicate balance of self-regulation that the body achieves flawlessly for non-diabetic patients. Biomedical polymers such as environment-sensitive polymers offer responsive properties that are sensitive to the changing environment for controlled insulin delivery. New systems including thermo-, pH-, and glucose-responsive hydrogels present attractive advantages for emerging oral and insulin delivery. Moreover, the synergy of charged polymers with potential biodegradability for block copolymer and polymer networks is relatively unexplored for insulin delivery.

3.2 *Introduction*

Insulin is an important peptide hormone for glucose homeostasis produced within the Beta-cells of the pancreas.[1-3] Although there are several hormones and signaling molecules that increase blood glucose such as glucagon,[4, 5] catecholamine,[3, 6] growth hormone,[7, 8] vasopressin,[9, 10] and corticosteroids,[11] only insulin possesses the capability to lower blood glucose levels.[3, 12] The insulin monomer is an asymmetric heterodimer protein comprised of an A-chain of 21 amino acids and a B-chain of 30 amino acids covalently linked together through two disulfide bonds .[13]

The entire chain of insulin is first synthesized in the body as the inactive preproinsulin form that contains a C-chain, the two active A and B chains, and a N-terminal sequence.[14] Post-translational modification cleaves the N-terminal sequence and C-chain.[15] The A-chain contains two α-helices while the B-chain contains one α-helix. Insulin contains three critical disulfide bonds that largely affect its activity. Two disulfide bonds connect the A and B chains at the A7-B7 and A20-B19 positions. The hydrophobic core of insulin surrounds the buried intramolecular A6-A11 disulfide bond.[2]

Moreover, insulin monomers form dimers; however, only the monomeric form stimulates activity. The insulin monomer consists of a hydrophobic core and a mostly hydrophilic surface. Hydrophobic surfaces are buried during dimer and hexamer formation. Three dimers are octahedrally coordinated into hexamers through two zinc(II) ions located on the threefold axis.[16, 17] Each zinc ion coordinates to three histadine residues (HisB10) and three water molecules. The hexameric formation relies heavily on the hydrogen-bonding interactions between glutamic acid residues (GluB13) and water molecules. The central portion of the hexamers that contains three layers of water perpendicular to the three-fold axis.[1] Hexamers associate at high insulin concentrations and pack to form rhombohedral crystals.[2, 17] Each rhombohedral unit cell

contains six molecules of insulin. The hexameric form embodies the main method of insulin storage within Beta-cell granules and blood stream. However, insulin dissociates into dimers and tetramers depending on protein concentration and pH. For example, insulin assembles into tetramers at pH 3 and dimers or monomers at pH 1.6-2.0.[18]

Insulin is a peptide hormone that acts as a signaling molecule. Insulin receptors found in the muscle and liver cells bind insulin and activate a signal transduction in the P1-3 kinase pathway for the translocation of GLUT-4 containing vesicles within the cytoplasm to the plasma membrane. GLUT-4 transmembrane proteins around the plasma membrane sequester glucose from the blood stream. Polymeric delivery systems aim to release insulin in a controlled and responsive manner similar. Polymer composition, molecular weight, and architecture all affect the structure-property relationship of insulin drug delivery.

3.3 *Challenges in Insulin Delivery*

The conventional method of insulin delivery is through transdermal injections. Although this method offers the most direct way to deliver insulin into the blood stream without potential degradation, the method also elicits painful and inconvenient therapeutic relief for patients.[19, 20] In addition, the release profile of insulin reveals an initial burst effect that causes the patient to be shortly hypoglycemic. The transdermal delivery of insulin in no way resembles the insulin release profile of a healthy individual without the aid of polymer delivery systems.

Polymer delivery systems for insulin reduces this burst effect and extend insulin residence within the blood stream. In addition to these advantages, polymer systems protect the insulin protein from proteases found within the gastrointestinal tract and allow one to exploit oral delivery of insulin. Because proper protein structure directly relates to its activity, the delivery

system must preserve the integrity of the protein folding. Protein misfolding eliminates its activity or present adverse side effects.[21] The goal of insulin-carrying polymer systems is to protect the protein during delivery for a regulated and triggered release.

Oral delivery of insulin provides the most socially accepted, non-invasive, and high compliance method for patients. Unfortunately, transporting protein drugs through the gastrointestinal tract (GIT) presents challenges such as low bioavailability. In particular, acidic pH, trypsin, pepsin, and other proteases residing within the stomach impart harsh conditions for protein drugs. Once the polymer-protein system proceeds from the stomach, it must once again endure pH changes in the small intestine.

The small intestine, although not as harsh in pH conditions as the stomach, presents different challenges. Enterocytes and goblet cells comprise the epithelium of the small intestine. Tight junctions surrounding enterocytes maintain the structural integrity of the epithelium and avert the passage of pathogens while allowing nutrients to be absorbed. Goblet cells produce a mucosal layer that prevents protein and peptide drugs from crossing the epithelial layer. M-cells located within the Peyer's patches of the small intestine increases uptake of peptide and vaccine drugs when associated with polymer drug carrying systems.[22-25] M-cells take up particles smaller than 10 μm; however, particles smaller than five μm are transported to the lymphatic system. Furthermore, drug delivery within the small intestine is transient, which may limit drug bioavailability.[26, 27]

Polymer systems offer many advantages to drug delivery systems. Specialized properties such as triggered[28-30], targeted[22-24] or prolonged release[31-33], allow for controlled or responsive drug delivery systems. Crosslinked hydrogels for drug entrapment is a major area in research that is heavily investigated for responsive and targeted insulin delivery.[19]

3.4 *Hydrogels in Insulin Delivery*

Hydrogels are 3-dimensional physical or chemical crosslinked networks that swell in aqueous solutions.[33-35] Hydrogels are commonly exploited for drug delivery due to their similarity to extracellular matrix, high biocompatibility through high water uptake, and porous structure for drug loading.[33] Moreover, polymer hydrophilicity, [33, 35, 36] composition, [37, 38] and crosslink density[39-42] largely affect the water content and swelling behavior. The kinetics of drug elution from hydrogels typically displayed Fickian diffusion whereby the rate of diffusion is first-order.[43, 44] Physical crosslinked networks with environment responsive properties achieved zero-order diffusion.[12, 45, 46]

Similar to surfactants, block copolymers spontaneously formed micelles depending on the hydrophobic and hydrophilic properties of the block and the solvating medium.[47-49] Amphiphilic block copolymers form spontaneous micelles[50] or hydrogels within aqueous mediums.[51] The size of the micelle depends on the composition of the block copolymer as well as the molar percent of hydrophilic block.[49] Hydrogels are of particular interest due to their ability to impart triggerable or responsive properties that change the structural character of the polymer.[36] This type of structural change could be a result of physiological changes,[29, 35, 52] biological factors,[36, 53] or external stimuli.[29, 31, 54] "Smart" or responsive hydrogel systems facilitates drug delivery through sustained and responsive release that mimics the metabolic system within the body.

3.4.1 Temperature-Responsive Hydrogels

Temperature-sensitive hydrogels have found wide use for their potential in subcutaneous injection drug delivery system.[37, 55-57] These systems reversibly converts from a gel state to a soluble state at a specific temperature called the phase transition temperature (T_p).[58, 59] Gelation describes the state in which polymer does not flow. The T_p stimulates changes in the hydrophobic interaction with the solvating medium, such as water, to facilitate sol-gel phase transition. These polymers were typically employed for injectable drug-delivery hydrogel systems for prolonged therapeutic relief.[57] Temperature-sensitive polymers are suitable for injectable drugs, because they transition from a liquid phase at room temperature to a gel at physiological temperature. The gel matrix prolongs the diffusion of insulin and eliminates the need for multiple injections for treatment.[60]

Temperature-sensitive hydrogels were typically comprised of amphiphilic blocks. Changes in the intermolecular interaction of hydrophobic groups versus hydrogen bonding to the solvent controlled the mechanism of the sol-gel transition.[61] Polymers, which have lower critical solution temperatures (LCST), exhibited T_p's close to body temperature and lost solubility as temperature increases.[35] At low temperatures, hydrogen-bonding interactions with the solvent dominated and resulted in a water-soluble polymer. At high temperatures, hydrophobic interactions within the polymer chain promoted aggregation of hydrophobic blocks into micelle-like structures and form reversible gels.[62-64]

Scheme 3.1. Synthesis of thermo-responsive biodegradable hydrogels from PEG and PLLA.

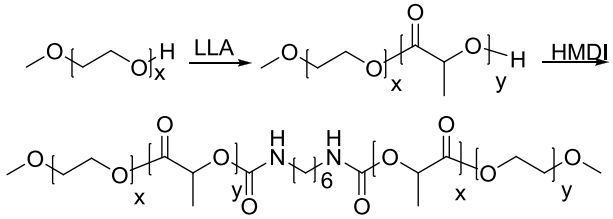

Early investigations on thermoreversible homopolymer and copolymer systems contained *N*-isopropylacrylamide[58, 65-67] and poly(ethylene oxide-*b*-propylene oxide-*b*-ethylene oxide) poly(PEG-*b*-PPO-*b*-PEG)[68-71]. However, these systems were toxic or nonbiodegradable and required surgical implantation.[72] The resulting copolymer and model protein drug, fluorescein isothiocyanate (FITC) labeled dextran, was soluble in aqueous solutions above 45 °C and entrapped within the hydrogel upon lowering the temperature to 37 °C. Since the drug loading procedure avoided the use of harsh solvents, the resulting polymer system was appropriate for large protein drug delivery. Moreover, **Figure 3.1** revealed simple changes in the drug and water content within the hydrogels induced noticeable differences in drug release. The authors suggested that mechanism insulin release occurs first through diffusion then degradation of the PLLA block.

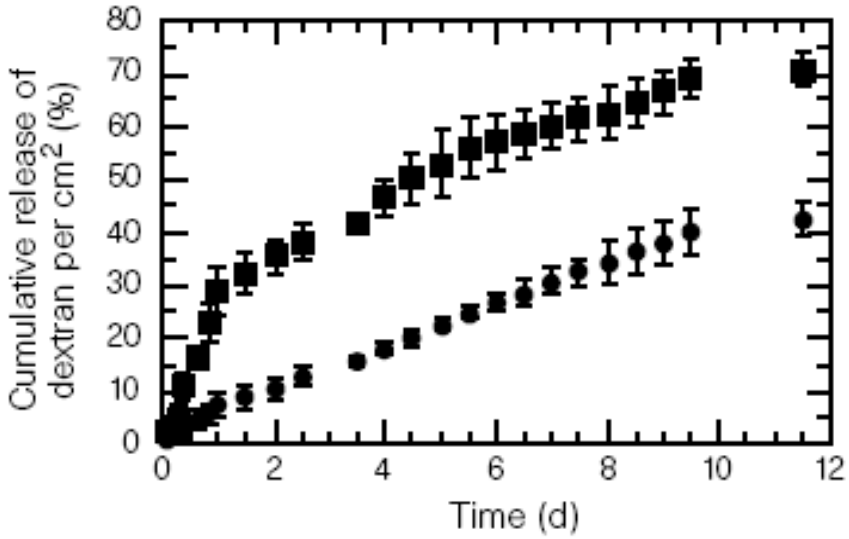

Figure 3.1 *In vitro* release of FITC labeled dextran. Filled squares and circles represent 23 and 35 weight% of polymer, respectively.[73]

Thermo-reversible biodegradable triblock hydrogels composed of poly(lactide-*co*-glycolide) (PLGA) and PEG have previously been described.[62, 64, 74] Aqueous-soluble polymers

spontaneously gelled at physiological temperature and remained within the body for approximately 4-6 weeks.[73] Temperature-sensitive block copolymers integrated PEG due to its low glass transition temperature, hydrophilicity, and biocompatibility. The triblock systems did not rely on chemical crosslinks and combined desirable properties from each constitutive segment. In this case, PEG contributed to the soluble block while PLGA added a biodegradable component for sustained insulin release through both diffusion and degradation. Because of their long residence time within the body, these polymers improved long-term injectable biomaterial for protein and poorly soluble drugs delivery.[64]

The drug release profiles of thermal responsive PLGA-PEG-PLGA triblocks for controlled release of protein and water-insoluble delivering thermal gels were dependent on the composition and molar content of PEG (**Table 3.1**).[73] Because hydrophobic and non-covalent interactions regulated gelation, there was no change in gelation after repetitive sol-gel interconversion.[64] Moreover, **Figure 3.2** indicated that the complex viscosity of the polymer in the sol state was independent of frequency or temperature until the gelation temperature was reached.[73] During the sol-gel transition, the viscosity increased four orders of magnitude. Although ReGel-1 and ReGel2 had the same composition, varying the PEG molecular weight and molar ratio of DL-lactide generated marked effects on insulin diffusion properties (**Figure 3.3**). ReGel-2 exhibited a much slower insulin release rate compared to ReGel-1.

Table 3.1 Two PLGA-PEG-PLGA polymers were synthesized from varying PEG molecular weights and molar ratios of DL-lactide: glycolide.

Polymer Composition	PEG M_n (g/mol)	DL-Lactide: Glycolide (molar ratio)	M_w (GPC)	PDI
ReGel-1	1000	3:1	4,200	1.3
ReGel-2	1450	4:1	---	---

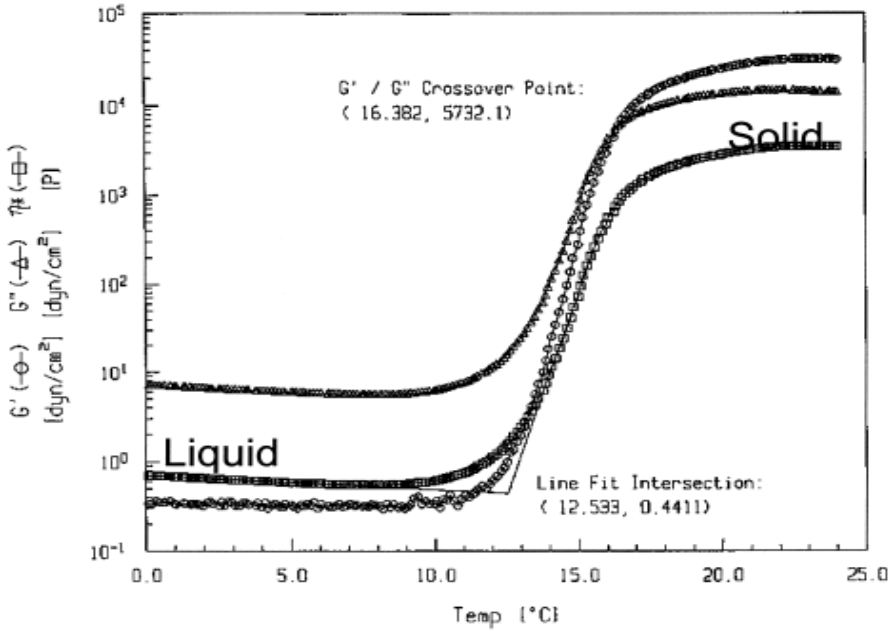

Figure 3.2. Shear storage modulus (G'), shear loss modulus (G"), and complex viscosity (ŋ*) show clear changes indicating the gelation temperature and sol-gel transition.[75] Reprinted with permission from Brahim, S.; Narinesingh, D.; Guiseppi-Elie, A., *Biomacromolecules* 2003, *4* (3), 497-503. Copyright 2003 American Chemical Society.

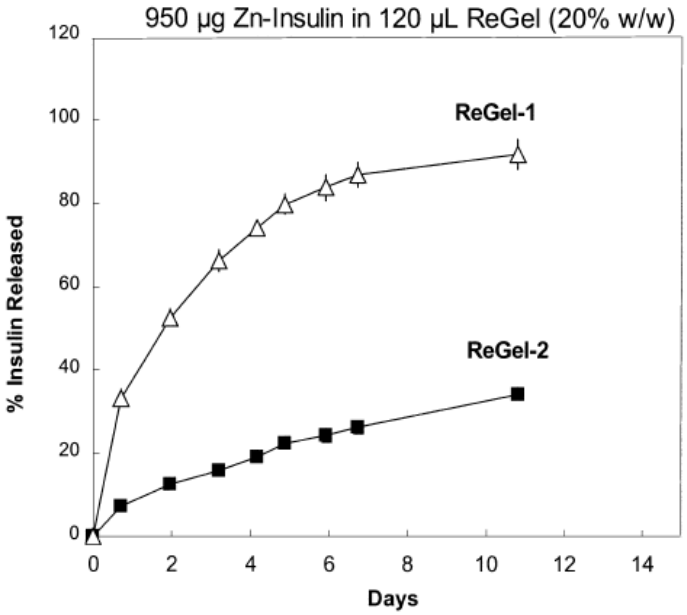

Figure 3.3. Comparison of insulin release rate for ReGel-1 and ReGel-2. ReGel-1 have a PEG unit of 1,000 g/mol and ReGel2: have a PEG unit of 1,450.[75] Reprinted with permission from Brahim, S.; Narinesingh, D.; Guiseppi-Elie, A., *Biomacromolecules* 2003, *4* (3), 497-503. Copyright 2003 American Chemical Society.

Since many protein drugs cannot tolerate much increase above physiological temperature, others have investigated biodegradable triblock copolymers with sol-to-gel (lower transition) and gel-to-sol (upper transition) transitions.[62] The phase transitions of PEG-PLGA-PEG triblock copolymers indicated a lower and upper transition. More importantly, the lower transition weakly depended on the polymer concentration while the upper transition revealed obvious changes to transition temperature as a function of concentration. This property permits drug loading at various concentrations in the sol phase and a better tailoring of drug release for individuals since the diffusion profile directly relates to water content within the hydrogel.[60, 75, 76]

The diffusive properties of hydrogels are dependent upon the composition and block length. Moreover, **Figure 3.4** demonstrated increasing the PLGA block length systematically decreased the critical gelation concentration (CGC). Larger hydrophobic units within the triblock encouraged micelle formation at lower polymer concentrations. The phase diagram of

PEG at varying block lengths indicated no change in the phase curve shape but imparted large variations in the critical gelation temperature (CGT) (**Figure 3.5**).

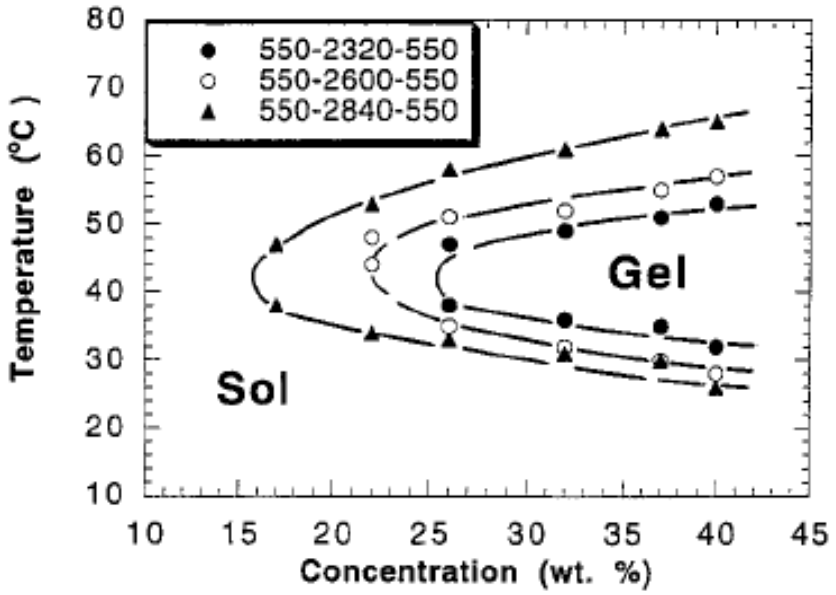

Figure 3.4. Effect of PLGA molecular weight on phase transition of PEG-PLGA-PEG.[62] Reprinted with permission from Jeong, B.; Bae, Y. H.; Kim, S. W., *Macromolecules* 1999, *32* (21), 7064-7069. Copyright 1999 American Chemical Society.

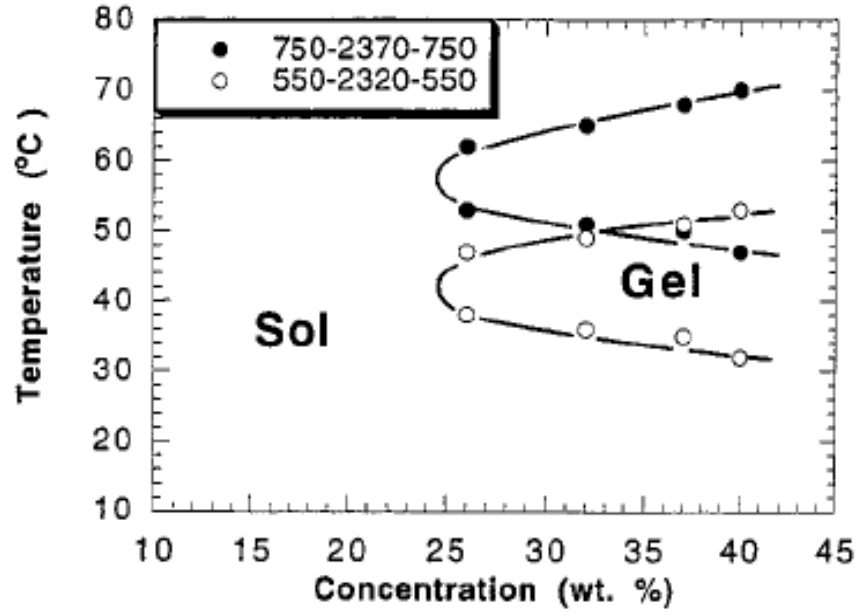

Figure 3.5. Phase diagram for PEG-PLGA-PEG triblocks.[62] Reprinted with permission from Jeong, B.; Bae, Y. H.; Kim, S. W., *Macromolecules* 1999, *32* (21), 7064-7069. Copyright 1999 American Chemical Society.

The ability to change the CGT and CGC allows one to modify the drug release profile for specific drug requirements. Further investigations on the salt effect and concentrations on the phase transitions elucidate the mechanism for micelle formation. Water structure making (NaCl) and water structure breaking (NaSCN) interactions were investigated for their effect on the phase transition. The addition of 1% NaCl results in a decrease of the CGT while the opposite effect occurred for 1% NaSCN. Salt effects screen hydrogen-bonding interactions between the polymer and water.

Others have incorporated pH-sensitive groups into thermosensitive hydrogels to modify drug delivery properties. Huynh et al. developed a pentablock thermoreversible hydrogel system that employed poly(β-amino ester) (PAE) as a pH-sensitive component as well as an electrostatic complexation group.[37] The polymer was composed of PAE, poly(caprolactone) (PCL), and PEG as the following pentablock: PAE-PCL-PEG-PCL-PAE. At low pH, PAE electrostatically complexes with insulin between the protonated nitrogen and the electronegative carbonyl oxygen (**Figure 3.6**). This ionic complex encourages insulin loading into the hydrogel; however, intramolecular complexation also occurs.

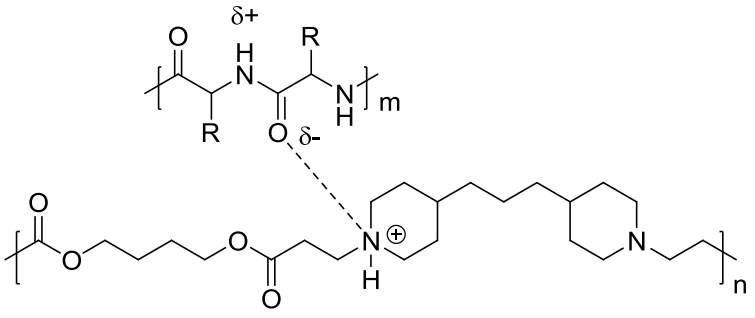

R= Amino acid side group

Figure 3.6. Electrostatic interactions provide strong complexes between the protonated PAE and partially negative carbonyl from the insulin amino acid. The dotted line depicts potential hydrogen bonding between the carbonyl and protonated amine.

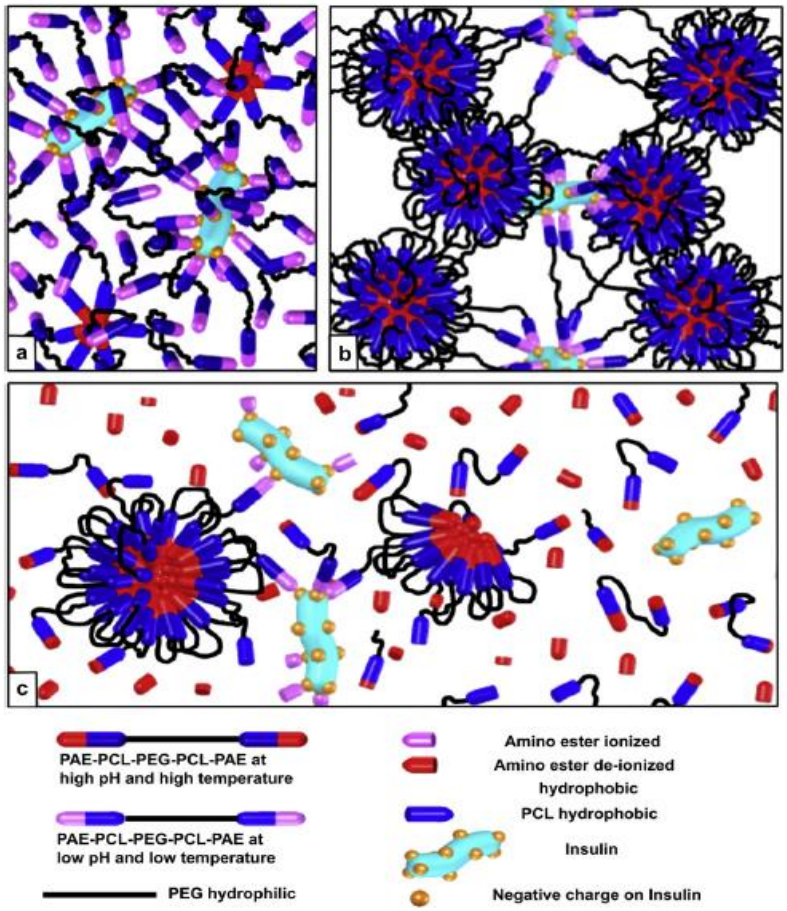

Figure 3.7. Mechanism controlling the complexation and release of insulin.[37] (Image reproduced from Ref. 37)

The PAE-PCL-PEG-PCL-PAE pentablock system functioned synergistically to improve insulin delivery through elimination of harsh burst effects, often experienced through insulin injections. At low pH, the amino ester partially ionizes and form electrostatic complexes with insulin; however, not all amino esters are completely ionized (**Figure 3.7**). The de-ionized amino esters aggregate and assimilate into micellular structures through hydrophobic interactions (**Figure 3.7**). Due to diffusion-controlled release of insulin, PAE-insulin complexes release first, followed by a slower degradation of PCL to extend insulin release. In this case, both temperature and pH components facilitate control of insulin release.

3.4.2 pH-Responsive Hydrogels

pH-Sensitive hydrogels are typically composed of amphoteric or ionizable groups, whose charge varies under changing pH.[35, 77, 78] Consequently, the structural properties of these hydrogels change dramatically due to electrostatic interactions compared to non-ion containing hydrogels.[60] Water uptake depends significantly on the protonation of the ionizable groups. pH-sensitive hydrogels are suitable for oral drug delivery because of the varying pH environment within the body.[19] The pH of the stomach is typically less than three, while that of the intestine is close to neutral.

Chitosan is a naturally derived polymer from the alkaline deacetylation of chitan.[27, 56, 79-81] Chitosan has received attention for biomedical applications due to their biocompatibility and biodegradability through naturally occurring enzymes within the body.[25, 81, 82] In addition, chitosan-based systems have also been found to possess thermo-responsive properties which are modified through pH and ionic strength.[83] Because of its ability to be positively charged at neutral pH, chitosan is used for many bioadhesive hydrogel applications.[84]

Zhou, et al. recently demonstrated successful photo-crosslinking of pH-sensitive hydrogels based on chitosan and poly(hydroxyethyl methacrylate) poly(HEMA) interpenetrating networks (IPN).[78] Interpenetrating networks offer desirable properties such as fast water absorption, porous microstructures, and enhanced mechanical properties.[85] Moreover, this system offer advantages over previously described chitosan-containing hydrogels because the preparation of ionized chitosan avoids the use of aqueous acid.[56, 67, 86, 87] HEMA and chitosan components were chosen for their ability to form ionizable and biocompatible hydrogels. Michael reaction of excess chitosan with acrylic acid resulted in the water-soluble monomer, N-carboxyethyl chitosan (CECS) (**Scheme 3.2**). Further Michael reaction of unreacted CECS

amine with tetraethylene glycol diacrylate and UV curing of HEMA and TEGDMA produced the crosslinked CECS/poly(HEMA) network. The resulting hydrogel exhibited different drug release profiles at pH 2.2 compared to pH 7.4. The authors attributed these variations to the electrostatic repulsion of the amine group at pH 2.2, which increased swelling behaviors.[78, 83] Chitosan's isoelectric point is pI 7.2 and thus, resulted in decreased swelling at physiological pH compared to an acidic condition.

Scheme 3.2. Synthesis of UV crosslinked CECS/poly(HEMA) with TEGDMA crosslinker.

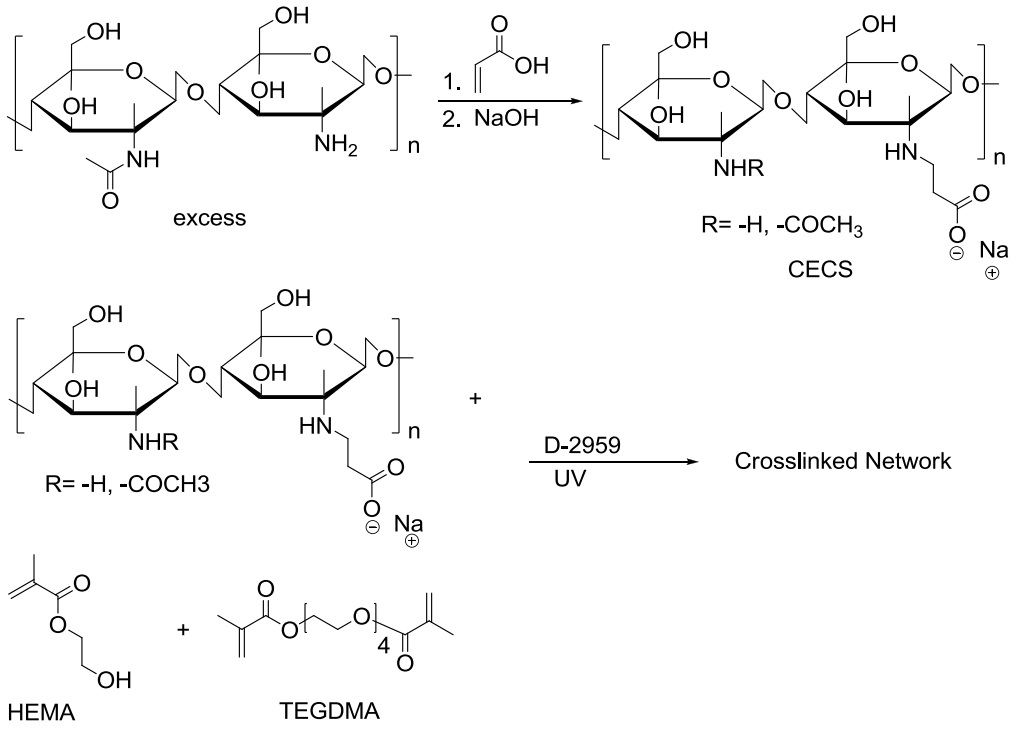

The synthesis and swelling properties of poly(methacrylic acid-*g*-ethylene glycol) poly(MAA-*g*-EG) networks were previously investigated for pH-sensitive oral insulin delivery carriers.[88] The swelling of grafted copolymer was less than that of the homopolymer. Moreover, the poly(MAA-*g*-EG) systems complexes with insulin more readily than the homopolymers at a higher range of concentrations and PEG molecular weights. The findings indicated that grafting

promoted a close proximity of PMAA and PEG, which eliminated complexation translational free energy for more favorable complexation.[88]

In addition, poly(MAA-*g*-EG) systems protected insulin within the enzymatic degradation and low pH environment of the stomach.[89-91] Polyacrylates and their derivatives such as Carbopol 934P (C934p) and polycarbophil (PCP), achieved enhanced protection against degradative enzymes.[46, 92-94] Negative charges on acrylate groups preferentially bound calcium and inhibited calcium-dependant enzymes such as trypsin. Calcium binding affinity of poly(MAA-*g*-EG) were substantially lower than C934p and PCP controls. However, slight increases in binding were observed in poly(MAA-*g*-EG) compositions with higher molar percent of MAA (Table 3.2). The increased hydrophobicity from the methyl group in PMAA and few negative charges in the graft copolymer contributed to the decrease in binding behavior.[90]

Table 3.2 Calcium binding affinity (mean ± standard deviation, *n*=3) of poly(MAA-*g*-EG) compared to C934p and PCP in buffered solution at pH 6.7.

Polymer	**PEG graft chain molecular weight (g/mol)**	**MAA: EG in hydrogel**	**Bound Ca^{2+} mg Ca^{2+}/ g polymer**
C934p	---	---	167.5 ± 16.2
PCP	---	---	170.1 ± 4.6
Poly(MAA-*g*-EG)	1000	1:1	66.1 ± 3.3
Poly(MAA-*g*-EG)	1000	2:1	75.5 ± 6.1
Poly(MAA-*g*-EG)	1000	4:1	86.1 ± 5.4
Poly(MAA-*g*-EG)	1000	1:2	55.5 ± 2.3
Poly(MAA-*g*-EG)	400	1:1	62.1 ± 3.9
Poly(MAA-*g*-EG)	200	1:1	51.5 ± 3.4

Further investigation into the oral bioavailability of insulin loaded poly(MAA-*g*-EG) (ILP) revealed the effect of the polymer in gastric and intestinal fluids.[95] After treatment of ILPs with gastric fluids, more than 80% of insulin remained within the hydrogel compared to insulin

alone, substantially protecting insulin from degradative enzymes. Moreover, the degree of insulin remaining intact within the hydrogel heavily depended on the molar ratio of MAA: EG. Specifically, higher molar ratios of MAA:EG resisted degradative effects from the gastric fluids. The authors attributed this effect to the extent of free MAA units that are free from EG complexation.[90]

Covalent crosslinking of poly(MAA-*g*-EG) systems with PEG dimethacrylate (PEGDMA) elucidated the effect of crosslink density and mesh size on the drug loading and diffusive properties.[96] The mesh size (ξ) was determined quantitatively using the polymer volume fraction and density. The pH-sensitive systems showed no apparent change in mesh size for varying formulations until the pK_a of the hydrogel was reached. More importantly, the release of insulin occurred when the pH of the aqueous environment was greater than the pK_a of the hydrogel and pI of insulin.

$$\frac{\tau}{\left(\alpha - \frac{1}{\alpha^2}\right)} = RT\rho_{2,r}\left(\frac{1}{\overline{M_e}} - \frac{2}{\overline{M_n}}\right)^{\frac{1}{3}}$$

$$\xi = \left(\frac{2C_n\overline{M_e}}{M_o}\right)^{\frac{1}{2}} lv_{2,s}^{\frac{1}{3}}$$

Insulin glargine is a chemically modified derivative of insulin that has the same molecular weight and size but possesses a higher pI.[96] The findings suggested that although the release of insulin was mainly due to diffusive control, diffusion only occurred during certain conditions directly related to an increase in mesh size as a function of pH environment.

3.4.3 Glucose-Responsive Hydrogels

Although sensitivity to temperature and pH may help drug-delivering hydrogels detect the changing environment and thus respond with an alteration of the structure, glucose-controlled delivery of insulin presents an exciting and relatively unexplored area in drug delivery. Glucose-sensitive components offer a physiological mimic to control insulin delivery. Glucose oxidase, lectin-loaded, and phenylboronic acid-containing hydrogels were incorporated into hydrogels to respond to varying glucose levels within the blood.[36]

pH-sensitivity with glucose recognition components further tailor glucose response for insulin delivery. Glucose oxidase (GOx) is a common glucose sensor that also detects changes in pH. Glucose oxidase oxidizes glucose to produce gluconic acid and hydrogen peroxide through the following reaction:

$$\text{glucose} + O_2 + H_2O \xrightarrow{\text{GOx}} \text{gluconic acid} + H_2O_2$$

Because H_2O_2 is harmful to the body, catalase further reduces H_2O_2 into water and oxygen:

$$H_2O_2 \xrightarrow{\text{catalase}} H_2O + 1/2\ O_2 .$$

The generation of gluconic acid effectively lowers the pH as GOx encounters increasing glucose concentrations.

Entirely cationic or anionic hydrogels have the advantage of being responsive towards external changes in pH. Because hydrogels do not typically retain mechanical properties in the swollen state, polyelectrolyte-containing composites were investigated for their enhanced mechanical properties.[51, 97] In a study by Zhang et al, glucose oxidase, catalase and poly(*N*-isopropylacrylaminde-*co*-methacrylic acid) (poly(NIPAm-*co*-MAA)) nanoparticles containing insulin were solution casted onto a hydrophobic ethylcellulose polymer.[98] As pH decreased due

to the increasing concentration of gluconic acid resulting from the oxidation of glucose, the anionic nanoparticles shrank and left voids within the composite membrane. The resulting polymer indicated fast and responsive insulin-eluting systems based on glucose concentration (**Figure 3.8**).

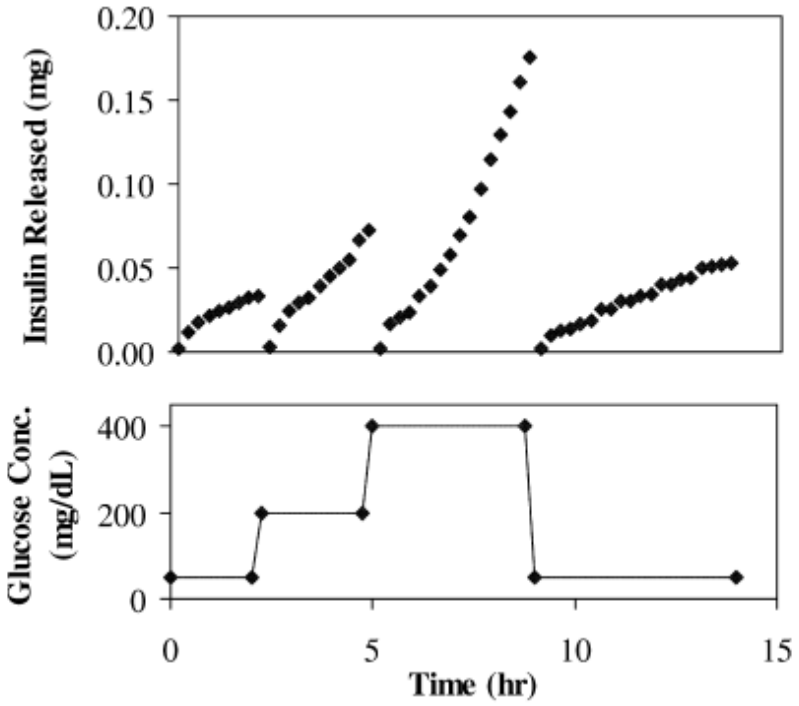

Figure 3.8. Insulin release profile showed clear response to the changes in glucose based on time and concentration.[98] (Image reproduced from Ref. 98)

A molecular model elucidated the diffusive properties of these nanoparticle-containing composites.[97] The diffusion of insulin from these hydrogels relates to the swelling or shrinking of the nanoparticles (**Figure 3.9**). Under high pH and low glucose concentrations, the nanoparticles occupied all of the pore spaces. This swollen state functioned as a nanovalve allowing small solutes to diffuse through while excluding larger solutes. At low pH, anionic nanoparticles shrank and imprinted water-filled pores. These pores permitted larger solutes to

diffuse; thus, the size of the diffusing solute experienced a different diffusion pattern based on the stimuli-response of the hydrogel.

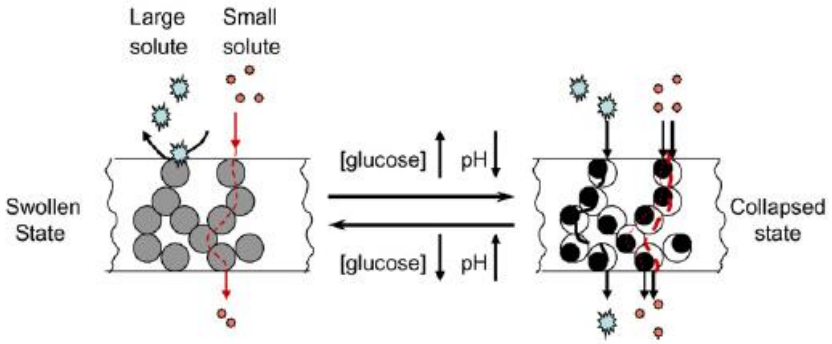

Figure 3.9. Changing glucose and pH concentrations control solute diffusion through swollen and collapsed hydrogels.[99] (Image reproduced from Ref. 99)

Glucose oxidase-containing hydrogels also integrates cationic polymers leading to the swelling of polymers and increase of network mesh size due to the electrostatic repulsion.[99] Previously investigated protonatable groups included tertiary amines found in *N*,*N*-diethylaminoethyl methacrylate (DEAEMA) and *N*,*N*-dimethylaminoethyl methacrylate (DMAEMA) (**Figure 3.10**).[36] Glucose and GOx must be present to control insulin release. Variations in the molar percent of DMAEMA affected the degree of swelling and hydration of the hydrogels.

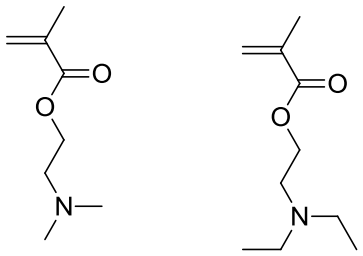

Figure 3.10. Examples of methacrylic tertiary amines used in pH-responsive polymeric systems.

A UV-crosslinked, 3-layer polymer matrix, each with a different concentration of insulin and GOx, was able to significantly lower the initial burst effect of insulin.[99] pH-sensitive

copolymer composed of HEMA, DMAEMA, 3-trimethoxysilylpropyl methacrylate (PMA), and tetraethylene glycol diacrylate (TEGDA) was synthesized with varying molar percent of DMAEMA. The degree of hydration increased with increasing molar percent of DMAEMA, as expected from increasing ionic content.

3.5 *Conclusions*

Stimuli-responsive hydrogels offer a controlled method for insulin delivery. Thermo-, pH-, and glucose-responsive hydrogel utilize the body's changing environment to induce a structural change in the hydrogel. Hydrogels from previous studies have demonstrated the ability to control the properties of insulin diffusion through simple changes in polymer block lengths and morphology. These properties offer a promising outlook for the future of insulin delivery. However, future studies should focus on the fundamental studies of polymer composition, charge, topology, and morphology on the ability to load and delivery insulin. Michael addition offers a unique, biocompatible, and simple method to incorporate charge-containing units into chemical crosslinked networks. Moreover, the prospect of calcium-triggered self-assembly of polymers and networks also presents a new direction for stimuli-responsive hydrogels.

3.6 *References*

1. Smith, G. D.; Pangborn, W. A.; Blessing, R. H., *Acta Crystallographica Section D* **2003,** *59* (3), 474-482.
2. Hodgkin, D. C., *Proceedings of the Royal Society of London. Series B, Biological Sciences* **1974,** *186* (1084), 191-215.
3. Riou, J. P.; Bernier-Valentin, F.; Beylot, M.; Laville, M.; Souquet, J. C.; Mornex, R., *Lyon Med.* **1983,** *250* (15), 121-41.
4. Lins, P. E.; Adamson, U.; Clausen, N.; Hamberger, B.; Efendic, S., *Acta Med. Scand.* **1986,** *220* (1), 39-46.
5. Svoboda, M.; Portois, L.; Malaisse, W. J., *Mol. Genet. Metab.* **1999,** *68* (2), 258-267.
6. Nonogaki, K., *Diabetologia* **2000,** *43* (5), 533-549.
7. Pusztai, P.; Sarman, B.; Ruzicska, E.; Toke, J.; Racz, K.; Somogyi, A.; Tulassay, Z., *Diabetes/Metab. Res. Rev.* **2008,** *24* (5), 343-352.
8. Sun, Y.; Asnicar, M.; Smith, R. G., *Neuroendocrinology* **2007,** *86* (3), 215-228.
9. Lampron, A.; Bourdeau, I.; Oble, S.; Godbout, A.; Schurch, W.; Arjane, P.; Hamet, P.; Lacroix, A., *J. Clin. Endocrinol. Metab.* **2009,** *94* (3), 750-756.
10. Tanoue, A., *J. Pharmacol. Sci. (Tokyo, Jpn.)* **2009,** *109* (1), 50-52.
11. Bell, A. W.; Greenwood, P. L.; Ehrhardt, R. A., *Biol. Grow. Anim.* **2005,** *3* (Biology of Metabolism in Growing Animals), 3-34.
12. Werle, M.; Makhlof, A.; Takeuchi, H., *Recent Pat. Drug Delivery Formulation* **2009,** *3* (2), 94-104.
13. Sanger, F., *Science* **1959,** *129* (3359), 1340-1344.
14. Weiss, M. A.; Insulin; Igfs, Chapter 2 The Structure and Function of Insulin: Decoding the TR Transition. In *Vitamins & Hormones*, Academic Press: 2009; Vol. Volume 80, pp 33-49.
15. Ciszak, E.; Beals, J. M.; Frank, B. H.; Baker, J. C.; Carter, N. D.; Smith, G. D., *Structure* **1995,** *3* (6), 615-622.
16. Maret, W.; Li, Y., *Chem. Rev.* **2009**.
17. Adams, M. J.; Blundell, T. L.; Dodson, E. J.; Dodson, G. G.; Vijayan, M.; Baker, E. N.; Harding, M. M.; Hodgkin, D. C.; Rimmer, B.; Sheat, S., *Nature* **1969,** *224* (5218), 491-495.
18. Nielsen, L.; Frokjaer, S.; Brange, J.; Uversky, V. N.; Fink, A. L., *Biochemistry* **2001,** *40* (28), 8397-8409.
19. Babu, V. R.; Patel, P.; Mundargi, R. C.; Rangaswamy, V.; Aminabhavi, T. M., *Expert Opinion on Drug Delivery* **2008,** *5* (4), 403-415.
20. D. R. Owens; B. Zinman; G. Bolli, *Diabetic Medicine* **2003,** *20* (11), 886-898.
21. Frokjaer, S.; Otzen, D. E., Protein drug stability: a formulation challenge. In *Nature Reviews Drug Discovery*, Nature Publishing Group: 2005; Vol. 4, pp 298-306.
22. Owen, R. L., *Semin. Immunol.* **1999,** *11* (3), 157-163.
23. Pukanud, P.; Peungvicha, P.; Sarisuta, N., *Drug Delivery* **2009,** *16* (5), 289-294.
24. Salman, H. H.; Gamazo, C.; Campanero, M. A.; Irache, J. M., *Journal of Nanoscience and Nanotechnology* **2006,** *6*, 3203-3209.
25. van der Lubben, I. M.; Verhoef, J. C.; van Aelst, A. C.; Borchard, G.; Junginger, H. E., *Biomaterials* **2001,** *22* (7), 687-694.

26. Patel, G. N.; Patel, G. C.; Patel, R. B.; Patel, S. S.; Patel, J. K.; Bharadia, P. D.; Patel, M. M., *Drug Delivery Technol.* **2006,** *6* (7), 62-71.
27. van der Merwe, S. M.; Verhoef, J. C.; Verheijden, J. H. M.; Kotzé, A. F.; Junginger, H. E., *European Journal of Pharmaceutics and Biopharmaceutics* **2004,** *58* (2), 225-235.
28. Amir, R. J.; Zhong, S.; Pochan, D. J.; Hawker, C. J., *Journal of the American Chemical Society* **2009**.
29. Bawa, P.; Pillay, V.; Choonara Yahya, E.; du Toit Lisa, C., *Biomed Mater* **2009,** *4* (2), 22001.
30. Nederberg, F.; Watanabe, J.; Ishihara, K.; Hilborn, J.; Bowden, T., *Biomacromolecules* **2005,** *6* (6), 3088-3094.
31. Cheng, J.; Teply, B.; Jeong, S.; Yim, C.; Ho, D.; Sherifi, I.; Jon, S.; Farokhzad, O.; Khademhosseini, A.; Langer, R., *Pharm. Res.* **2006,** *23* (3), 557-564.
32. Davaran, S.; Omidi, Y.; Mohammad Reza Rashidi; Anzabi, M.; Shayanfar, A.; Ghyasvand, S.; Vesal, N.; Davaran, F., *Journal of Bioactive and Compatible Polymers* **2008,** *23* (2), 115-131.
33. Hoare, T. R.; Kohane, D. S., *Polymer* **2008,** *49* (8), 1993-2007.
34. Kuckling, D., *Colloid. Polym. Sci.* **2009,** *287* (8), 881-891.
35. Qiu, Y.; Park, K., *Advanced Drug Delivery Reviews* **2001,** *53* (3), 321-339.
36. Miyata, T.; Uragami, T.; Nakamae, K., *Advanced Drug Delivery Reviews* **2002,** *54* (1), 79-98.
37. Huynh, D. P.; Nguyen, M. K.; Pi, B. S.; Kim, M. S.; Chae, S. Y.; Lee, K. C.; Kim, B. S.; Kim, S. W.; Lee, D. S., *Biomaterials* **2008,** *29* (16), 2527-2534.
38. Huynh, D. P.; Im, G. J.; Chae, S. Y.; Lee, K. C.; Lee, D. S., *J. Controlled Release* **2009,** *137* (1), 20-24.
39. Singh, B.; Sharma, N., *Biomacromolecules* **2009,** *10* (9), 2515-2532.
40. Keppeler, S.; Ellis, A.; Jacquier, J. C., *Carbohydr. Polym.* **2009,** *78* (4), 973-977.
41. Kulkarni, R. V.; Sa, B., *Journal of Bioactive and Compatible Polymers* **2009,** *24* (4), 368-384.
42. Tai, H.; Howard, D.; Takae, S.; Wang, W.; Vermonden, T.; Hennink, W. E.; Stayton, P. S.; Hoffman, A. S.; Endruweit, A.; Alexander, C.; Howdle, S. M.; Shakesheff, K. M., *Biomacromolecules* **2009**.
43. Kou, J. H., *Drugs Pharm. Sci.* **2000,** *102* (Transport Processes in Pharmaceutical Systems), 445-471.
44. Divis, P.; Docekalova, H.; Rezacova, V., *Chem. Listy* **2005,** *99* (9), 640-646.
45. Yadav, N.; Morris, G.; Harding, S. E.; Ang, S.; Adams, G. G., *Endocrine, Metabolic & Immune Disorders - Drug Targets(Formerly Current Drug Targets - Immune, Endocrine & Metabolic Disorders)* **2009,** *9*, 1-13.
46. Tribello, G. A.; Liew, C.; Parrinello, M., *J. Phys. Chem. B* **2009,** *113* (20), 7081-7085.
47. Matsuoka, H.; Matsutani, M.; Mouri, E.; Matsumoto, K., *Macromolecules* **2003,** *36* (14), 5321-5330.
48. Nie, T.; Zhao, Y.; Xie, Z.; Wu, C., *Macromolecules* **2003,** *36* (23), 8825-8829.
49. Wang, D.; Liu, J.; Ye, G.; Wang, X., *Polymer* **2009,** *50* (2), 418-427.
50. Blanazs, A.; Armes, S. P.; Ryan, A. J., *Macromol. Rapid Commun.* **2009,** *30* (4-5), 267-277.
51. Bae, Y. H.; Kim, S. W., *Advanced Drug Delivery Reviews* **1992,** *11* (1-2), 109-135.
52. Wu, D. C.; Liu, Y.; He, C. B., *Macromolecules* **2008,** *41* (1), 18-20.

53. Traitel, T.; Cohen, Y.; Kost, J., *Biomaterials* **2000,** *21* (16), 1679-1687.
54. Sershen, S.; West, J., *Advanced Drug Delivery Reviews* **2002,** *54* (9), 1225-1235.
55. Guillot, S.; Tomsic, M.; Sagalowicz, L.; Leser, M. E.; Glatter, O., *J. Colloid Interface Sci.* **2009,** *330* (1), 175-179.
56. Chang, Y.; Xiao, L.; Du, Y., *Polym. Bull.* **2009,** *63* (4), 531-545.
57. Yu, L.; Ding, J., *Chem. Soc. Rev.* **2008,** *37* (8), 1473-1481.
58. Maeda, Y.; Sakamoto, J.; Wang, S.-y.; Mizuno, Y., *The Journal of Physical Chemistry B* **2009,** *113* (37), 12456-12461.
59. Weber, C.; Becer, C. R.; Hoogenboom, R.; Schubert, U. S., *Macromolecules* **2009,** *42* (8), 2965-2971.
60. Firestone, B. A.; Siegel, R. A., *J. Appl. Polym. Sci.* **1991,** *43* (5), 901-914.
61. Khairuzzaman, A., *Drug Delivery Technol.* **2009,** *9* (6), 50, 52-55.
62. Jeong, B.; Bae, Y. H.; Kim, S. W., *Macromolecules* **1999,** *32* (21), 7064-7069.
63. Jiang, Z.; Hao, J.; You, Y.; Liu, Y.; Wang, Z.; Deng, X., *Journal of Biomedical Materials Research Part A* **2008,** *87A* (1), 45-51.
64. Zhang, H.; Yu, L.; Ding, J., *Macromolecules* **2008,** *41* (17), 6493-6499.
65. Chee, C.-K.; Hunt, B. J.; Rimmer, S.; Rutkaite, R.; Soutar, I.; Swanson, L., *Soft Matter* **2009,** *5* (19), 3701-3712.
66. Misra, G. P.; Singh, R. S. J.; Aleman, T. S.; Jacobson, S. G.; Gardner, T. W.; Lowe, T. L., *Biomaterials* **2009,** *30* (33), 6541-6547.
67. Verestiuc, L.; Nastasescu, O.; Barbu, E.; Sarvaiya, I.; Green, K. L.; Tsibouklis, J., *Journal of Biomedical Materials Research Part A* **2006,** *77A* (4), 726-735.
68. Cohn, D.; Sagiv, H.; Benyamin, A.; Lando, G., *Biomaterials* **2009,** *30* (19), 3289-3296.
69. Zhao, F.; Xie, D.; Zhang, G.; Pispas, S., *The Journal of Physical Chemistry B* **2008,** *112* (20), 6358-6362.
70. Yang, C.; Li, J., *The Journal of Physical Chemistry B* **2008,** *113* (3), 682-690.
71. Chiappetta, D. A.; Sosnik, A., *European Journal of Pharmaceutics and Biopharmaceutics* **2007,** *66* (3), 303-317.
72. Jeong, B.; Bae, Y. H.; Lee, D. S.; Kim, S. W., *Nature* **1997,** *388* (6645), 860-862.
73. Zentner, G. M.; Rathi, R.; Shih, C.; McRea, J. C.; Seo, M.-H.; Oh, H.; Rhee, B. G.; Mestecky, J.; Moldoveanu, Z.; Morgan, M.; Weitman, S., *J. Controlled Release* **2001,** *72* (1-3), 203-215.
74. Li, S.; Vert, M., *Macromolecules* **2003,** *36* (21), 8008-8014.
75. Brahim, S.; Narinesingh, D.; Guiseppi-Elie, A., *Biomacromolecules* **2003,** *4* (3), 497-503.
76. dos Santos, J.-F. R.; Couceiro, R.; Concheiro, A.; Torres-Labandeira, J.-J.; Alvarez-Lorenzo, C., *Acta Biomaterialia* **2008,** *4* (3), 745-755.
77. Bayramo, G.; gbreve; lu; Ar, M. Y.; inodot; ca, *Macromolecular Symposia* **2003,** *203* (1), 213-218.
78. Zhou, Y.; Yang, D.; Ma, G.; Tan, H.; Jin, Y.; Nie, J., *Polym. Adv. Technol.* **2008,** *19* (8), 1133-1141.
79. Cui, F.; He, C.; He, M.; Tang, C.; Yin, L.; Qian, F.; Yin, C., *Journal of Biomedical Materials Research Part A* **2009,** *89A* (4), 1063-1071.
80. Cui, F.; Qian, F.; Yin, C., *Int. J. Pharm.* **2006,** *316* (1-2), 154-161.
81. Ta, H. T.; Dass, C. R.; Dunstan, D. E., *J. Controlled Release* **2008,** *126* (3), 205-216.
82. Sarmento, B.; Ribeiro, A.; Veiga, F.; Ferreira, D.; Neufeld, R., *Biomacromolecules* **2007,** *8* (10), 3054-3060.

83. Zhou, H. Y.; Chen, X. G.; Kong, M.; Liu, C. S., *J. Appl. Polym. Sci.* **2009,** *112* (3), 1509-1515.
84. Berger, J.; Reist, M.; Mayer, J. M.; Felt, O.; Gurny, R., *European Journal of Pharmaceutics and Biopharmaceutics* **2004,** *57* (1), 35-52.
85. Yin, L.; Zhao, Z.; Hu, Y.; Ding, J.; Cui, F.; Tang, C.; Yin, C., *J. Appl. Polym. Sci.* **2008,** *108* (2), 1238-1248.
86. Kaewpirom, S.; Boonsang, S., *Eur. Polym. J.* **2006,** *42* (7), 1609-1616.
87. Ng, L.-T.; Swami, S., *Carbohydr. Polym.* **2005,** *60* (4), 523-528.
88. Klier, J.; Scranton, A. B.; Peppas, N. A., *Macromolecules* **2002,** *23* (23), 4944-4949.
89. Kim, B.; Peppas, N. A., *Int. J. Pharm.* **2003,** *266* (1-2), 29-37.
90. Madsen, F.; Peppas, N. A., *Biomaterials* **1999,** *20* (18), 1701-1708.
91. Perakslis, E.; Tuesca, A.; Lowman, A., Complexation hydrogels for oral protein delivery: an in vitro assessment of the insulin transport-enhancing effects following dissolution in simulated digestive fluids. In *Journal of Biomaterials Science -- Polymer Edition*, VSP International Science Publishers: 2007; Vol. 18, pp 1475-1490.
92. Thaurer, M. H.; Deutel, B.; Schlocker, W.; Bernkop-Schnuerch, A., *J. Microencapsulation* **2009,** *26* (3), 187-194.
93. Bulo, R. E.; Donadio, D.; Laio, A.; Molnar, F.; Rieger, J.; Parrinello, M., *Macromolecules (Washington, DC, U. S.)* **2007,** *40* (9), 3437-3442.
94. Leeuw, B. J. d.; Luessen, H. L.; Perard, D.; Verhoef, J. C.; de Boer, A. G.; Junginger, H. E., *Proc. Int. Symp. Controlled Release Bioact. Mater.* **1995,** *22nd*, 528-9.
95. Yamagata, T.; Morishita, M.; Kavimandan, N. J.; Nakamura, K.; Fukuoka, Y.; Takayama, K.; Peppas, N. A., *J. Controlled Release* **2006,** *112* (3), 343-349.
96. Tuesca, A.; Lowman, A., *Macromolecular Symposia* **2008,** *266* (1), 101-107.
97. Abdekhodaie, M. J.; Wu, X. Y., *Journal of Membrane Science* **2009,** *335* (1-2), 21-31.
98. Zhang, K.; Wu, X. Y., *J. Controlled Release* **2002,** *80* (1-3), 169-178.
99. Guiseppi-Elie, A.; Brahim, S. I.; Narinesingh, D., *Adv. Mater.* **2002,** *14* (10), 743-746.

Chapter 4: Melt Transesterification and Characterization of Segmented Block Copolyesters Containing 2,2,4,4-Tetramethyl-1,3-cyclobutanediol

(Published in *Journal of Polymer Science Part A: Polymer Chemistry* **2012,** *50* (18), 3710-3718.)

Musan Zhang, Robert B. Moore, and Timothy E. Long

Department of Chemistry, Macromolecules and Interfaces Institute
Virginia Tech, Blacksburg, VA 24061-0212

4.1 *Abstract*

Conventional melt transesterification successfully produced high molecular weight segmented copolyesters. A rigid, high-T_g polyester precursor containing the cycloaliphatic monomers, 2,2,4,4-tetramethyl-1,3-cyclobutanediol and dimethyl-1,4-cyclohexane dicarboxylate, allowed molecular weight control and hydroxyl difunctionality through monomer stoichiometric imbalance in the presence of a tin catalyst. Subsequent polymerization of a 4,000 g/mol polyol with monomers comprising the low-T_g block yielded high molecular weight polymers that exhibited enhanced mechanical properties compared to an non-segmented copolyester controls and soft segment homopolymers. Reaction between the polyester polyol precursor and a primary or secondary alcohol at melt polymerization temperatures revealed reduced transesterification of the polyester hard segment as a result of enhanced steric hindrance adjacent to the ester linkages. Differential scanning calorimetry, dynamic mechanical analysis, and tensile testing of the copolyesters supported the formation of a segmented multiblock architecture. Further investigations with atomic force microscopy uncovered unique needle-like, interconnected, microphase separated surface morphologies. Small-angle X-ray scattering confirmed the presence of microphase separation in the segmented copolyesters bulk morphology.

4.2 *Introduction*

Segmented block copolymers demonstrate immense commercial impact in thermoplastic elastomer applications including pressure- and temperature-sensitive adhesives,[1] coatings,[2] and food packaging.[3, 4] These segmented copolymers derive strength and flexibility from microphase separation and combine melt processibility for facile processing. Due to increasing environmental awareness, polymer researchers strive for greener synthetic approaches through the elimination of volatile organic solvents and the identification of monomers derived from renewable resources.[5-8] Polyesters offer both of these features in addition to hydrolytic reactivity that permits post-consumer degradation and monomer recovery. In addition, hydrolytic reactivity allows new applications in the growing biomedical field for controlled drug delivery vehicles and biodegradable tissue scaffolds.[9, 10] Thus, exceptional thermomechanical properties of segmented copolymers and environmentally sustainable syntheses of polyesters serve as primary motivations for our research.

Despite many advances and emerging applications for segmented copolyesters, there remain few examples in the literature describing an entirely polyester-based segmented block copolymer. Contemporary examples of polyester block copolymers feature sequential ring-opening polymerization of bio-derived lactide and menthide monomers to form ABA triblock copolymers[11] and enzymatic catalysis of monohydroxyl-terminated homopolymers with divinyl adipate to obtain AB diblocks copolymers.[12] However, these synthetic approaches require cyclic monomers, which limit the range of polymer compositions. In addition, organic solvents in the polymerization process remain a disadvantage for many biomedical and electronic applications due to more difficult isolation and the potential for residual solvent. The main obstacle to melt processible block copolyester compositions originates from the inherent reactivity of the ester

carbonyl allowing for hydrolysis and alcoholysis of the polymer backbone. Our research group previously investigated the impact of tailored polyester topologies on their degradative, thermal, mechanical, and rheological properties.[13-22] However, there remain many growing opportunities for new families of all-polyester segmented block copolymers.

Recently, polymers containing the rigid cyclic monomer 2,2,4,4-tetramethyl-1,3-cyclobutanediol (CBDO) have garnered increasing attention as a potential bisphenol-A (BPA) replacement. Staudinger[23] first reported in 1906 the spontaneous cyclic dimerization of dimethylketene to produce the cyclic 1,3-diketone. Hasek et al.[24] later described the successful hydrogenation of 2,2,4,4-tetramethyl,1,3-cyclobutanediketone using a ruthenium catalyst to produce an equal mixture of *cis/trans* CBDO isomers. Interestingly, the *cis* CBDO isomers exhibited a higher melting temperature of 163 °C compared to the *trans* CBDO isomer at 148 °C. Furthermore, the *trans* CBDO crystal structure revealed a unique planar structure arising from steric hindrance,[25] which was distinctly different from enhanced puckering attributed to hydrogen bonding in the *cis* CBDO crystal structure.[26] The planar conformation enabled exclusive acid dehydration of the *trans* CBDO isomer through a coordinated intramolecular transition state to yield pure *cis* CBDO from isomeric mixtures.[27]

Eastman Chemical Company extensively investigated several CBDO-containing (co)polyester compositions and noted exceptionally high melt viscosities during the polymerization process, significantly higher glass transition temperatures (T_g), and excellent polyester hydrolytic stabilities.[28, 29] The high melt viscosities and lower diol reactivity required reactive cyclic diester monomers, strong metal hydride bases, and high reaction temperatures to produce high molecular weight polyesters. Further studies from Kelsey et al.[30] also observed amorphous CBDO-based terephthalate copolyesters with unusually high glass transition

temperatures and exceptional impact properties exceeding BPA-polycarbonates. Recently, Hawker and others described the synthesis of novel cyclobutanediol monomers with unique alkyl groups using ketene chemistry[31] and demonstrated their polymerization in high-Tg polyesters.[32] Eastman's recent Tritan™ copolyester exemplifies the significant commercial impact of CBDO-copolyesters as alternatives for BPA-polycarbonates.

In this manuscript, we report a convenient one-pot melt transesterification approach to synthesize segmented multiblock copolyesters from high-T_g polyester precursors containing CBDO. Transesterification studies of CBDO-based polyester polyols revealed the effects of reaction temperature, alcohol reactivity, and sterics surrounding the ester carbonyl. The reduced alcoholysis of the ester linkage enabled the polyol to retain its compositional integrity throughout chain extension under melt transesterification conditions to yield high molecular weight segmented copolyesters containing varying hard segment contents. Differential scanning calorimetry (DSC) and dynamic mechanical analysis (DMA) supported the absence of phase mixing and the formation of a segmented multiblock architecture. Atomic force microscopy (AFM) and small-angle X-ray scattering (SAXS) further confirmed multiphase morphologies, which were consistent with dynamic mechanical and thermal analyses.

4.3 *Experimental Section*

Materials

2,2,4,4-Tetramethyl-1,3-cyclobutanediol (CBDO, 45/55 *cis/trans* mixture) and dimethyl-1,4-cyclohexanedicarboxylate (DMCD, 99% *trans* mixture) were generously provided by Eastman Chemical Company and used as received. Diethylene glycol (DEG, 99% purity) and dimethyl adipate (DMAp, 99% purity) were purchased from Sigma-Aldrich and used without subsequent

purification. Dibutyltin oxide catalyst and titanium tetra(isopropoxide) (99% purity) were purchased from Sigma-Aldrich, and a 0.01 g/mL titanium solution in anhydrous 1-butanol was prepared according to previously described procedures.[33]

Synthesis of Poly(CBDO-DMCD) Polyester Polyols

DMCD (10.0 g, 50 mmol), excess diol, CBDO (8.63 g, 60 mmol), and dibutyltin oxide (600 ppm) were introduced into a dry 100-mL, round-bottomed flask equipped with a mechanical overhead stirrer, nitrogen inlet, and condenser. The polymerization of the degassed reactants proceeded at temperatures from 200 – 240 °C over 5 h, and subsequent reaction under reduced pressure (0.1 mmHg) proceeded for an additional 2 h. End group analysis using ^{1}H NMR spectroscopy and chloroform size exclusion chromatography (SEC) determined number-average molecular weights of poly(CBDO-DMCD).

Synthesis of Poly[(CBDO-DMCD)-*co*-(DEG-DMAp)] Segmented Copolyesters

Conventional melt transesterification methods produced segmented copolyesters with varying weight percent of hard segment content. All reactions were conducted in a dry 50-mL, round-bottomed flask equipped with an overhead stirrer, nitrogen inlet, and condenser. For a 30 wt% hard segment copolyester (abbreviated poly[(CBDO-DMCD)-*co*-(DEG-DMAp)], poly(CBDO-DMCD) (3.12 g, 37 wt % solid), DEG (2.23 g, 21 mmol), and DMAp (3.12 g, 11.2 mmol) were introduced into a flask. Dibutyltin oxide (600 ppm) and titanium tetra(isoproxide) (100 ppm) were added to facilitate the reaction. The reactants were degassed under vacuum, and purged with nitrogen three times. The molar ratio of hydroxyl end groups to diester end groups was 1.0:1.0 to allow for high molecular weight. The reaction occurred at 180 °C for 5 h under a

constant nitrogen purge and subsequent reduced pressure (0.1 mmHg) for an additional 2 h. Chloroform solutions containing 20 wt % copolyesters were prepared and allowed to evaporate slowly for 2 d at 23 °C and annealed under reduced pressure for 1 d at 80 °C prior to thermal, mechanical, and morphological analysis.

Determination of Poly(CBDO-DMCD) Transesterification Resistance

Reaction of poly(CBDO-DMCD) with either 1-dodecanol or 2-dodecanol in the melt determined the propensity for polymer transesterification. Poly(CBDO-DMCD) oligomers, 1-dodecanol (8 molar excess), and titanium tetra(isoproxide) (100 ppm) were charged to a round-bottomed flask equipped with an overhead mechanical stirrer, nitrogen inlet, and condenser. The flask was degassed under vacuum and purged with nitrogen three times before heating the reaction. The reaction was heated from 180 – 220 °C at 10 °C increments over 5 h. ^{1}H NMR spectroscopy in $CDCl_3$ determined number-average molecular weight (M_n) of polymers that were aliquotted hourly.

Polymer Characterization

^{1}H NMR spectroscopy conducted in $CDCl_3$ at 23 °C with a Varian 400 MHz INOVA spectrometer provided chemical compositional analyses of all poly(CBDO-DMCD) and segmented copolyesters poly[(CBDO-DMCD)-*co*-(DEG-DMAP)]. A TA Instruments Hi-Res thermogravimetric analyzer (TGA) 2950 determined the onset of weight loss with increasing temperature under a nitrogen purge and heat ramp rate of 10 °C/min. Dynamic scanning calorimetry (DSC) heat/cool/heat experiments conducted on a TA Instruments Q1000 DSC at a heating rate of 10 °C/min from -100 to 150 °C and cooling rate of 50 °C/min under a constant

nitrogen purge of 50 mL/min determined polymer thermal transitions. DMA measured thermomechanical transitions of the segmented copolyesters using a TA Instruments Q800 in tension mode at a frequency of 1 Hz from -80 to 150 °C (heating rate of 3 °C/min) or until the storage modulus reached 0.1 MPa. The peak maximum from the tan δ curve determined T_g. An Instron 4411 universal testing instrument tested tensile properties of the segmented copolyesters at a crosshead speed of 10 mm/min. Tensile data represent an average of five specimens.

SEC was performed at 30 °C in $CHCl_3$ (HPLC grade) at 1.0 mL/min using polystyrene standards on a Waters 707 Autosampler equipped with Waters 1515 isocratic HPLC pump, a Waters 2414 refractive index detector, and Viscotek 270 MALLS/viscometric dual detector. Reported number-average and weight-average molecular weights were relative to polystyrene standards using the refractive index detector. A Veeco MultiMode atomic force microscope uncovered the surface morphology of the segmented copolyesters using a tapping mode (tip spring constant = 42 N/m). The free air amplitude setpoint was 3.00 V, and the amplitude setpoint during analysis was 1.70-1.80 V. Small-angle X-ray scattering was performed using a Rigaku S-Max 3000 pinhole SAXS system equipped with a CuK_α x-ray source (λ = 0.154 nm). SAXS sample-to-detector distance was calibrated with silver behanate. A SAXSGUI software obtained plots of scattering intensity, *I(q)*, as a function of the scattering wave vector, *q*. The scattering wave vector is $4\pi\sin(\theta)/\lambda$, where θ is the scattering angle, and λ is the wavelength of the incident beam.

4.4 *Results and Discussion*

Segmented block copolyesters offer the potential for polymer hydrolysis in biomedical applications or recyclable commercial products.[34-36] However, segmented copolymers

containing only ester linkages represents a challenge due to potential transesterification in both the hard and soft segments which may cause sequence scrambling especially at elevated temperatures.[11, 37, 38] Thus, we proposed a sterically hindered polyester precursor containing CBDO to maintain compositional sequence integrity for segmented multiblock architecture. The hydroxyl-functionalized, high-T_g poly(CBDO-DMCD) polyols were chain extended with monomers that will comprise the soft segments and afford segmented copolyesters. **Scheme 4.1** describes synthesis of amorphous cycloaliphatic polyols from 99% *trans* DMCD and 45/55 *cis/trans* CBDO. A controlled stoichiometric excess of CBDO afforded hydroxyl-functionalized polyester polyols. The conventional transesterification catalyst, titanium tetra(isopropoxide), produced polyols with insufficient molecular weights and required long reaction times. Kelsey et al. hypothesized that the titanium catalyst coordinated with the *cis*-CBDO isomer and reduced catalytic activity.[30] Based on previous literature describing the synthesis of CBDO-containing copolyesters, $(Bu)_2SnO$ catalyst resulted in high molecular weight copolymers using shorter reaction times compared to other transesterification metal catalysts.[30]

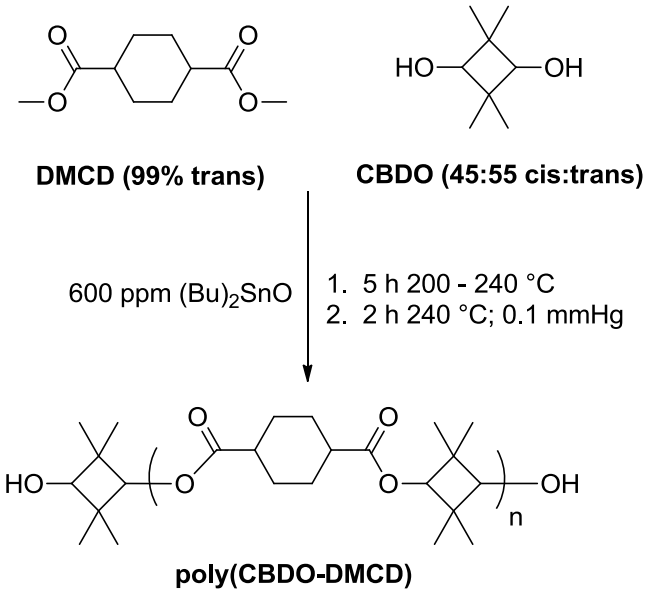

Scheme 4.1. Synthesis of high-T_g CBDO-containing polyester polyols.

The synthesis of poly(CBDO-DMCD) produced a colorless glassy polymer. ^{1}H NMR spectroscopy revealed no change in the *cis/trans* CBDO ratio incorporated into the polyester. Stoichiometric imbalance of diol to diester monomers effectively controlled the molecular weights. **Table 4.1** compares the theoretical polyol molecular weights as calculated using the modified Carothers's equation to ^{1}H NMR spectroscopic- and chloroform SEC-derived M_n values. At low M_n, the theoretical and experimental M_n agreed well; however, higher M_n oligomers deviated from theoretical values. This difference presumably reflected relative M_n generated from SEC polystyrene standards. In addition, the lower reactivity and steric hindrance of the CBDO secondary diol presumably contributed to the departure from the theoretical M_n. High melt viscosity also influenced molecular weight control and prevented the synthesis of high molecular weight poly(CBDO-DMCD). However, earlier reports described the synthesis of high molecular weight CBDO-based polyesters using a more reactive 1,4-diphenylcyclohexane dicarboxylate and metal hydride catalysts.[29] Nevertheless, ^{1}H NMR spectroscopy and chloroform SEC M_n agreed well over the desired range.

Table 4.1. Molecular weight control of poly(CBDO-DMCD) polyols using stoichiometric imbalance.

CBDO : DMCD Molar Ratio	Calc. M_n (g/mol)	M_n[a] (g/mol)	M_n[b] (g/mol)	M_w[b] (g/mol)	M_w/M_n
1.0 : 1.0	High MW	NA	NA	NA	NA
1.1 : 1.0	5,880	3,500	3,450	4,900	1.42
1.2 : 1.0	3,080	2,300	2,710	4,520	1.67
1.5 : 1.0	1,400	1,450	1,715	2,890	1.69

[a] Calculated from ^{1}H NMR spectroscopy

[b] Chloroform SEC: Refractive index detector (30 °C) universal calibration relative to polystyrene standards

NA = not available due to high melt viscosity

The literature extensively discusses the relationship between the glass transition temperature and molecular weight.[39] Properties such as T_g are proportional to molecular weight according to the classical equation:[40]

$$T_g = T_\infty - \frac{K}{M_n}$$

where T_∞ is the T_g for high molecular weight polymer, and K is a constant related to the end-group contribution and polymer free-volume. Thus, as the molecular weight increases, the impact of the second term decreases and approaches the T_g of high molecular weight polymer due to diminishing end group effects and increasing chain entanglement contributions.[40] **Figure 4.1** depicts the T_g values from DSC as a function of M_n. Molecular weights ranging from approximately 1,000 – 3,000 g/mol resulted in dramatic increases in the T_g which plateaued above 3,000 g/mol.

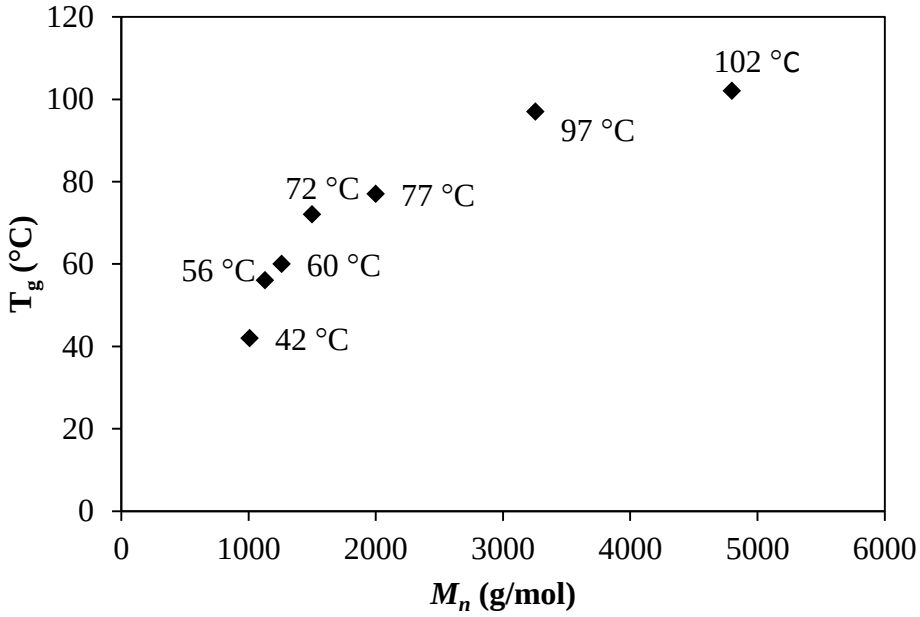

Figure 4.1. Plot of T_g as a function of poly(CBDO-DMCD) M_n.

Figure 4.2 illustrates the glass transition temperature as a function of the inverse number-average molecular weight. The extrapolated *y*-intercept value using the equation above predicted the high molecular weight T_g at 118 °C.

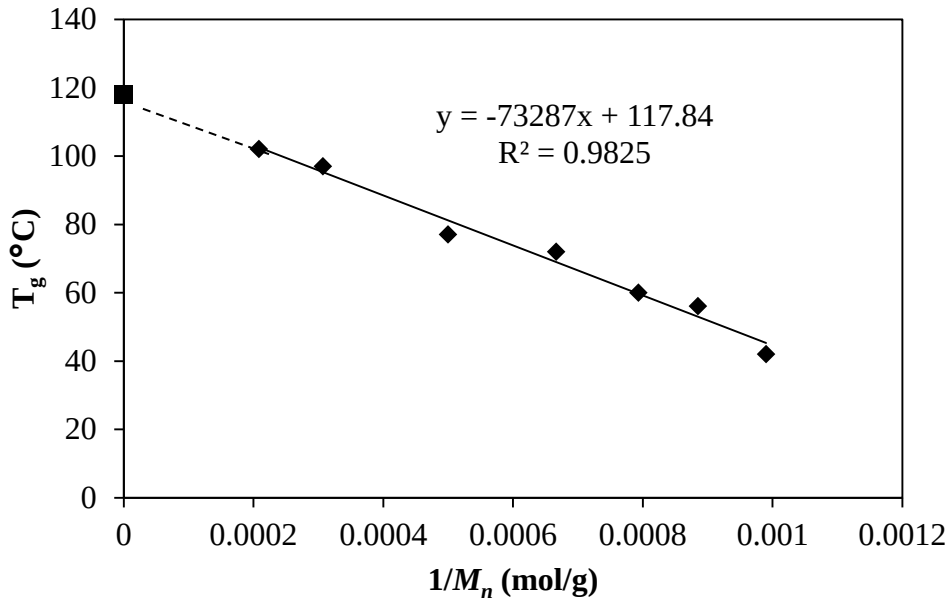

Figure 4.2. Plot of T_g as a function of inverse M_n provides a theoretical T_g for high molecular weight poly(CBDO-DMCD).

Despite the high-T_g of the poly(CBDO-DMCD) oligomeric precursors and elevated temperatures required for melt transesterification, a successful synthesis of segmented block copolyesters must maintain the hard segment sequence composition during chain extension. Parameters that influence polyester transesterification and hydrolysis include reaction temperature, catalysts, carbonyl sterics, and reactivities of the alcohol.[41] Park and Kang[42] investigated the compositional sequence redistribution during melt processing between a random ternary aliphatic copolyester and poly(butylene terephthalate) (PBT). Decreased degree of crystallinity, appearances of multiple peaks in ^{1}H NMR spectroscopy, and shifts in T_g implied a relationship between melt processing time and transesterification of the block copolyesters.[42]

However, the authors did not consider the influence of melt processing temperature on transesterification because the process required a homogenous molten state above the melting temperature of PBT. Nevertheless, the findings demonstrated the significance of transesterification in polyesters at elevated temperatures.

In our investigations, careful selection of DMCD and CBDO cyclic monomers produced a transesterification resistant, hydrolytically robust hard segment with a sterically hindered ester linkages arising from both the bulky tetramethyl groups and the adjacent cyclohexyl ring. Transesterification studies with primary and secondary alcohols emphasized the importance of the hard segment polyol structural robustness for subsequent melt polymerization to produce suitable segmented copolyesters. The poly(CBDO-DMCD) hard segments in the presence of added high boiling primary or secondary alcohols reacted at varying melt transesterification temperatures from 160-220 °C. ^{1}H NMR spectroscopy with end group analysis followed the changes in molecular weight as a function of the reaction temperature. These investigations probed the influence of the reaction temperature and alcohol on the transesterification behavior of poly(CBDO-DMCD). **Figure 4.3** illustrates the change in poly(CBDO-DMCD) M_n during reaction with a primary or secondary alcohol as a function of temperature. The results reflected a decrease in poly(CBDO-DMCD) molecular weights when reacted with a less sterically hindered primary alcohol, 1-dodecanol. However, the poly(CBDO-DMCD) molecular weights displayed no change when reacted with a more sterically hindered secondary alcohol, 2-dodecanol, at temperatures up to 220 °C.

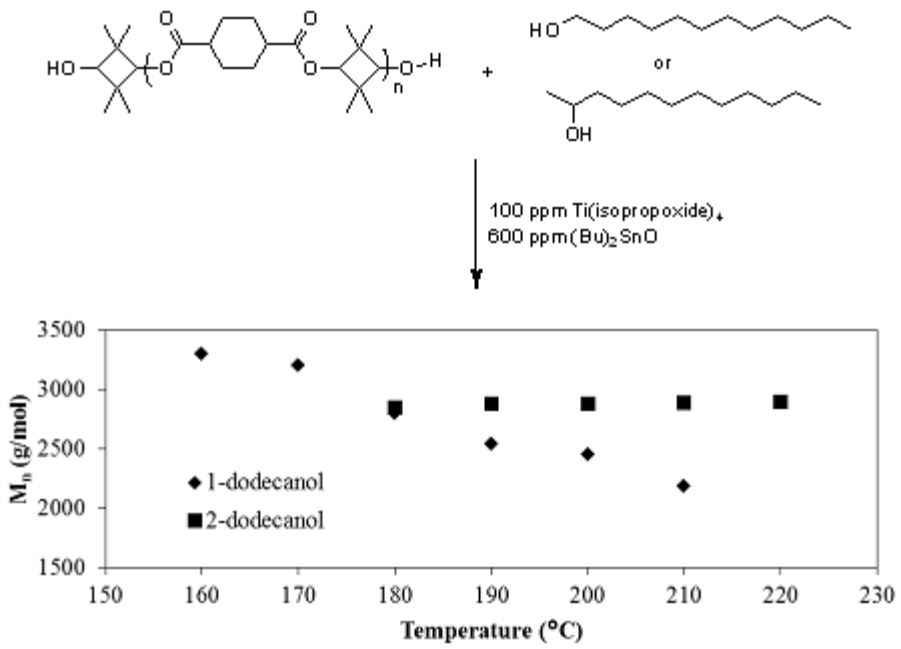

Figure 4.3. Transesterification study demonstrated a decrease in M_n as a function of reaction temperature and alcohol steric hindrance.

Flory's molecular weight distribution derivation and fundamental kinetics studies for step-growth polymerization assumed equal reactivity of functional groups.[43-45] However, further investigations of polyester polymerization of 1,2-propylene glycol with various anhydrides revealed differences in primary and secondary alcohol reactivity.[46-49] Zetterlund et al.[48] developed a self-catalyzed polyesterification kinetic model based on primary and secondary alcohol reactivities of 2.6 and 1.0, respectively, to accurately simulate the polymerization of 1,2 propylene glycols with anhydrides for unsaturated polyester resins. Our transesterification study further emphasized the importance of alcohol reactivity and concluded the less reactive 2-dodecanol maintained hard segment molecular weight over a range of temperatures compared to the more reactive 1-dodecanol. Furthermore, temperature played a larger role in preserving the hard segment when using a primary diol during subsequent soft segment synthesis. Our results revealed the importance of the sterics of the poly(CBDO-DMCD) ester carbonyl, diol reactivity

selected for the soft segment composition, reaction temperature, and reaction time on the extent of transesterification within the hard segment.

The monomers for the soft segment, DEG and DMAp, produced low-T_g, flexible polyester soft segments. Our previous studies of the rheological behavior of poly(DEG-DMAp) demonstrated their potential as low-T_g pressure-sensitive, potentially biodegradable polyester adhesives.[18] **Scheme 4.2** describes the synthesis of segmented poly[(CBDO-DMCD)-*co*-(DEG-DMAp)].

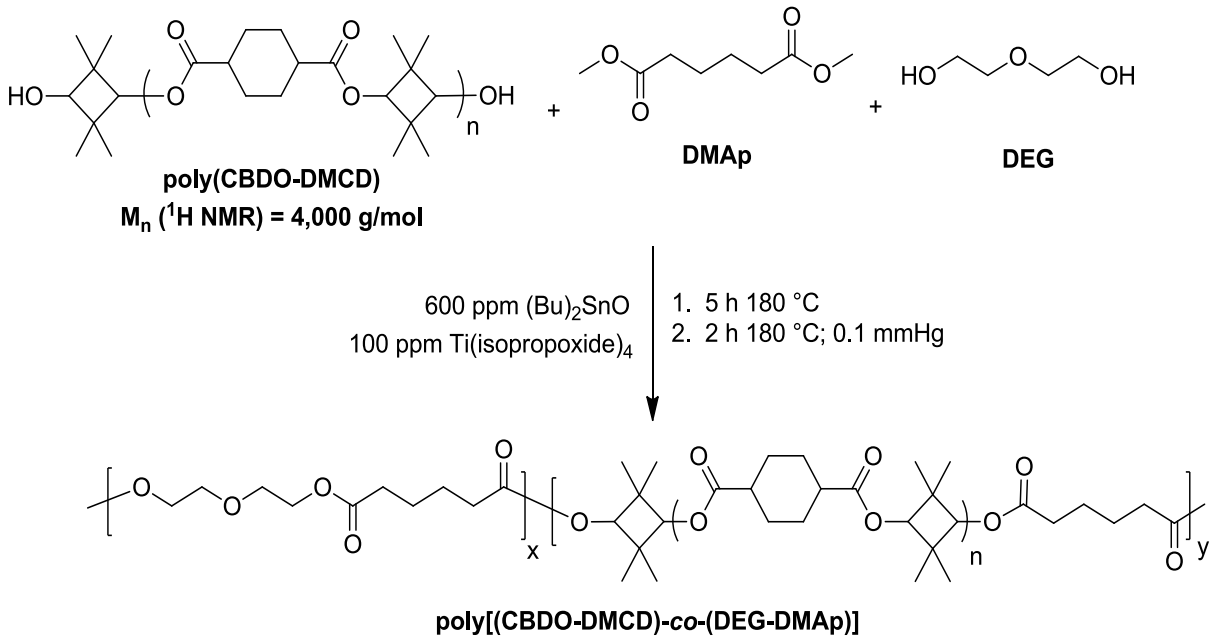

Scheme 4.2 Synthesis of poly(CBDO-DMCD)-based segmented copolyesters.

Scheme 4.3 shows the synthesis of a high molecular weight low-T_g poly(DEG-DMAp) homopolymer control for the soft segment. Melt transesterification of poly(CBDO-DMCD) polyols, DEG, and DMAp produced copolyesters containing varying hard segment content. The combination of titanium and tin catalysts facilitated polymerization, and high molecular weight copolyesters suggested the absence of deleterious catalytic interactions or inactivation.

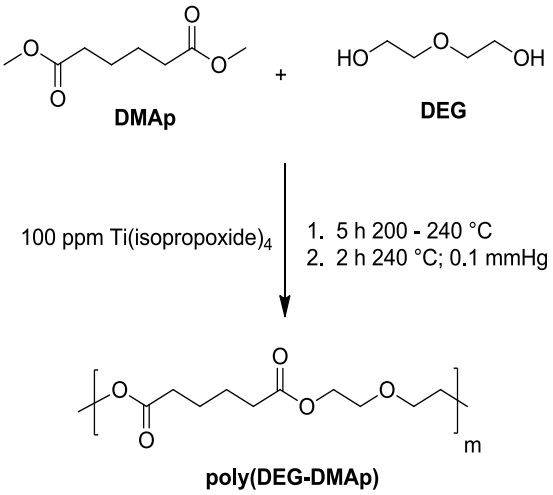

Scheme 4.3. Synthesis of low-T_g poly(DEG-DMAp) homopolymer.

A non-segmented copolyester provided a comparison to the properties of poly(CBDO-DMCD)-containing segmented copolyesters. **Scheme 4.4** summarizes the synthesis of a copolyester from equimolar diester and diol monomers that yielded a viscous low-T_g polymer composed of four repeating units. In sharp contrast, polyesters synthesized with poly(CBDO-DMCD) polyols afforded a transparent solid which was soluble and readily solution cast to form thin films. Thus, a unique structural integrity in the segmented copolyesters was distinctly different from the non-segmented copolyesters.

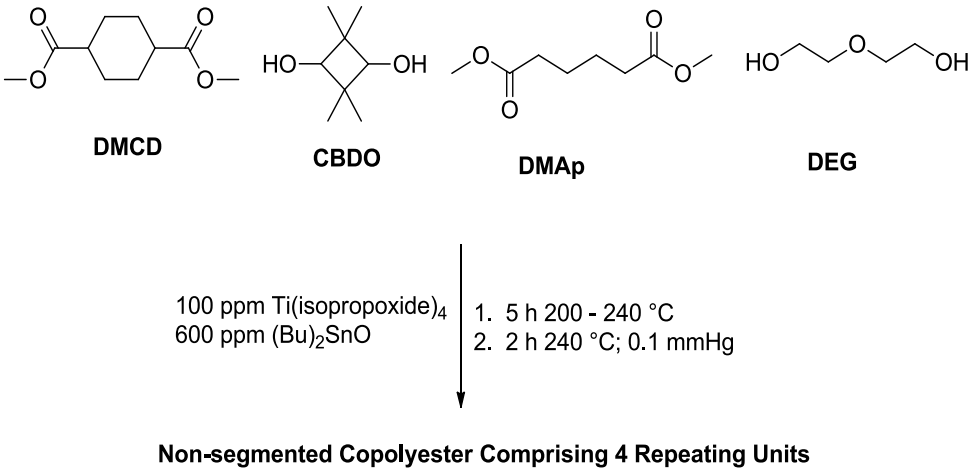

Scheme 4.4. Synthesis of CBDO-containing non-segmented copolyesters.

Table 4.2 summarizes copolyester molecular weights and T_g values observed with both DSC and DMA. SEC analysis indicated high molecular weight copolyesters obtained from melt transesterification. The poly(DEG-DMAp) homopolymer exhibited a T_g of -50 °C. In contrast, the non-segmented copolyesters possessed a higher T_g at -20 °C from the contribution of rigid cyclic rings that restricted segmental motion.[18] The segmented block copolyesters displayed a single T_g at -46 °C similar to the poly(DEG-DMAp) homopolymers T_g, and this strongly indicated a preserved poly(DEG-DMAp) phase and absence of phase mixing from hard segment transesterification.

Table 4.2. Molecular weight characterization of poly[(CBDO-DMCD)-*co*-(DEG-DMAp)] copolyesters.

Polymer Composition	M_n[a] (g/mol)	M_w[a] (g/mol)	M_w/M_n	T_g[b] (°C)	T_g[c] (°C)	T_{flow}[c] (°C)
Random	13,200	21,300	1.61	-20	----	----
Poly(DEG-DMAp)	24,490	43,800	1.79	-50	----	----
20 wt% HS	24,500	38,300	1.56	-45	-25	78
30 wt% HS	29,300	41,300	1.41	-47	-26	139
40 wt% HS	31,500	50,000	1.59	-47	-22	139

[a]Chloroform SEC: Refractive index detector (30 °C) universal calibration relative to polystyrene standards
[b]DSC: Heat/Cool/Heat, 2nd Heat, N_2, Heating rate = 10 °C/min
[c] DMA: Tension mode, 1 Hz, Heating rate = 3 °C/min

DMA further confirmed a segmented copolyester structure and microphase separation of the polyester blocks. **Figure 4.4** depicts the DMA results for 20, 30, and 40 wt% segmented copolyesters. The increase in hard segment weight content increased moduli and lengthened the rubbery plateau. Copolyesters containing 30 and 40 wt% hard segments showed two tan δ maxima corresponding to the soft and hard phases of the copolyesters at -26 °C and 130 °C. The

flow temperature increased from 78 to 139 °C with increasing hard segment content from 20 to 30 wt%. Increasing incorporation of the hard segment content from 20 to 40 wt% increased the broadness of the lower T_g presumably due to physical crosslinks restricting chain mobility within the soft phase.[32, 33] However, the segmented copolyesters maintained a consistent lower T_g at -26 °C with varying hard segment content. Furthermore, the rubbery plateau modulus systematically increased with hard segment weight content due to greater physical crosslink density, and the length of the rubbery plateau reflected a large processing temperature and application window.

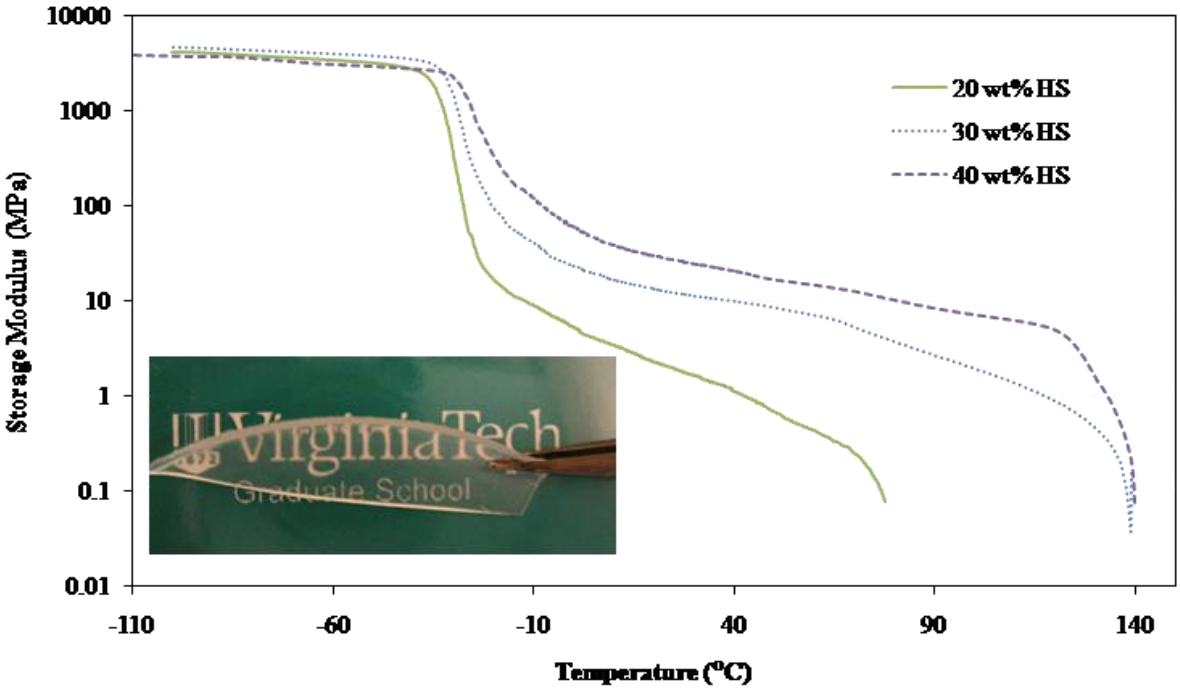

Figure 4.4. Dynamic mechanical analysis of 20, 30, and 40 wt% hard segment copolyesters. Dynamic mechanical properties analyzed in tension mode: 1 Hz, 3 °C/min.

Tensile testing probed the mechanical properties of these novel segmented copolyesters. The tensile properties were consistent with DMA results and exhibited an increase in Young's modulus, tensile stress, and tensile strain with increasing hard segment content (**Figure 4.5**). An

increase in hard segment content enhanced polymer toughness, a property derived from the area under a stress-strain curve. However, these values were significantly lower than commercial segmented polyurethanes, which was likely due to the higher poly(DEG-DMAp) soft segment T_g compared to conventional polyether-based copolymers. In addition, intermolecular interactions such as hydrogen bonding in polyurethanes reinforce and enhance mechanical properties. We will explore non-covalent intermolecular interactions including hydrogen bonding and ionic groups in future studies to enhance microphase separation and mechanical properties of these polyester-based thermoplastic elastomers.[19, 33, 50-52]

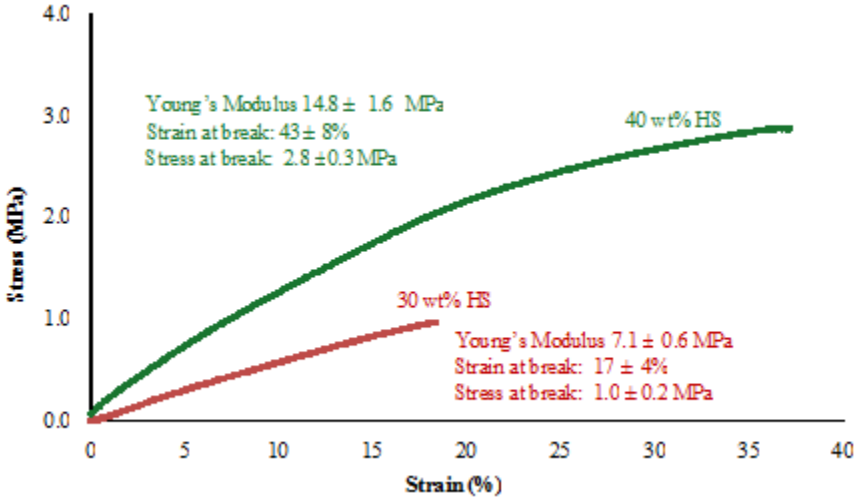

Figure 4.5. Tensile properties of 30 and 40 wt% hard segment (HS) copolyesters. Tensile data are reported as an average of 5 replications under tensile mode and crosshead speed of 10 mm/min.

Earlier studies in the literature employed AFM to elucidate the multiphase morphologies of segmented multiblock copolymers.[53-57] Morphological investigations using AFM uncovered a microphase separated surface morphology for 30 and 40 hard segment wt% segmented copolyesters **Figure 4.6**. The non-segmented copolyester did not produce suitable films; thus, images were not obtained. The surface morphology for 30 and 40 wt% hard segment copolyesters exhibited needle-like hard segments (light colored) percolated throughout a soft

segment matrix (dark colored). In addition, higher hard segment content promoted a more regular surface morphology. The increase in hard segment content generated a denser physical network as observed in AFM images and correlated with the increase in the DMA rubbery plateau modulus and Young's modulus. The absence of periodic long range, microphase separated morphologies is typical for segmented multiblock copolymers, and surface morphologies in our segmented copolyesters compare well with other microphase separated, segmented multiblock copolymers.[54, 56, 57]

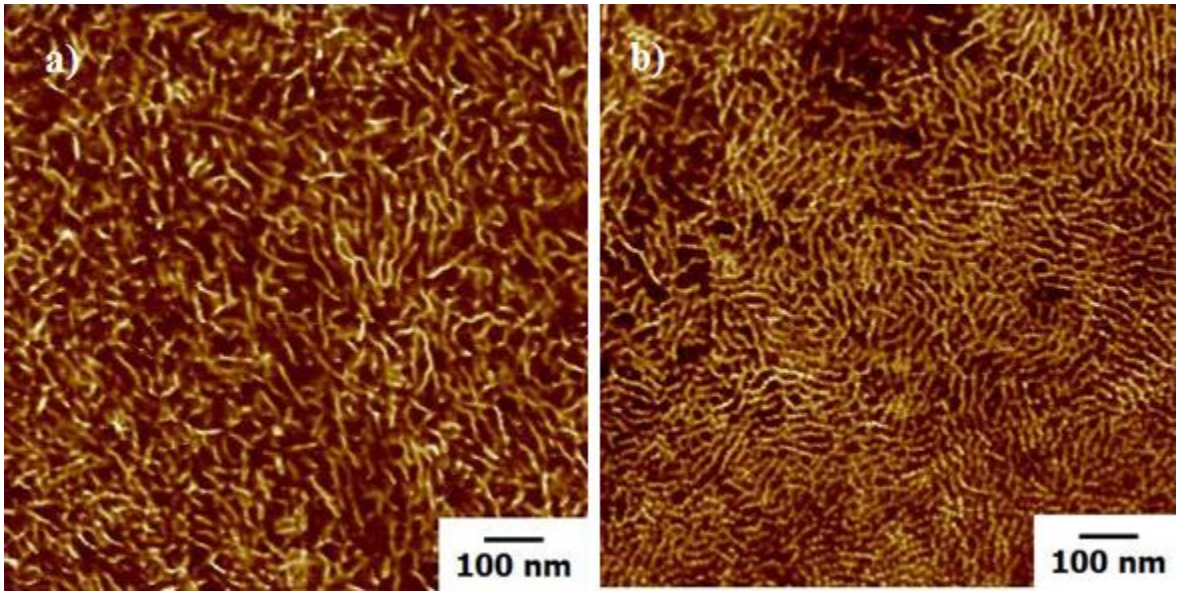

Figure 4.6. Atomic force images in tapping mode of segmented copolyesters. (a) 30 wt% hard segment content. (b) 40 wt% hard segment content.

SAXS experiments complemented AFM morphological findings and determined the presence of bulk microphase separation (**Figure 4.7**). Scattering intensity peaks were broad, weak, and characteristic of non-uniform microphase separation seen in multiblock segmented copolymers. The scattering vector peak maximum, q_m, corresponds to the average interdomain spacing, L, according to Bragg's law:

$$L = \frac{2\pi}{q_m}$$

Small-angle X-ray scatterings of the 30 and 40 wt% hard segment segmented copolyesters showed a q_m of 0.361 and 0.402 nm^{-1}, which were equivalent to 17.4 and 15.6 nm interdomain spacings, respectively. The SAXS profiles exhibited a shift to higher q values, smaller interdomain spacings, with increasing hard segment content and related to a denser physical network microphase separation with increasing hard segment content. In addition to the smaller interdomain spacings, the 40 wt% hard segment segmented copolyester possessed a sharper scattering intensity profile compared to the 30 wt% hard segment copolyester. The sharper intensity corresponds to a more regular and uniform morphology compared to the 30 wt% hard segment copolyester. The SAXS results agreed well with AFM images of the segmented copolyester surface morphology. Current efforts in electron microscopy involve investigations of selective staining strategies, and in addition, metal sulfonated introduction will add sufficient contrast.

The literature extensively describes the dynamics and structural parameters that dictate block copolymers microphase separation.[58, 59] The polymer block molecular weight, polydispersity, and Flory-Huggins interaction parameter contribute to polymer phase-mixing. More importantly, these parameters are tailored through careful selection of the copolymer composition and well-controlled polymerization techniques. Periodic, long-range microphase separated morphologies in well-defined block copolymers arise from the incompatibility and weight content of the constitutive blocks. Segmented multiblock copolymers such as polyurethanes and polyether-esters exploit differences in the polymer segment interaction energies to achieve microphase separation.[60] For instance, polar hydrogen bonding phases in polyurethanes promote preferential microphase separation of the hard segment from less polar polyether phases. Furthermore, our group reported the microphase separation and morphologies

of segmented copolymers are highly sensitive to competitive non-covalent interactions.[61] Segmented PTMO-based polyurethanes containing phosphonium salts within the hard segment significantly reduced the hydrogen bonding interactions, effectively modified their thermomechanical behavior, and reduced tensile properties of the ionic elastomers. Thus, an entirely polyester-based segmented copolymer that lacks strong differences in block polarity may benefit from dynamic, non-covalent interactions in future studies.

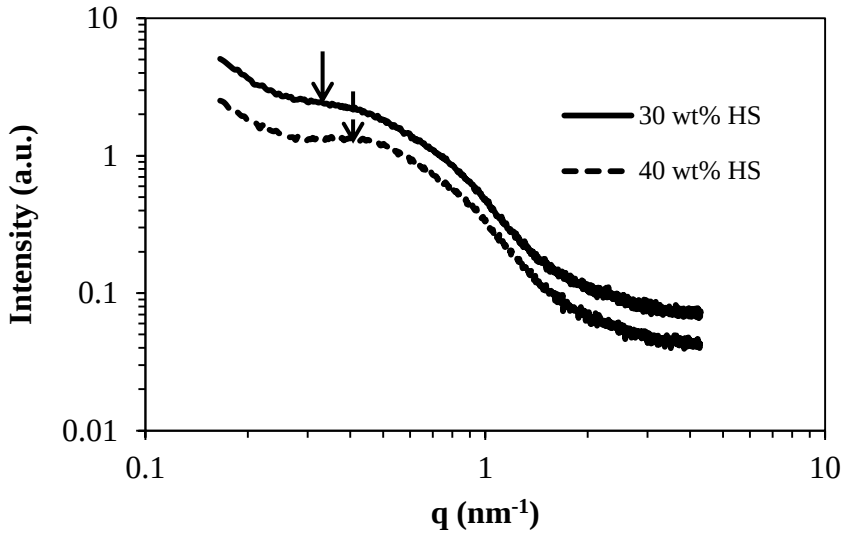

Figure 4.7. SAXS profiles of scattering intensity versus scattering vector for poly[(CBDO-DMCD)-*co*-(DEG-DMAp)] copolyester.

4.5 *Conclusions*

Conventional polyester melt transesterification polymerization produced a series of well controlled high-T_g poly(CBDO-DMCD) polyols. A transesterification study demonstrated the influence of alcohol steric hindrance and reaction temperature on the degree of transesterification in poly(CBDO-DMCD) oligomers. This study also determined the appropriate melt reaction conditions for the subsequent chain extension of the polyols with DEG and DMAp. The one-pot synthesis of poly[(CBDO-DMCD)-*co*-(DEG-DMAp)] occurred at 180 °C to reduce hard segment sequence scrambling through transesterification during chain extension. DSC and DMA revealed a low T_g for all segmented copolyesters consistent with the T_g of the poly(DEG-DMAp) homopolymer. In addition, a systematic increase with hard segment weight content seen in the DMA rubbery plateau modulus and plateau breadth further supported a segmented block topology. AFM of these segmented copolyesters revealed an elaborate microphase separated surface morphology with increasing hard segment phases from 30 to 40 wt% hard segment and correlated well with DMA and tensile testing results.

Acknowledgements
This work is supported in part by the U.S. Army Research Laboratory and the U.S. Army Research Office under the Army Materials Center of Excellence Program, contract W911NF-06-2-0014. The authors would also like to thank Eastman Chemical Company for providing CBDO and DMCD monomers and the Riffle research group for chloroform GPC analysis. In addition, the authors thank Steve McCartney at the Virginia Tech Institute of Critical Technology and Applied Sciences (ICTAS) Nanoscale Characterization and Fabrication Laboratory (NCFL) for atomic force microscopy assistance and training.

4.6 *References*

1. Brown, K.; Hooker, J. C.; Creton, C., *Macromolecular Materials and Engineering* **2002,** *287* (3), 163-179.
2. Louie, J. S.; Pinnau, I.; Ciobanu, I.; Ishida, K. P.; Ng, A.; Reinhard, M., *Journal of Membrane Science* **2006,** *280* (1-2), 762-770.
3. Spontak, R. J.; Patel, N. P., *Current Opinion in Colloid & Interface Science* **2000,** *5* (5-6), 333-340.
4. Fasolka, M. J.; Mayes, A. M., *Annual Review of Materials Research* **2001,** *31* (1), 323.
5. Raquez, J. M.; Deléglise, M.; Lacrampe, M. F.; Krawczak, P., *Prog. Polym. Sci.* **2010,** *35* (4), 487-509.
6. Williams, C. K.; Hillmyer, M. A., *Polymer Reviews* **2008,** *48* (1), 1-10.
7. Petrović, Z. S., *Polymer Reviews* **2008,** *48* (1), 109-155.
8. Liu, C.; Liu, F.; Cai, J.; Xie, W.; Long, T. E.; Turner, S. R.; Lyons, A.; Gross, R. A., *Biomacromolecules* **2011,** *12* (9), 3291-3298.
9. Wanamaker, C. L.; Tolman, W. B.; Hillmyer, M. A., *Biomacromolecules* **2009,** *10* (2), 443-448.
10. Wang, X.; Xie, X.; Cai, C.; Rytting, E.; Steele, T.; Kissel, T., *Macromolecules* **2008,** *41* (8), 2791-2799.
11. Wanamaker, C. L.; O'Leary, L. E.; Lynd, N. A.; Hillmyer, M. A.; Tolman, W. B., *Biomacromolecules* **2007,** *8* (11), 3634-3640.
12. Dai, S.; Xue, L.; Zinn, M.; Li, Z., *Biomacromolecules* **2009,** *10* (12), 3176-3181.
13. Mather, B. D.; Viswanathan, K.; Miller, K. M.; Long, T. E., *Prog. Polym. Sci.* **2006,** *31* (5), 487-531.
14. Ozturk, G.; Long, T. E., *J. Polym. Sci., Part A: Polym. Chem.* **2009,** *47* (20), 5437-5447.
15. Unal, S.; Ozturk, G.; Sisson, K.; Long, T. E., *J. Polym. Sci., Part A: Polym. Chem.* **2008,** *46* (18), 6285-6295.
16. Unal, S.; Long, T. E., *Macromolecules* **2006,** *39* (8), 2788-2793.
17. McKee, M. G.; Unal, S.; Wilkes, G. L.; Long, T. E., *Prog. Polym. Sci.* **2005,** *30* (5), 507-539.
18. Ozturk, G. I.; Pasquale, A. J.; Long, T. E., *The Journal of Adhesion* **2010,** *86* (4), 395-408.
19. Lin, Q.; Unal, S.; Fornof, A. R.; Armentrout, R. S.; Long, T. E., *Polymer* **2006,** *47* (11), 4085-4093.
20. Karikari, A. S.; Williams, S. R.; Heisey, C. L.; Rawlett, A. M.; Long, T. E., *Langmuir* **2006,** *22* (23), 9687-9693.
21. Karikari, A. S.; Mather, B. D.; Long, T. E., *Biomacromolecules* **2006,** *8* (1), 302-308.
22. Karikari, A. S.; Edwards, W. F.; Mecham, J. B.; Long, T. E., *Biomacromolecules* **2005,** *6* (5), 2866-2874.
23. Staudinger, H.; Klever, H. W., *Berichte der deutschen chemischen Gesellschaft* **1906,** *39* (1), 968-971.
24. Hasek, R. H.; Elam, E. U.; Martin, J. C.; Nations, R. G., *The Journal of Organic Chemistry* **1961,** *26* (3), 700-704.
25. Margulis, T. N., *Chemical Communications (London)* **1969,** (5), 215-16.
26. Shirrell, C. D.; Williams, D. E., *Acta Crystallographica Section B* **1976,** *32* (6), 1867-1870.

27. Hasek, R. H.; Clark, R. D.; Chaudet, J. H., *The Journal of Organic Chemistry* **1961,** *26* (9), 3130-3133.
28. Clark, R. D. Treatment of 2,2,4,4-Tetramethyl-1,3-Cyclobuntaediols. 3,236,899, February 23, 1961, 1966.
29. Elam, E. U.; Martin, J. C.; Gilkey, R. Linear polyesters and polyester-amids from 2,2,4,4-tetraalkyl-1,3-cyclobutanediols. 3,313,777, 1967.
30. Kelsey, D. R.; Scardino, B. M.; Grebowicz, J. S.; Chuah, H. H., *Macromolecules* **2000,** *33* (16), 5810-5818.
31. Leibfarth, F. A.; Kang, M.; Ham, M.; Kim, J.; Campos, L. M.; Gupta, N.; Moon, B.; Hawker, C. J., *Nature Chemistry* **2010,** *2* (3), 207-212.
32. Wolffs, M.; Kade, M. J.; Hawker, C. J., *Chem. Commun.* **2011,** *47* (38), 10572-10574.
33. Kang, H.; Lin, Q.; Armentrout, R. S.; Long, T. E., *Macromolecules* **2002,** *35* (23), 8738-8744.
34. Poirier, Y.; Dennis, D. E.; Klomparens, K.; Somerville, C., *Science* **1992,** *256* (5056), 520-523.
35. Martina, M.; Hutmacher, D. W., *Polym. Int.* **2007,** *56* (2), 145-157.
36. Fenouillot, F.; Rousseau, A.; Colomines, G.; Saint-Loup, R.; Pascault, J. P., *Prog. Polym. Sci.* **2010,** *35* (5), 578-622.
37. Wang, C. S.; Lin, C. H., *Polymer* **2000,** *41* (11), 4029-4037.
38. Wanamaker, C. L.; Tolman, W. B.; Hillmyer, M. A., *Macromolecular Symposia* **2009,** *283-284* (1), 130-138.
39. Gibbs, J., *J. Chem. Phys.* **1958,** *28* (3), 373.
40. Cown, J. M. G., *Eur. Polym. J.* **1975,** *11* (4), 297-300.
41. Bryant, W. M. D.; Smith, D. M., *J. Am. Chem. Soc.* **1936,** *58* (6), 1014-1017.
42. Park, S. S.; Kang, H. J., *Polym. J.* **1999,** *31* (3), 238-245.
43. Flory, P. J., *Principles of polymer chemistry*. Cornell University Press: Ithaca, 1953.
44. Flory, P. J., *J. Am. Chem. Soc.* **1940,** *62* (9), 2261-2264.
45. Flory, P. J., *J. Am. Chem. Soc.* **1939,** *61* (12), 3334-3340.
46. Chen, S. A.; Wu, K. C., *Journal of Polymer Science Part a-Polymer Chemistry* **1982,** *20* (7), 1819-1831.
47. Jedlovčnik, R.; Šebenik, A.; Golob, J.; Korbar, J., *Polymer Engineering & Science* **1995,** *35* (17), 1413-1417.
48. Zetterlund, P. B.; Weaver, W.; Johnson, A. F., *Polym. React. Eng.* **2002,** *10* (1-2), 41-57.
49. Nalampang, K.; Johnson, A. F., *Polymer* **2003,** *44* (19), 6103-6109.
50. Anderson, E. B.; Long, T. E., *Polymer* **2009,** *51* (12), 2447-2454.
51. Schmalz, H.; Abetz, V.; Lange, R.; Soliman, M., *Macromolecules* **2001,** *34* (4), 795.
52. Yamauchi, K.; Kanomata, A.; Inoue, T.; Long, T. E., *Macromolecules* **2004,** *37* (10), 3519-3522.
53. Klinedinst, D. B.; Yilgör, E.; Yilgör, I.; Beyer, F. L.; Wilkes, G. L., *Polymer* **2005,** *46* (23), 10191-10201.
54. Sheth, J. P.; Wilkes, G. L.; Fornof, A. R.; Long, T. E.; Yilgor, I., *Macromolecules* **2005,** *38* (13), 5681-5685.
55. McLean, R. S.; Sauer, B. B., *Macromolecules* **1997,** *30* (26), 8314-8317.
56. Sheth, J. P.; Unal, S.; Yilgor, E.; Yilgor, I.; Beyer, F. L.; Long, T. E.; Wilkes, G. L., *Polymer* **2005,** *46*, 10180-10190.

57. Yilgor, I.; Yilgor, E.; Das, S.; Wilkes, G. L., *J. Polym. Sci., Part B: Polym. Phys.* **2009,** *47* (5), 471-483.
58. Leibler, L., *Macromolecules* **1980,** *13* (6), 1602-1617.
59. Bates, F. S., *Science* **1991,** *251* (4996), 898-905.
60. Velankar, S.; Cooper, S. L., *Macromolecules* **1998,** *31* (26), 9181-9192.
61. Williams, S. R.; Wang, W.; Winey, K. I.; Long, T. E., *Macromolecules* **2008,** *41* (23), 9072-9079.

Chapter 5: Influence of Charge Placement on the Thermal and Morphological Properties of Sulfonated Segmented Copolyesters

(Submitted to *Polymer*)

Musan Zhang, Mingqiang Zhang, Robert B. Moore, and Timothy E. Long

Department of Chemistry, Macromolecules and Interfaces Institute
Virginia Tech, Blacksburg, VA 24061-0212

5.1 *Abstract*

A new synthetic strategy using melt transesterification enabled selective control of ionic charge placement into the hard segment or soft segment block of segmented copolyesters. Dynamic mechanical analysis of sulfonated soft segment copolyesters revealed an increase in the low-T_g transition and rubbery plateau storage modulus as a function of sulfonation level. Sulfonated hard segment copolyesters displayed similar rubbery plateau moduli and decreasing flow temperature from 145 to 90 °C. Dynamic melt rheology and *in situ*, variable temperature small-angle X-ray scattering determined the non-sulfonated copolyester order-disorder transition at 150 ± 5 °C, which was ~60 °C above the hard segment T_g. Atomic force microscopy revealed sulfonated hard segment copolyesters contained more disordered surface morphologies. Sulfonated soft segment copolyesters demonstrated increased tensile stress and improved tensile strain from 18 to 170% with increasing ion content. The enhanced mechanical performance of sulfonated soft segment was attributed to the preserved microphase-separated morphology and the presence of physical crosslinks from electrostatic interactions.

5.2 *Introduction*

Segmented block copolyesters represent an important class of commercial thermoplastic elastomers. Typical segmented block copolyesters contain low glass transition temperature (T_g), flexible soft segments (SS) that provide high tensile strains, and high-T_g hard segments (HS) that serve as mechanically reinforcing phases. In contrast to chemically crosslinked thermosets, microphase separation in block copolymers often incorporates noncovalent, intermolecular, interactions that function as thermally labile, physical crosslinks.[1] Microphase separation in block copolymers primarily depends on polymer incompatibility as a function of the interaction parameter, χ, block molecular weights, and polydispersity.[2] Due to inherent polydispersity obtained from traditional step-growth polymerization, segmented block copolymers often possess hydrogen bonding, electrostatic interactions, or crystallization to increase χ and thermodynamically promote microphase separation.[1, 3]

Ionomers are defined as polymers with low levels of ionic sites, often less than 15 mol%.[4, 5] Depending on the ionic composition, ionic concentration, and polymer matrix polarity, ionic sites microphase separate into ion-rich domains called *multiplets* or *clusters*.[6, 7] These ionic associations afford thermally labile, multifunctional, physical crosslinks that improve polymer properties. Ionic block copolymers impart unique and desirable thermomechanical properties and morphology for emerging applications including conductive electroactive devices,[8-10] high performance adhesives,[11] and drug delivery vehicles.[12, 13] The presence of ionic interactions in segmented block copolymers presents a potential synergy between the microphase-separated morphology and ionic association. For example, segmented block copolymers based on ammonium[14, 15] and imidazolium[16] ionenes offered controlled ionic distribution and charge density, which influenced the local and long-range morphology that dictated charge-transport properties.[17] McGrath and coworkers also observed improved proton conductivity for segmented

sulfonated poly(arylene ethers) due to a higher degree of ionic interconnectivity originating from the microphase separated morphology.[18, 19]

In segmented polyesters[19] and polyurethanes (PU),[20, 21] the addition of pendant ionic sites within the HS dramatically influences the thermomechanical properties and morphologies. The ionic aggregate size and electrostatic strength directly correlated to the degree of microphase separation and thermomechanical properties. Polyurethanes with higher dielectric constants for the SS, such as poly(ethylene glycol) (PEG) and poly(propylene glycol) (PPG), resulted in frequent and smaller ionic aggregates because the polymer matrix effectively solubilized the ion pairs.[20] Further investigations of PU that contain phosphonium cations in the HS reduced hydrogen-bonding interactions, but effectively served as the principal driving force for microphase separation.[22] Despite numerous reported examples of ion-containing segmented multiblock copolymers, few examples isolate the influence of ionic associations from competing interactions. Furthermore, the challenging synthetic methods previously employed often limit the investigations on controlled placement of ionic groups within the HS or SS. However, the incorporation of ionic interactions generates significant changes in the polymer properties and provides an additional approach to tailor specific polymer properties for more sophisticated applications such as electroactive transducers and polymeric water purification membranes.

This manuscript describes an efficient synthetic approach that permitted precise control of the charge location and content in amorphous, segmented block copolyesters, which enabled a systematic investigation of electrostatic interactions on physical properties. Melt polymerization temperatures at 180 °C of preformed, sterically hindered polyester polyols prevented the HS transesterification during chain-extension, which proved critical in preserving the segmented chemical composition. [23] Nederberg and coworkers subsequently reported on melt derived

block copolyesters with fluorinated isophthalic-based segments.[24] The incorporation of electrostatic interactions has developed our understanding of structure-property relationships in ionomeric, segmented block copolymers. The majority of charged segmented block copolymers described in the literature contain hydrogen-bonding interactions or crystallization. This present study removed other noncovalent interactions in order to isolate the effects of electrostatic interactions on polymer morphology and physical properties. The impact of the electrostatic interactions depends largely on the ability of the surrounding polymer matrix to solvate the ionic group. The charge placement significantly impacted the local, morphological ordering; sulfonated HS copolyesters resulted in a more disordered morphology. Tensile testing revealed significantly improved mechanical properties for sulfonated SS copolyesters due to the preservation of nanoscale morphology.

5.3 *Experimental Section*

Dimethyl-1,4-cyclohexane dicarboxylate (95% trans, DMCD), dimethyl isophthalate (DMI), and 2,2,4,4-tetramethyl-1,3-cyclobutanediol (45/55 *cis/trans*, CBDO) were graciously provided from Eastman Chemical Company and used without subsequent purification. Dimethyl 5-sulfoisophthalate sodium salt (99.9%, sDMI), dimethyl adipate (99%, DMAp), and diethylene glycol (99.9%, DEG), and dibutyltin oxide (99.9%) were purchased from Sigma-Aldrich and used as received. A titanium tetraisopropoxide (99%, Sigma-Aldrich) solution in anhydrous 1-butanol was prepared according to previous procedures.[25] The synthesis of the non-sulfonated copolyester was polymerized according to previously described procedures.[23]

Synthesis of sulfonated poly(sCBDO-DMCD) polyols

Melt transesterification of DMCD, CBDO, and sDMI produced sulfonated HS polyols, and a stoichiometric excess of CBDO afforded hydroxyl-terminated oligomers for subsequent chain extension. In a representative synthesis, DMCD (1.0 mol eq), CBDO (1.2 mol eq), sDMI (0.01, 0.03, or 0.05 mol eq), and dibutyltin oxide (600 ppm) were charged into a 100-mL, round-bottomed flask equipped with a mechanical stirrer and condenser. The reaction flask was purged and degassed with nitrogen three times before polymerization at 200 – 240 °C over 5 h under a constant N_2 purge. Reduced pressure (<0.1 mmHg) was subsequently applied for 2 h.

Synthesis of sulfonated segmented copolyesters

Non-sulfonated HS polyols were chain extended with DEG, DMAp, and sDMI to produce sulfonated SS copolyesters. Sulfonated HS copolyesters were synthesized with sulfonated HS polyol precursors. In a representative synthesis, poly(sCBDO-DMCD) (30 wt%), DEG, DMAp, titanium tetraisopropoxide (40 ppm), and dibutyltin oxide (600 ppm) were charged into a 100-mL, round-bottomed flask equipped with a mechanical stirrer, nitrogen inlet, and condenser. The reaction mixture was purged and degassed three times before polymerization at 180 °C for 5 h under a N_2 purge. Reduced pressure (<0.1 mmHg) was applied for 2 h.

Solution cast, polymeric films were coated onto silicon-coated Mylar™ substrates using a drawdown blade (1 mm coating thickness) from 90/10 (w/w %) chloroform/methanol (18 wt% solids). The films were dried at ambient conditions for 1 d and subsequently dried under reduced pressure for 1 d at 23 °C, and 1 d at 80 °C. Samples were annealed at 80 °C under reduced pressure for 1 d immediately prior to characterization.

Polymer Characterization

^{1}H NMR spectroscopic analysis (Varian INOVA 400 MHz) confirmed the polymer chemical composition in $CDCl_3$. Size exclusion chromatography (SEC) in chloroform (flow rate 1.0 mL/min, Waters 707 Autosampler with Waters 1515 isocratic HPLC pump, Waters 2414 refractive index detector, and Viscotek 270 MALLS/viscometric dual detector) determined the relative molecular weights of uncharged polyester polyols using polystyrene standards. Differential scanning calorimetry (DSC) (TA Instruments Q1000) heat/cool/heat experiments from -60 to 200 °C, measured the polymer thermal transitions from the second heating cycle (N_2, heating rate 10 °C/min). Thermogravimetric analysis (TGA) (TA Instruments Q500) provided the onset degradation temperature of the polyesters (N_2, heating rate 10 °C/min). Dynamic mechanical analysis (DMA) (TA Instruments Q800) temperature ramp experiments analyzed the nonionic and sulfonated segmented copolyesters thermomechanical property from -100 to 150 °C (film tension mode, 1 Hz, heating rate 3 °C/min). A TA Instruments Discovery HR-2 rheometer performed isothermal, dynamic oscillatory shear experiments using an 8 mm, parallel plate geometry. The temperature ranged from 80 to 200 °C, and dynamic measurements were obtained at 5 °C intervals. All rheological experiments were conducted from 0.125 – 1.000% strain, and the linear viscoelastic region was confirmed using strain sweep experiments. An Instron 4411 universal testing instrument measured tensile properties of the segmented copolyesters (crosshead speed 10 mm/min, average of five specimens). Tensile cyclic hysteresis experiments consisted of three loading and unloading cycles for the 7 mol% sulfonated SS copolyester strained to 80% or 120% at 80 mm/min with 30 sec delays between cycles.

Atomic force microscopy (AFM) (Veeco MultiMode) investigated the surface morphology under tapping mode using a 42 N/m spring constant cantilever tip. The tapping amplitude to free air amplitude setpoint ratio was approximately 0.66 corresponding with

medium to hard tapping. *In situ* VT-SAXS was performed at Advanced Photon Source (APS), Argonne National Laboratory (Beamline 5-ID DND-CAT). The wavelength of X-ray is 0.07293 nm. Scattering from a silver behenate standard was used to calibrate the sample-to-detector distance, and the sample-to-detector distance was 2974 mm. SAXS images were obtained using a low-noise, Mar USA Inc, 162 mm, marCCD camera, with a 4 second exposure time. *In situ* VT-SAXS data was collected approximately every 10 sec from 30 ºC to 200 ºC at a heating ramp rate of 10°C/min. All SAXS data was corrected for sample transmission and background scattering. All SAXS data were analyzed using the in-house software package provided in APS to obtain radically integrated SAXS intensity versus scattering vector q (SAXS), where $q=(4\pi/\lambda)\sin(\theta)$, θ is one half of the scattering angle and λ is the wavelength of X-ray.

5.4 *Results and Discussion*

Polymer Synthesis

The polymerization of sulfonated segmented block copolyesters with controlled ionic placement utilizes our recently reported melt transesterification procedures for segmented block segmented block copolyesters containing poly(CBDO-DMCD) HS.[23] Steric hindrance surrounding the ester carbonyls prevented HS sequence scrambling under melt polymerization conditions and successfully produced high molecular weight segmented copolyesters. The results determined that the melt polymerization temperature and duration significantly influenced the extent of HS transesterification. Based on these conclusions, non-sulfonated and sulfonated HS were chain extended with SS monomers to obtain segmented block copolyesters (30 wt% HS) with controlled charge placement.

Scheme 5.1 illustrates the polymerization strategy used to obtain high-T_g polyols with varying levels of sulfonation (1, 3, or 5 mol% sDMI). Even at low molecular weights, high melt viscosities during the polymerization prevented >5 mol% sulfonation in the polyols. Subsequent chain extension with DEG and DMAp, which formed the SS, afforded sulfonated HS copolyesters (**Scheme 5.2**). Alternatively, non-sulfonated polyol chain extended with DEG, DMAp, and sDMI yielded sulfonated SS copolyesters (**Scheme 5.3**). ^{1}H NMR spectroscopy confirmed polymer compositions, and end group analysis determined the absolute M_n of sulfonated polyols (**Figure S 5.2**). ^{13}C NMR spectroscopies of the segmented copolyesters exhibited two distinct resonances corresponding to the SS and HS carbonyls and confirmed the absence of HS transesterification (**Figure S 5.3**). This efficient, synthetic approach generated segmented block copolyesters with selectively located sodium sulfonates of various concentrations in the HS or SS.

Scheme 5.1. Synthesis of high-T_g sulfonated poly(sCBDO-DMCD) polyols using melt-transesterification.

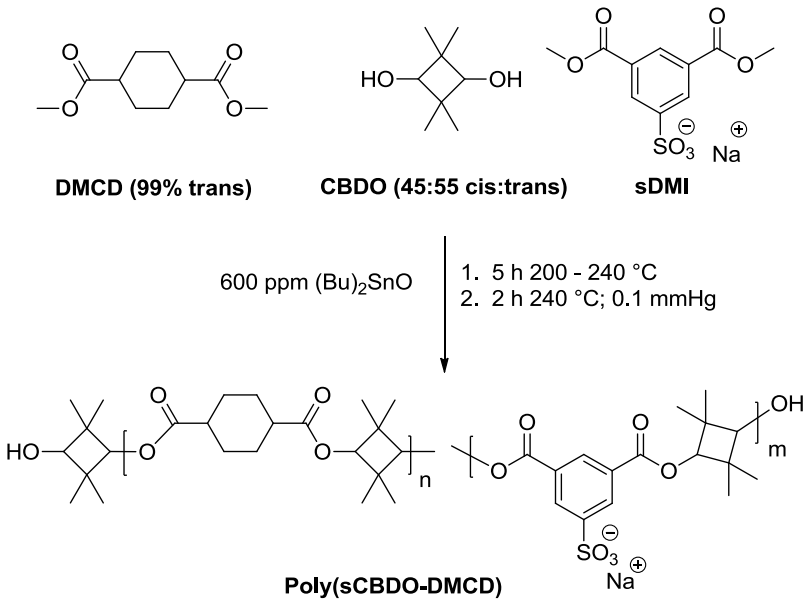

Scheme 5.2. Synthesis of segmented copolyesters containing sulfonated poly(CBDO-DMCD) hard segments using metal-catalyzed melt transesterification.

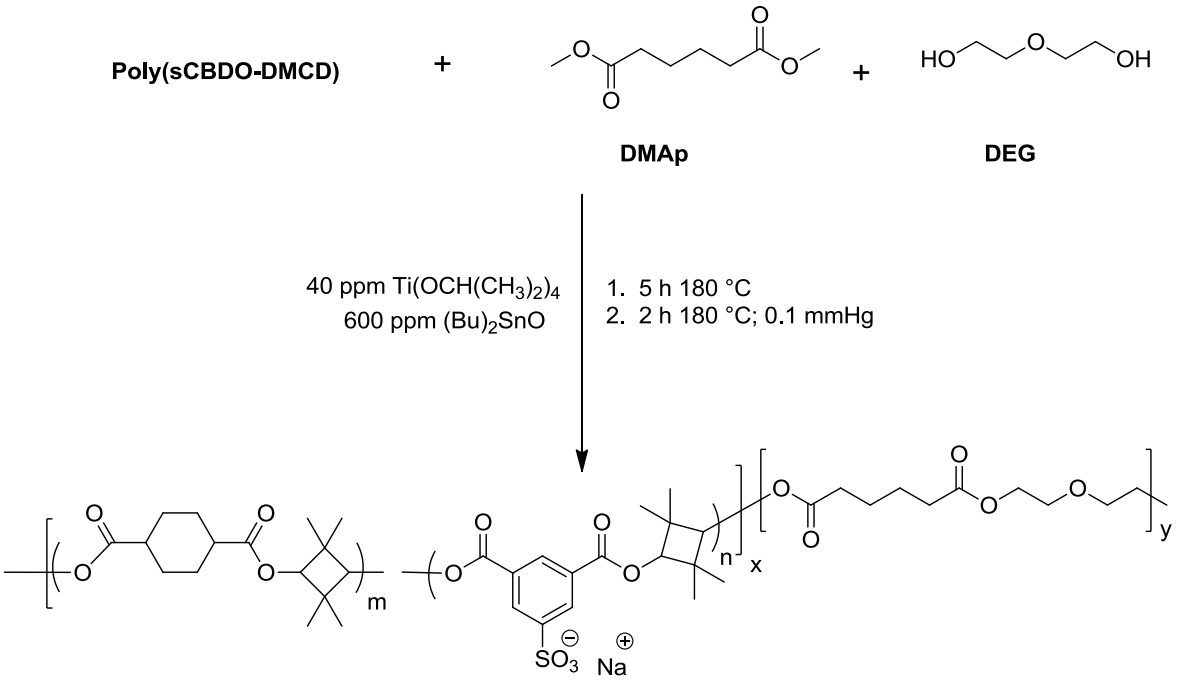

Scheme 5.3. Synthesis of soft segment sulfonated segmented copolyesters containing poly(CBDO-DMCD) hard segments.

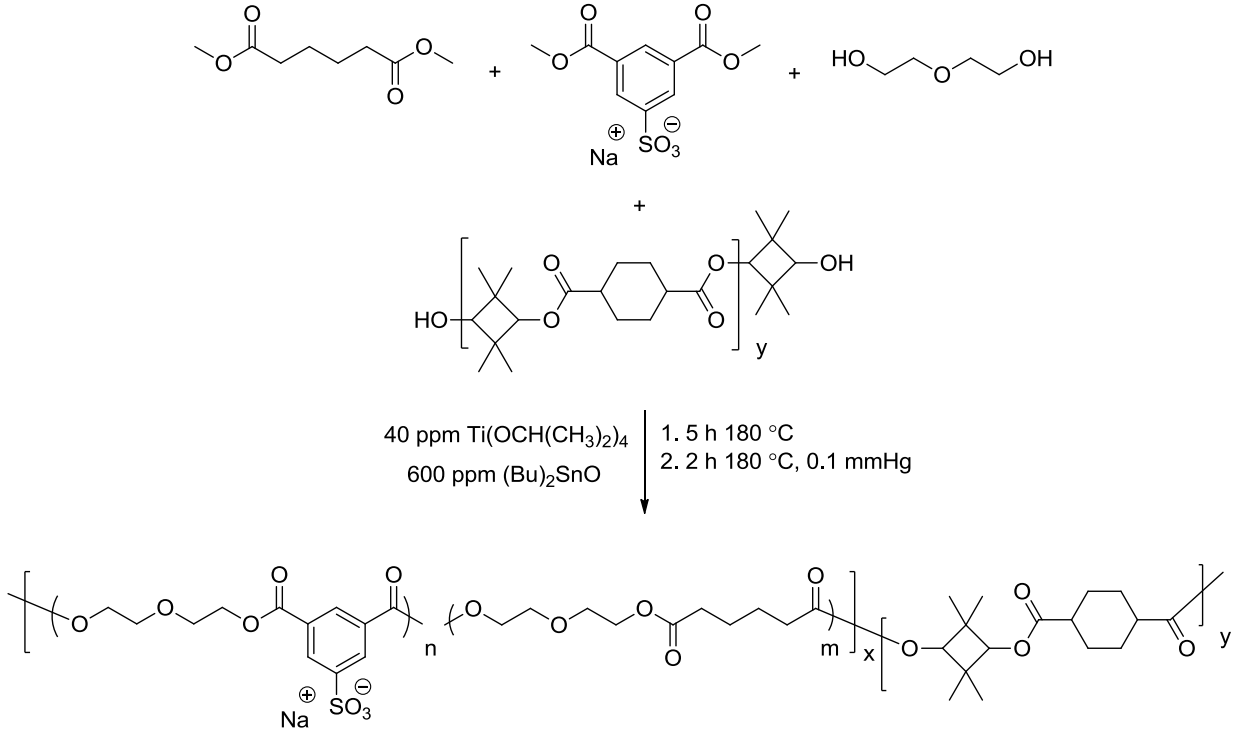

Thermal Properties

Sulfonated and non-sulfonated high-T_g polyols enabled investigations of ionic content on thermal properties (**Figure S 5.4**). **Figure 5.1** illustrates the effect of sulfonation content on the polyol precursor T_g. Although the M_n of the charged polyols remained similar with increasing sulfonation content from 1 to 5 mol%, the T_g increased from 106 to 148 °C. Incorporation of ionic groups in the HS substantially restricted polymer segmental mobility and consequently, increased T_g values. As reported earlier, the extent of increase at low ionic content depends primarily on the ionic concentration, cationic charge, and ion-ion distance. [26]

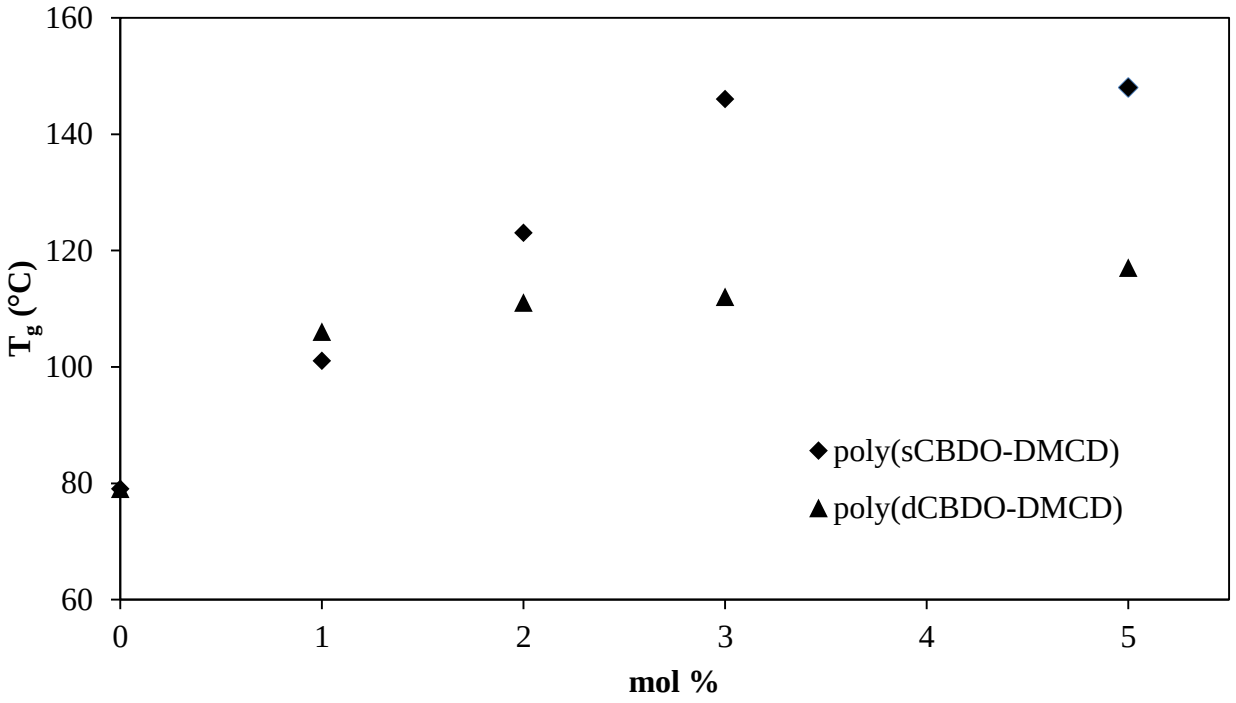

Figure 5.1. HS T_g as a function of sulfonated dimethylisophthalate (poly(sCBDO-DMCD)) or dimethyl isophthalate (poly(dCBDO-DMCD)) molar content.

Table 5.1 summarizes the thermal transitions of sulfonated copolyesters obtained from DSC. The sulfonation placement in either the HS or SS at various concentrations did not affect the low-T_g transition, suggesting an absence of appreciable phase mixing. Although sulfonated

HS polyols had significantly higher T_g's, DSC did not detect the high-T_g transition in the sulfonated HS copolyesters. Low HS content, extent of microphase separation, and reduced heat capacities associated with the HS rigidity offer explanations for the absence of the high-T_g transition in DSC.[27] Interestingly, the HS T_g in sulfonated SS copolyesters was detected (**Figure S 5.5**). Complementary characterization using dynamic mechanical analysis confirmed the presence of the high-T_g transition in all segmented copolyester compositions.

Table 5.1. T_g of soft segment sulfonated copolyesters. T_g values are determined from the second heat of a heat/cool/heat experiment.

Segmented Copolymer	**T_{g1} (°C)**	**T_{g2} (°C)**
30 wt% HS non-sulfonated control	-42	ND
SHSP-1	-44	ND
SHSP-3	-43	ND
SHSP-5	-42	ND
SSSP-1	-41	ND
SSSP-3	-40	102
SSSP-5	-40	109
SSSP-7	-40	115

ND: Not detected using DSC.

Thermomechanical Characterization

Dynamic mechanical analysis evaluated the thermomechanical properties of nonionic and sulfonated copolyester films. In sulfonated HS copolyesters, the low-T_g transition appeared at -

31 °C similar to the non-sulfonated analog (**Figure 5.2**). Our group observed earlier an increase in the SS T_g and loss of the PEG T_m in PEG-based sulfonated hard segment PU.[28] The presence of ion-dipole interactions between the sulfonate anions and ether oxygens promoted phase-mixing and led to the observed thermal transitions. In the sulfonated HS copolyesters, however, a constant SS T_g and similar rubbery plateau moduli indicated the sulfonated groups did not promote phase-mixing (at temperatures less than about 50 °C) or contribute to additional physical crosslinking. Furthermore, increasing sulfonation in the HS systematically reduced the onset of polymer flow (shortened the rubbery plateau) despite an increase in the HS polyol T_g observed in DSC. This trend presumably implied either a change in the copolyester morphology due to electrostatic interactions or a decrease in the solubility-interaction parameter, χ, leading to a lower phase-mixing temperature (i.e., ODT).[29]

In sharp contrast, the sulfonated SS copolyesters displayed an increase in the low-T_g transition from -31 °C to -23 °C (**Figure 5.3**). Although DSC determined the low-T_g transition remained unchanged, DMA data showed an increase in the low-T_g transition with sulfonation content. The T_g variation obtained from DSC and DMA emphasized the complementary analytical methods necessary to characterize segmented copolymers. Sulfonated SS copolyesters with 5 and 7 mol% ionic content possessed higher rubbery plateau moduli, which indicated the sulfonate groups provided additional physical crosslinking in the SS matrix. A broadening and increase of the low-T_g transition resulted from a heterogeneous electrostatic network restricting segmental mobility.

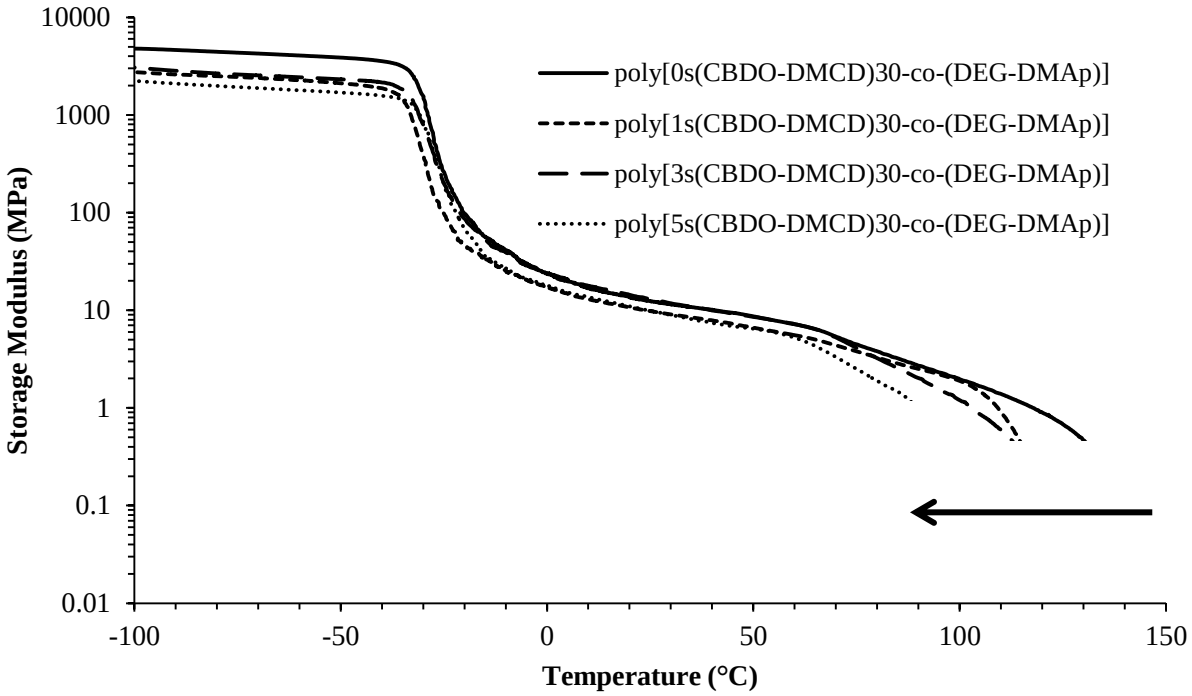

Figure 5.2. Dynamic mechanical analysis of sulfonated HS copolyesters.

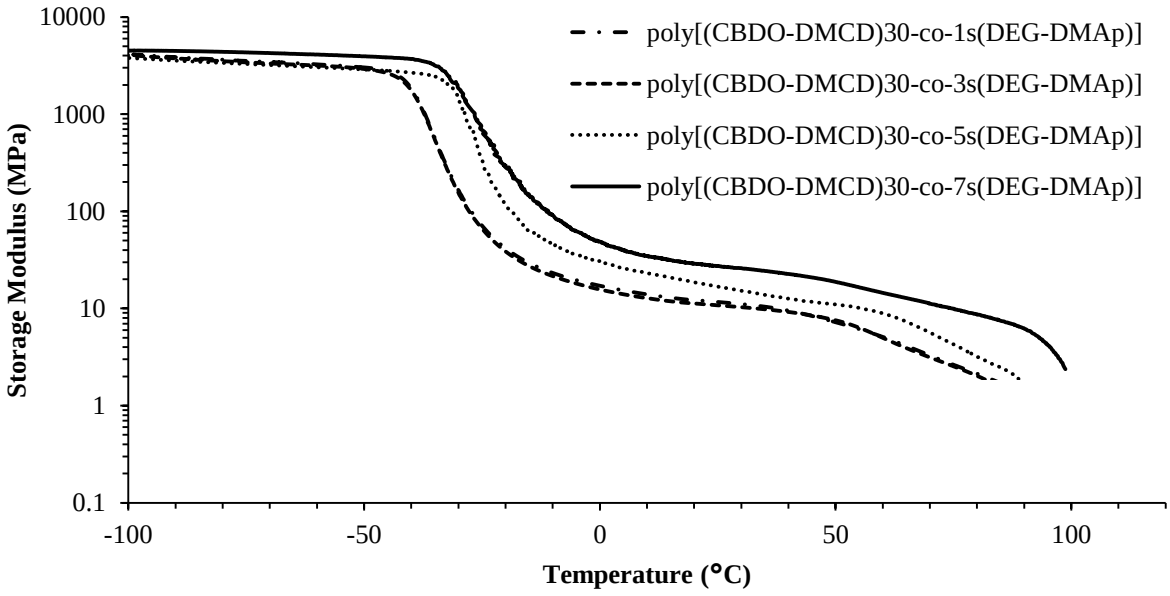

Figure 5.3. Dynamic mechanical analysis of sulfonated SS copolyesters.

The thermomechanical analysis suggested that ionic multiplets presumably formed at 5 mol% sulfonation leading to a discontinuous increase in both the rubbery plateau modulus and

low-T_g transition. Previous investigations on the influence of ionic concentration in ionomers also observed an abrupt transition in polymer properties such as T_g,[30] melt viscosity,[31, 32] and flow activation[33] at a critical ion concentration. The Eisenberg-Hird-Moore multiplet-cluster model for random ionomers explained this phenomena as a transition from isolated ion pairs to the formation of multiplets.[6] The precise transition depended on the strength of the electrostatic interaction and the proximity between ionic groups. The presence of multiplets restricts the segmental mobility of the local polymer matrix surrounding the multiplets and changes the polymer viscoelastic properties.

Morphological Characterization

Several reports on the microphase separation behavior of segmented block copolymers identified the transition from a microphase-separated domains to a disordered, homogenous polymer phase, known as the ODT temperature.[34] *In situ*, variable temperature SAXS investigated the influence of temperature on the non-sulfonated copolyester morphology (**Figure 5.4**). At temperatures below 130 ºC, a scattering peak maximum was observed at $q \approx 0.35$ nm^{-1}, which indicated a microphase-separated morphology between the hard and soft domains. As the temperature increased from 130 – 140 ºC, the broad scattering peak suddenly decreased in intensity. At 145 ºC, the scattering peak was completely indiscernible, which suggested the transition to a more disordered, homogeneous morphology.

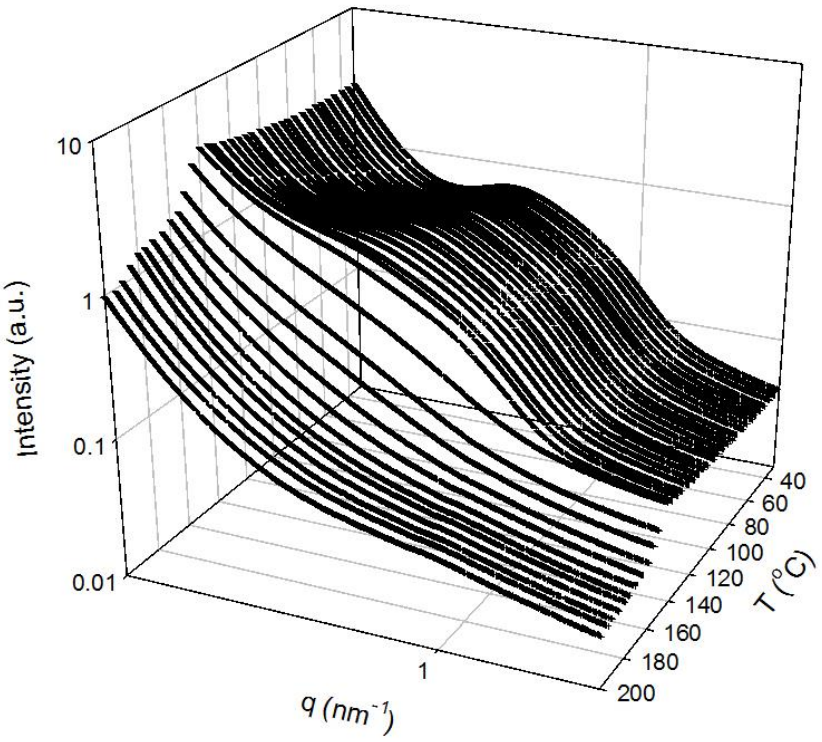

Figure 5.4. ***In situ*** **VT-SAXS profile demonstrating the disappearance of the scattering peak maximum (q ≈ 0.35 nm^{-1}) from 130 to 145 °C. VT-SAXS profiles were collected approximately every 10 sec from 30 – 200 °C under a heating ramp rate of 10 °C/min. Each scattering profile represents a 5 °C interval.**

Dynamic melt rheology confirmed the ODT transition temperature observed from the VT-SAXS analysis. **Figure 5.5** represents log-log plots of *G'* vs. *G''* at various temperature steps. The ODT is defined rheologically as the transition at which *G'* vs. *G''* become independent of temperature, usually identified by the characteristic slope of two. **Figure 5.5** clearly demonstrates the *G'* vs. *G''* curves systematically collapsed along a single curve, whose slope = 2, at 160 ± 5 °C. Previous melt rheological studies of segmented block copolymers utilized *G'* and *G''* vs. temperature plots to identify the ODT.[34] However, these experiments were highly sensitive to the block volume fraction, and the ODT became increasingly difficult to discern in copolymer systems with less homogenous morphologies.[35] To the best of our knowledge, log-log plots of *G'* vs. *G''* have never been applied to segmented block copolymer

systems to determine the ODT. Our melt rheological studies supported the VT-SAXS results and successfully determined the ODT.

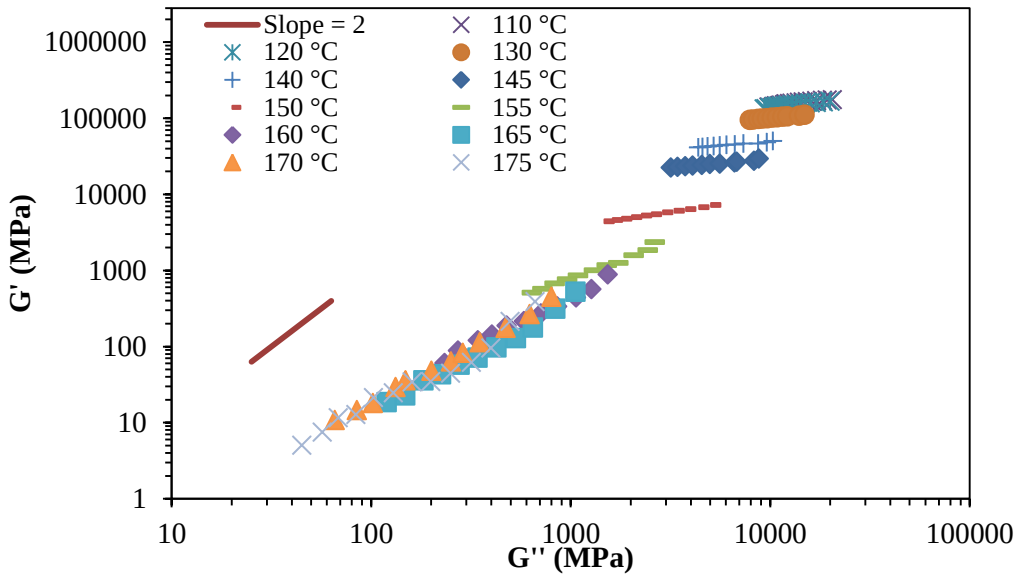

Figure 5.5. Log-log plots of *G'* vs. *G''* obtained from dynamic melt rheology. The transition to temperature-independent *G'* vs. *G''* curves (slope = 2) was used to identify the ODT.

Interestingly, the ODT of the non-sulfonated copolyester was consistent with the DMA polymer flow temperature (T_{flow} = 145 °C), which suggested the thermomechanical integrity was extended beyond the HS T_g until the loss of microphase separation at the ODT. This trend presumably implied either a change in the copolyester morphology due to electrostatic interactions or a decrease in the solubility-interaction parameter, χ, leading to a lower phase-mixing temperature.[36] It is important to note the difference between a phase-mixed morphology and the phase-mixing temperature, which relates to the ODT. The sulfonate group within the HS maintained a microphase-separated morphology; however, due to the presence of ionic sulfonate reduces the ODT temperature due to possible a decrease in the solubility-interaction parameter.

The SAXS and oscillatory rheological data suggest the flow temperature relates to the order-disorder transition.

The ionic placement demonstrated significant differences in the thermomechanical properties of the sulfonated segmented copolyesters and prompted us to investigate further the polymer morphology using AFM. AFM phase images in **Figure 5.6** reflect the copolyester surface morphology as a function of ionic charge placement and content. The non-sulfonated copolyester displayed unique thread-like, interconnected, microphase-separated morphology, which exhibited regularity in the local ordering. The sulfonated SS copolyesters surface morphology closely resembled the non-sulfonated copolyester. However, sulfonated HS copolyesters exhibited a more disordered surface morphology with less well-defined surface features.

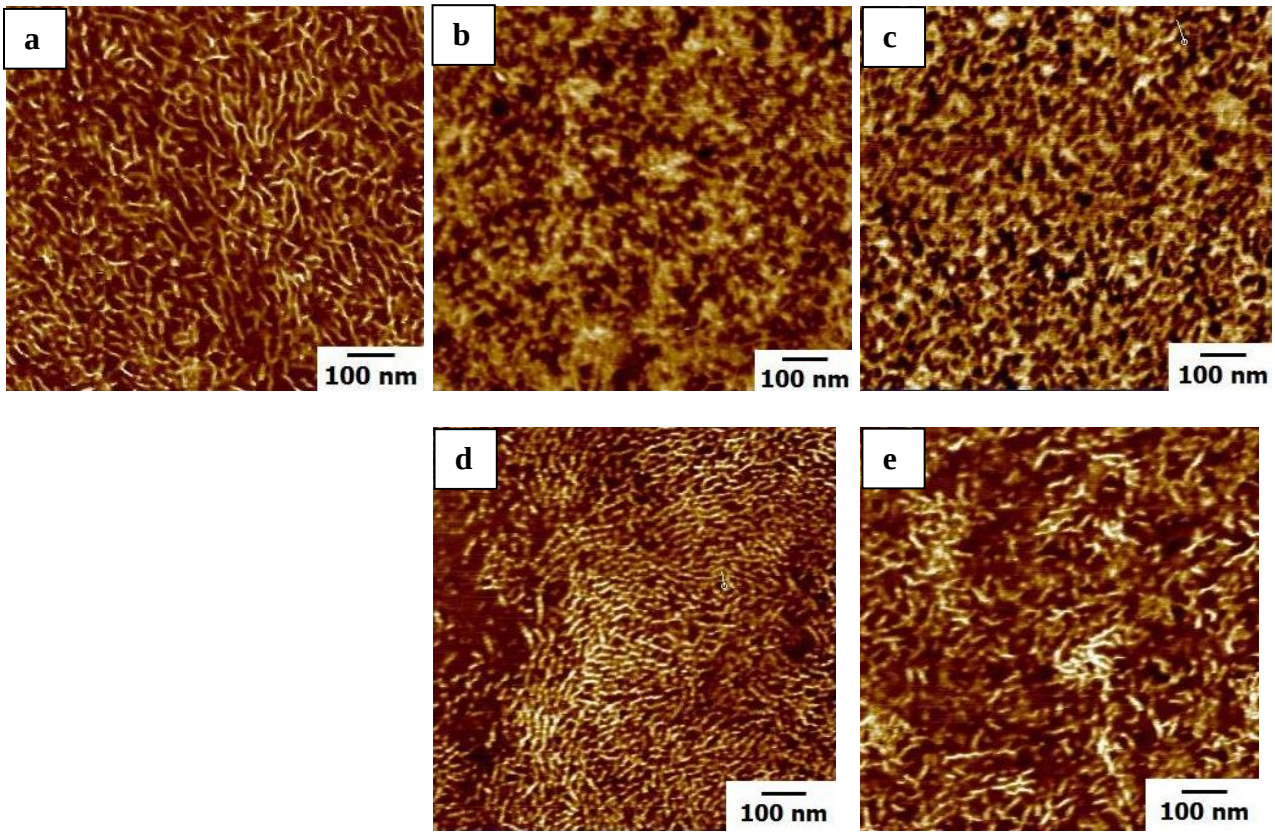

Figure 5.6. Atomic force microscopy phase images of non-sulfonated and sulfonated segmented block copolyesters containing 30 wt% HS. a) Non-sulfonated, b) 3 mol% sulfonated HS, c) 5 mol% sulfonated HS, d) 3 mol% sulfonated SS, and e) 5 mol% sulfonated SS.

Tensile Properties

Tensile studies elucidated the influence of ionic interactions on the segmented copolyesters mechanical properties. **Figure 5.7.a** reflects the stress at break for sulfonated HS and SS copolyesters. Increasing sulfonation in SS copolyesters systematically increased the stress at break from 1 to 3 MPa and improved the strain at break from 18% to >150% (**Figure 5.7.b**). **Figure 5.7.c** represents the Young's modulus as a function of SS or HS sulfonation content. Most encouragingly, the results from tensile testing further developed our understanding of the importance of ionic charge placement on the mechanical properties. Incorporation of the ionic group in the SS resulted in enhanced tensile stress and strain at break.

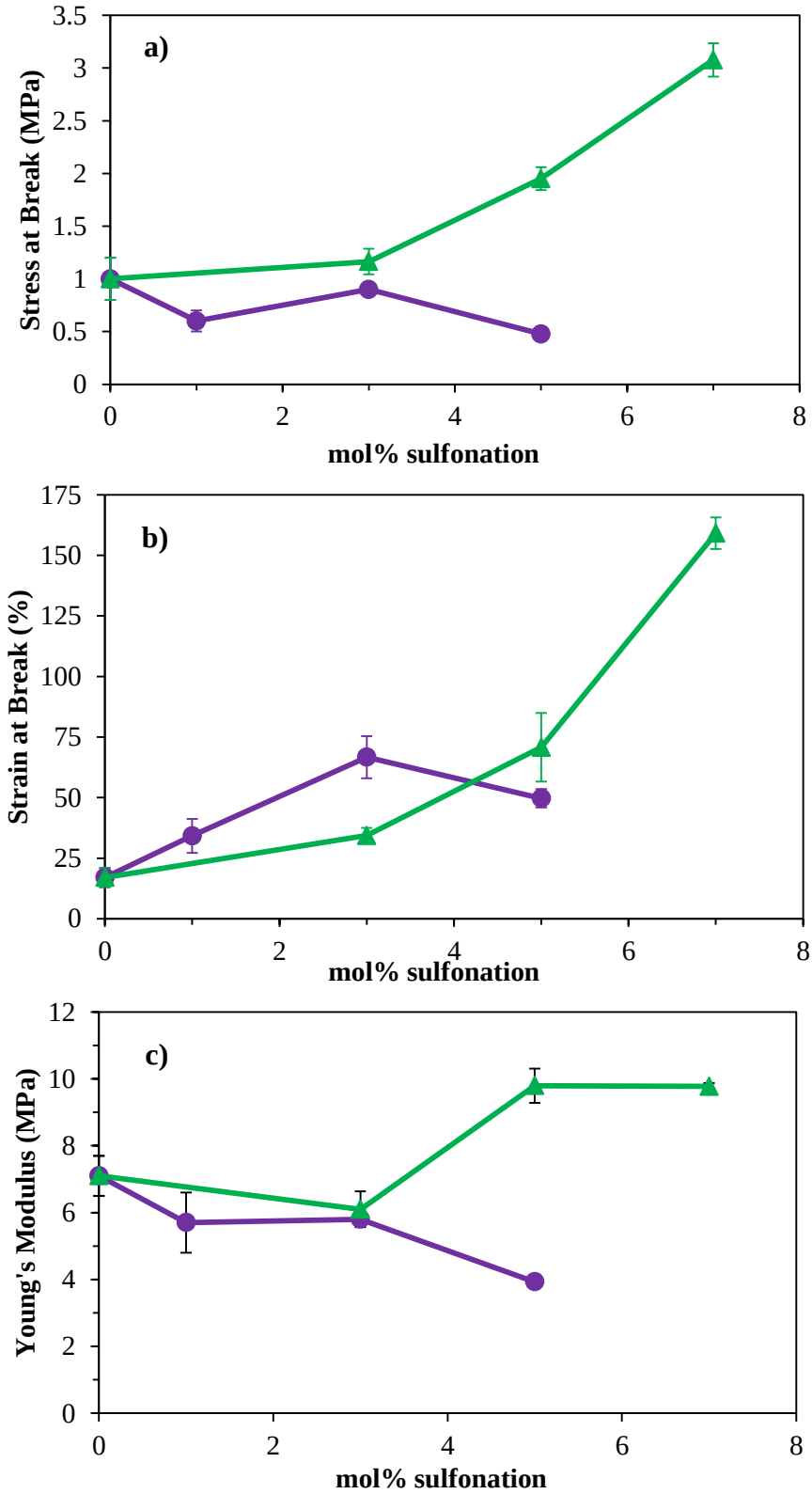

Figure 5.7. Tensile testing plots displaying a) stress at break, b) strain at break, and c) Young's modulus as a function of sulfonation content in HS (circle) or SS (triangle). Tensile data are represented as an average of five samples.

Tensile cyclic hysteresis studies of the 7 mol% sulfonated SS copolyester elucidated their elastomeric properties. The sample was subjected to three loading (80% or 120%) and unloading (0%) cycles at a strain rate of 80 mm/min with 30 sec delays between cycles. As shown in **Figure 5.8.a**, the 7 mol% sulfonated SS copolyester exhibited significant hysteresis after the first loading cycle, which implied the sample experienced permanent plastic deformation. The sample remained approximately 20% elongated after each loading cycle, but recovered 10% during the 30 sec delay between loading cycles. The tensile hysteresis loss between the first and second cycle was approximately 42%. Interestingly, the elastic response was significant between the second and third loading-unloading cycles, which displayed only a 5% hysteresis loss and similar elastic recovery to the first cycle. The stress at the final loading of 80% remained at 2 MPa between all three cycles. The cyclic hysteresis study to 120% strain behaved similarly (**Figure 5.8.b**). Again, the largest hysteresis loss of 39% occurred after the first cycle and only 6% loss was observed after the second and third cycles. The tensile and cyclic hysteresis studies demonstrated the influential role of electrostatic interactions in improving mechanical performance. Compared to the non-sulfonated control, incorporation of ionic interactions in the SS improved tensile stress, strain, and improved elastomeric performance.

Melt transesterification of sterically hindered, polyester polyol precursors efficiently generated segmented copolyesters with precise control of charge placement and content in the HS or SS. We hypothesize the ionic placement in the HS or SS directly impacted ion solvation effects, which depends largely on the polarity of the surrounding polymer matrix. In sulfonated SS copolyesters, the polar SS matrix promotes ion-dipole interactions with the ether oxygens to solvate the ionic sulfonates. In contrast, the sulfonated HS copolyesters contain ionic groups within a more nonpolar matrix and present two possible ionic interactions. In one scenario, the

nonpolar matrix promotes ionic aggregation within the HS matrix. In the second scenario, ion-dipole solvation effects from the SS promote phase-mixing interactions particularly at the HS-SS phase interface. The decreased flow temperatures observed in the thermomechanical behavior, presence of a disordered surface morphology, and reduced mechanical properties suggested the sulfonated HS copolyesters likely contained a more phase-mixed HS-SS interface.

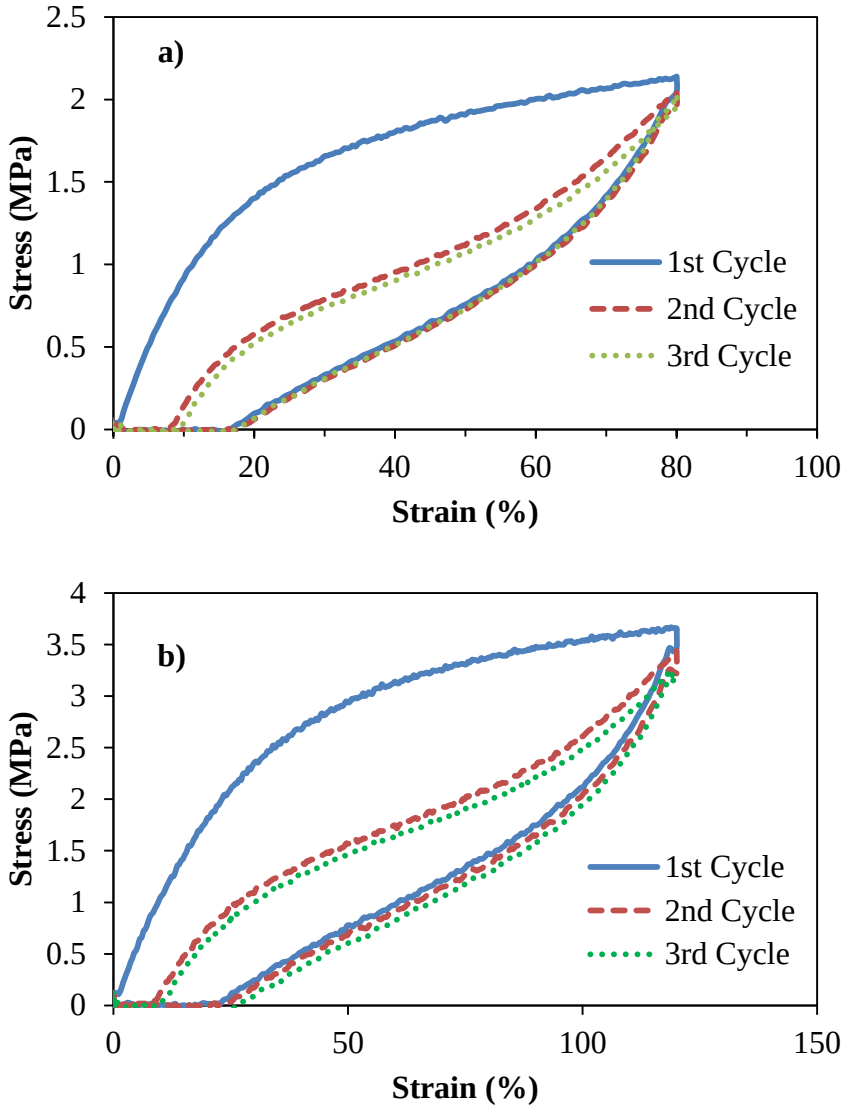

Figure 5.8. Hysteresis studies depicting three loading and unloading cycles for 7 mol% soft segment sulfonated copolyesters pulled to a) 80% and b) 120% strain at 80 mm/min with 30 sec delays between cycles.

5.5 *Conclusions*

Melt transesterification efficiently produced amorphous, microphase-separated, segmented copolyesters with controlled charge placement in the SS or HS. The sulfonated segmented copolyesters enabled systematic investigations of the influence of ionic content and charge placement on the thermomechanical properties and morphology. Sulfonated polyol precursors significantly increased the T_g from 80 to 148 °C, but showed decreased onset of T_{flow} when incorporated into segmented copolyesters. In contrast, sulfonated SS copolyesters displayed an increase in the low-T_g transitions and the rubbery plateau moduli with sulfonation levels. *In situ*, variable temperature small-angle X-ray and dynamic melt rheological studies determined the order-disorder was consistent with the onset of T_{flow}. Atomic force microscopy further verified a microphase-separated surface morphology for the sulfonated segmented copolyesters. Tensile and cyclic hysteresis studies further emphasized the effects of ionic charge placement on mechanical and elastomeric properties. Sulfonated SS copolyesters possessed significantly enhanced tensile stress and strain compared to the non-sulfonated control. Electrostatic interactions in the SS serve as noncovalent, physical crosslinks and improved mechanical performance without disrupting the microphase-separated morphology.

Acknowledgements. This work is supported in part by the U.S. Army Research Laboratory and the U.S. Army Research Office under the Army Materials Center of Excellence Program, contract W911NF-06-2-0014. We acknowledge the Advanced Photon Source supported by the U. S. Department of Energy, Office of Science, Office of Basic Energy Sciences, under Contract No. W-31-109-Eng-38, for access to the beamtime 5ID-D, operated by DND-CAT. The DND-CAT is supported by the E.I. DuPont de Nemours & Co., The Dow Chemical Company, the U.S. National Science Foundation through Grant DMR-9304725 and the State of Illinois through the

Department of Commerce and the Board of Higher Education Grant IBHE HECA NWU 96. The diode beam stops were constructed at DuPont by Robert F. Knox and Mark G. Bradigan under J. David Londono's direction. The authors would also like to thank Eastman Chemical Company for providing CBDO and DMCD monomers and the Riffle research group for chloroform GPC analysis. We extend our gratitude to Ninad Dixit for his collaboration on this project and Professor Garth Wilkes for his expertise and discussions. In addition, the authors thank Steve McCartney at the Virginia Tech Institute of Critical Technology and Applied Sciences (ICTAS) Nanoscale Characterization and Fabrication Laboratory (NCFL) for atomic force microscopy assistance and training.

5.6 *References*

1. Cella, R. J., *Journal of Polymer Science: Polymer Symposia* **1973,** *42* (2), 727-740.
2. Spontak, R. J.; Patel, N. P., *Current Opinion in Colloid & Interface Science* **2000,** *5* (5-6), 333-340.
3. Gabriëlse, W.; Soliman, M.; Dijkstra, K., *Macromolecules* **2001,** *34* (6), 1685-1693.
4. Capek, I., *Adv. Colloid Interface Sci.* **2005,** *118* (1–3), 73-112.
5. Mauritz, K. A., *Journal of Macromolecular Science, Part C* **1988,** *28* (1), 65-98.
6. Eisenberg, A.; Hird, B.; Moore, R. B., *Macromolecules* **1990,** *23* (18), 4098-4107.
7. Lefelar, J. A.; Weiss, R. A., *Macromolecules* **1984,** *17* (6), 1145-1148.
8. Duncan, A. J.; Akle, B. J.; Long, T. E.; Leo, D. J., *Smart Mater. Struct.* **2009,** *18* (10), 104005.
9. Green, M. D.; Wang, D.; Hemp, S. T.; Choi, J. H.; Winey, K. I.; Heflin, J. R.; Long, T. E., *Polymer* **2012,** *53* (17), 3677-3686.
10. Green, M. D.; Choi, J.-H.; Winey, K. I.; Long, T. E., *Macromolecules* **2012,** *45* (11), 4749-4757.
11. Delpech, M. C.; Coutinho, F. M. B., *Polym. Test.* **2000,** *19* (8), 939-952.
12. Hemp, S. T.; Smith, A. E.; Bryson, J. M.; Allen, M. H., Jr.; Long, T. E., *Biomacromolecules* **2012**.
13. Olson, D. A.; Gratton, S. E. A.; DeSimone, J. M.; Sheares, V. V., *J. Am. Chem. Soc.* **2006,** *128* (41), 13625-13633.
14. Williams, S. R.; Long, T. E., *Prog. Polym. Sci.* **2009,** *34* (8), 762-782.
15. Williams, S. R.; Borgerding, E. M.; Layman, J. M.; Wang, W.; Winey, K. I.; Long, T. E., *Macromolecules* **2008,** *41* (14), 5216-5222.
16. Williams, S. R.; Salas-de la Cruz, D.; Winey, K. I.; Long, T. E., *Polymer* **2010,** *51* (6), 1252-1257.
17. Das, S.; Goff, J. D.; Williams, S.; Salas-De La Cruz, D.; Riffle, J. S.; Long, T. E.; Winey, K. I.; Wilkes, G. L., *Journal of Macromolecular Science, Part A: Pure and Applied Chemistry* **2010,** *47* (3), 215 - 224.
18. Roy, A.; Hickner, M. A.; Yu, X.; Li, Y.; Glass, T. E.; McGrath, J. E., *J. Polym. Sci., Part B: Polym. Phys.* **2006,** *44* (16), 2226-2239.
19. Szymczyk, A.; Ezquerra, T.; Roslaniec, Z., *Journal of Macromolecular Science: Physics* **2001,** *40* (5), 669.
20. Visser, S. A.; Cooper, S. L., *Macromolecules* **1991,** *24* (9), 2576-2583.
21. Visser, S. A.; Cooper, S. L., *Macromolecules* **1991,** *24* (9), 2584-2593.
22. Williams, S. R.; Wang, W.; Winey, K. I.; Long, T. E., *Macromolecules* **2008,** *41* (23), 9072-9079.
23. Zhang, M.; Moore, R. B.; Long, T. E., *J. Polym. Sci., Part A: Polym. Chem.* **2012,** *50* (18), 3710-3718.
24. Drysdale, N. E.; Brun, Y.; McCord, E. F.; Nederberg, F., *Macromolecules* **2012,** *45* (20), 8245-8256.
25. Lin, Q.; Unal, S.; Fornof, A. R.; Armentrout, R. S.; Long, T. E., *Polymer* **2006,** *47* (11), 4085-4093.
26. Eisenberg, A., *Macromolecules* **1971,** *4* (1), 125-128.
27. Chen, T. K.; Chui, J. Y.; Shieh, T. S., *Macromolecules* **1997,** *30* (17), 5068-5074.
28. Gao, R.; Zhang, M.; Dixit, N.; Moore, R. B.; Long, T. E., *Polymer* **2012,** *53* (6), 1203-1211.

29. Wu, L.; Cochran, E. W.; Lodge, T. P.; Bates, F. S., *Macromolecules* **2004,** *37* (9), 3360-3368.
30. Matsuura, H.; Eisenberg, A., *Journal of Polymer Science: Polymer Physics Edition* **1976,** *14* (7), 1201-1209.
31. Weiss, R. A.; Zhao, H., *J. Rheol.* **2009,** *53* (1), 191-213.
32. Bagrodia, S.; Pisipati, R.; Wilkes, G. L.; Storey, R. F.; Kennedy, J. P., *J. Appl. Polym. Sci.* **1984,** *29* (10), 3065-3073.
33. Greener, J.; Gillmor, J. R.; Daly, R. C., *Macromolecules* **1993,** *26* (24), 6416-6424.
34. Ryan, A. J.; Macosko, C. W.; Bras, W., *Macromolecules* **1992,** *25* (23), 6277-6283.
35. Han, C. D.; Baek, D. M.; Kim, J. K.; Ogawa, T.; Sakamoto, N.; Hashimoto, T., *Macromolecules* **1995,** *28* (14), 5043-5062.
36. Szymczyk, A.; Ezquerra, T. A.; Roslaniec, Z., *Journal of Macromolecular Science, Part B: Physics* **2001,** *40* (5), 685 - 708.

5.7 *Supporting Information*

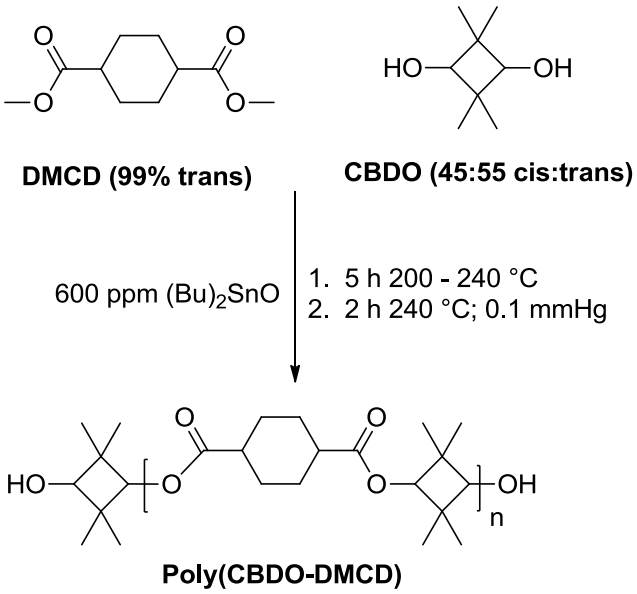

Figure S 5.1. Synthesis of high-T_g CBDO-containing polyester polyols.

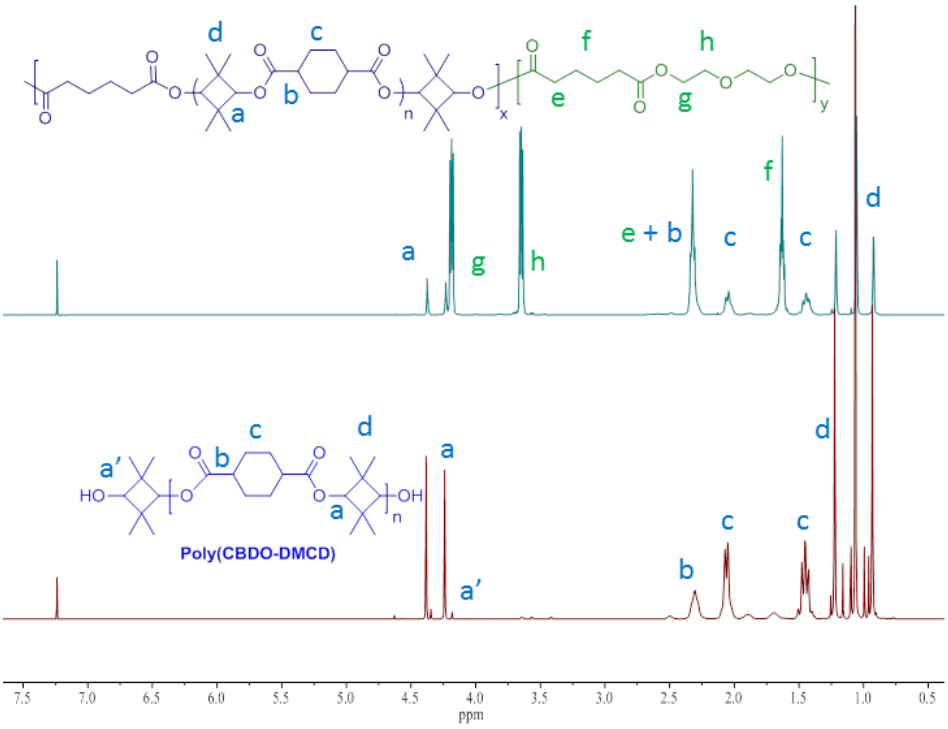

Figure S 5.2. ^{1}H NMR spectroscopy of the hard segment precursor polyol and final segmented copolyester. The integration ratio of a to a' resonances from the CBDO provides the degree of polymerization (X_n) of the polyol.

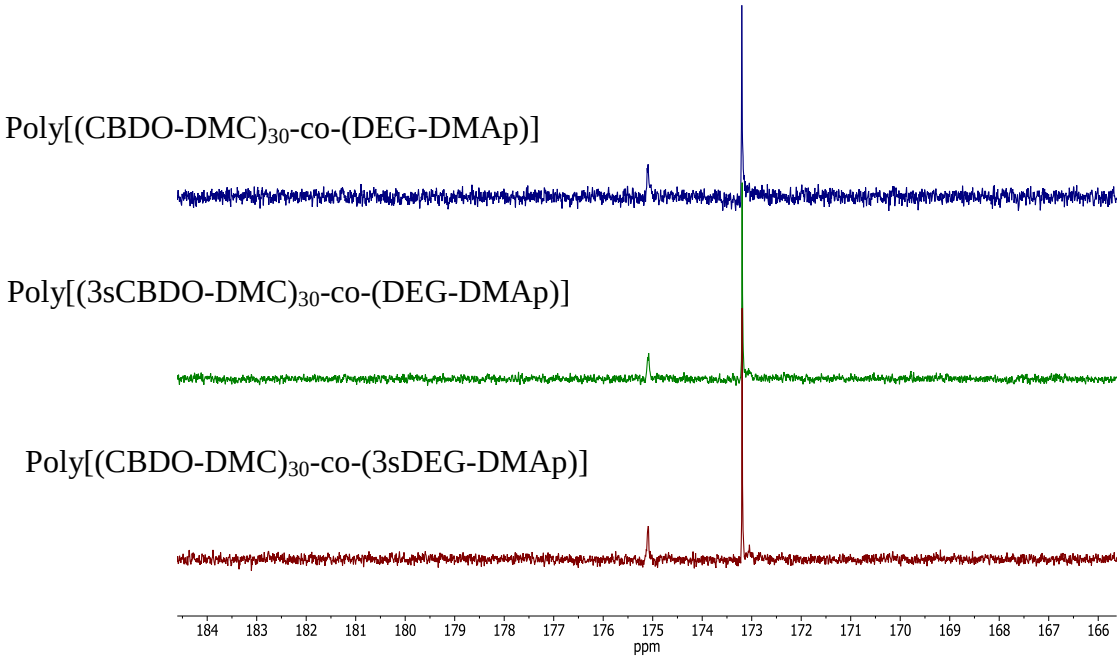

Figure S 5.3. ^{13}C NMR spectroscopy of the carbonyl region showing two distinct carbonyls associated with the two repeating units of the hard segment and soft segment.

Mol % DMI	M_n[a] (g/mol)	M_w[a] (g/mol)	T_g (°C)	Mol% sDMI	M_n[b] (g/mol)	T_g (°C)
0	3,700	4,700	85			
1	3,120	6,010	106	1	3,500	106
2	2,880	4,950	111	2	3,560	123
3	3,210	5,780	112	3	3,410	146
5	3,840	6,960	117	5	3,330	148

[a]Chloroform SEC refractive index detector determined molecular weight relative to polystyrene standards.

[b] ^{1}H NMR spectroscopy determined M_n due to ionic aggregation in SEC solvents.

Figure S 5.4 Molecular weights and T_g of polyester polyols containing dimethyl isophthalate or sulfonated dimethyl isophthalate. T_g values are determined from the DSC second heat.

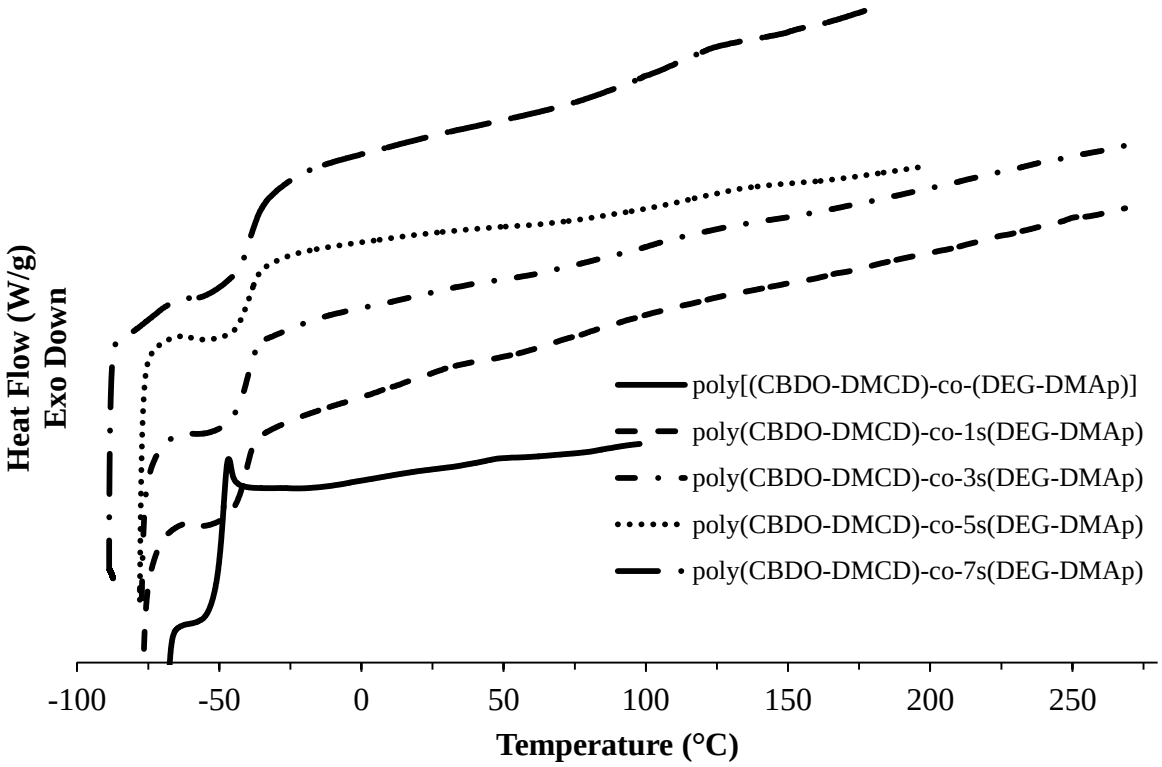

Figure S 5.5. Differential scanning calorimetry indicating the T_g's of soft segment sulfonated copolyesters containing 30 wt% hard segment poly(CBDO-DMCD). Thermographs are depicted as the second heat in a heat/cool/heat experiment.

Chapter 6: Impact of Divalent Metal Cations on Thermal and Rheological Properties of Randomly Sulfonated Polyesters

Musan Zhang and Timothy E. Long

Department of Chemistry, Macromolecules and Interfaces Institute
Virginia Tech, Blacksburg, VA 24061-0212

6.1 *Abstract*

Melt transesterification of low-T_g, sodium sulfonate-containing copolyesters generated a series of ionomeric copolyesters with 0 – 15 mol% ionic content. Systematic viscoelastic and solution characterization elucidated the impact of electrostatic interactions. Thermal analysis revealed weak T_g effects as a function of ionic content most likely due to the ion-dipole solvation from polar ester groups. Dynamic light scattering of sodium sulfonated copolyesters at 10 and 15 mol% ionic content generated aqueous dispersions with solution particle sizes < 100 nm depending on the ionic content and solvent composition. Cation dialysis exchange eliminated molecular weight effects and efficiently achieved Mg^{2+}, Ca^{2+}, and Zn^{2+} sulfonated copolyester compositions. Thermal analysis revealed the ionic content and divalent cation composition did not significantly affect the T_g. In contrast, dynamic mechanical analysis and melt rheology demonstrated that stronger, divalent electrostatic interactions achieved higher melt viscosities, broader rubbery plateau moduli, and much slower polymer relaxations compared to the monovalent sodium form. Time-temperature superposition shifted master curves were obtained in sulfonated copolyesters with low ionic content (≤5 mol%). At high ionic content (15 mol%), only the Zn^{2+} form demonstrated successful TTS shifted master curves.

6.2 *Introduction*

Ionomers represent a class of charge-containing polymer, which contain less than 15 mol% ionic groups.[1, 2] The electrostatic interactions function as thermally labile, dynamic crosslinks to achieve reversible networks that afford melt processibility and enhance thermomechanical performance. Ionomers have applications as electro-active actuators, fuel cell membranes, water purification membrane, self-healing materials, and high performance thermoplastics.[3] The influence of the electrostatic interactions on the polymer viscoelastic properties have been studied extensively in the past. The Eisenberg-Hird-Moore model has been heavily sited to explain the influence of the electrostatic interactions and ionic aggregates on the polymer viscoelasticity and consequently the morphology.[4] One unique feature of ionomers is the ability of electrostatic interactions to create a region of restricted mobility, which results in phase separated-like properties. Ionic groups potentially aggregate into microphase separated domains depending on the charge content, electrostatic strength, and polarity of the polymeric matrix.[4] The counterion composition affords control of the electrostatic strength and tunes the thermomechanical, viscoelastic, and conductive properties.[5-9]

Melt rheology of ionomers probe the viscoelastic dynamics elucidate the effects of electrostatic interactions on the studies determined sulfonated ethylene-propylene-diene polymers containing divalent cations such as Mg^{2+} and Ca^{2+} exhibited higher melt viscosities compared to Zn^{2+}.[10, 11] Noncovalent interactions such as hydrogen bonding potentially solvate the ionic groups and reduce the effects of electrostatic forces. Small-angle X-ray scattering (SAXS) of neutralized ionomers with multivalent cations exhibited complex coordination chemistry, which impacted the arrangement of the ionic aggregates. Neutralization of acid-containing polymers is one method to generate ionomers with multivalent countercations. The

influence of neutralization depends on the chemical structure of the acid, cation charge, and degree of neutralization.[12] Neutralization in sulfonic acid-containing dramatically influences properties including thermal weight loss stability and water uptake.[13]

Polyester-containing ionomers contribute immensely to biodegradable adhesives, which have potential in biomedical applications.[14] Furthermore, sulfonated copolyesters represent an important class of water-dispersible copolymers often used in aqueous ink formulations and aqueous dispersants.[15] Aqueous dispersions afford nontoxic, nonflammable, and environmentally conscious alternatives to organic-based dispersions. Solution rheology and light scattering reflect the solution complexities of ionomers. Factors including charge repulsion and screening, polymer composition, molecular weight, and solution concentration affect the solution properties.[16] Solvent polarity also impacts the polymer solution conformation through solvating or ionizing the ionic group.[17, 18] As a result, the extent of charge repulsion and screening contributes to extended or random coil-like polymeric solution structures, which lead to changes in solution viscosity and hydrodynamic sizes.[19-21]

This manuscript probes the influence of metal sulfonate structure and content on the polymer thermomechanical properties. Dynamic light scattering investigated the charged polymeric solution behavior and discovered freely dispersed, non-aggregated, nano-sized particles in water. The unique water dispersible property enabled dialysis cation exchange with monovalent sodium cations to various divalent cations including Mg^{2+}, Ca^{2+}, and Zn^{2+}. This approach in cation exchange from a single polymer precursor eliminated potential molecular weight effects, which may complicate the analysis. Thermogravimetric sorption analysis investigated the water sorption/desorption/sorption behavior of the various forms of sulfonated copolyesters. Further analysis of these sulfonated copolyester thermomechanical properties

demonstrated the sodium sulfonated form exhibited a rubbery plateau. The cation exchange from sodium to magnesium or calcium generated a more stable thermomechanical curve and extended the rubbery plateau to higher temperatures, with little change in the rubbery modulus.

6.3 *Experimental Section*

Materials

All chemical reactants used for polymerization and salts (LiCl, $MgCl_2$, $CaCl_2$, and $ZnCl_2$) used to perform cation exchanges were purchased from Sigma-Aldrich. Diethylene glycol (99.9%, DEG), dimethyl adipate (99%, DMAp), dimethyl 5-sulfoisophthalate sodium salt (99.9%, sDMI), sodium acetate were used without further purification. A titanium tetraisopropoxide (99%) solution was prepared in anhydrous 1-butanol according to previously described procedures.[22] All polymers were dried at 80 °C for 12 h under reduced pressure prior to characterization and analysis. Standard regenerated cellulose dialysis tubing (Spectrapor, MWCO = 3,500 g/mol) was purchased from VWR.

Synthesis of sulfonated poly(diethylene glycol adipate)

All polymerizations were performed at a 1.2:1.0 molar ratio of diol to diester. The following polymerization procedure for 10 mol% sulfonated poly(diethylene glycol adipate) (abbreviated Na-10s) serves as a representative example. Diethylene glycol (120 mmol), DMAp (90 mmol), sDMI (10 mmol), Ti catalyst solution (15 ppm), and NaOAc (0.01 mmol) were charged into a flame dried, 100-mL round-bottomed flask equipped an overhead mechanical stirrer, nitrogen inlet, and distillation outlet. A nitrogen purge and vacuum degasing cycle was applied three times to the system to ensure complete removal of air. The reaction was heated to 200 °C, and the temperature was increased to 240 °C over 5 h under a constant nitrogen purge and stirring. The pressure was gradually reduced to <0.1 mmHg, and the polymerization

proceeded for an additional 2 h. The polyester was isolated and characterized without further purification.

Cation exchange of sulfonated poly(diethylene glycol adipate)

The cation exchange of water-soluble Na-15s polyesters was readily achieved using dialysis. In a typical dialysis cation exchange, 5 g of Na-15s polyester (3.2 mmol of DEG-sDMI repeating unit) was dissolved in 10 mL of deionized water and added to a solution of 2.342 g of $CaCl_2 \cdot 2H_2O$ dissolved 10 mL of deionized water. The solution was transferred carefully into a dialysis tube, which was placed into a beaker of deionized water. After 6 and 12 h, the water was changed and 2.342 g of $CaCl_2 \cdot 2H_2O$ was subsequently added to ensure complete exchange. The water was changed after an additional 6 and 12 h, and the polymer solution was lyophilized.

Polymer Characterization

A TA Instruments Q50 thermogravimetric analyzer provided onset degradation temperatures of sulfonated polyesters (10 °C/min, N_2). Differential scanning calorimetry obtained the polymer thermal transitions between -70 to 200 °C using heat/cool/heat experiments (TA Instruments Q1000, 10 °C/min, N_2). A TA Instruments Q5000 thermogravimetric sorption analyzer (TGA-SA) performed sorption/desorption/sorption experiments at 25 °C using 5% relative humidity (RH) steps from 0 to 70% RH. In addition to drying the sample under reduced pressure for 18 h at 80 °C, an instrumental drying procedure (0% RH, 50 °C, 1 h) was applied to the sample prior to the start of the experimental procedure. Each RH step occurred for a maximum duration of 2 h or until the wt% change stabilizes (stabilization condition: wt% change < 0.01% over 15 min). The wt% change was converted to λ, which is defined as the molar ratio of H_2O to sulfonates. Dynamic light scattering (Malvern Zetasizer Nano ZS) measured the hydrodynamic diameters of 5 wt% Na-10s and Na-15s polyesters in water, or water 0.25 M NaBr.

In addition, DLS monitored the salting-out effects of monovalent or divalent salts at varying solution concentrations. Initial Na-15s polyester (15 mg/mL) and salt (0.40 M) stock solutions were prepared in water. In a typical DLS procedure, 500 μL of the Na-15s solution was added into a disposable sizing cuvette. An appropriate volume of the salt solution was added to the cuvette to achieve a targeted final molar content. Water was subsequently added to the solution to achieve a final volume of 750 μL, and the final polymer concentrations (10 mg/mL) were consistent between all samples.

To obtain films, a solution containing 10 wt% polyester in a 90/10 (w/w%) chloroform/methanol solvent mixture was coated onto a silicon-coated Mylar™ substrate using a micrometer adjustable doctor blade (1 mm coating thickness). The films were allowed to dry slowly at ambient conditions for 1 d, followed by subsequent drying under reduced pressure for 1 d at 23 °C, and an additional 2 d at 80 °C. A TA Instruments Q800 DMA performed single frequency – temperature ramp experiments from -100 to 200 °C in film tension mode (1 Hz, 3 °C/min). A TA Instruments Discovery HR-2 rheometer equipped with an 8 mm, parallel plate geometry performed isothermal, dynamic oscillatory shear experiments. Time-temperature superposition (TTS) master curves (T_{ref} = 40 °C) were obtained for Na-sulfonated polyester compositions with ≤ 5 mol% ionic content. Although TTS experiments were performed on Na-15s, Mg-15s, Ca-15s, and Zn-15s, only the Zn-15s generated suitable master curves. Strain sweep experiments confirmed the dynamic rheological studies were performed in the linear viscoelastic region. Shear sweep experiments obtained zero-shear viscosities (η_o) at various temperature steps well above the polymer glass transition temperature ($T > T_g + 100$ °C).

6.4 *Results and Discussion*

The impact of electrostatic interactions in ionomers is well described in the literature for free radical polymers. Low levels of ionic content significantly influence polymeric properties including melt viscosity, solubility, thermomechanical behavior, and morphology. The considerable increase in melt viscosity with low ionic content presents a synthetic challenge for melt-phase polymerizations to achieve high molecular weights. In order to avoid excessively high melt viscosities during melt transesterification, low-T_g copolyesters based on poly(diethylene glycol adipate) were generated with varying levels of sDMI. The molar ratio of sDMI to DMAp determined the sulfonation mol%. Melt transesterification using a titanium catalyst yielded a range copolymer compositions with sulfonation levels between 0 – 15 mol% (abbreviated Na-(*x*)s, where *x* represents the mol% of DEG-sDMI repeating units) (**Scheme 6.1**).

One desirable advantage of generating low-T_g copolymers with a broad range of ionic content is the ability to investigate these ionomers systematically. Moreover, the Na-10s and Na-15s copolyesters were readily water-soluble and displayed water-dispersible properties, a phenomenon which has been reported numerously in the past. Efficient and mild cation exchanges of a single Na-15s precursor varied the countercation chemical composition without molecular weight effects. Interestingly, macroscopic precipitation was observed during cation exchanges with divalent salts upon a critical concentration. If the aqueous medium as decanted, the sulfonated polyester becomes once again readily soluble in pure water. This behavior prompted us to follow-up our observations with more detailed dynamic light scattering experiments.

Table 6.1 provides a summary of the Na-sulfonated copolyester compositions achieved using melt transesterification. The conversion of mol% to wt% emphasizes the sDMI

contribution to the overall copolymer content. The 5% weight loss temperatures decreased with increasing Na-sulfonate content. The T_g of poly(DEGA) was -48 °C and agreed with previously reported literature values. Interestingly, the Na-sulfonated copolyesters demonstrated a weak T_g effect with ionic content. The T_g effect varies substantially depending on the composition of the ionomer and counterion. The weak T_g correlation to ionic content suggests that even at 15 mol% Na-sulfonate content, the thermal behavior of the polymer remains similar to the nonionic poly(DEGA) polymer matrix. A summary of the copolyester compositions containing divalent cations and their thermal properties are represented in **Table 6.2**. The divalent compositions show reduced thermal weight loss stabilities compared to the Na form. The divalent compositions displayed similar T_g's to the Na-15s.

In addition to being able to explore the influence of the ionic content on the randomly sulfonated copolyesters, dialysis cation exchanges from one polymeric precursor enabled us isolate the impact of the divalent metal cations on the physical properties. The Na-10s and Na-15s copolyesters were readily water-soluble without any additional heat and produced clear aqueous solutions. Dynamic light scattering (DLS) demonstrated both Na-sulfonated copolyesters exhibited non-aggregated, monomodally sized particles <100 nm in water (**Figure 6.1**). Increasing the Na-sulfonate content decreased the particle size and polydispersity in water. In 0.25 M NaBr, the salt presumably screened the polymer ionic interactions, which further reduced the particle size and polydispersity.

DLS further probed the influence of various monovalent and divalent salt compositions on the solution particle size. **Figure 6.2** displays the influence of the particle hydrodynamic diameter as a function salt concentration. Addition of salts that contained monovalent cations demonstrated an overall decrease in the particle diameter. Conversely, divalent salt

incorporation resulted in an increase in the particle size at approximately 16 mmol salt content. The increase in the particle size corresponds to a salting-out effect presumably due to the displacement of the monovalent sodium cation to a multifunctional divalent cation.

Although the DSC analysis suggested little to no correlation between the T_g and ionic content, DMA and melt rheology observe more discernible impact of the ionic groups on the polymer viscoelastic properties. The thermomechanical behavior for both Na-10s and Na-15s compositions exhibited a sharp drop in the glassy storage modulus and a maximum in the tan δ at the low-T_g transition at -30 °C (**Figure 6.3**). The low-T_g transitions were the same for both the Na-10s and Na-15s compositions, which were similar to the values obtained from DSC. The Na-10s possessed a rubbery plateau until the polymer flow temperature at 70 °C. The higher rubbery modulus and extended rubbery plateau for Na-15s indicated increasing ionic content generated improved the crosslink density. In addition, higher ionic content led to a more cohesive copolymer network, which was confirmed by the increase in the polymer flow temperature to 140 °C. The influence of the ionic contribution was clearly noticeable in transforming a low-T_g viscoelastic liquid such as poly(DEGA), into a film-forming copolymer, whose thermomechanical behavior was readily tailored by the ionic content. Distinct thermal transitions in the storage modulus and evidence of a rubbery plateau are characteristic features often observed in microphase-separated materials, such as well-defined block copolymers. In these randomly sulfonated copolyesters, the strong electrostatic interactions presumably led to ionic aggregations, which influences their surrounding polymer matrix and results in a separate, viscoelastically distinct phase.

Figure 6.4 represents the thermomechanical behavior of Na-15s and the divalent analogues, Ca-15s and Mg-15s. At temperatures between 0 – 60 °C, all three compositions

displayed similar rubbery moduli, which confirmed the ionic content contributed significantly to the noncovalent crosslink density. The Ca-15s and Mg-15s copolyesters demonstrated improved thermomechanical stabilities at higher temperatures compared to the Na-15s. The sulfonated copolyesters with divalent cations exhibited a broad rubbery plateau that persisted to 180 °C. The extended rubbery plateaus suggested the divalent cations perhaps afforded stronger electrostatic interactions, which improved the thermoreversible crosslink density of the noncovalent network.[23, 24]

The Zn-15s interestingly did not produce free-standing films despite its divalent cationic charge. Therefore, dynamic melt rheological temperature sweep experiments were conducted to obtain Zn-15s viscoelastic properties. **Figure 6.5** displays the temperature sweep rheological experiments for 15 mol% sulfonated copolyesters. The oscillatory shear temperature sweep experiments confirmed the results from DMA. The various forms of the 15 mol% sulfonated copolyesters displayed similar initial rubbery plateau moduli up to 80°C. A monovalent to divalent countercation exchange effectively extended the rubbery plateau to higher temperatures. The temperature of the G'' > G' crossover, the onset of the polymer terminal flow region, increased from $Zn^{2+} < Na^{+} < Ca^{2+} < Mg^{2+}$. This result suggested the divalent countercations, Ca^{2+} and Mg^{2+}, stabilized the physical crosslinks at higher temperatures compared to the monovalent Na^{+}. The thermomechanical stabilization most likely related to the increased electrostatic forces in divalent systems, which relates proportionally to the charge valence. Interestingly, the Zn-15s copolyesters observed the lowest flow temperature.

TGA-SA probed the impact of countercation on the water sorption. Sorption/desorption/sorption experiments probed the effects of relative humidity on the sample water vapor sorption behavior. The sorption analyses provide insight on the moisture sensitivity

of sulfonated copolyesters, which may significantly alter the polymer physical behavior. **Figure 6.6** displays a representative thermogravimetric sorption/desorption/sorption curve, which may exhibit hysteresis in the moisture uptake depending on moisture absorption or desorption. Interestingly, the overall water sorption content measured during the first and second cycle generated similar results and displayed very little hysteresis. The observations suggested the sulfonated copolyester water absorption did not permanently alter subsequent water absorptions after drying.[25] In each sample, the desorption curve exhibited deviations in the wt% at each relative humidity step from the initial and final sorption curves. Both the Zn-15s and Mg-15s copolyesters generated similar sorption-desorption-sorption profiles, which were higher compared to Na-15s and Ca-15s.

Melt rheological studies investigated the cation effects on the copolyester viscoelastic properties. **Figure 6.7** shows the TTS shifted mastercurves for copolyesters containing ≤5 mol% sulfonation. In some ionomers with low ionic content below the threshold concentration that form ionic aggregates, WLF behavior is still observed. As the ionic content increased, the relaxation time at the G' = G'' crossover systematically shifted to lower frequencies. This behavior suggested the incorporation of ionic interactions significantly altered the polymer viscoelastic dynamics and reduced segmental mobility. At high frequencies, the ionomers behaved as viscoelastic solids displaying high storage moduli. Conversely, at low frequencies, the ionomers exhibited viscoelastic liquid properties. The transition towards the terminal relaxation broadened with the incorporation of Na-sulfonates, which implicated ionic interactions contributing to whole chain relaxations. The terminal flow behavior is denoted by the characteristic ratio $G' = \omega^2$ and $G'(\omega)$. Ion-containing polymers typically do not display suitable master curves due do the presence of ionic aggregation influencing the viscoelastic

properties at elevated temperatures. The failure of TTS strongly indicates multiple relaxation mechanisms, which cannot be accurately described using one shift factor.[26]

Zero shear viscosity values as a function of the inverse temperature ($T > T_g + 100$) demonstrated a linear Arrhenius behavior, whose slope related to the flow activation energy (**Figure S 6.1**). Suitable linear relationships were observed only at temperatures well above T_g. Interestingly, the Zn-form showed suitable Arrhenius behavior at moderate temperatures above its T_g and suggested its properties resembled more closely to the nonsulfonated controls. (Insert sentences about Zn as a plasticizer). **Figure 6.8** further confirms the unique properties of the Zn-15s sulfonated copolyester, which displayed successful TTS shifting. All other forms of the charged copolyesters failed TTS shifting as expected from the electrostatic interactions, which influenced the viscoelastic properties at long timescales.

6.5 *Conclusions*

Melt transesterification produced a series of low-T_g, sodium sulfonate-containing copolyesters with 0 – 15 mol% ionic content. A broad range of ionic compositions afforded systematic investigations on the thermal, mechanical, and viscoelastic behaviors of sodium sulfonated copolyesters. Sodium sulfonated copolyesters at 10 and 15 mol% ionic content exhibited water dispersibility and generated solution particle sizes < 100 nm depending on the ionic content and solvent composition. Furthermore, dynamic light scattering revealed the effect of monovalent vs. divalent metal cations on the size and stability of the solution nanoparticle. Cation dialysis exchange efficiently achieved sulfonated copolyester compositions with Mg^{2+}, Ca^{2+}, and Zn^{2+} countercations at identical molecular weights. Thermal analysis revealed the ionic content and divalent cation composition did not significantly influence the T_g. Dynamic mechanical analysis and melt rheology demonstrated that stronger, divalent electrostatic interactions achieved higher melt viscosities, broader rubbery plateau moduli, and much slower polymer relaxations compared to the monovalent sodium form. Time-temperature superposition shifted master curves were obtained in sulfonated copolyesters with low ionic content (≤5 mol%). At 15 mol% sulfonate content, only the Zn^{2+} form exhibited successful TTS shifted master curves.

Acknowledgements. This work is supported in part by the U.S. Army Research Laboratory and the U.S. Army Research Office under the Army Materials Center of Excellence Program, contract W911NF-06-2-0014. This material is also based upon work supported in part by the US Army Research Office under Grant no. W911NF-07-1-0452 Ionic Liquids in Electro-active Devices (ILEAD) MURI. In addition, the authors thank the Virginia Tech Institute of Critical

Technology and Applied Sciences (ICTAS) Nanoscale Characterization and Fabrication Laboratory (NCFL) for atomic force microscopy characterization.

Scheme 6.1. Synthesis of sodium sulfonated random copolyesters.

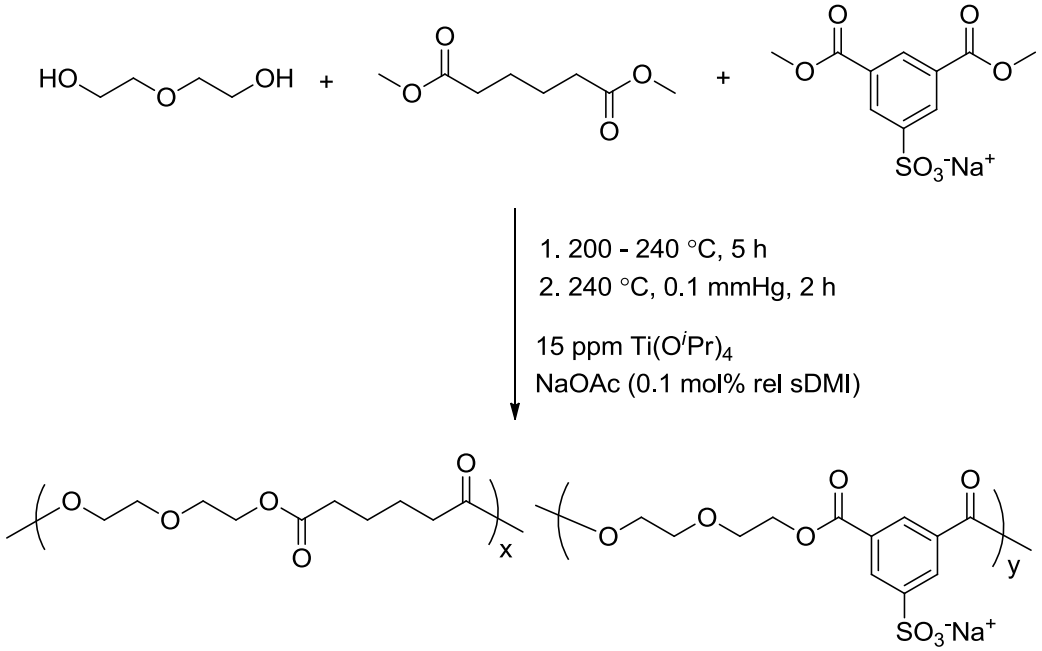

Table 6.1. Summary of sodium sulfonated random copolyester compositions and thermal properties.

Polyester	Mol% sDMI	Wt% sDMI	$T_{d5\%}$[a] (°C)	T_g[b] (°C)
0sDEGDMAP	0	0.0	340	-48
Na-1s	1	1.6	334	-47
Na-3s	3	4.6	333	-46
Na-5s	5	7.6	332	-45
Na-7s	7	10.5	327	-43
Na-10s	10	14.8	324	-42
Na-15s	15	21.6	320	-42

[a]TGA: N_2, 10 °C/min.
[b]DSC: T_g determined from 2nd heating cycle, N_2, 10 °C/min.

Table 6.2. Summary of thermal properties and flow activation energies for 15 mol% sulfonated copolyesters containing various countercations. The molecular weights of the sulfonated copolyesters are identical.

Polyester	$T_{d5\%}$[a] (°C)	T_g[b] (°C)	E_a[c] (kJ/mol)
15 mol% DMI	295	-42	53.8
Na-15s	331	-42	62.7
Ca-15s	319	-41	
Mg-15s	308	-40	175.1
Zn-15s	240	-39	70.9

[a]TGA: N_2, 10 °C/min.
[b]DSC: T_g determined from 2nd heating cycle, N_2, 10 °C/min.
[c]DHR-2 : 8 mm parallel plate, N_2

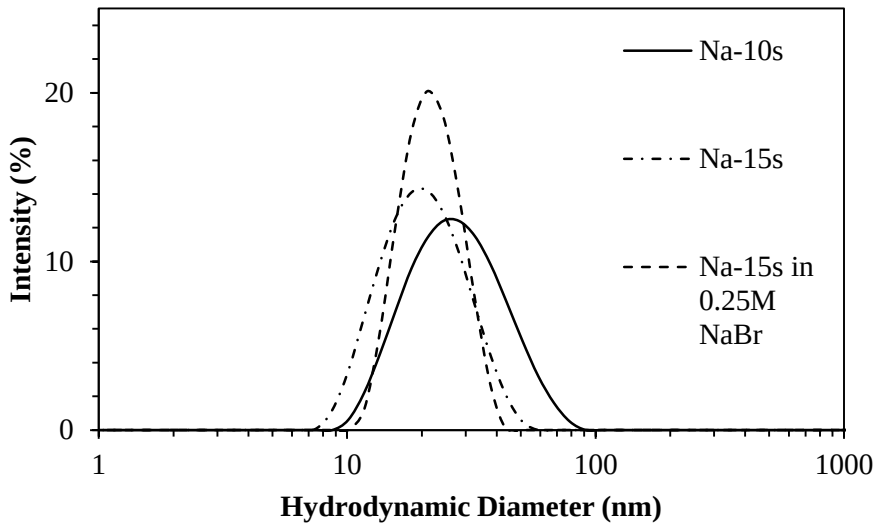

Figure 6.1. Dynamic light scattering traces of 5 wt% sodium sulfonated polyesters in water and water with 0.25 M NaBr.

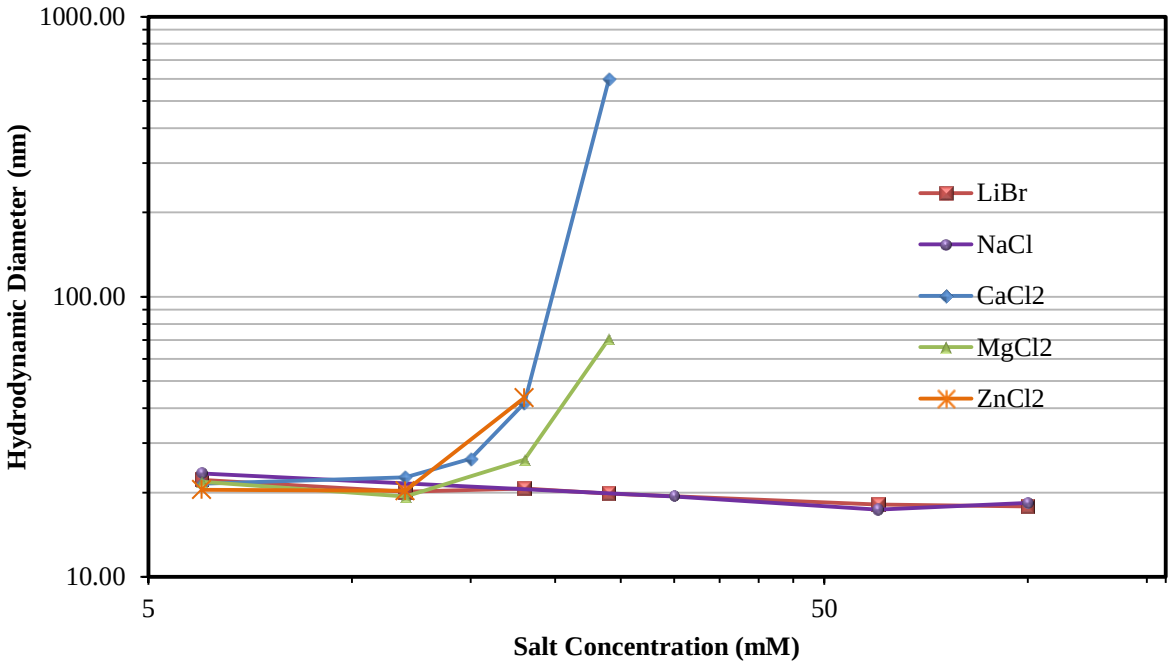

Figure 6.2. Influence of monovalent and divalent salt concentrations on the hydrodynamic diameter of 15 mol% sulfonated copolyesters in 10 wt% polymer solutions. Divalent salts increased the polymer hydrodynamic diameter at approximately 16 mM salt concentrations.

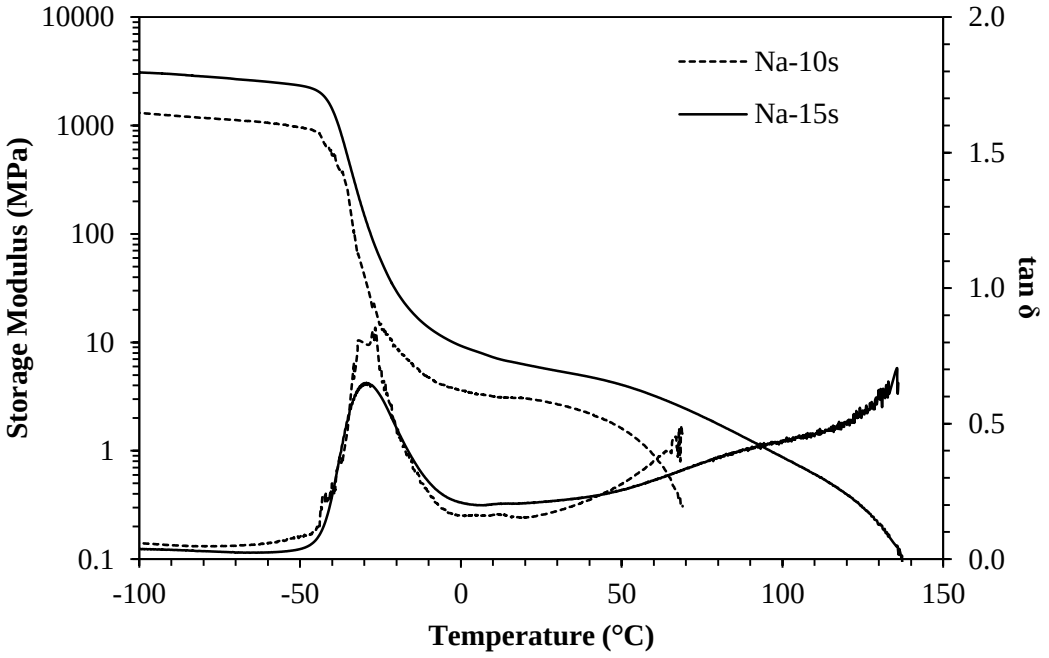

Figure 6.3. Dynamic mechanical analysis of Na-10s and Na-15s copolyesters.

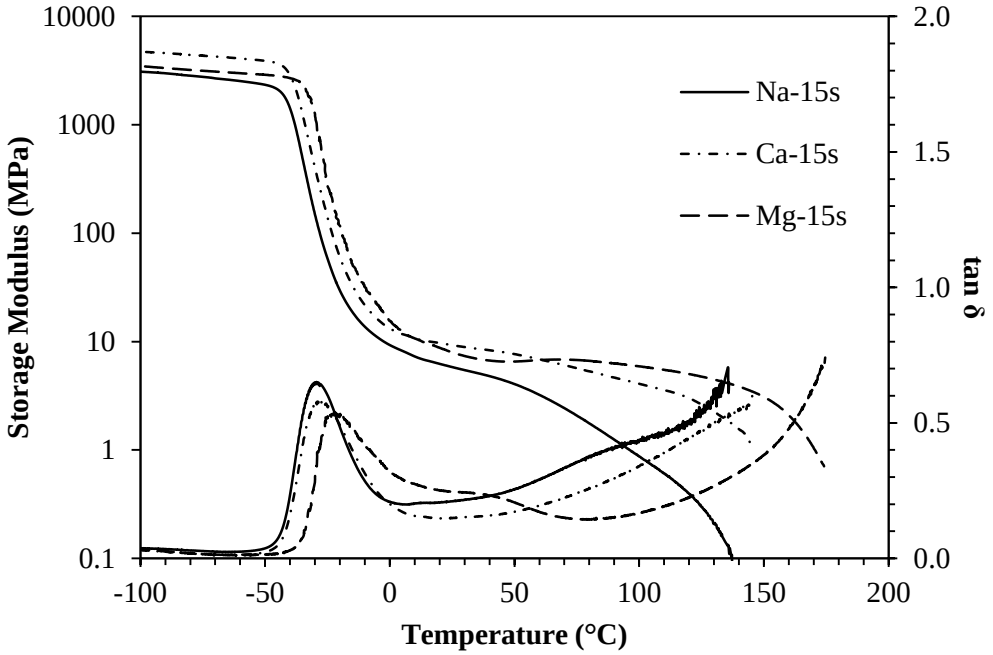

Figure 6.4. Dynamic mechanical analysis of 15 mol% sulfonated copolyesters as a function of countercation composition.

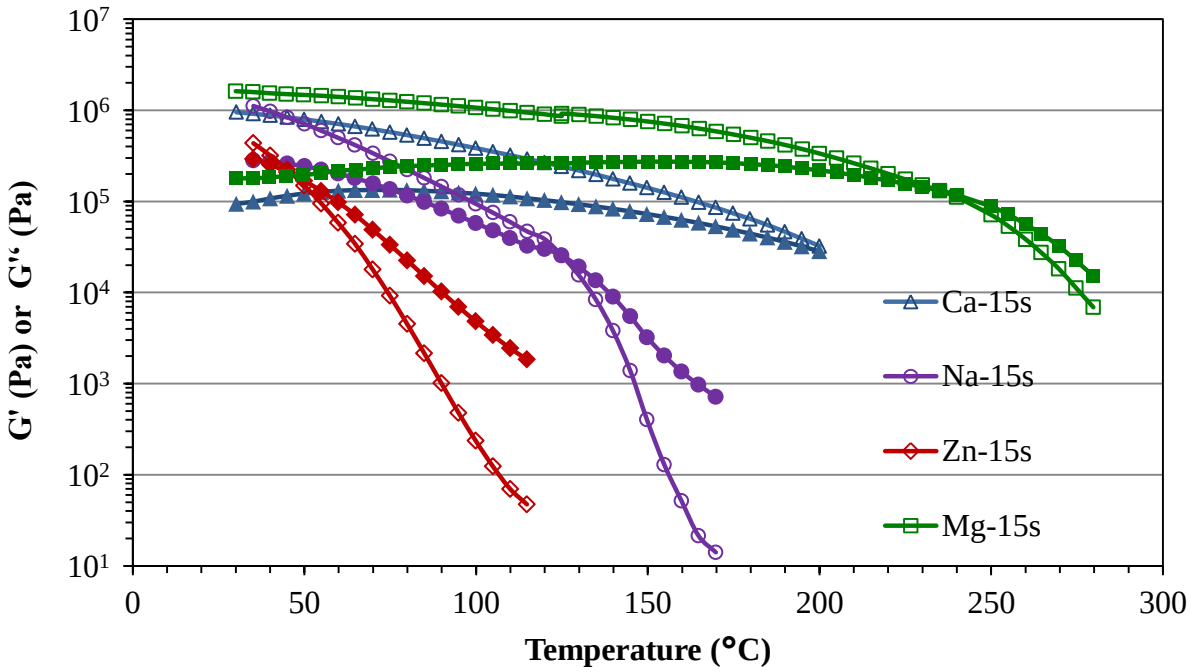

Figure 6.5. Temperature sweep experiments obtained from dynamic melt rheology demonstrates the influence of divalent metal cations on 15 mol% sulfonated copolyesters. Molecular weight influences were eliminated using dialysis cation exchange.

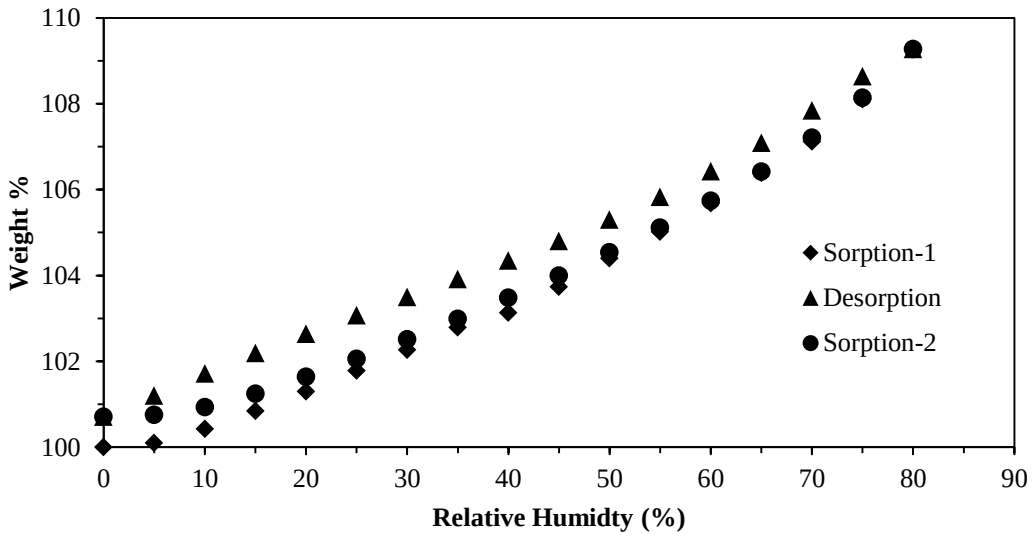

Figure 6.6. Representative thermogravimetric sorption/desorption/sorption curve obtained from Mg-15s copolyester.

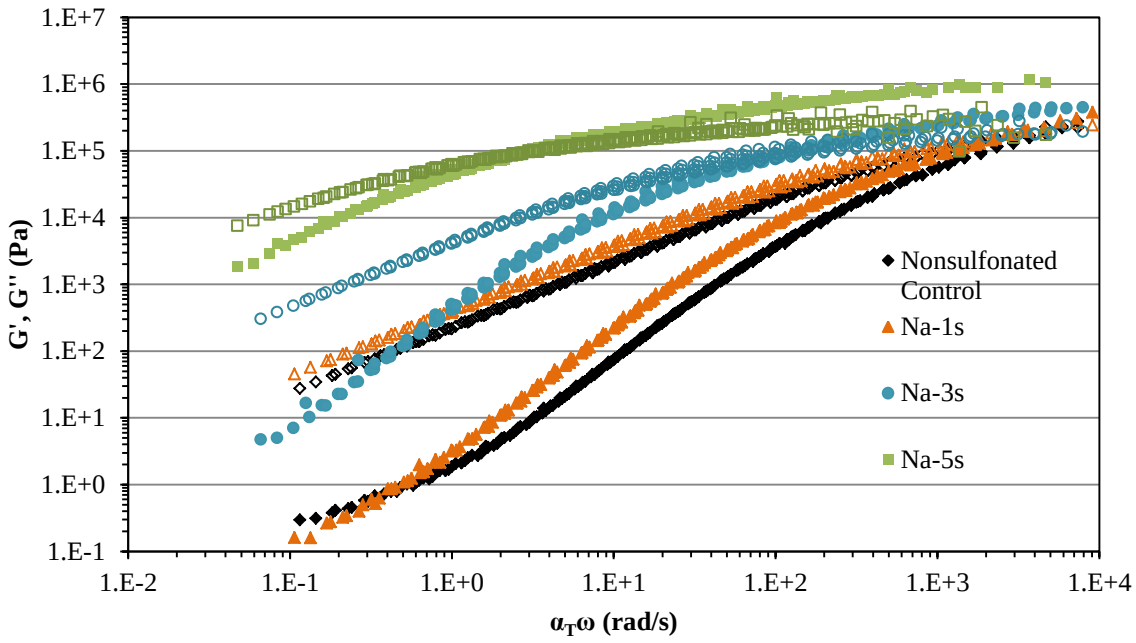

Figure 6.7. TTS master curves of ≤ 5 mol% sodium sulfonated copolyester (T_{ref} = 40 °C) demonstrating an extended rubbery plateau as a function of sulfonation level. Filled and unfilled symbols represent the storage and loss moduli, respectively.

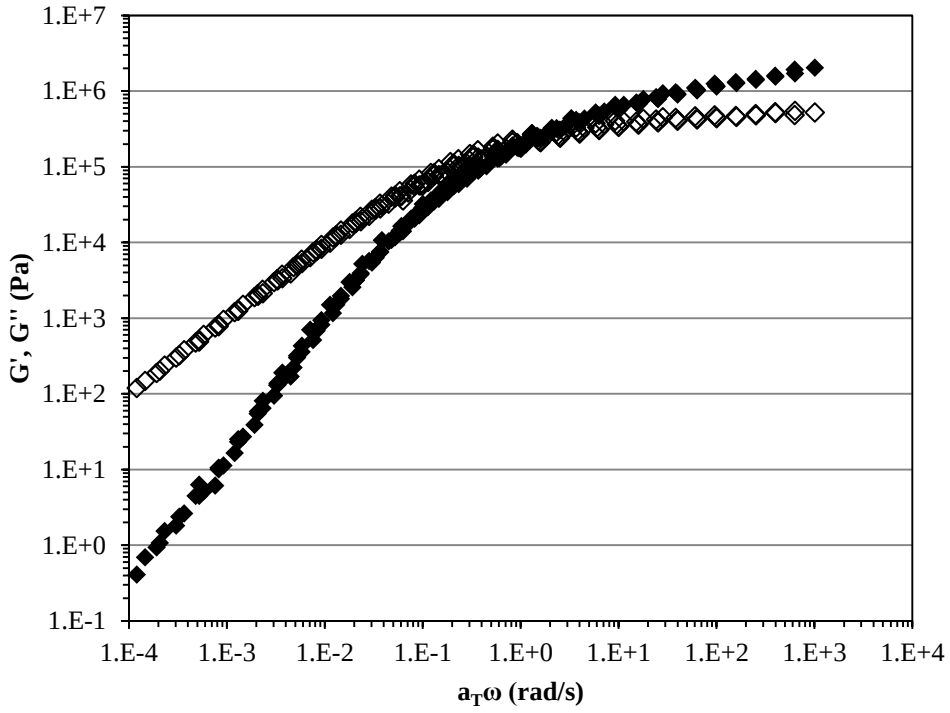

Figure 6.8. TTS master curve of Zn-15s copolyester (T_{ref} = 30 °C). Filled and unfilled symbols represent the storage (G') and loss (G'') moduli, respectively.

6.6 *References*

1. Schlick, S., *Ionomers : characterization, theory, and applications*. CRC Press: Boca Raton, 1996.
2. Tant, M. R.; Mauritz, K. A.; Wilkes, G. L.; Editors, *Ionomers: Synthesis, Structure, Properties and Applications*. 1997; p 514 pp.
3. Varley, R. J.; van der Zwaag, S., *Acta Mater.* **2008,** *56* (19), 5737-5750.
4. Eisenberg, A.; Hird, B.; Moore, R. B., *Macromolecules* **1990,** *23* (18), 4098-4107.
5. Hall, L. M.; Seitz, M. E.; Winey, K. I.; Opper, K. L.; Wagener, K. B.; Stevens, M. J.; Frischknecht, A. L., *J. Am. Chem. Soc.* **2011,** *134* (1), 574-587.
6. Fitzgerald, J. J.; Weiss, R. A., Cation-Anion and Cation-Cation Interactions in Sulfonated Polystyrene Ionomers. In *Coulombic Interactions in Macromolecular Systems*, American Chemical Society: 1986; Vol. 302, pp 35-53.
7. Lee, M.; Choi, U. H.; Colby, R. H.; Gibson, H. W., *Chem. Mater.* **2010,** *22* (21), 5814-5822.
8. Page, K. A.; Cable, K. M.; Moore, R. B., *Macromolecules* **2005,** *38* (15), 6472-6484.
9. Cheng, S.; Zhang, M.; Wu, T.; Hemp, S. T.; Mather, B. D.; Moore, R. B.; Long, T. E., *J. Polym. Sci., Part A: Polym. Chem.* **2011**, n/a-n/a.
10. Castagna, A. M.; Wang, W.; Winey, K. I.; Runt, J., *Macromolecules* **2011,** *44* (8), 2791-2798.
11. Agarwal, P. K.; Makowski, H. S.; Lundberg, R. D., *Macromolecules* **1980,** *13* (6), 1679-1687.
12. Fan, X.-D.; Bazuin, C. G., *Macromolecules* **1995,** *28* (24), 8216-8223.
13. Tsonos, C.; Apekis, L.; Pissis, P., *Journal of Materials Science* **2000,** *35* (23), 5957-5965.
14. Pilati, F.; Manaresi, P.; Ruperto, M. G.; Bonora, V.; Munari, A.; Fiorini, M., *Polymer* **1993,** *34* (11), 2413-2421.
15. Capek, I., *Adv. Colloid Interface Sci.* **2005,** *118* (1–3), 73-112.
16. Lantman, C. W.; MacKnight, W. J.; Peiffer, D. G.; Sinha, S. K.; Lundberg, R. D., *Macromolecules* **1987,** *20* (5), 1096-1101.
17. Hara, M.; Wu, J. L., *Macromolecules* **1988,** *21* (2), 402-407.
18. Pedley, A. M.; Higgins, J. S.; Peiffer, D. G.; Burchard, W., *Macromolecules* **1990,** *23* (5), 1434-1437.
19. Dieterich, D., *Prog. Org. Coat.* **1981,** *9* (3), 281-340.
20. Hunley, M. T.; England, J. P.; Long, T. E., *Macromolecules* **2010,** *43* (23), 9998-10005.
21. McKee, M. G.; Hunley, M. T.; Layman, J. M.; Long, T. E., *Macromolecules* **2005,** *39* (2), 575-583.
22. Lin, Q.; Unal, S.; Fornof, A. R.; Armentrout, R. S.; Long, T. E., *Polymer* **2006,** *47* (11), 4085-4093.
23. Calhoun, B. H.; Moore, R. B., *Journal of Vinyl and Additive Technology* **1996,** *2* (4), 358-362.
24. Landis, F. A.; Moore, R. B., *Macromolecules* **2000,** *33* (16), 6031-6041.
25. Majsztrik, P. W.; Satterfield, M. B.; Bocarsly, A. B.; Benziger, J. B., *Journal of Membrane Science* **2007,** *301* (1–2), 93-106.
26. Tierney, N. K.; Register, R. A., *Macromolecules* **2003,** *36* (4), 1170-1177.

6.7 *Supporting Information*

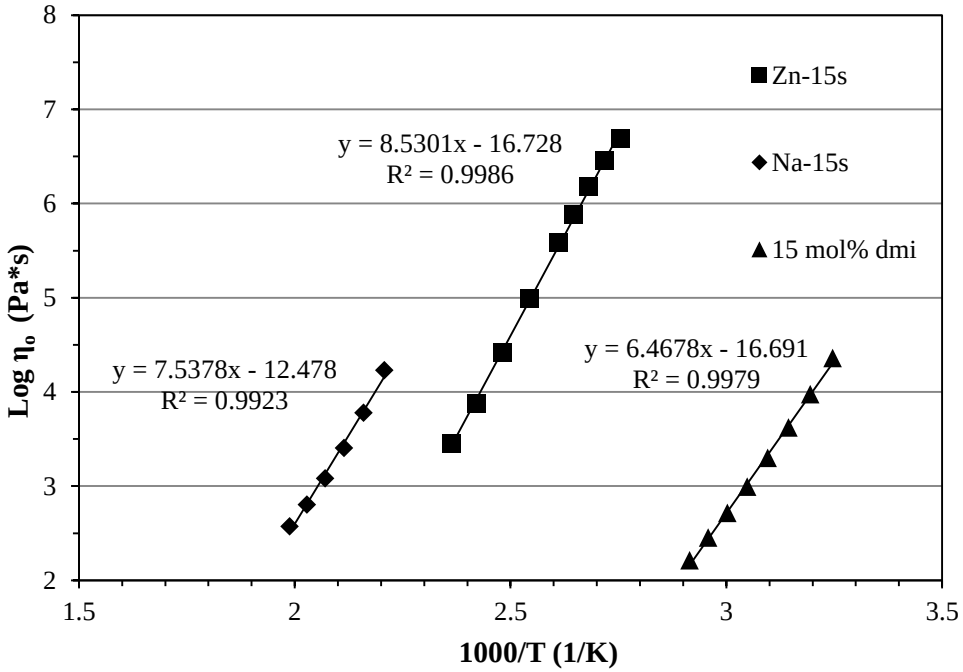

Figure S 6.1. Flow activation energy of 15 mol% sulfonated polyester containing various countercations.

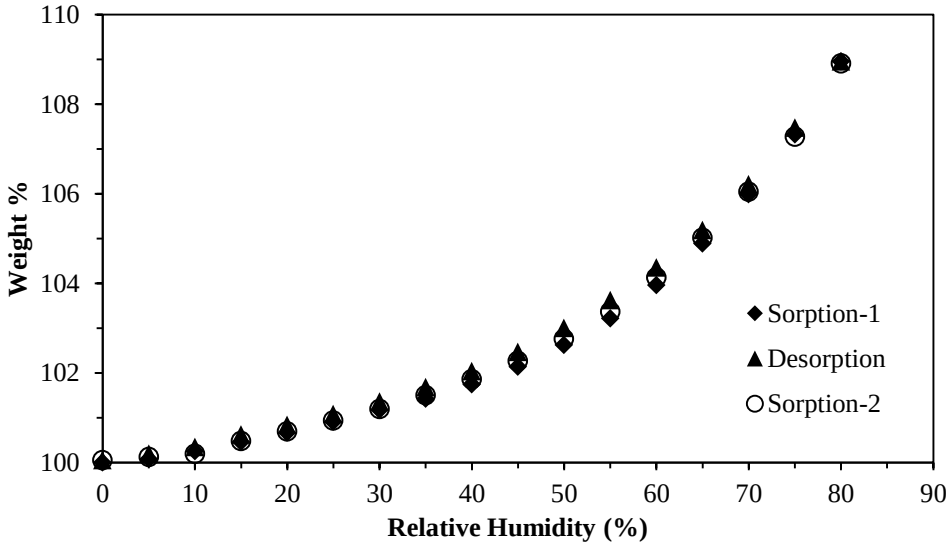

Figure S 6.2. Isothermal sorption curve for Na-15s obtained at 25 °C.

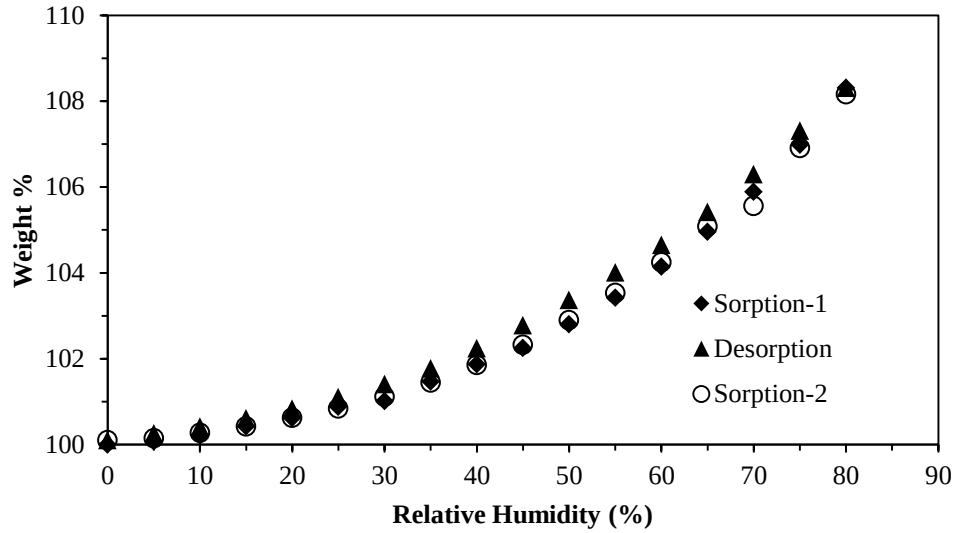

Figure S 6.3. Isothermal sorption curve for Ca-15s obtained at 25 °C.

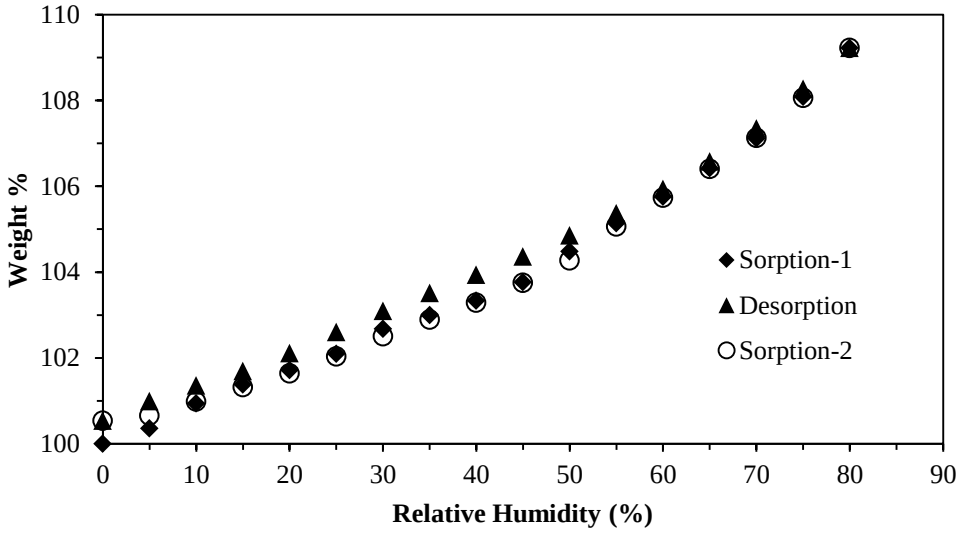

Figure S 6.4 Isothermal sorption curve for Zn-15s obtained at 25 °C.

Chapter 7: Water-Dispersible Cationic Polyurethanes Containing Pendant Trialkylphosphoniums

Musan Zhang, Sean T. Hemp, Mingqiang Zhang, Michael H. Allen, Jr., Richard N. Carmean, Robert B. Moore, and Timothy E. Long*

Department of Chemistry, Macromolecules and Interfaces Institute
Virginia Tech, Blacksburg, VA 24061-0212

7.1 *Abstract*

Novel trialkylphosphonium ionic liquids chain extenders enabled the successful synthesis of poly(ethylene glycol)-based, cationic polyurethanes with pendant phosphoniums in the hard segments (HS). Aqueous size exclusion chromatography (SEC) confirmed the charged polyurethanes, which varied the phosphonium alkyl substituent length (ethyl and butyl) and cationic HS content (25, 50, 75 mol%), achieved high absolute molecular weights. Dynamic mechanical analysis (DMA) demonstrated the triethylphosphonium (TEP) and tributylphosphonium (TBP) polyurethanes displayed similar thermomechanical properties, including increased rubbery plateau moduli and flow temperatures. Fourier transform infrared spectroscopy (FTIR) emphasized the significance of ion-dipole interaction on hydrogen bonding. Atomic force microscopy (AFM), small-angle X-ray scattering (SAXS), and wide-angle X-ray diffraction (WAXD) supported microphase separated morphologies in the trialkylphosphonium polyurethanes, despite the presence of ionic interactions. Sorption isotherm experiments revealed TBP polyurethanes displayed similar water sorption profiles to the noncharged analogue and lower water absorptivity compared to TEP. The phosphonium polyurethanes displayed significantly improved tensile strain; however, lower tensile stress of the TEP polyurethane was presumably due to absorbed water. In addition, we also explored applications of the trialkylphosphonium polyurethanes as nucleic acid delivery vectors and demonstrated their abilities to form colloidally stable polyplexes in salt-containing media.

7.2 *Introduction*

The critical fields of biomedical technology and high performance materials demand innovative macromolecular design for multifunctional applications. The literature extensively describes the success of ion-containing polymers, including polyelectrolytes and ionomers, to meet the challenges of emerging technologies from water purification membranes, conductive thin films, and electro-active actuators to antimicrobial bioadhesives, tissue scaffolds, and drug delivery vehicles.[1-3] Although relatively unexplored compared to ammonium analogues, phosphonium cations afford many advantages resulting from the phosphorous electronic distribution, which dictates electronegativity, nucleophilicity, and polarizability.[4, 5] A subtle atomic modification from nitrogen to phosphorus in quaternary salts results in significant differences in properties including electrostatic strength, ionic conductivity, thermal stability, and chemical resistivity. Phosphonium-containing salts and polymers displayed enhanced resistance to the deleterious Hoffman elimination, which is often observed for quaternary ammoniums. Recently, our research initiative to explore ammonium-alternative, cationic structures led to the first report of phosphonium polyelectrolytes and phosphonium diblock copolymers as macromolecular nucleic acid delivery vehicles.[6, 7]

Many researchers have elucidated the significance of noncovalent interactions, including electrostatics and hydrogen bonding, on nanoscale morphologies of polymers with various architectures.[8-10] Random copolymers of *n*-butyl acrylate and trialkylphosphonium styrenics demonstrated tunable thermomechanical properties depending on the alkyl length and counteranion.[11] In many instances, hydrogen bonded self-assembly produced synergistic effects with ionic interactions, which resulted in unique microphase separated, nanostructured morphologies.[12, 13] The versatility of the phosphonium cation and significance of morphology extend beyond bulk polymer properties. Diblock copolymers containing a phosphonium

complexation block and poly(ethylene glycol)-based (PEG) stabilizing block produced colloidally stable polymer-DNA polyplexes most likely due to the formation of complex solution structure.[6, 7]

The impact of electrostatic interactions on the morphology of segmented copolymers, have been described in segmented copolyesters,[14] polyurethanes,[15, 16] poly(arylene ethers),[17] and ionenes.[18, 19] Polyurethanes are ideal segmented copolymers to probe the interactions between electrostatics and hydrogen bonding. Several studies reported the electrostatic interactions in charged polyurethanes disrupted the hydrogen bonding, which eliminated the microphase separated morphology necessary to maintain suitable mechanical properties.[16, 20] Although the electrostatic interactions partially restored the mechanical properties lost from disrupted hydrogen bonding, a sacrifice in the tensile properties was often observed.

Quaternary nitrogens represent the most common example of cationic polyurethanes, and only one example currently exists for phosphonium polyurethanes.[15] This manuscript describes water-dispersible, phosphonium-containing polyurethanes synthesized using novel phosphonium ionic liquid chain extenders. Aqueous size exclusion chromatography (SEC) confirmed high absolute molecular weight polymers. Dynamic mechanical analysis (DMA) supported the presence of a microphase separated morphology, which was further confirmed using complementary characterization techniques including atomic force microscopy (AFM), small-angle X-ray scattering (SAXS), and wide-angle X-ray diffraction (WAXD). Fourier transform infrared spectroscopy (FTIR) confirmed the phosphonium polyurethanes maintained a hydrogen bonded physical network. Thermogravimetric sorption analysis probed the water absorption properties, which provided valuable information for interpretation tensile behavior. Our results indicated that ion-dipole interactions promoted more cohesive, microphase separated networks

and suppressed hydrogen bonding to the polar PEG SS leading to undesired phase-mixing. Compelling preliminary nucleic acid delivery investigations further demonstrated versatility of the phosphonium polyurethanes for future biological applications.

7.3 *Experimental Section*

Materials

Triethylphosphine (99%), tri-*n*-butylphosphine (anhydrous, 99%), and 1,4-butanediol (BD, anhydrous, 99.5%) were purchased from Sigma-Aldrich and used as received. Poly(ethylene glycol) (PEG, Sigma-Aldrich, M_n = 2000 g/mol) was dried at 60 °C under reduced pressure (10 mmHg) for 18 h. Anhydrous *N,N*-dimethylformamide (DMF, 99.8%) was obtained from Fischer Scientific. Dibutyltin dilaurate (DBTDL, Sigma-Aldrich, 95%) catalyst solution was prepared at 1 wt% in anhydrous tetrahydrofuran (THF). Dicyclohexylmethane-4,4'-diisocyanate (HMDI, 99.5%), which was graciously donated from Bayer MaterialScience, was used without further purification. 2-(Bromomethyl)-2-methyl-1,3-propanediol was synthesized according to procedures described in the literature and dried at 40 °C under reduced pressure (10 mmHg) for 12 h.[21]

Synthesis of trialkylphosphonium diols

The synthesis of tri-*n*-butyl(1,3-dihydroxypropyl)phosphonium bromide serves as a representative example; the triethylphosphonium diol was prepared similarly. 2-(Bromomethyl)-2-methyl-1,3-propanediol (1.05 molar excess) was charged into a flame-dried, 100-mL, round-bottomed flask with a magnetic stir bar and purged with dry N_2. Tri-*n*-butylphosphine was added using dry syringe techniques, and the reaction proceeded at 100 °C for 2 d under vigorous stirring. The initial, biphasic reaction was homogenous after completion. Unreacted reagents

were distilled from the reaction at 100 °C (<1 mmHg). The product was washed multiple times with diethyl ether and dried at 90 °C under reduced pressure (0.5 mmHg) for 24 h.

Tri-n-butyl(1,3-dihydroxypropyl)phosphonium bromide - Yield: 94% as a clear, viscous ionic liquid, T_d(5%) = 368 °C, T_g = -29 °C, T_m = 66 °C. ^{1}H NMR (400 MHz, D_2O, 25 °C) δ (ppm): 0.93 (t, -$CH_2CH_2CH_2CH_3$, 9H, *J* = 7.2 Hz), 1.06 (s, -CH_3, 3H), 1.30-1.55 (m, -$CH_2CH_2CH_2CH_3$, 12H), 2.10-2.22 (m, -PCH_2-, 8H), 3.33-3.44 (m, -CH_2OH, 4H). ^{31}P NMR (400 MHz, D_2O, 25 °C) δ (ppm): 33.73. Mass Spectrometry: Theoretical, *m/z* 305.2604; Experimental, *m/z* 305.2605.

Triethyl(1,3-dihydroxypropyl)phosphonium bromide - Yield: 85% as white solid, T_d(5%) = 370 °C, T_g = -39 °C, T_m = 124 °C. ^{1}H NMR (400 MHz, D_2O, 25 °C) δ (ppm): 1.06 (s, -CH_3, 3H), 1.20-1.28 (m, -CH_2CH_3, 9H), 2.24-2.35 (m, -PCH_2-, 8H), 3.44-3.53 (dd, -CH_2OH, 4H). ^{31}P NMR: 38.87. Mass Spectrometry: Theoretical, *m/z* 221.1670; Experimental, *m/z* 221.1652.

Synthesis of polyurethanes

The following procedure for 75 mol% HS tri-*n*-butylphosphonium (TBP(75)) polyurethane serves as a representative polymerization. Dry PEG (2.5 mmol) was charged into a flame-dried, three-necked, round-bottomed flask equipped with an addition funnel, nitrogen inlet, and overhead mechanical stirrer and purged thoroughly with N_2. The DBTDL catalyst solution (50 ppm) and HMDI (10 mmol) were syringed into the addition funnel. The reaction flask was first heated to 70 °C, and the DBTDL and HMDI mixture was added after the PEG thoroughly melted. The reaction continued under constant stirring for 5 h at 70 °C. The dry chain extender, tributylphosphonium diol (7.5 mmol), was charged into a separate flame-dried, round-bottomed flask and purged with N_2. Dry DMF (~10 mL) was cannulated into the flask. The dissolved solution was transferred into the addition funnel and slowly added drop-wise to the reaction. The addition funnel was washed with additional anhydrous DMF and added to the reaction to achieve

a final 10 wt% polymer concentration. The following equation determined the hard segment weight content (HS wt%):

$$HS\ wt\% = \frac{HMDI + chain\ extender}{HMDI + chain\ extender + PEG} \times 100\%$$

Characterization

All monomers and polymers were dried under reduced pressure (0.5 mmHg) at 80 °C overnight prior to characterization. ^{1}H NMR spectroscopy (Varian Inova, 400 MHz, D_2O) and mass spectrometry (Agilent 6220 LC-TOF-MS) confirmed monomer composition. Dynamic light scattering (DLS, Malvern Zetasizer NanoZS) confirmed the absence of polymer aggregation in the aqueous mobile phase (54/23/23 (v/v/v %) water/methanol/acetic acid with 0.1 M sodium acetate). Aqueous size exclusion chromatography (SEC) provided absolute molecular weights using a Water 1515 Isocratic HPLC Pump and Waters 717plus Autosampler with Waters 2414 refractive index and Wyatt MiniDAWN MALLS detectors (flow rate 0.8 mL/min). A Wyatt Optilab T-rEX differential refractometer measured offline *dn/dc* values at 658 nm and 35 °C. A TA Instruments thermogravimetric analyzer (TGA 2950) determined the temperature (T_d) at 5% weight loss of monomers and polymers (N_2, 25 to 600 °C, ramp 10 °C/min). Differential scanning calorimetry (DSC, TA Instruments, Q1000) measured monomer and polymer thermal transitions from heat/cool/heat experiments (N_2, -80 to 200 °C, ramp 10 °C/min). A TA Instruments Q5000 thermogravimetric sorption analyzer (TGA-SA) investigated the water sorption behavior of polyurethane samples (75 mol% HS) using a 5% relative humidity (RH) step procedure from 0 – 95% RH. Each RH step proceeded for 2 h or until the weight stabilized (<0.01% change over 10 min). An instrumental pre-drying method was applied to each sample before the experiment at 50 °C and 0% RH. Dynamic mechanical analysis (DMA, TA Instruments, Q800) revealed PU thermomechanical properties from

temperature ramp experiments under an oscillatory tension mode (-100 to 180 °C, ramp 3 °C/min, 1 Hz). A 5500R Instron universal testing instrument performed tensile testing at a cross-head speed of 50 mm/min; the polyurethane tensile stress, % elongation, and Young's moduli are reported based on an average of five specimens. Fourier transform infrared (FTIR) spectroscopy (Varian ATR-FTIR) evaluated the extent of hydrogen bonding at ambient conditions (128 scans, background subtraction, and ATR corrected). Atomic force microscopy (Veeco Multimode AFM) probed the polyurethane surface morphology under tapping mode (tip spring constant 42 N/m, free air amplitude 3.00 V, tapping to free air amplitude ratio = 0.6). [SAXS/WAXD method characterization]

7.4 *Results and Discussion*

Water-dispersible, phosphonium polyurethanes were successfully generated using novel trialkylphosphonium diol chain extenders. An efficient, one-step, nucleophilic substitution reaction between 2-(bromomethyl)-2-methyl-1,3-propanediol and trialkylphosphine produced trialkyl(1,3-dihydroxypropyl)phosphonium bromide in high yields (**Scheme 7.1**). Both triethylphosphonium (TEP) and tributylphosphonium (TBP) diols exhibited high thermal stabilities above 370 °C. The TEP diol displayed a glass transition temperature (T_g) and melting point at -40 and 124 °C, respectively. In contrast, the amorphous TBP diol revealed a single T_g at -33 °C, which classified this monomer as a room temperature ionic liquid. Trialkylphosphonium diols that contain primary hydroxyls served as efficient chain extenders to afford cationic polyurethanes with pendant phosphonium groups in the HS. The rationale for the pendant phosphonium position was to presumably promote facile ionic interactions.

Scheme 7.1 Synthesis of trialkyl(1,3-dihydroxypropyl)phosphonium bromide.

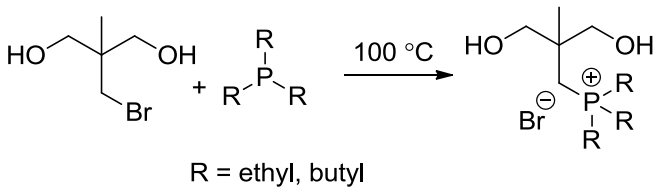

Scheme 7.2. Synthesis of trialkylphosphonium polyurethanes.

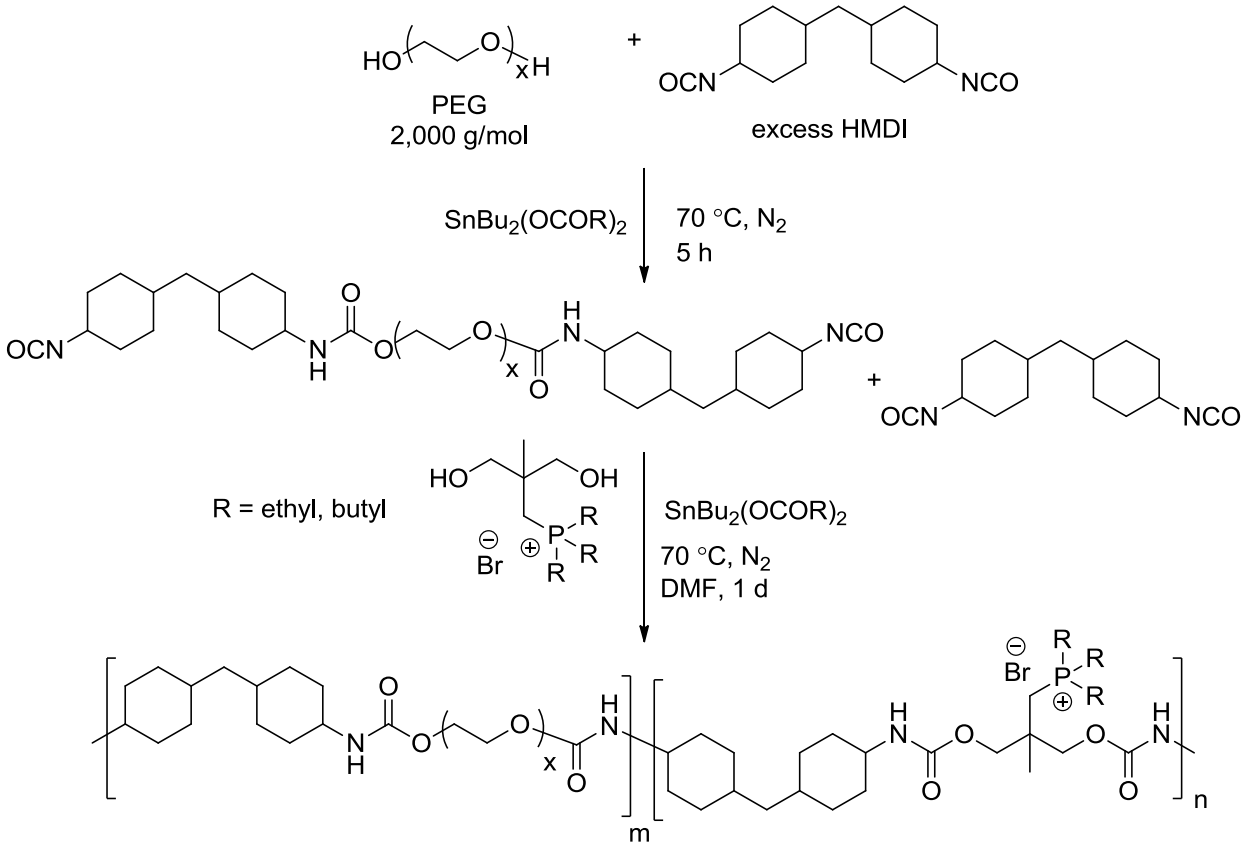

Scheme 7.2 illustrates the two-step synthesis of noncharged (BD(*x*)), triethylphosphonium (TEP(*x*)), and tri-*n*-butylphosphonium (TBP(*x*)) polyurethanes, where *x* represents the mol% HS. Chain extension of the HMDI-endcapped PEG prepolymer with trialkylphosphonium diols afforded cationic phosphonium polyurethanes. Dynamic light scattering of the phosphonium polyurethanes confirmed the absence of polymer aggregation in

the aqueous SEC solvent (**Figure S 7.3**). **Figure 7.1** displays representative aqueous SEC light scattering traces for various phosphonium polyurethanes. **Table 7.1** summarizes the absolute molecular weights using experimentally determined *dn/dc* values. Possible inefficient SEC separation presumably accounted for the low polydispersity; however, all polyurethanes exhibited M_n > 23,000 g/mol with monomodal distributions.

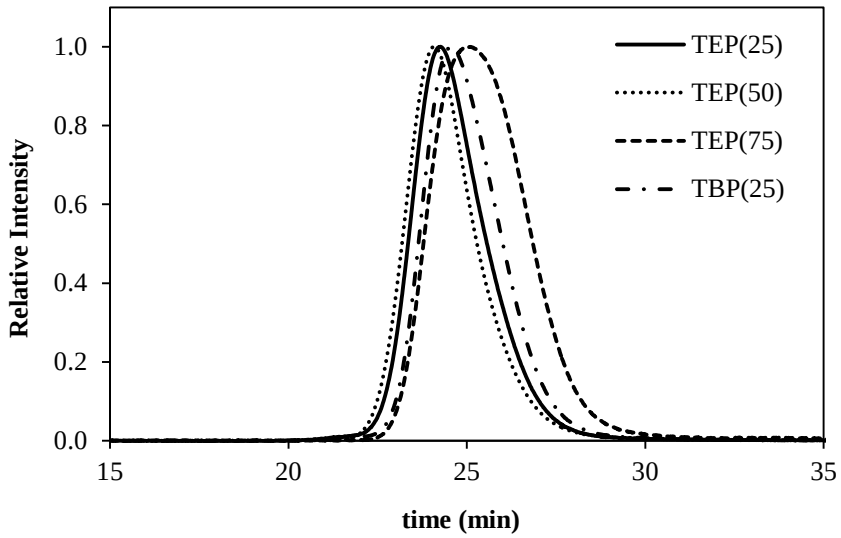

Figure 7.1. Representative aqueous SEC light scattering chromatograms of phosphonium PU (54/23/23 water/methanol/acetic acid (v/v/v %), 0.1 M sodium acetate).

Table 7.2 summarizes the polyurethane thermal properties, and phosphonium polyurethanes demonstrated higher thermal stabilities compared to noncharged polyurethanes. The TBP polyurethanes exhibited comparable thermal stabilities to the TEP polyurethanes at equivalent HS content. Increasing the HS content systematically reduced the thermal stability, which suggested the initial weight loss occurred primarily within the HS. The phosphonium-based polyurethanes offered higher thermal stabilities relative to ammonium-based polyurethanes, which showed evidence of Hoffman elimination at 180 °C.[22] The phosphonium polyurethanes exhibited a single T_g at approximately -55 °C, which was attributed to the PEG SS. Noncharged polyurethanes displayed SS melting transitions at approximately 35 °C. The

phosphonium polyurethanes exhibited similar melting transitions at high SS content, however, both TEP(75) and TBP(75) polyurethanes had lower T_m values compared to noncharged controls. Thermal analysis suggested both the noncharged analogue and phosphonium polyurethanes possessed a microphase separated morphology.

Table 7.1. Absolute molecular weights of butanediol (BD), triethylphosphonium diol (TEP), tributylphosphonium diol (TBP) chain extended polyurethanes (PU) containing various mol% hard segment (HS) content.

PU	M_n[a] (g/mol)	M_w/M_n[a]	HS mol%	HS wt%
BD(50)[b]	20,300	1.54	50	26
BD(75)[b]	22,100	2.05	75	43
TEP(25)	46,500	1.19	25	21
TEP(50)	55,800	1.30	50	31
TEP(75)	25,400	1.37	75	53
TBP(25)	50,200	1.17	25	22
TBP(50)	38,500	1.28	50	33
TBP(75)	46,500	1.10	75	56

[a]Aqueous SEC-MALLS detector unless otherwise indicated.
[b]DMF 0.05 M LiBr SEC-MALLS detector.

Table 7.2. Thermal properties of BD, TEP, and TBP chain extended PU containing various mol% HS content.

PU	$T_{d5\%}$[a] (°C)	T_g(SS)[b] (°C)	T_c(SS)[b] (°C)	T_m(SS)[b] (°C)
BD(50)	310	-50	-4	36
BD(75)	311	-52	ND	31
TEP(25)	328	-52	-2	36
TEP(50)	321	-55	-8	34
TEP(75)	303	-50	ND	9
TBP(25)	337	-52	-4	36
TBP(50)	330	-54	-9	33
TBP(75)	324	-56	-9	11

[a]TGA: N_2, 10 °C/min.
[b]DSC: T_g and T_m determined from 2nd heating cycle, T_c from cooling cycle.
ND: Crystallization temperatures not detected using DSC.

DMA probed the thermomechanical properties of noncharged and phosphonium polyurethanes containing 75 mol% HS. **Figure 7.2** reflects at least three major thermal transitions in the storage modulus and tan δ curves as a function of temperature. The lowest transition at -51 °C corresponded to the PEG T_g. The second transition at approximately 1 °C indicated the melting of the PEG SS. The noncharged BD(75) displayed a broad transition at higher temperatures compared to the phosphonium polyurethanes. Both TEP(75) and TBP(75) consistently achieved higher storage moduli between the T_g and T_m transitions compared to BD(75). DMA thermal transitions associated with the PEG SS agreed well with the DSC results. The third transition was attributed to the disruption of hydrogen bonding interactions. In the noncharged BD(75), the hydrogen bonding dissociation occurred at 60 °C leading to a sharp onset of polymer flow. In sharp contrast, TEP(75) and TBP(75) demonstrated higher storage moduli and increased breadth of the rubbery plateau compared to BD(75). Interestingly, the alkyl substituent did not influence the rubbery plateau modulus, which implied the extent of physical crosslinks in the phosphonium polyurethanes were similar at equivalent HS content. The TEP(75) hydrogen bonding dissociation near the onset of polymer flow resulted in a broad transition at approximately 120 °C. TBP(75) displayed two distinct transitions associated with hydrogen bonding dissociation and viscous flow at 110 °C and 160 °C, respectively. The sharp contrast in the thermomechanical properties of the noncharged analogue and phosphonium polyurethanes suggested that the phosphonium charge promoted a more well-defined, microphase separated

morphology, which resulted in higher storage moduli and extended rubbery plateau. Painter and coworkers reported hydrogen bonded urethane N-H and ether oxygen occurred more frequently in polyurethanes containing a more polar SS such as PEG, which accounted for more phase-mixing.[23] The incorporation of phosphonium cations into the polyurethane HS functioned synergistically with hydrogen bonding interactions, which led to improved microphase separation and enhanced thermomechanical properties compared to the noncharged control. Goddard and Copper observed similar trends in ammonium polyurethanes and concluded the cationic ammonium group promoted hydrogen bonding and microphase separation.[24]

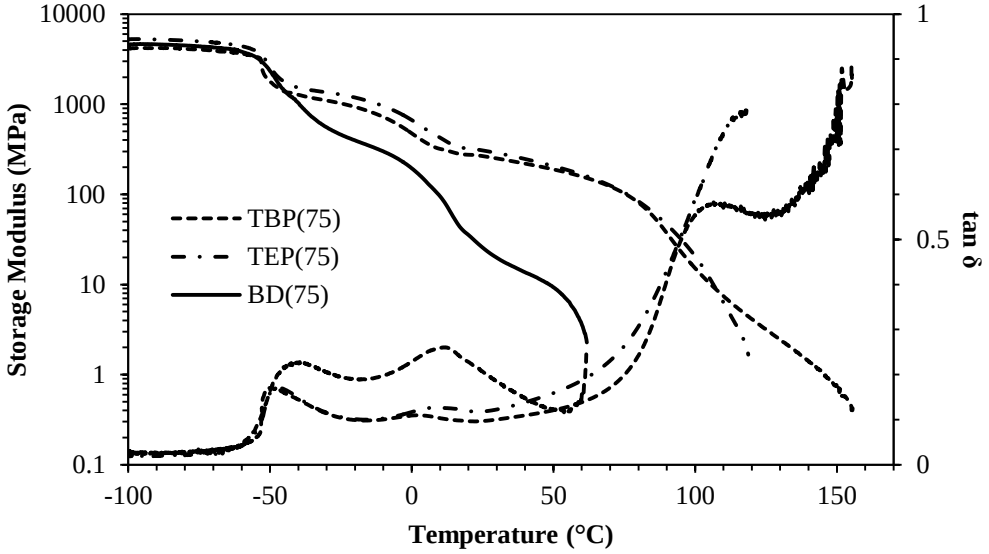

Figure 7.2. Dynamic mechanical analysis of noncharged and phosphonium PU (75 mol% HS).

Fourier transform infrared spectroscopy (FTIR) probed various hydrogen bonding interactions in noncharged and phosphonium polyurethanes using the urethane N-H (~3100 – 3550 cm^{-1}) and carbonyl (~1650 – 1800 cm^{-1}) stretching regions (**Figure 7.3**). Noncharged polyurethanes typically display two main N-H absorption bands associated with the "free" N-H stretch at 3500 cm^{-1} and hydrogen bonded N-H at lower wavenumbers.[25] Several investigations

reported on the complex hydrogen bonding interactions arising from multiple proton donor-acceptor pairs.[26-28] In the noncharged BD(75), the two primary hydrogen bond acceptors are urethane carbonyls and PEG ether oxygens (**Figure 7.3.a**). The BD(75) FTIR spectra displays a small shoulder at 3326 cm^{-1} and a dominant stretch at 3300 cm^{-1} corresponding to the N-H – ether oxygen and N-H – urethane carbonyl interactions, respectively. BD(75) demonstrated a greater extent of N-H – urethane carbonyl hydrogen bonding due to stronger associations. The phosphonium polyurethanes demonstrated an additional broad shoulder at 3260 cm^{-1}, which corresponded with hydrogen bonding between the N-H and bromide anion. Several investigations on cationic polyurethanes observed similar N-H bands.[20, 22, 29-31] The absorbance at lower frequencies reflected lower energies associated with increasing hydrogen bonding strength to anions. More importantly, unlike hydrogen bonding interactions between the N-H and ether oxygens, which promotes phase-mixing, the stronger ion-dipole interactions in phosphonium polyurethanes occurred preferentially within the HS and provided an explanation for the improved thermomechanical behavior.

The FTIR carbonyl spectral region provides additional characterization of the hydrogen bonding associations and supports similar trends observed in the N-H region (**Figure 7.3.b**). Polyurethanes with high SS content display a low-frequency absorbance at 1730 – 1740 cm^{-1} commonly assigned to free carbonyls.[25, 27, 32, 33] In conventional polyurethanes, weak, disordered hydrogen bonding typically occurred within the phase-separated interface, SS matrix, or phase-mixed regions,[23] and well-aligned, stronger hydrogen bonding existed within the HS matrix. BD(75) revealed two distinct peaks of similar intensities at 1712 and 1695 cm^{-1} corresponding to the disordered and weakly associating, ordered hydrogen bonded urethane carbonyls, respectively. In contrast, phosphonium polyurethanes presented a peak at 1700 cm^{-1} assigned to

weakly associating, ordered carbonyls. The alkyl substituents presumably resulted in sterically hindered, ordered hydrogen bonds compared to the linear butanediol, shifting the carbonyl peak to lower wavenumbers.

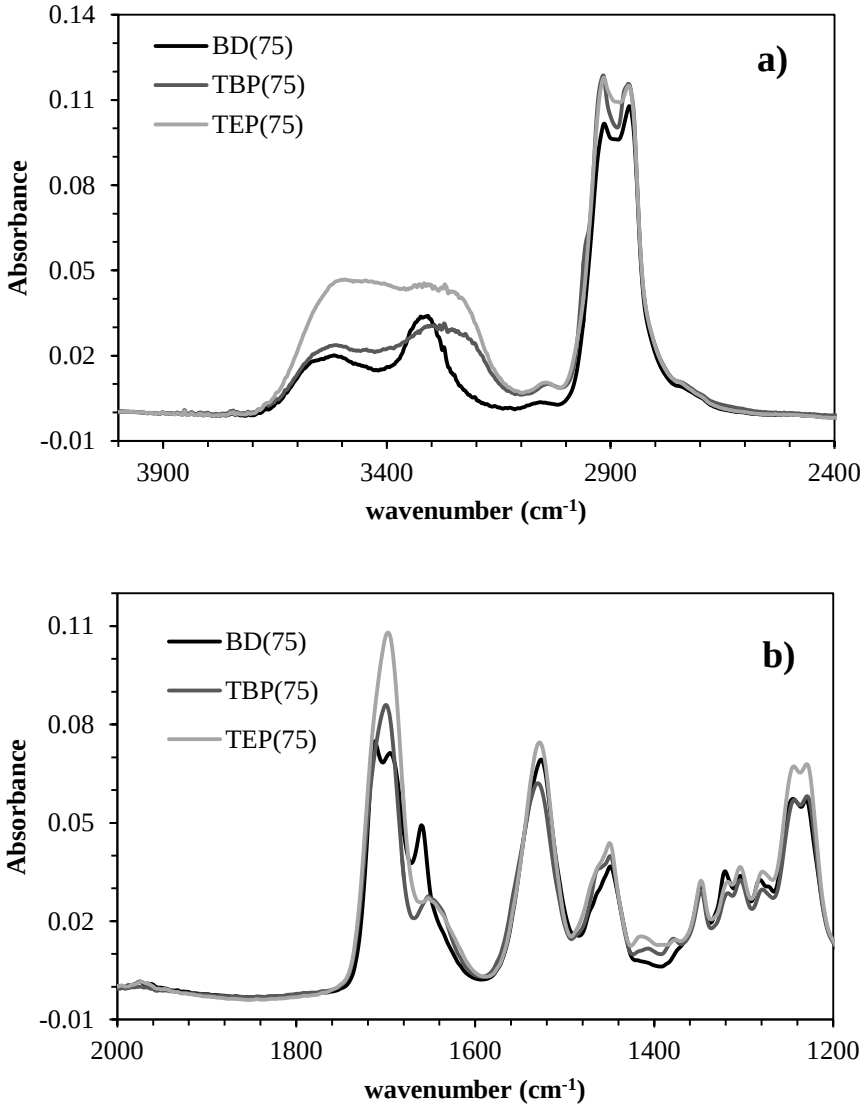

Figure 7.3. FTIR spectra of noncharged and phosphonium polyurethanes: a) N-H stretch between 3000 – 3500 cm^{-1} and b) carbonyl stretch between 1600 – 1750 cm^{-1}.

Strongly associated, ordered hydrogen bonding in BD(75) was assigned to the higher frequency stretch at 1660 cm^{-1}. Several studies on semicrystalline polyurethanes reported

evidence of ordered, hydrogen bonding occurring within the HS crystalline matrix. Wilkes and coworkers demonstrated that the diisocyanate symmetry served a critical role in determining polyurethane semicrystallinity.[34] The HMDI *cis/trans* stereoisomers effectively prevented crystallization of the HS, and the strongly associated, ordered hydrogen bonding presumably occurred in regions of high stereoregularity.[35] In TEP(75) and TBP(75), the strongly associated, ordered hydrogen bonding stretch located at lower wavenumbers (1655 cm^{-1}) was attributed to the more polar HS character. FTIR analysis demonstrated that the phosphonium polyurethanes maintained ordered, hydrogen bonding in the presence of electrostatic interactions. Furthermore, the stronger N-H – anion interactions occurred preferentially compared to weaker N-H – ether hydrogen bonding, which promoted microphase separation and led to more defined morphologies.

Atomic force microscopy elucidated the influence of phosphonium cations on the polymer surface morphology. Both the noncharged and phosphonium polyurethanes contained irregularly structured, hard domains (light colored) dispersed within the SS matrix (dark colored) (**Figure 7.4**).[36, 37] BD(75) exhibited the least defined microphase separated morphology, suggesting evidence of phase-mixing particularly at the HS-SS interface. In contrast, microphase separation improved for the phosphonium polyurethanes from the ethyl to butyl substituents. The HS-SS interface becomes increasingly distinct relative to the noncharged control. Furthermore, the TBP(75) hard phase appeared smaller and more percolated throughout the low-T_g matrix, suggesting a higher degree of HS interconnectivity.

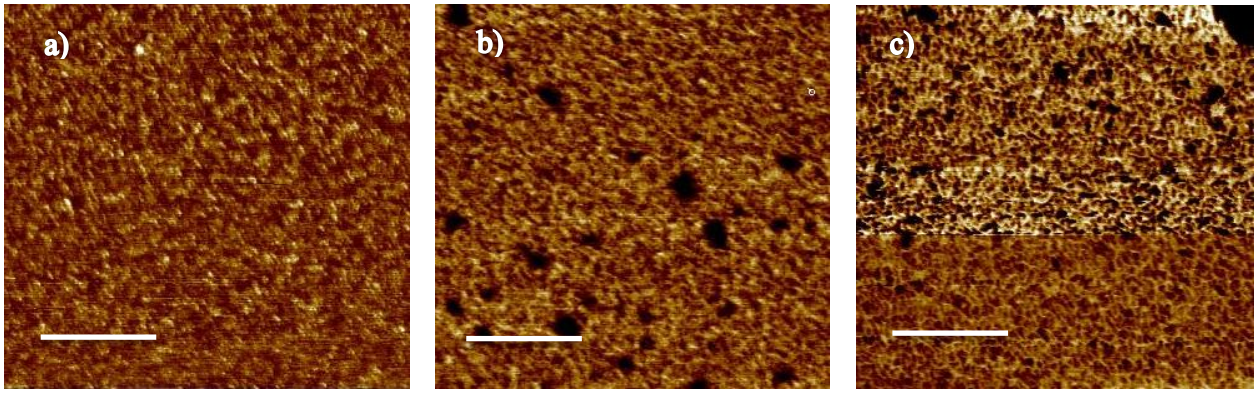

Figure 7.4. Atomic force microscopy phase images: a) BD(75), b) TEP(75), and c) TBP(75) polyurethanes. The scale bars represent 200 nm.

SAXS provided complementary analysis of the bulk morphology to confirm the presence of microphase separation.

Table 7.3 summarizes the interdomain spacing from SAXS analysis for BD(75), TEP(75), and TBP(75). Both the noncharged and phosphonium polyurethanes exhibited a single, broad intensity peak characteristic of the non-uniform microphase-separated morphology often observed in segmented block copolymers (**Figure S 7.6**).[36, 38-42] The peak position at maximum scattering intensity, q_{max}, relates to the interdomain spacing, d, according to Bragg's law:

$$d = \frac{2\pi}{q_{max}}$$

The phosphonium-containing polyurethanes exhibited smaller interdomain spacing compared to the noncharged analogue. Increasing the phosphonium alkyl substituent length from ethyl to butyl further reduced the size of the domain spacing

Table 7.3. Summary of SAXS scattering peak position, q, and interdomain spacing, *d*, of noncharged and phosphonium polyurethanes.

PU	q (nm^{-1})	*d* (nm)
BD(75)	0.523	12.0
TEP(75)	0.548	11.5
TBP(75)	0.577	10.9

SAXS: Peak position determined at maximum scattering intensity: $d=2\pi/q$

Table 7.4. Tensile properties of noncharged and phosphonium polyurethanes.

PU	Young's Modulus (MPa)	Stress at Break (MPa)	Strain at Break (%)
BD(75)	10.0 ± 0.5	7.1 ± 0.3	354 ± 35
TEP(75)	21.0 ± 5.6	4.6 ± 0.7	862 ± 13
TBP(75)	134 ± 16	10.8 ± 1.0	857 ± 20

Tensile: Crosshead speed 50 mm/min; values reported as an average of five samples.

Tensile testing indicated that the phosphonium polyurethanes offered significantly improved mechanical properties compared to neutral controls (**Table 7.4**). Both TEP(75) and TBP(75) had 100% increase in tensile strains compared to BD(75) (**Figure 7.5**). The semicrystalline PEG phase in BD(75) possibly reduced SS flexibility, which resulted in lower elongations. In the phosphonium polyurethanes, the combination of an amorphous, low-T_g phase and improved microphase separation likely contributed to increased elongations and Young's moduli. Higher Young's moduli in the phosphonium polyurethanes reflected greater hard domain cohesive strength.[31, 43] Furthermore, evidence of modest strain hardening, associated

with ordered alignment of the HS domains during deformation, further supported a well-defined, microphase separated morphology.

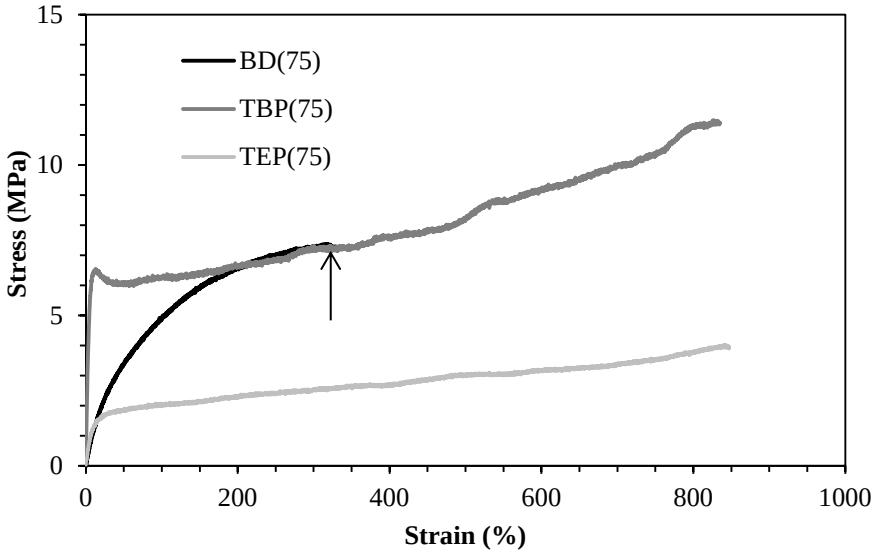

Figure 7.5. Representative tensile stress-strain curves of noncharged and phosphonium polyurethanes. Arrow designates the stress and strain at break for BD(75).

Tensile analyses also supported the impact of alkyl length on mechanical properties. The TBP(75) displayed a distinct yield point corresponding to plastic deformation of the hydrogen bonded, highly interconnected hard phase. In contrast, the TEP(75) displayed a noticeably lower tensile stress compared to both TBP(75) and BD(75). This observation led to an investigation of the polyurethane water sorption behavior. **Figure 7.6** illustrates the sample weight% as a function of %RH during a thermogravimetric water sorption experiment. The TEP(75) clearly exhibited the highest water absorption at every %RH. Interestingly, the TBP(75) revealed a similar water absorption profile to the BD(75), and this observation suggested the tributylphosphonium group did not significantly contribute to water absorption properties. The results suggested the shorter ethyl substituent in TEP(75) contributed significantly to the enhanced hydrophilicity. The higher absorbed water content in TEP(75) presumably functioned

as a HS plasticizer, which lowered the tensile stress. Previous investigations reported increased tensile strengths and reduced strains in ionic polyurethanes when the extent of electrostatic interactions exceeded hydrogen bonding associations.[44, 45] Our results demonstrated that the phosphonium polyurethanes possessed desirable synergistic interactions, which significantly contributed to the overall improved mechanical performance.

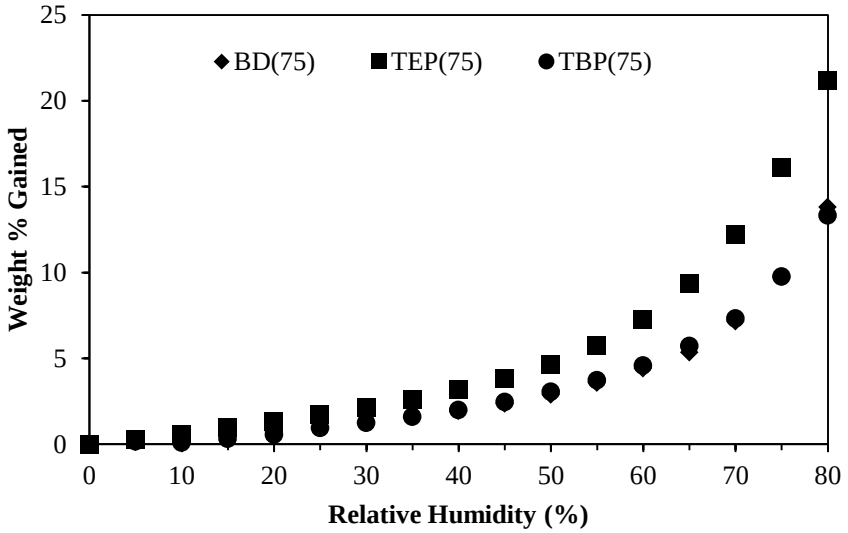

Figure 7.6. Sorption isotherm of noncharged and phosphonium polyurethanes (75 mol% HS) at 25 °C.

A desirable feature of the phosphonium polyurethanes was their spontaneous water-dispersibility and formation of non-aggregated, nanoparticles in solution. DLS investigations showed the phosphonium polyurethanes with longer butyl substituents produced larger nanoparticles in solution compared to ethyl analogues (**Figure S 7.4**). Furthermore, the size of the particle decreased with increasing HS content. Typically, ionic polymers in salt-free aqueous conditions exhibit large-scale aggregation due to hydrophobic interactions.[46, 47] DLS results

suggested that the phosphonium polyurethanes possess unique solution structure that arises from cationic structure, segmented block composition, and hydrogen bonding interactions.[48]

The water-dispersible phosphonium polyurethanes demonstrated potential as nonviral, macromolecular gene delivery vehicles. DNA binding gel shift assays confirmed DNA binding at low charge (+/-) ratios, where (+) represents the number of positive polymer cationic sites and (–) represents the number of negative DNA phosphate groups (Figure 7.7). As expected, the +/- ratio at complete DNA binding decreased from 4 to 2 with increasing HS content due to a higher cationic content. In general, DLS investigations found that the size of the polyplexes systematically decreased with increasing HS content, which presumably related to stronger DNA-polymer interactions with increasing cationic charge density. Furthermore, DLS studies verified the polyplexes formed from TBP(50) and TBP(75) maintained particle stability over 24 h in physiological salt solutions (Figure 7.8). However, TBP(25) showed an increase in the particle size attributed to the release of DNA after 24 h from weaker binding. These preliminary investigations indicated that phosphonium polyurethanes serve as promising vectors for nucleic acid delivery.

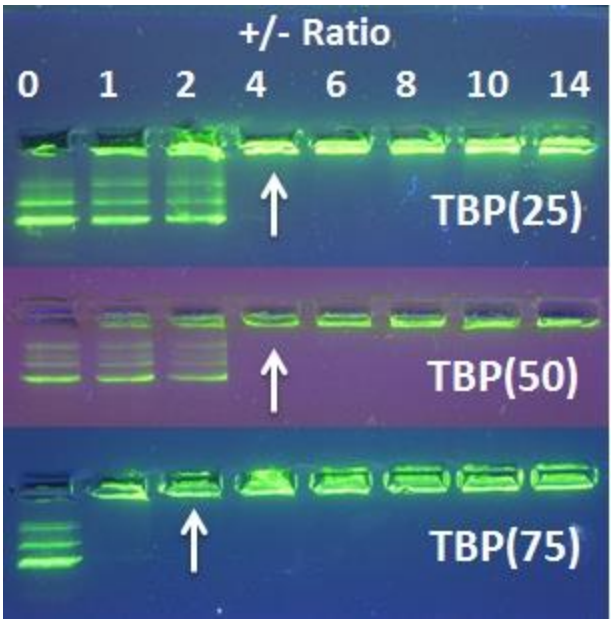

Figure 7.7. DNA binding gel shift assay of cationic polyurethanes with various TBP mol% content. Arrows designate +/- ratio at complete DNA binding.

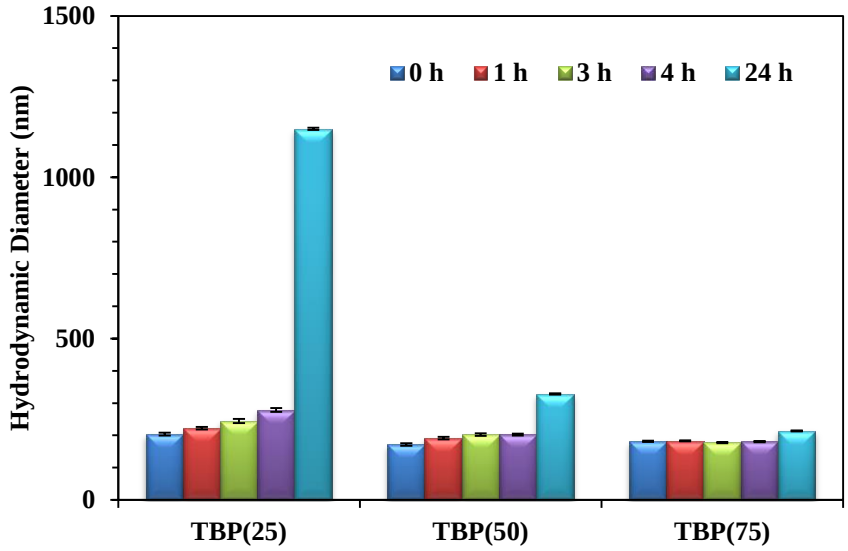

Figure 7.8. Polyplex stability (+/- ratio = 4) over 24 h in salt solution, Dulbecco's modified Eagle's media (DMEM).

7.5 *Conclusions*

Cationic polyurethanes possess several desirable advantages including improved microphase separation and mechanical performance for a variety of applications from high performance engineering thermoplastics to novel biomaterials. This manuscript reports the synthesis of cationic polyurethanes bearing pendant trialkylphosphoniums from novel, ionic liquid, phosphonium chain extenders. Polyurethane compositions varied the HS content and alkyl substituent to elucidate their influence on thermomechanical properties and morphology. The phosphonium polyurethanes demonstrated significantly higher rubbery plateau moduli, increased flow temperature from 60 to 160 °C, and evidence of microphase separation. FTIR spectroscopy revealed the phosphonium polyurethanes maintained hydrogen bonding, and hydrogen bonding to anions within the HS most likely served as the predominant driving force for microphase separation. Morphological investigations employed both AFM and SAXS, and confirmed microphase separated morphologies with more defined HS features in tributylphosphonium polyurethane compared to the ethyl substituent. The enhanced microphase separation led to improved tensile stress and strain properties compared to the noncharged control. Preliminary nucleic acid delivery studies verified the TBP polyurethanes bound DNA at low charge ratios, and DLS confirmed increasing polyplex stability with higher cationic charge. Our investigations demonstrated the phosphonium polyurethanes offered desirable properties for a broad range of emerging applications.

Acknowledgements. This work is supported in part by the U.S. Army Research Laboratory and the U.S. Army Research Office under the Army Materials Center of Excellence Program, contract W911NF-06-2-0014. This material is also based upon work supported in part by the US Army Research Office under Grant no. W911NF-07-1-0452 Ionic Liquids in Electro-active

Devices (ILEAD) MURI. This material is partially based upon work supported by the National Science Foundation under Grant No. DMR-0923107. The authors thank Bayer Material Science for providing the dicyclohexylmethane-*4,4'*-diisocyanate monomer. We extend our gratitude to Amanda Hudson and Jennifer Ludwig for their collaborations on this project and Professor Garth Wilkes for insightful discussions. In addition, the authors thank the Virginia Tech Institute of Critical Technology and Applied Sciences (ICTAS) Nanoscale Characterization and Fabrication Laboratory (NCFL) for atomic force microscopy characterization.

7.6 *References*

1. Green, M. D.; Long, T. E., *Polymer Reviews* **2009,** *49* (4), 291 - 314.
2. Yuan, J.; Antonietti, M., *Polymer* **2011,** *52* (7), 1469-1482.
3. Merle, G.; Wessling, M.; Nijmeijer, K., *Journal of Membrane Science* **2011,** *377* (1–2), 1-35.
4. Jaeger, W.; Bohrisch, J.; Laschewsky, A., *Prog. Polym. Sci.* **2010,** *35* (5), 511-577.
5. Wang, S.-W.; Liu, W.; Colby, R. H., *Chem. Mater.* **2011,** *23* (7), 1862-1873.
6. Hemp, S. T.; Allen, M. H.; Green, M. D.; Long, T. E., *Biomacromolecules* **2011,** *13* (1), 231-238.
7. Hemp, S. T.; Smith, A. E.; Bryson, J. M.; Allen, M. H.; Long, T. E., *Biomacromolecules* **2012,** *13* (8), 2439-2445.
8. Allen, M. H.; Hemp, S. T.; Zhang, M.; Zhang, M.; Smith, A. E.; Moore, R. B.; Long, T. E., *Polymer Chemistry* **2013**.
9. Wu, T.; Wang, D.; Zhang, M.; Heflin, J. R.; Moore, R. B.; Long, T. E., *ACS Applied Materials & Interfaces* **2012,** *4* (12), 6552-6559.
10. Green, M. D.; Choi, J.-H.; Winey, K. I.; Long, T. E., *Macromolecules* **2012,** *45* (11), 4749-4757.
11. Cheng, S.; Zhang, M.; Wu, T.; Hemp, S. T.; Mather, B. D.; Moore, R. B.; Long, T. E., *J. Polym. Sci., Part A: Polym. Chem.* **2011**, n/a-n/a.
12. Mather, B. D.; Baker, M. B.; Beyer, F. L.; Green, M. D.; Berg, M. A. G.; Long, T. E., *Macromolecules* **2007,** *40* (13), 4396-4398.
13. Hemp, S. T.; Long, T. E., *Macromolecular Bioscience* **2012,** *12* (1), 29-39.
14. Kang, H.; Lin, Q.; Armentrout, R. S.; Long, T. E., *Macromolecules* **2002,** *35* (23), 8738-8744.
15. Williams, S. R.; Wang, W.; Winey, K. I.; Long, T. E., *Macromolecules* **2008,** *41* (23), 9072-9079.
16. Gao, R.; Zhang, M.; Dixit, N.; Moore, R. B.; Long, T. E., *Polymer* **2012,** *53* (6), 1203-1211.
17. Ghassemi, H.; Riley, D. J.; Curtis, M.; Bonaplata, E.; McGrath, J. E., *Appl. Organomet. Chem.* **1998,** *12* (10-11), 781-785.
18. Tamami, M.; Williams, S. R.; Park, J. K.; Moore, R. B.; Long, T. E., *J. Polym. Sci., Part A: Polym. Chem.* **2010,** *48*, 4159-4167.
19. Williams, S. R.; Long, T. E., *Prog. Polym. Sci.* **2009,** *34* (8), 762-782.
20. Dieterich, D.; Keberle, W.; Witt, H., *Angewandte Chemie International Edition in English* **1970,** *9* (1), 40-50.
21. Mindemark, J.; Bowden, T., *Polymer* **2011,** *52* (25), 5716-5722.
22. Goddard, R. J.; Cooper, S. L., *Macromolecules* **1995,** *28* (5), 1390-1400.
23. Coleman, M. M.; Lee, K. H.; Skrovanek, D. J.; Painter, P. C., *Macromolecules* **1986,** *19* (8), 2149-2157.
24. Goddard, R. J.; Cooper, S. L., *J. Polym. Sci., Part B: Polym. Phys.* **1994,** *32* (8), 1557-1571.
25. Brunette, C. M.; Hsu, S. L.; MacKnight, W. J., *Macromolecules* **1982,** *15* (1), 71-77.
26. Christenson, C. P.; Harthcock, M. A.; Meadows, M. D.; Spell, H. L.; Howard, W. L.; Creswick, M. W.; Guerra, R. E.; Turner, R. B., *J. Polym. Sci., Part B: Polym. Phys.* **1986,** *24* (7), 1401-1439.

27. Srichatrapimuk, V. W.; Cooper, S. L., *Journal of Macromolecular Science, Part B* **1978,** *15* (2), 267-311.
28. Yoon, S. C.; Sung, Y. K.; Ratner, B. D., *Macromolecules* **1990,** *23* (20), 4351-4356.
29. Al-Salah, H. A.; Xiao, H. X.; McLean Jr, J. A.; Frisch, K. C., *J. Polym. Sci., Part A: Polym. Chem.* **1988,** *26* (6), 1609-1620.
30. Dieterich, D., *Prog. Org. Coat.* **1981,** *9* (3), 281-340.
31. Chen, S.-A.; Chan, W.-C., *J. Polym. Sci., Part B: Polym. Phys.* **1990,** *28* (9), 1499-1514.
32. Senich G, A.; Mac Knight W, J., A Dynamic Mechanical Study of Phase Segregation in Toluene Diisocyanate, Block Polyurethanes. In *Multiphase Polymers*, AMERICAN CHEMICAL SOCIETY: 1979; Vol. 176, pp 97-127.
33. Zharkov, V. V.; Strikovsky, A. G.; Verteletskaya, T. E., *Polymer* **1993,** *34* (5), 938-941.
34. Das, S.; Cox, D. F.; Wilkes, G. L.; Klinedinst, D. B.; Yilgor, I.; Yilgor, E.; Beyer, F. L., *Journal of Macromolecular Science: Physics* **2007,** *46*, 853-875.
35. Yilgor, I.; Yilgor, E.; Guler, I. G.; Ward, T. C.; Wilkes, G. L., *Polymer* **2006,** *47* (11), 4105-4114.
36. Zhang, M.; Moore, R. B.; Long, T. E., *J. Polym. Sci., Part A: Polym. Chem.* **2012,** *50* (18), 3710-3718.
37. McLean, R. S.; Sauer, B. B., *Macromolecules* **1997,** *30* (26), 8314-8317.
38. Velankar, S.; Cooper, S. L., *Macromolecules* **1998,** *31* (26), 9181-9192.
39. Visser, S. A.; Cooper, S. L., *Macromolecules* **1991,** *24* (9), 2576-2583.
40. Yarusso, D. J.; Cooper, S. L., *Macromolecules* **1983,** *16* (12), 1871-1880.
41. Wilkes, G. L.; Emerson, J. A., *J. Appl. Phys.* **1976,** *47* (10), 4261-4264.
42. Das, S.; Yilgor, I.; Yilgor, E.; Wilkes, G. L., *Polymer* **2008,** *49* (1), 174-179.
43. Kim, B. K.; Lee, S. Y.; Xu, M., *Polymer* **1996,** *37* (26), 5781-5793.
44. Miller, J. A.; Hwang, K. K. S.; Cooper, S. L., *Journal of Macromolecular Science, Part B* **1983,** *22* (2), 321-341.
45. Yang, C.-Z.; Grasel, T. G.; Bell, J. L.; Register, R. A.; Cooper, S. L., *J. Polym. Sci., Part B: Polym. Phys.* **1991,** *29* (5), 581-588.
46. McKee, M. G.; Hunley, M. T.; Layman, J. M.; Long, T. E., *Macromolecules* **2006,** *39* (2), 575-583.
47. Layman, J. M.; Borgerding, E. M.; Williams, S. R.; Heath, W. H.; Long, T. E., *Macromolecules* **2008,** *41* (13), 4635-4641.
48. Hemp, S. T.; Hunley, M. T.; Cheng, S.; DeMella, K. C.; Long, T. E., *Polymer* **2012,** *53* (7), 1437-1443.

7.7 *Supporting Information*

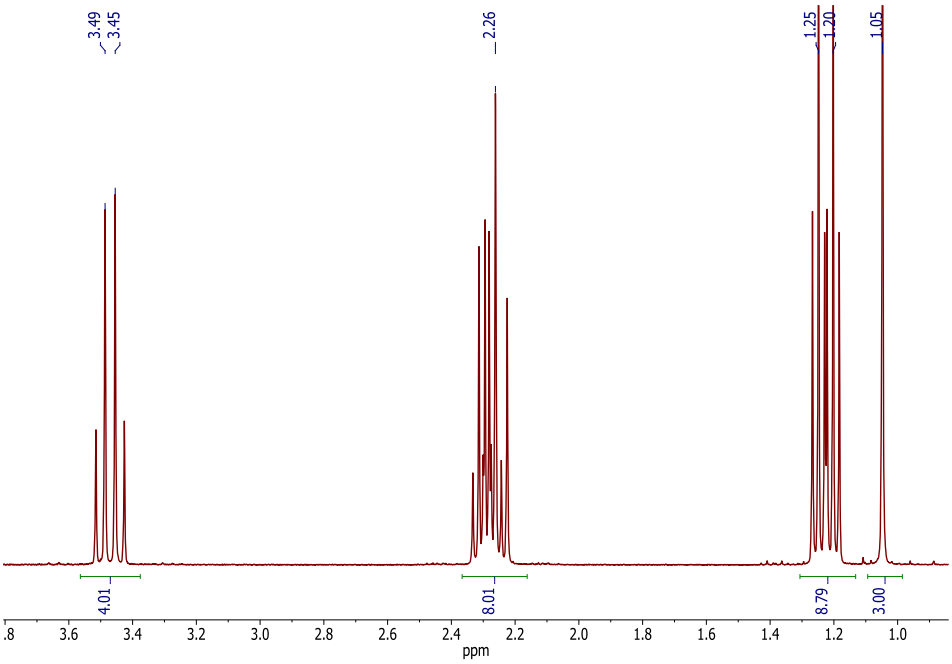

Figure S 7.1. ^{1}H NMR spectrum of triethyl(1,3-dihydroxypropyl)phosphonium bromide in D_2O.

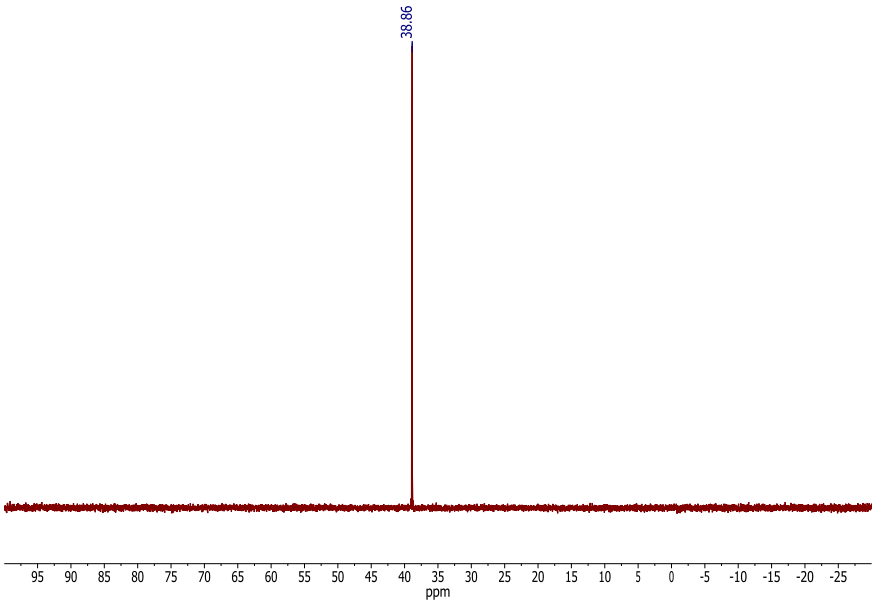

Figure S 7.2. ^{31}P NMR spectrum of triethyl(1,3-dihydroxypropyl)phosphonium bromide in D_2O.

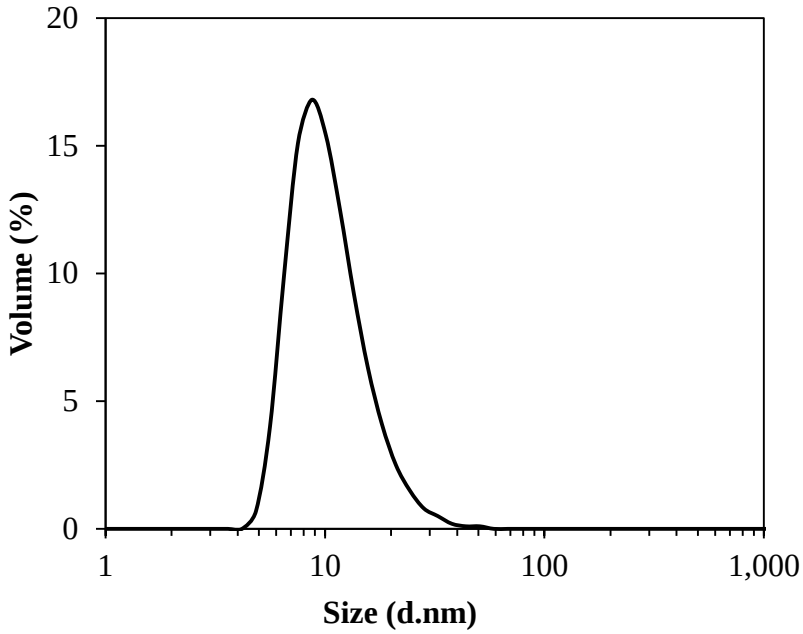

Figure S 7.3. A representative monomodal DLS trace for phosphonium polyurethanes in aqueous SEC solvent (54/23/23 water/methanol/acetic acid (v/v/v %), 0.1 M sodium acetate).

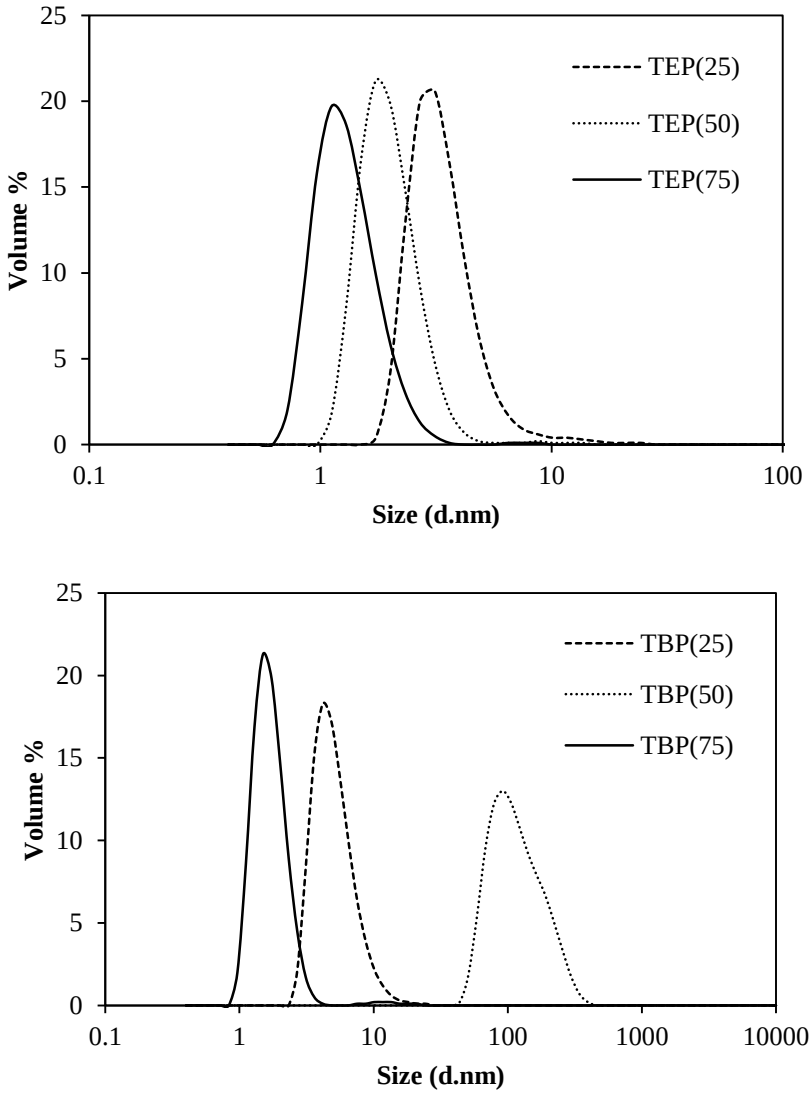

Figure S 7.4. A representative DLS trace for phosphonium polyurethanes in water.

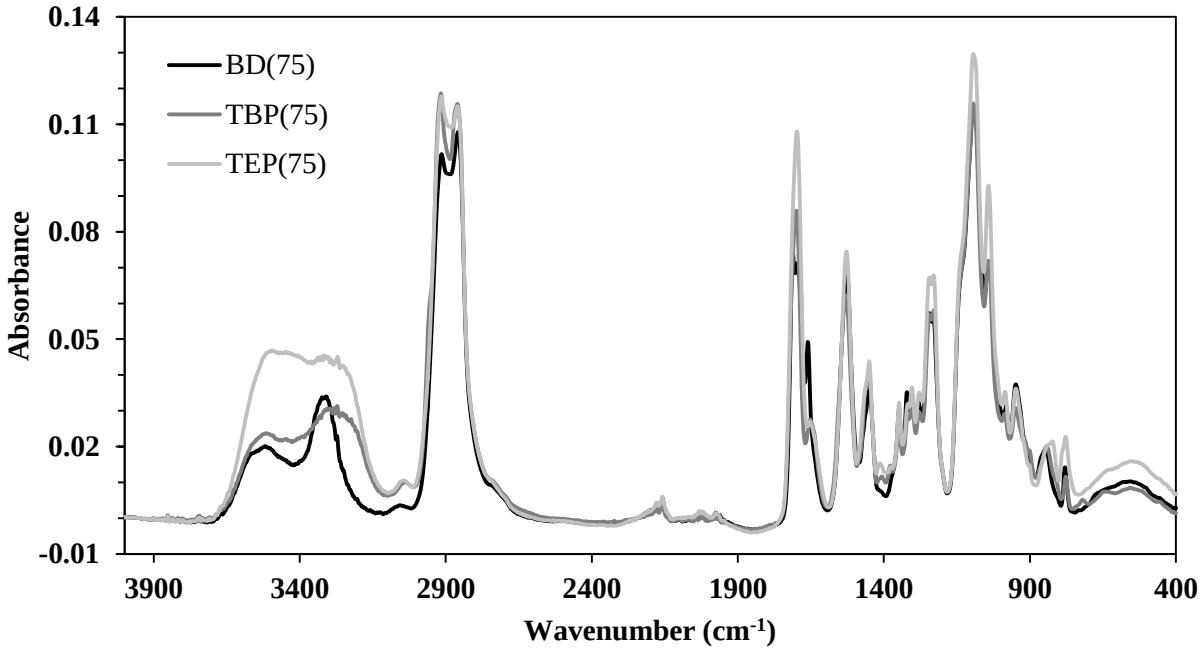

Figure S 7.5. FTIR spectra of BD, TEP, and TBP chain extended PU containing 75 mol% HS.

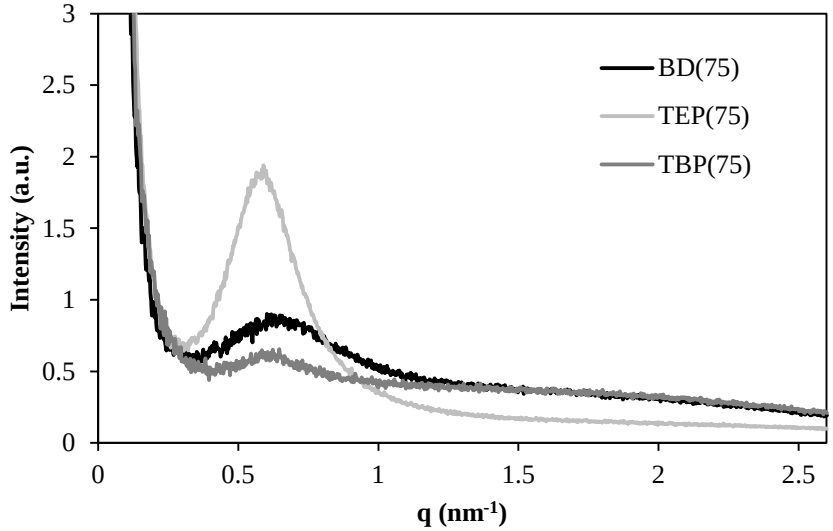

Figure S 7.6. Small-angle X-ray scattering profile of noncharged and phosphonium polyurethanes.

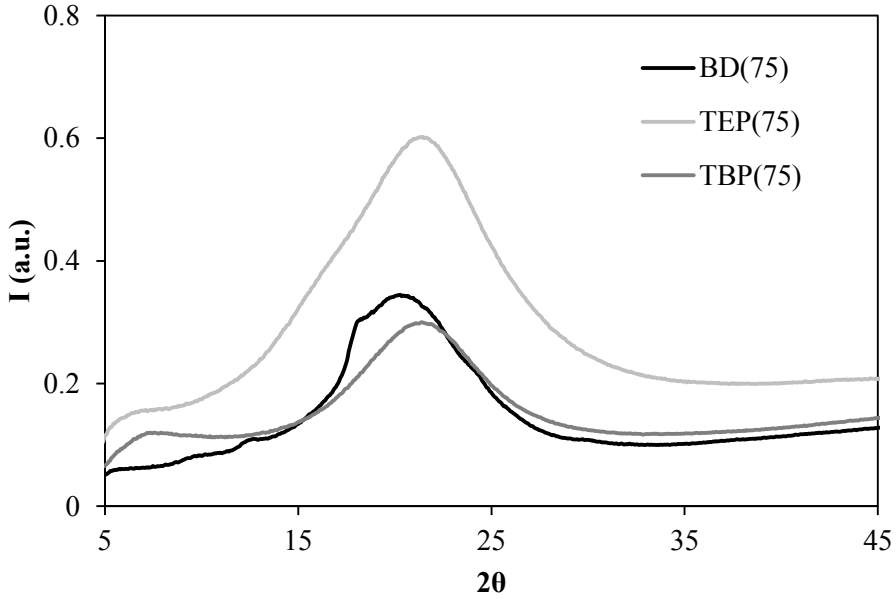

Figure S 7.7. Wide-angle X-ray diffraction (WAXD) of noncharged and phosphonium polyurethanes.

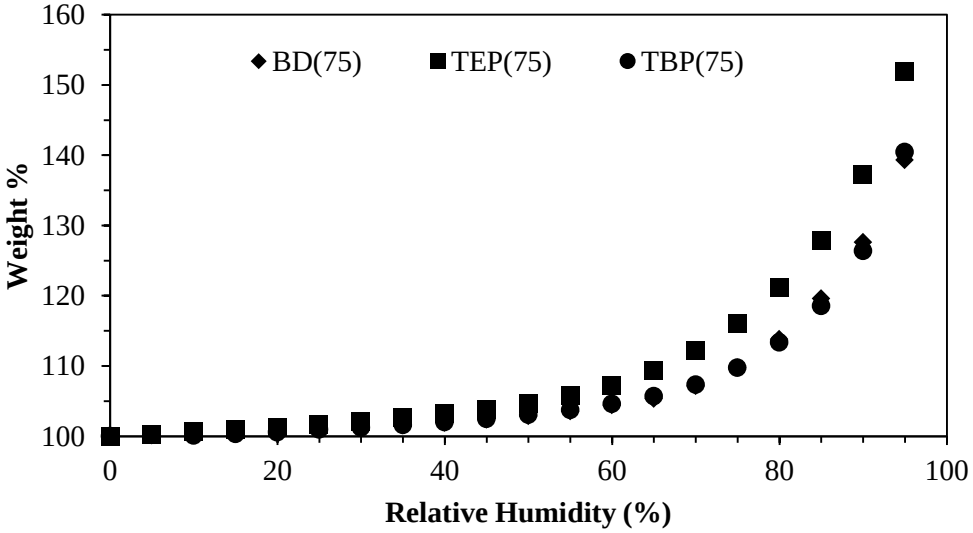

Figure S 7.8. Thermogravimetric sorption analysis of noncharged and phosphonium polyurethanes (75 mol% HS) at 25 °C.

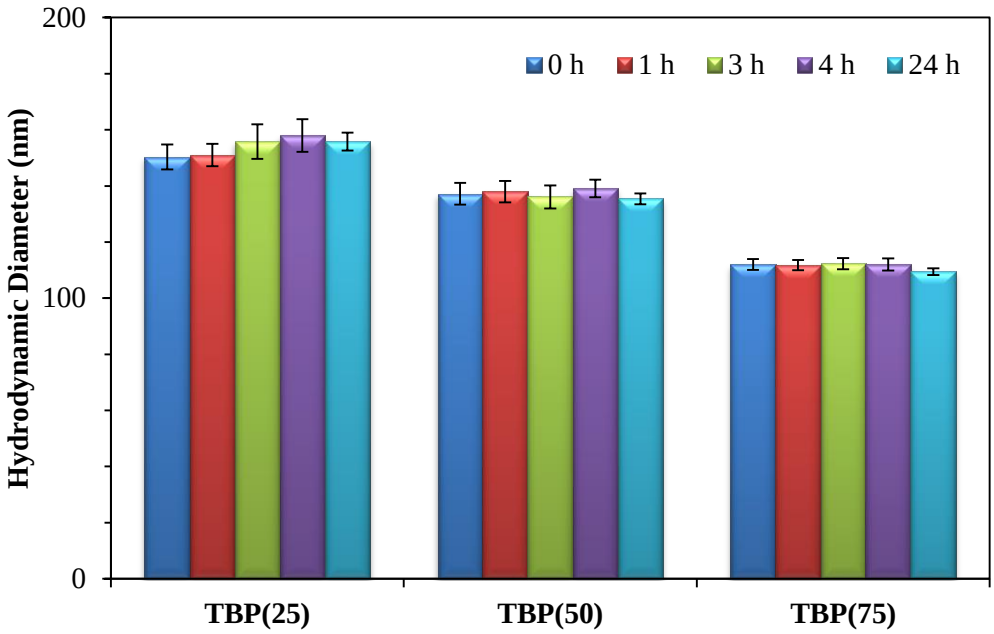

Figure S 7.9. Dynamic light scattering of polyplex stability (+/- ratio = 4) in water over 24 h.

Chapter 8: Trialkylphosphonium Polyesters for Nonviral Nucleic Acid Delivery

Musan Zhang, Sean T. Hemp, Richard N. Carmean, and Timothy E. Long

Department of Chemistry, Macromolecules and Interfaces Institute
Virginia Tech, Blacksburg, VA 24061-0212

8.1 *Abstract*

Melt-phase polycondensation of novel, thermally stable trialkylphosphonium diols afforded water-dispersible polyesters with pendant phosphonium cation. The diacid compositions, succinic and adipic acids, and phosphonium alkyl substituent length tuned the polymer water solubility. Mono-/difunctional poly(ethylene glycol) generated segmented and triblock copolyesters. A nonionic polyester analogue using neopentylglycol enabled absolute molecular weight analysis. Trialkylphosphonium polyesters exhibited higher T_g's compared to their nonionic analogue. For the first time, a series of water-soluble, phosphonium polyesters were investigated as potentially biodegradable DNA delivery vectors. The polyester water solubility and trialkylphosphonium charge density influenced DNA binding. DNA gel shift assays demonstrated the tributylphosphonium-containing polyester did not bind DNA. However, poly(triethylphosphonium adipate) exhibited DNA binding at a +/- charge ratio of 8. *In situ* FTIR indicated the polyesters were hydrolytically stable in water for up to 1 d. MTT assays demonstrated the polyesters were nontoxic at high polymer concentrations. Phosphonium polyesters did not express GFP. Varying the chemical compositions and macromolecular architecture tuned the polymer physical properties and achieved promising for these polymers

8.2 *Introduction*

Ion-containing monomers impart strong electrostatic interactions, which results in thermoreversible, dynamic physical crosslinks. Ionomers with high melt viscosities presents synthetic challenges, particularly for melt-phase polymerization. High melt viscosities during the polymerization may limit the molecular weight and require high polymerization temperatures, which may lead to thermally-induced, deleterious byproducts.[1, 2] Polyester monomers commonly contain aromatic, cycloaliphatic, or long chain diols to eliminate possible thermal degradation including thermo-oxidation, which most likely limit the molecular weight, polymer coloration, and crosslinking.[3, 4] The undesired side reactions limit accessibility of novel monomers for melt-phase polycondensation, particularly for polyesters. In order to avoid potential side reactions related to the monomers, inert reactions, with no other functionality beyond the diester, diacid, or diol reactive group are often used.[5-7] The limited functionality for current, commonly existing copolymer remains the greatest synthetic challenge. Because step-growth polymers contribute significantly to industrial applications, simple, efficient, high yielding reactions are desired.

The literature extensively describes several examples of sodium-sulfonated copolyesters, often achieved through the monomer sodium sulfonated dimethyl isophthalate (sDMI).[8-10] These sulfonated, ionomeric copolyesters exhibited unique dispersible behavior in water. The dispersions formed well-defined nanoparticles in solution with hydrodynamic radii (<200 nm) depending on the solvent ionizing or solvating quality on the charged, ionic group in the polyester. Other anionic functionalities, such as carboxylates, are not easily generated due to the possible reaction.[11] Cationic polyesters are even less common due to thermal instabilities

leading to reverse S_N2 reaction or Hoffman elimination.[12-15] Furthermore, unreacted tertiary amines act as base catalysts for ester hydrolysis, which reduced molecular weight.

In addition to high melt viscosities achieved during the polymerization extent, water associated with the charged monomers also lead to limited molar weights. Finally, reliable size exclusion chromatography (SEC) are difficult to generate with cationic polyesters, therefore many cationic polyesters require post-functionalization reaction onto a nonionic, polymer precursor. However, post-functionalization reactions also observe significant challenges in complete functionalization onto the polymer backbone due to steric interactions. To achieve high functionalization, larger, less basic leaving groups, heat, and solvent are often employed to observe high conversions.

Polyesters generate growing interest for the development of drug delivery and biomedical technologies due to their potential biodegradation into nontoxic, biocompatible components. Ring-opening polymerization of polylactide, poly(lactide-*co*-glycolide), and poly(caprolactones), are commonly used in biomedical applications. One potential drawback to these polyesters is their crystallinity, which leads to variations in their degradation and erosion profile.[16-20] Furthermore, hydrolysis of these polymers generates carboxylic acids, which acts as a catalyst for degradation. Tuning the macromolecular structure and introducing novel functionalities control the degree of crystallinity and degradation profiles.

In this manuscript, melt-phase polycondensation of a novel, cationic trialkylphosphonium diol generated water-dispersible polyesters depending on the polyester composition. Phosphonium diols with ethyl, propyl, or butyl alkyl substituents were efficiently generated in quantitative yields. Biocompatible diacids, succinic acid and adipic acid, and poly(ethylene glycol) with mono- or difunctionality tuned the macromolecular architecture. Melt viscosity

experiments confirmed the monomer stoichiometric effectively controlled the phosphonium polyester molecular weight. Nonionic polyesters using neopentylglycol (NPG) further verified our polymerization method generated polyesters with controlled molecular weights using SEC. We explored these cationic polyesters as potentially biodegradable, DNA delivery vectors.

8.3 *Experimental Section*

Materials

Triethylphosphine (99%), tri-*n*-propylphosphine (99%), tri-*n*-butylphosphine (anhydrous, 99%), neopentylglycol, succinic acid (SA, 99.5%) and adipic acid (AA, 99.0%) were purchased from Sigma-Aldrich and used as received. HPLC grade tetrahydrofuran (THF) was purchased from EMD solvents. Poly(ethylene glycol) methyl ether (PEGME, Sigma-Aldrich, M_n = 2,000 g/mol) was dried at 60 °C under reduced pressure (10 mmHg) for 18 h. A titanium tetraisopropoxide (99%, Sigma-Aldrich) solution in anhydrous 1-butanol was prepared according to previous procedures.[21] 2-(Bromomethyl)-2-methyl-1,3-propanediol was prepared according to procedures described in the literature, dried at 40 °C under reduced pressure (10 mmHg) for 12 h, and stored in a dry box.[22] All polymers were dried under reduced pressure (<10 mmHg) at 50 °C for 24 h prior to characterization.

Synthesis of trialkylphosphonium diols

The synthesis of tri-*n*-butyl(1,3-dihydroxypropyl)phosphonium bromide serves as a representative example; the triethylphosphonium diol was prepared similarly. 2-(Bromomethyl)-2-methyl-1,3-propanediol (1.05 molar excess) was charged into a flame-dried, 100-mL, round-bottomed flask with a magnetic stir bar and purged with dry N_2. Tri-*n*-butylphosphine was added using dry syringe techniques, and the reaction proceeded at 100 °C for 2 d under vigorous stirring. The initial, biphasic reaction was homogenous after completion. Unreacted reagents

were distilled from the reaction at 100 °C (<1 mmHg). The product was washed multiple times with diethyl ether and dried at 90 °C under reduced pressure (0.5 mmHg) for 24 h.

Tri-n-butyl(1,3-dihydroxypropyl)phosphonium bromide - Yield: 94% as a clear, viscous ionic liquid, T_d(5%) = 368 °C, T_g = -29 °C, T_m = 66 °C. ^{1}H NMR (400 MHz, D_2O, 25 °C) δ (ppm): 0.93 (t, -$CH_2CH_2CH_2CH_3$, 9H, *J* = 7.2 Hz), 1.06 (s, -C*H*$_3$, 3H), 1.30-1.55 (m, -$CH_2CH_2CH_2CH_3$, 12H), 2.10-2.22 (m, -P*CH*$_2$-, 8H), 3.33-3.44 (m, -*CH*$_2$OH, 4H). ^{31}P NMR (400 MHz, D_2O, 25 °C) δ (ppm): 33.73. Mass Spectrometry: Theoretical, *m/z* 305.2604; Experimental, *m/z* 305.2605.

Triethyl(1,3-dihydroxypropyl)phosphonium bromide - Yield: 85% as white solid, T_d(5%) = 370 °C, T_g = -39 °C, T_m = 124 °C. ^{1}H NMR (400 MHz, D_2O, 25 °C) δ (ppm): 1.06 (s, -C*H*$_3$, 3H), 1.20-1.28 (m, -CH_2CH_3, 9H), 2.24-2.35 (m, -P*CH*$_2$-, 8H), 3.44-3.53 (dd, -*CH*$_2$OH, 4H). ^{31}P NMR: 38.87. Mass Spectrometry: Theoretical, *m/z* 221.1670; Experimental, *m/z* 221.1652.

Synthesis of trialkylphosphonium-containing polyesters

The following melt polycondensation procedure for poly(tributylphosphonium adipate) (poly(TBPA)) serves as a synthetic representation for all polyester homopolymers. TBP diol (1.0 mol eq.) and adipic acid (1.0 mol eq.) was charged into a flame-dried, 50-mL, round-bottomed flask equipped with an overhead mechanical stirrer, nitrogen inlet, and condenser. The reaction was purged with dry N_2 and degassed under reduced pressure (<1 mmHg) three times prior to polymerization. The polymerization temperature was ramped from 130 – 200 °C over 24 h, and the pressure was gradually reduced (<0.1 mmHg) for the remaining 6 h. The polyester displayed good coloration after the polymerization and exhibited increased melt viscosity over the extent of polymerization. Stoichiometric excess of TBP diol to diacid monomers controlled the polyester homopolymer molecular weight. Incorporating monohydroxyl PEGME endcapped

the polyesters to achieve PEGME outer blocks and control the polyester middle block molecular weight.

Polymer Characterization

All monomers and polymers were dried under reduced pressure (0.5 mmHg) at 80 °C overnight prior to characterization. ^{1}H NMR spectroscopy (Varian Inova, 400 MHz, D_2O) and mass spectrometry (Agilent 6220 LC-TOF-MS) confirmed monomer composition. Dynamic light scattering (DLS, Malvern Zetasizer NanoZS) screened for the presence of polymer aggregation in various SEC solvents to enable reliable absolute molecular weight. THF size exclusion chromatography (SEC) provided absolute molecular weights using a Water 1515 Isocratic HPLC Pump and Waters 717plus Autosampler with Waters 2414 refractive index and Wyatt MiniDAWN MALLS detectors (flow rate 1.0 mL/min). A Wyatt Optilab T-rEX differential refractometer measured offline *dn/dc* values at 658 nm and 35 °C. A Metler Toledo 45M *in situ* Fourier transform infrared (FTIR) spectroscopy evaluated the hydrolytic stability of aqueous dispersible, poly(TBPS) in pure water (pH = 7.0) over 24 h.

DNA Binding Assay. Agarose gels (0.6 g, 8-well lanes) were prepared from 60 mL of 1x Tris-acetate-EDTA (TAE, Sigma-Aldrich) buffer, and 6 μL of SYBR green. Polymer only solutions from an initial 1 mg/mL polymer solution in H_2O and 0.2 μL of gWiz-Luc plasmid DNA only solutions (1 μg/μL in H_2O, Aldevron) were prepared separately from calculated, desired charge ratios. Polyplexes were incubated at 25 °C for 30 min, and 7 μL of DNA loading buffer (30 wt% glycerol in H_2O) was added to the polyplex solution. The polyplex solution (20 μL) was loaded and electrophoresed in 1x TAE buffer at 70 V for 30 min. DNA gels were imaged using a MultiDoc-it Digital Imaging System (UVP).

Cytotoxicity Assay and GFP Expression. Human cervical cancer (HeLa) cells (100 μL of 20,000 cells/mL in complete DMEM) were plated onto 96-well plates or 24-well plates and incubated at 37 °C for 24 h. Procedures for polymer cytotoxicity and GFP expressions (gWiz-GFP plasmid DNA) were strictly followed.

8.4 *Results and Discussion*

Phosphonium-containing polyelectrolytes serve as chemical and structural cationic analogues to ammonium-containing polyelectrolytes. In melt-phase polycondensation of polyesters, cationic functionalities proved difficult to achieve due to possible detrimental thermal side reactions. Furthermore, ion-containing polyesters reflect high melt viscosities, which may limit the molecular weight. This manuscript describes the synthesis of novel, thermally stable trialkylphosphonium diols, which enabled melt-phase polycondensation of cationic, phosphonium polyesters. The synthesis of a brominated 1,3-propanediol with two primary hydroxyls provided equal reactivity. Nucleophilic substitution of the brominated diol, 2-(Bromomethyl)-2-methyl-1,3-propanediol, with trialkylphosphine in the absence of solvent efficiently generated trialkylphosphonium diols in quantitative yields (**Scheme 8.1**). Tributylphosphonium diols was a low-T_g, colorless ionic liquid, whereas the triethyl- and tripropylphosphonium diols were isolated as white solids.

Scheme 8.1. Synthesis of trialkylphosphonium diols.

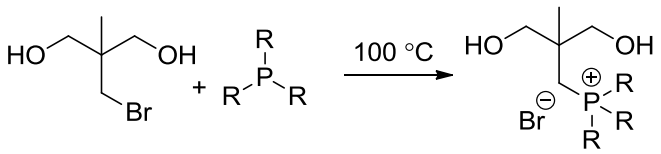

R = Ethyl, Propyl, Butyl

Melt-phase polycondensation of poly(trialkylphosphonium succinate) (poly(TAPS)) and poly(trialkylphosphonium adipate) (poly(TAPA)) demonstrated increasing viscosity over the extent of the polymerization procedure described in **Scheme 8.2**. Due to the catalytic behavior of the carboxylic acid endgroups, direct esterification does not require the use of a metal or acid esterification catalyst. Introducing metal catalysts may also lead to discoloration of the polyester, which was not observed in our polymers (**Figure 8.1**). In addition to avoiding potentially bio-incompatible metal catalysts, melt-phase polycondensation eliminates the use of harmful, volatile organic solvents and requires no additional purification, which is often needed in chain-growth polymerizations.

Scheme 8.2. Synthesis of poly(trialkylphosphonium succinate) (poly(TAPS)).

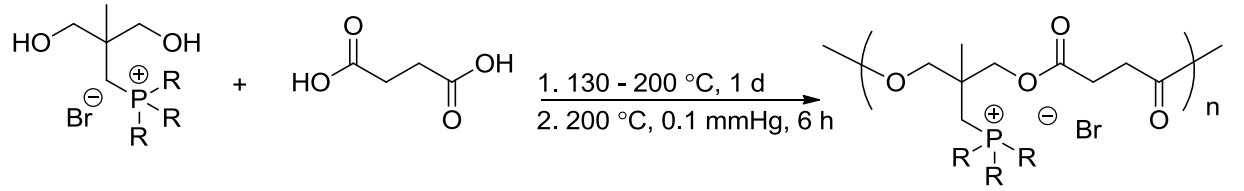

R = Ethyl, Propyl, Butyl

Poly(trialkylphosphonium succinate)

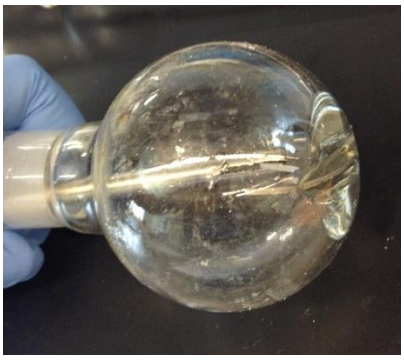

Figure 8.1. Picture of phosphonium polyesters demonstrating colorless appearance.

Dynamic light scattering of our cationic polyesters revealed aggregation in our aqueous and DMF 0.05 M LiBr SEC solvents, which prevented accurate molecular weight analysis. To ensure our polymerization procedure generated high molecular weight polyesters, nonionic polyester analogues were obtained using NPG (**Scheme 8.3**). THF SEC and experimentally determined *dn/dc* values afforded absolute molecular weights.

Table 8.1 summarizes the thermal analysis of trialkylphosphonium polyesters. The glass transition temperatures systematically increased when a longer alkylene diacid spacer was used. Longer alkyl substituents and the diacid composition also tuned the water solubility of these polyesters.

Scheme 8.3. Melt polycondensation of poly(neopentylglycol succinate) (poly(NPGS)).

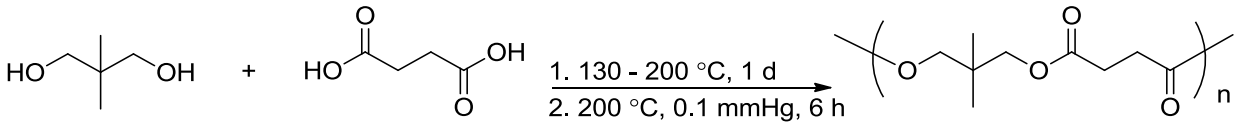

Table 8.1 Summary of trialkylphosphonium-containing polyester compositions and thermal properties.

Trialkylphosphonium Diol	Aliphatic Diacid	Polyester Composition	$T_{d,5\%}$ (°C)	T_g (°C)
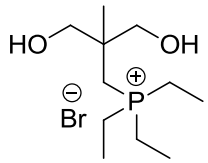	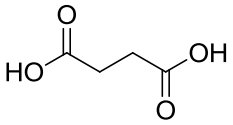	**TEPS**		
	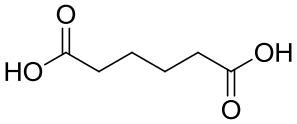	**TEPA**	294	13
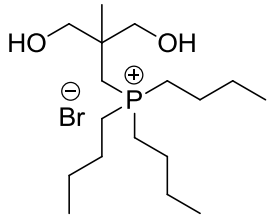	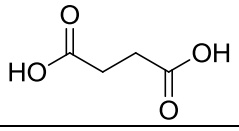	**TPPS**	290	20
	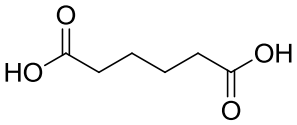	**TPPA**	289	21
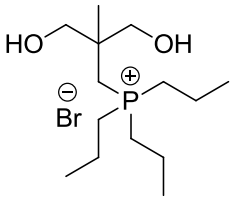	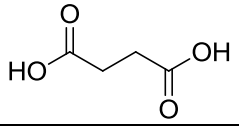	**TBPS**	280	10
	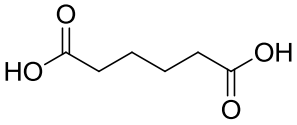	**TBPA**	280	-23

Due to the cationic and water-dispersible properties of the trialkylphosphonium polyesters, DNA delivery was investigated. DNA binding gel shift assays of TBP-containing compositions suggested the phosphonium polyesters did not bind DNA. Dynamic light scattering observed the formation of polyplexes in water. The incorporation of stabilizing PEG groups effectively reduced the polyplex hydrodynamic diameter and narrowed the polyplex size polydispersity. Upon the addition of salt-containing DMEM media, the polymer-DNA presumably dissociated. We currently hypothesize the more diffuse TBP charge density bound DNA less efficiently compared to TEP-containing polyesters, which led to a release of DNA upon the addition of salt.[14, 23] This occurrence contrasted to our recent observations in

tributylphosphonium styrenic polyelectrolytes, which exhibited enhanced DNA binding and improved GFP protein expression after transfection.

Furthermore, MTT cytotoxicity assays indicated our polymers were not cytotoxic up to polymer concentrations of 200 μg/mL (**Figure 8.2**). The MTT assay confirmed our observations from GFP expression, which displayed no GFP expression and high confluence compared to Jet-PEI controls (**Figure 8.3**). Our group recently published on phosphonium polyelectrolyte DNA delivery vectors, which suggested longer butyl chains may provide a method of escape within the endosome through alkyl interdigitating into the endosomal membrane.[14, 23] The techniques employed in this current report cannot delineate whether or not the polyplex is being uptaken into the cell.

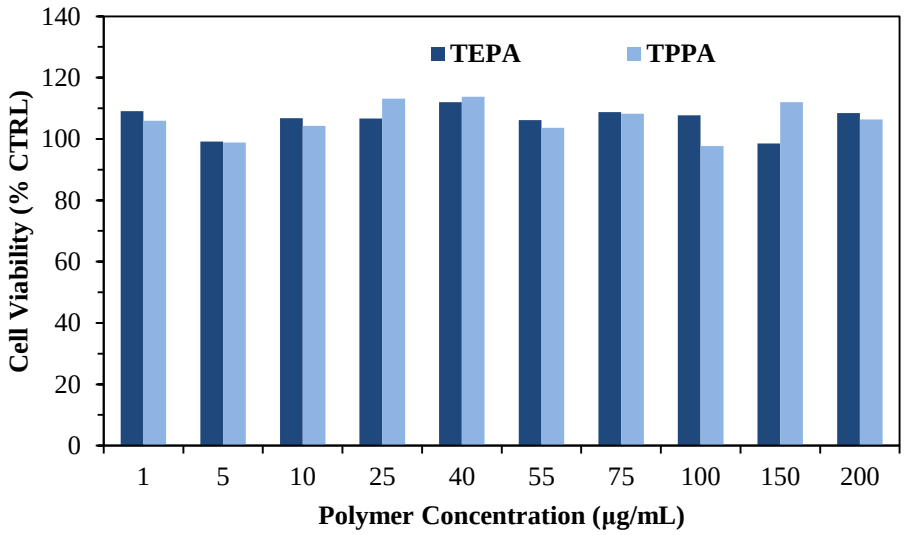

Figure 8.2 MTT cytotoxicity as a function of polymer concentration after 4 h incubation on HeLa cell viability.

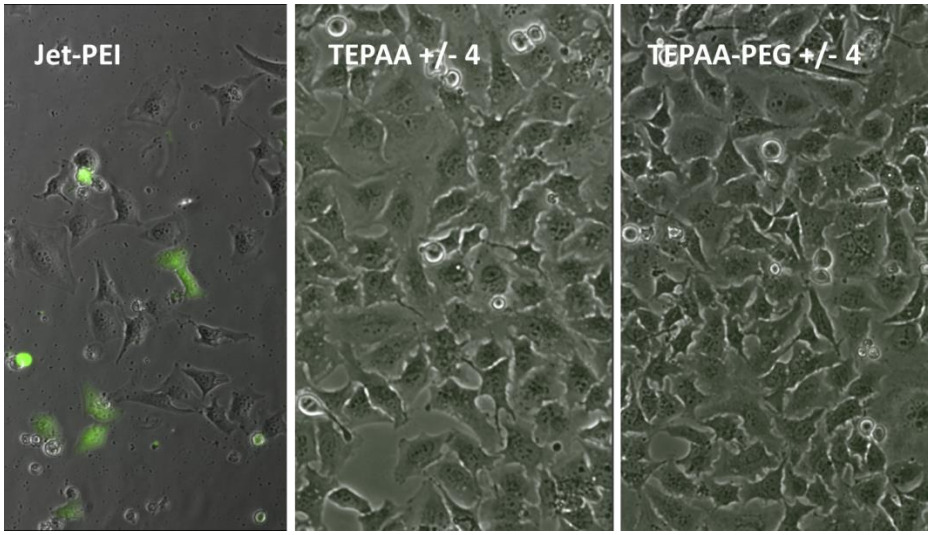

Figure 8.3 GFP expression in HeLa cells using TEPAA and poly(TEPAA-co-PEG) segmented copolyester.

8.5 *Conclusions*

Novel trialkylphosphonium diols containing ethyl, propyl, and butyl substituents were synthesized in quantitative yields. The difunctional primary alcohols, which afforded equal reactivity and absence of β-hydrogens improved the thermal stability. The polyesters maintained good coloration and exhibited an increase in their melt viscosity during the polymerization. Thermal analysis reflected an increase in the T_g with the incorporation of cationic phosphoniums. Nonionic polyesters using the structural analogue, neopentylglycol, demonstrated monomer stoichiometric imbalance and polymerization conditions generated polyesters with controlled molecular weight. Variations in monomer structure and composition tuned the macromolecular architecture to enable structure-property characterization. Depending on the phosphonium diol alkyl substituent length and diacid structure, these polyesters were readily soluble in water. DNA delivery studies of the water-soluble polyesters were investigated.

Acknowledgements. This work is supported in part by the U.S. Army Research Laboratory and the U.S. Army Research Office under the Army Materials Center of Excellence Program, contract W911NF-06-2-0014. This material is also based upon work supported in part by the US Army Research Office under Grant no. W911NF-07-1-0452 Ionic Liquids in Electro-active Devices (ILEAD) MURI. This material is partially based upon work supported by the National Science Foundation under Grant No. DMR-0923107. In addition, the authors thank the Virginia Tech Institute of Critical Technology and Applied Sciences (ICTAS) Nanoscale Characterization and Fabrication Laboratory (NCFL) for atomic force microscopy characterization.

8.6 *References*

1. Goddard, R. J.; Cooper, S. L., *J. Polym. Sci., Part B: Polym. Phys.* **1994,** *32* (8), 1557-1571.
2. Goddard, R. J.; Cooper, S. L., *Macromolecules* **1995,** *28* (5), 1401-1406.
3. Evans, S. J.; Haines, P. J.; Skinner, G. A., *Thermochim. Acta* **1996,** *278* (0), 77-89.
4. Pohl, H. A., *J. Am. Chem. Soc.* **1951,** *73* (12), 5660-5661.
5. Zhang, M.; June, S. M.; Long, T. E., 5.02 - Principles of Step-Growth Polymerization (Polycondensation and Polyaddition). In *Polymer Science: A Comprehensive Reference*, Matyjaszewski, K., Ed. Elsevier: Amsterdam, 2012; pp 7-47.
6. Rogers, M. E.; Long, T. E.; Turner, S. R., Introduction to Synthetic Methods in Step-Growth Polymers. In *Synthetic Methods in Step-Growth Polymers*, John Wiley & Sons, Inc.: 2003; pp 1-16.
7. Fradet, A.; Tessier, M., Polyesters. In *Synthetic Methods in Step-Growth Polymers*, John Wiley & Sons, Inc.: 2003; pp 17-134.
8. Han, S.-I.; Im, S. S.; Kim, D. K., *Polymer* **2003,** *44* (23), 7165-7173.
9. Pilati, F.; Manaresi, P.; Ruperto, M. G.; Bonora, V.; Munari, A.; Fiorini, M., *Polymer* **1993,** *34* (11), 2413-2421.
10. Szymczyk, A.; Baltá Calleja, F. J.; Roslaniec, Z.; Wlochowicz, A.; Slusarczyk, C., *Journal of Macromolecular Science: Physics* **2002,** *41* (3), 507.
11. Visser, S. A.; Cooper, S. L., *Macromolecules* **1991,** *24* (9), 2576-2583.
12. Rana, U. A.; Vijayaraghavan, R.; Walther, M.; Sun, J.; Torriero, A. A. J.; Forsyth, M.; MacFarlane, D. R., *Chem. Commun.* **2011,** *47* (42), 11612-11614.
13. Jaeger, W.; Bohrisch, J.; Laschewsky, A., *Prog. Polym. Sci.* **2010,** *35* (5), 511-577.
14. Hemp, S. T.; Allen, M. H.; Green, M. D.; Long, T. E., *Biomacromolecules* **2011,** *13* (1), 231-238.
15. Williams, S. R.; Long, T. E., *Prog. Polym. Sci.* **2009,** *34* (8), 762-782.
16. Liu, Q.; Jiang, L.; Shi, R.; Zhang, L., *Prog. Polym. Sci.* **2012,** *37* (5), 715-765.
17. Okada, M., *Prog. Polym. Sci.* **2002,** *27* (1), 87-133.
18. Pitt, C. G.; Hendren, R. W.; Schindler, A.; Woodward, S. C., *J. Controlled Release* **1984,** *1* (1), 3-14.
19. Middleton, J. C.; Tipton, A. J., *Biomaterials* **2000,** *21* (23), 2335-2346.
20. McKee, M. G.; Unal, S.; Wilkes, G. L.; Long, T. E., *Prog. Polym. Sci.* **2005,** *30* (5), 507-539.
21. Lin, Q.; Unal, S.; Fornof, A. R.; Armentrout, R. S.; Long, T. E., *Polymer* **2006,** *47* (11), 4085-4093.
22. Mindemark, J.; Bowden, T., *Polymer* **2011,** *52* (25), 5716-5722.
23. Hemp, S. T.; Smith, A. E.; Bryson, J. M.; Allen, M. H.; Long, T. E., *Biomacromolecules* **2012,** *13* (8), 2439-2445.

8.7 *Supporting Information*

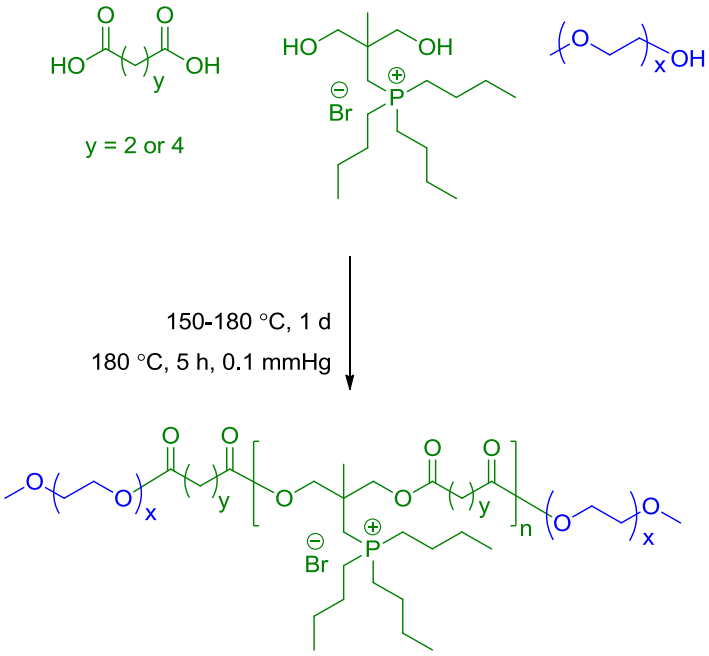

Figure S 8.1 Synthesis of poly(ethylene glycol) methylether endcapped phosphonium triblock copolyester.

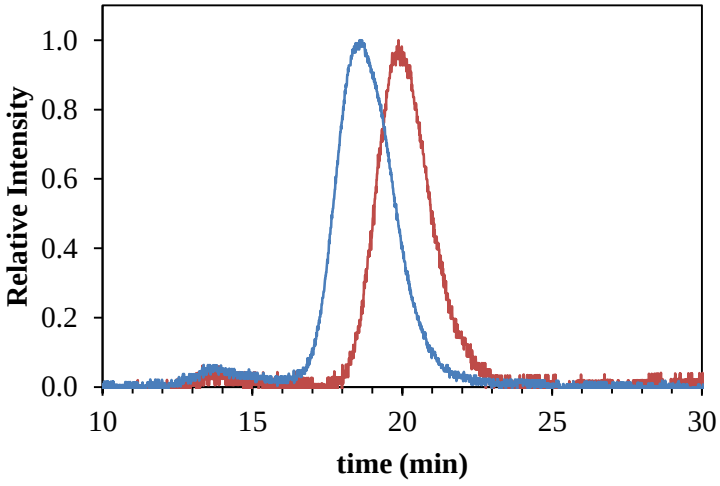

Figure S 8.2 Absolute molecular weight confirmed poly(NPGS) demonstrated molecular weight control through monomer stoichiometric imbalance.

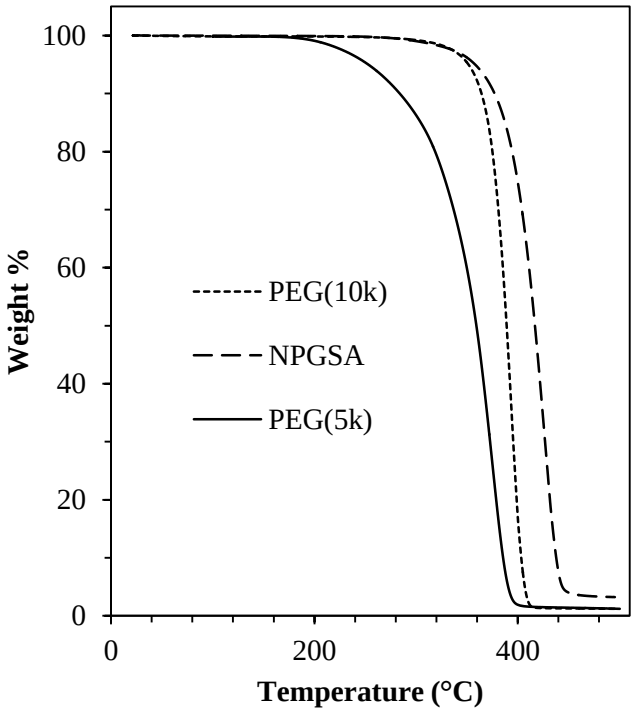

Figure S 8.3 Thermogravimetric analysis of poly(NPGS) demonstrated enhanced thermal weight loss stability.

[NPG]: [SA]: [PEGME]	PEGME M_n (g/mol)	Target M_n (g/mol)	Expt M_n (g/mol)	PDI
1.00 : 1.00 : 0.00	-----	High MW	14,600	1.58
1.04 : 1.00 : 0.00	-----	2,400	2,400	1.83
1.00 : 1.00 : 0.02	750	4,600	4,300	1.52
1.00 : 1.00 : 0.02	2,000	7,100	6,700	1.53

Figure S 8.4 Nonionic, PEGME endcapped poly(NPGS) triblock copolyesters to demonstrate molecular weight control using monofunctional endcapping polyol.

Chapter 9: Overall Conclusions

The polymer synthesis and motivation described in this dissertation reflects the interdisciplinary efforts of step-growth research to bridge together the fields of biochemistry, polymer chemistry, and life sciences, take advantage of nature's design, and respond to the growing challenges of sustainability. There is a renewed interest in discovering novel monomers, functionalities, and methods for future step-growth processes. As polymer scientists, the techniques and synthetic methods used to generate traditional step-growth polymers have developed significantly since Carothers's early pioneering work. However, the current trends and applications observed for mainly ion-containing chain growth polymers continue to serve as the inspiration for interesting morphological and physical polymer properties. Step-growth polymers have proven to be especially useful in achieving a variety of macromolecular structures with tailored performance. In order to address future challenges in polymer science, we must tackle questions in an interdisciplinary manner. We must strive to reduce our dependency on petroleum feedstocks, and we need to design high performance polymers with a keen attention to sustainability. Step-growth polymerization processes are excellent platforms to achieve these critical goals.

Chapter 10: Suggested Future Work

10.1 *Polymerized Imidazolium and Phosphonium Ionic Liquids for Step-Growth Biopolymers*

We described the efficient synthesis of imidazolium and phosphonium diols in previous chapters. The thermal stability and primary hydroxyl difunctionality affords a synthetic handle for further transformations. Although we demonstrate potential applications in DNA delivery for the trialkylphosphonium polyurethanes, other applications are certainly available to expand the library functional ionic liquids. Cationic polyesters may be suitable for melt adhesives due to the low melt viscosity generated compared to anionic sulfonated polyesters. Furthermore, our results suggest the trialkylphosphonium polyesters exhibited low cytotoxicity, which may enable them to find applications as nontoxic bioadhesives.

One area of interest is in the synthesis of surfactant-like or lipid-like ionic liquids using our imidazolium ionic liquid platform. **Scheme 10.1** shows the synthesis and alkylation of imidazolium diols. This synthetic pathway efficiently achieves simple modification with longer alkyl tails to afford surfactant-like characteristics, a polar headgroup and long hydrophobic tail. A primary challenge of introducing novel functional groups and monomers into the area of polyester research is the polymerization scale, which often requires gram-scale quantities of reactants to achieve suitable polymerization conditions. The cost of reaction, monomer yield, and efficient isolation and purification are critical in order to probe novel monomers in meaningful ways. One of the advantages highlighted in **Scheme 10.1** is that the synthesis for the brominated diol is low cost, high yielding, and simple to purify. The imidazole diol obtained in the first step is a versatile monomer that serves as a platform to explore polymer properties. These monomers are completely novel and presumably eliminate potential thermal degradation compared to fatty acid derivatives (**Figure 10.1**). The ability to generate polyesters from the

melt allows us to achieve various polyester chemical compositions and macromolecular architecture. However, it is important to note that residual free amines from unalkylated imidazole diols may act as a catalyst to facilitate base hydrolysis of ester linkages and will need to be carefully eliminated in order to achieve high molecular weight polyesters. In applications such as drug delivery where degradability is desirable, the noncharged imidazole diol may allow tuning of the degradation profile.

Scheme 10.1. Synthesis of imidazole diol and alkylation with alkyl halide to afford imidazolium diols

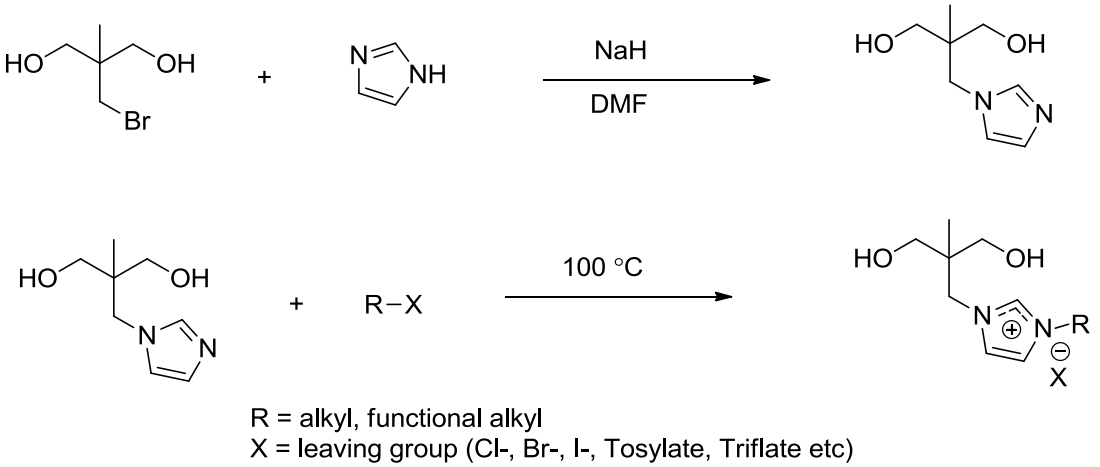

R = alkyl, functional alkyl
X = leaving group (Cl-, Br-, I-, Tosylate, Triflate etc)

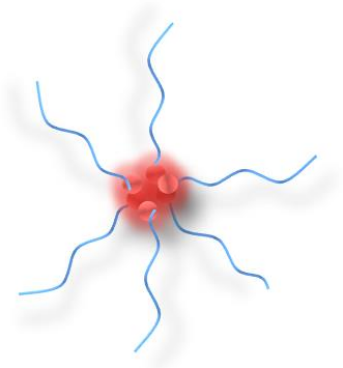

Figure 10.1 Representative micelle structure formed from ionic associations of surfactant polar headgroups.

In order to progress the growing interests of polyester, it is critical to develop a novel family of thermally stable monomers that incorporate desirable functionality. There is a growing scientific effort to progress the areas of polymer research towards environmentally responsible synthesis and polymerizations. Melt-phase polymerizations serve as an attractive method that eliminates the use of volatile organic solvents (VOCs) and improve processibility. **Figure 10.2** show possible structures to probe using step-growth polymerization to generate functional polyesters, polyurethanes, and polyoxalates. In addition to their use as functional monomers, these ionic liquids may also afford interesting properties such as liquid crystallinity, birefringence, and tunable ionic conductivity. Structure **A** represents an alkylated imidazolium diol using any alkyl halide. Depending on the alkyl substituent length, the physical properties of the diol may afford surfactant-like qualities. The literature extensively describes examples of ionic liquids that afford liquid crystalline properties and optical properties.

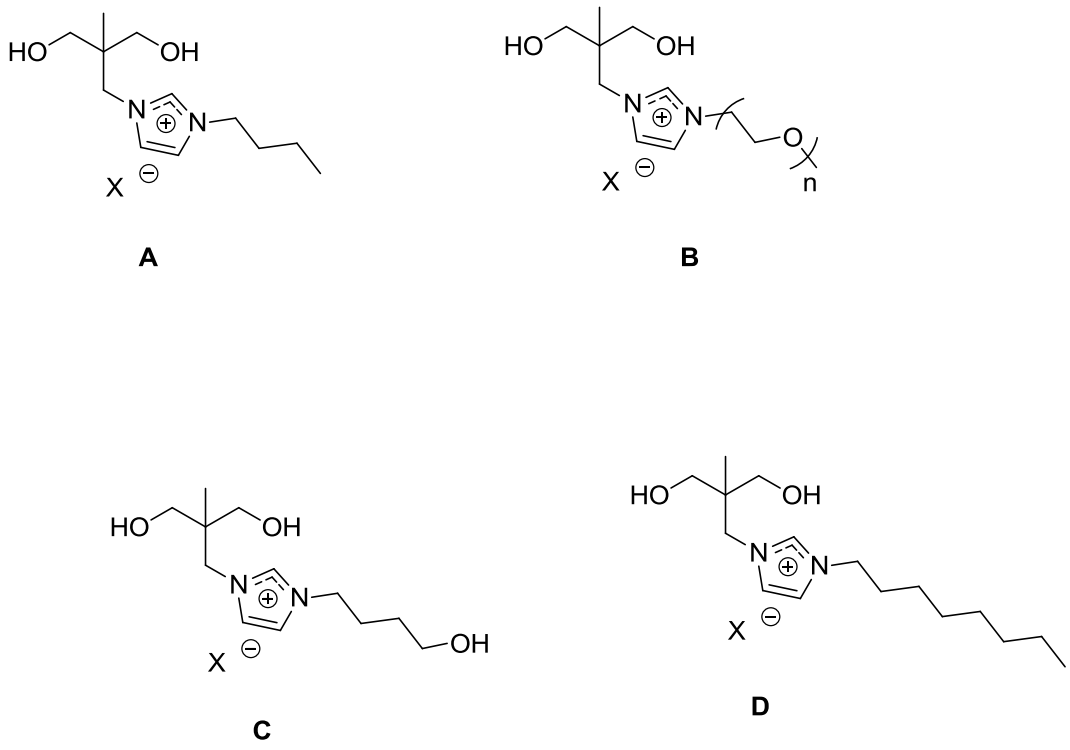

Figure 10.2. Versatile imidazolium diols with various functionality.